BioMed Research International

Imaging Neurodegenerative Diseases: Mechanisms and Interventions

Guest Editors: Lijun Bai, Lin Ai, Mingzhou Ding, Yong He, Lixing Lao, and Fanrong Liang

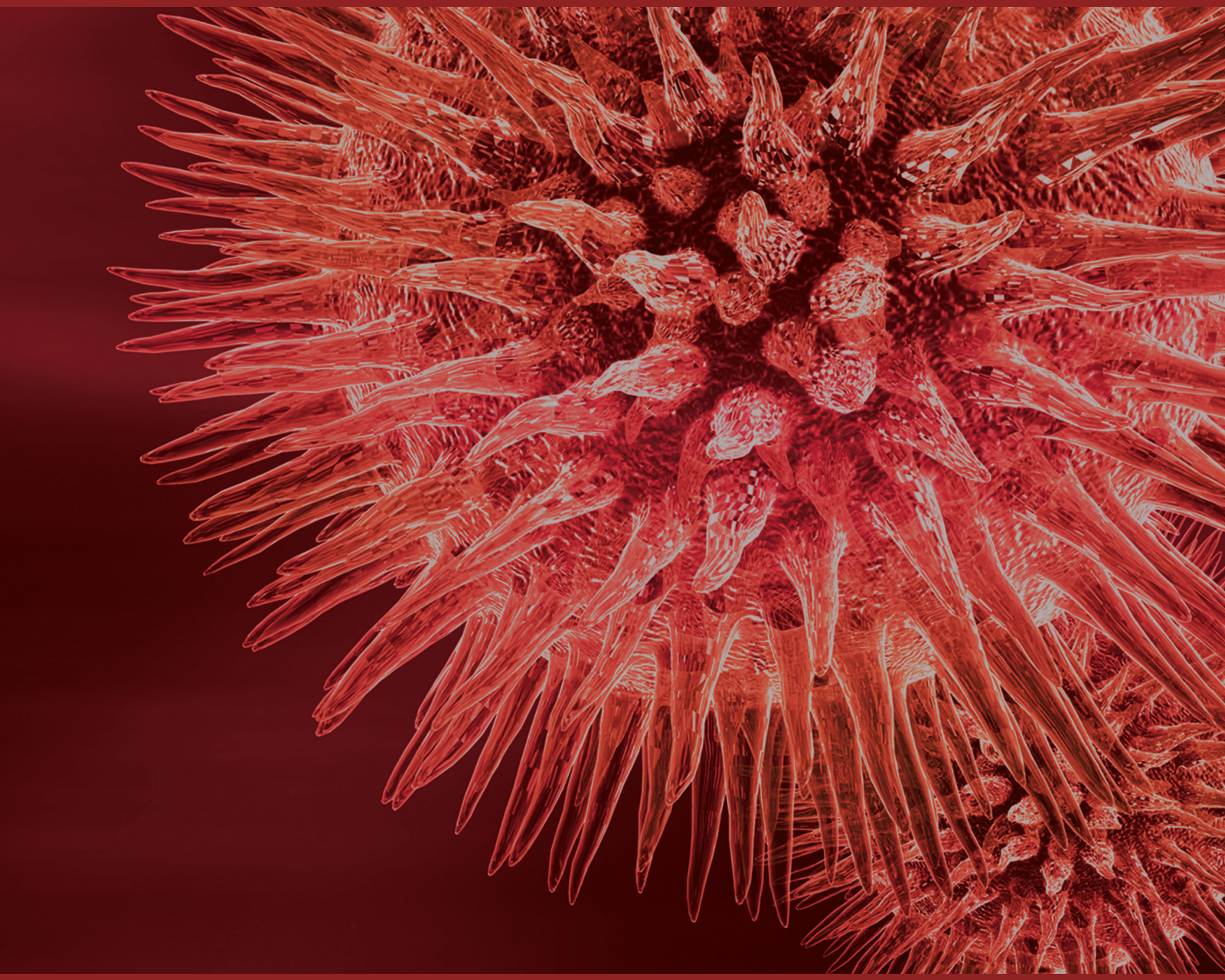

Imaging Neurodegenerative Diseases: Mechanisms and Interventions

BioMed Research International

Imaging Neurodegenerative Diseases: Mechanisms and Interventions

Guest Editors: Lijun Bai, Lin Ai, Mingzhou Ding, Yong He, Lixing Lao, and Fanrong Liang

Contents

Hindawi Publishing Corporation
BioMed Research International
Volume 2014, Article ID 419317, 2 pages
http://dx.doi.org/10.1155/2014/419317

Editorial

Imaging Neurodegenerative Diseases: Mechanisms and Interventions

Lijun Bai,[1] Lin Ai,[2] Mingzhou Ding,[3] Yong He,[4] Lixing Lao,[5,6] and Fanrong Liang[7]

[1] *The Key Laboratory of Biomedical Information Engineering, Ministry of Education, Department of Biomedical Engineering, School of Life Science and Technology, Xi'an Jiaotong University, Xi'an 710049, China*
[2] *Department of Nuclear Medicine, Beijing Tiantan Hospital, Capital Medical University, Beijing 100050, China*
[3] *J.Crayton Pruitt Family Department of Biomedical Engineering, University of Florida, Gainesville, FL 32610, USA*
[4] *State Key Laboratory of Cognitive Neuroscience and Learning and IDG/McGovern Institute for Brain Research, Beijing Normal University, Beijing 100875, China*
[5] *School of Chinese Medicine, University of Hong Kong, 10 Sassoon Road, Pokfulam, Hong Kong*
[6] *Center for Integrative Medicine, School of Medicine, University of Maryland, Baltimore, Baltimore, MD 21201, USA*
[7] *Chengdu University of Traditional Chinese Medicine, Chengdu 610075, China*

Correspondence should be addressed to Lijun Bai; bailj4152615@gmail.com

Received 10 September 2014; Accepted 10 September 2014; Published 21 December 2014

Neurodegenerative diseases as diverse as Alzheimer's disease, Parkinson's disease, amyotrophic lateral sclerosis, multiple sclerosis, stroke, and depression are thought to share a common pathogenesis mechanism—the aggregation and deposition of misfolded proteins, which leads to progressive central nervous system impairments. This special issue compiled 11 articles, most of which are novel and excellent investigations in this field.

Two modalities of neuroimaging techniques (PET and MRS) are leading to a greater understanding of quantification for the early and differential diagnosis of Alzheimer's disease. P. Daniela et al. conducted a meta-analysis and GRADE analysis reporting differences in the levels of sensitivity and specificity for the standard visual FDG PET scan or dichotomous readout based amyloid PET with respect to parametric or semiquantitative analysis. The review by Radoslaw Magierski and Tomasz Sobow summarized the main results obtained from the application of neuroimaging techniques in Dementia with Lewy bodies (DLB) cases, mainly focusing on proton magnetic resonance spectroscopy (1H-MRS). DLB and Parkinson's disease share clinical symptoms and neuropsychological profiles. Proton magnetic resonance spectroscopy (1H-MRS) provides a noninvasive method of assessing an *in vivo* biochemistry of brain tissue.

The altered brain mechanisms underlying potential progress state related with neurodegenerative disease are addressed in four articles. As a subtype of mild cognitive impairments (MCI), amnestic mild cognitive impairment (aMCI) most often leads to Alzheimer's disease. Z. Zhao and colleagues aimed to elucidate the altered resting brain in patients with aMCI. They found increased activities in the frontal lobe of aMCI patients, which might indicate effective recruitment of compensatory brain resources. Traumatic brain injury (TBI) is one of the most consistent candidates for initiating the molecular cascades that result in Alzheimer's disease. Y. Zhu et al. enrolled only "probable and symptomatic" TBI with no visible lesions by using conventional and SWI neuroimaging techniques, while DTI analysis indicated widespread declines in the fractional anisotropy (FA) of gray matter and white matter, particularly in the limbic-subcortical structures. A better understanding of the acute changes occurring following symptomatic TBI may increase our understanding of neuroplasticity and continuing degenerative change, which in turn, may facilitate advances in management and intervention. S. Zheng et al. evaluated relationship between degree of internal carotid artery (ICA) stenosis and frontal activations induced by working memory (WM) task using fMRI. They demonstrated that cognitive

impairments in ICA stenosis were associated with frontal lobe dysfunctions. Furthermore, D. Rong et al. investigated the involvement and changes of the corticospinal tract (CST) in patients with medulla infarct during motor recovery. The degree of degeneration and spared peri-infarct CST compensation may reflect important motor recovery mechanism.

Two researches mainly focus on the pathophysiological changes and nuclear neuroimaging diagnostic work-up for amyotrophic lateral sclerosis (ALS) in assessing the evolution of the disease and/or the effectiveness of therapeutic action. A. Cistaro et al. offered a comprehensive overview of the different radiotracers for the assessment of the metabolism of glucose (FDG), the measurement of cerebral blood flow (CBF), or the evaluation of neurotransmitters, astrocytes, and microglia in clinically diffuse radiopharmaceuticals in ALS. Q. Zhang et al. investigated abnormal lateralization of brain gray matter (GM) in the ALS patients and focused on the relationship between GM abnormalities and side of disease onset in limb-onset patients. They found a negative relationship between regional atrophy and disease progression rate, indicating the possible correspondence between disease progression and cortical abnormality. Depression is a risk factor for neurodegenerative diseases in general, including Alzheimer's disease (AD). Its premorbid signs are commonly observed, and the morbidity of depression is higher in dementia patients. R. Yang and colleagues examined the effects of antidepressant treatment (sertraline) on hypothalamus-related resting brain networks. People with multiple sclerosis (MS) are also at high risk of depression. One study from Y. Shen et al. reported that there was a significant relation between the depression symptoms in relapsing-remitting MS and global microstructural changes both in brain white matter and gray matter. P. Zhang et al. demonstrated altered functional connectivity (FC) in the affective network (AN) in patients with poststroke depression.

By gathering these papers, we hope to enrich our readers and researchers with respect to the underlying neurological mechanism of neurodegenerative diseases. We look forward to an increasing number of both clinical trials and experimental studies to further identify early disease biomarkers and more effective therapies to improve the quality of life and cognitive function of the patients affected by these devastating illnesses.

Lijun Bai
Lin Ai
Mingzhou Ding
Yong He
Lixing Lao
Fanrong Liang

Hindawi Publishing Corporation
BioMed Research International
Volume 2014, Article ID 809503, 7 pages
http://dx.doi.org/10.1155/2014/809503

Review Article

Magnetic Resonance Spectroscopy in the Diagnosis of Dementia with Lewy Bodies

Radoslaw Magierski[1] and Tomasz Sobow[2]

[1] *Department of Old Age Psychiatry and Psychotic Disorders, Medical University of Lodz, Czechoslowacka 8/10, 92-216 Lodz, Poland*
[2] *Department of Medical Psychology, Medical University of Lodz, Sterlinga 5, 91-425 Lodz, Poland*

Correspondence should be addressed to Radoslaw Magierski; radoslaw.magierski@umed.lodz.pl

Received 25 January 2014; Revised 21 May 2014; Accepted 20 June 2014; Published 6 July 2014

Academic Editor: Fan-Rong Liang

Dementia with Lewy bodies (DLB) is considered to be the second most frequent primary degenerative dementing illness after Alzheimer's disease (AD). DLB, together with Parkinson's disease (PD), Parkinson's disease with dementia (PDD) belong to α-synucleinopathies—a group of neurodegenerative diseases associated with pathological accumulation of the α-synuclein protein. Dementia due to PD and DLB shares clinical symptoms and neuropsychological profiles. Moreover, the core features and additional clinical signs and symptoms for these two very similar diseases are largely the same. Neuroimaging seems to be a promising method in differential diagnosis of dementia studies. The development of imaging methods or other objective measures to supplement clinical criteria for DLB is needed and a method which would accurately facilitate diagnosis of DLB prior to death is still being searched. Proton magnetic resonance spectroscopy (^{1}H-MRS) provides a noninvasive method of assessing an *in vivo* biochemistry of brain tissue. This review summarizes the main results obtained from the application of neuroimaging techniques in DLB cases focusing on ^{1}H-MRS.

1. Introduction

Dementia with Lewy bodies (DLB) is considered to be the second most frequent primary degenerative dementing illness after Alzheimer's disease (AD). According to some investigators from research centres and brain banks it comprises up to 20% of all dementia cases [1]. DLB, together with Parkinson's disease (PD), Parkinson's disease with dementia (PDD) belong to α-synucleinopathies—a group of neurodegenerative diseases related by the pathological accumulation of the α-synuclein protein [2, 3]. The clinical and neuropathologic criteria for DLB and consensus criteria were published by McKeith et al. [4–7].

DLB is characterized by dementia (a progressive cognitive decline with deficits in attention, executive functions, and visuospatial ability associated with fluctuations), visual hallucinations, and parkinsonism. Presence of parkinsonism, visual hallucinations, and specific profile of cognitive deficits allows for differential diagnosis with AD or frontotemporal lobar degeneration (FTLD), especially at the early stage of disease. Dementia due to PD and DLB shares clinical symptoms and neuropsychological profiles. Moreover, the core features and additional clinical signs and symptoms for these two very similar diseases are largely the same. Researchers have spent over decade debating whether these are two different diseases or simply different phenotypes of one single entity. PDD and DLB are separated mostly by the "one-year rule" of dementia onset, which is frequently the only criterion applied in differential diagnosis. It seems that the temporal sequence of symptoms and clinical features of PDD and DLB justify distinguishing these disorders. Details on doubts and boundary issues are well covered in the paper by Lippa et al. [8] and review on clinical presentation of DLB was published lately by Morra and Donovick [9].

Conflicting data are present on cognitive decline rate and duration of the illness. In the study by Williams et al. [10] DLB was characterised by increased risk of death compared with AD, but the two groups did not differ in rate of cognitive decline. More rapid progression of cognitive decline and shorter duration of dementia were found in DLB in

comparison to AD in the naturalistic study by Magierski et al. [11], but no differences between these two types of dementia in the rate of progression were found in other studies [12].

Accurate *ante mortem* diagnosis of DLB is essential for several reasons. First, the detailed and exact diagnosis of dementia subtype is needed in clinical studies on efficacy and safety of treatment. Second, current treatment options that are effective in one type of dementia may not be useful or dangerous in other types [13, 14]. A patient with DLB usually responds well to cholinesterase inhibitors [15–17] and improvement in some neuropsychiatric symptoms was confirmed [18]. The antipsychotic treatment is known to be a dangerous treatment option in DLB because of the risk of exacerbation of extrapyramidal symptoms and is generally contraindicated in this disorder [19–21], but in the study by Johnell at al. [22] the use of antipsychotics in DLB patients was surprisingly high (16% in DLB patients) with an adjusted odds ratio of 4.2 compared to AD patients. Third, in clinical studies it is essential to identify uniform diagnostic groups. According to Watson et al. [23] in light of the poor sensitivity of the consensus criteria, it is important to establish additional markers which, when combined with clinical assessment, can improve diagnostic accuracy. Vernon et al. [24] stated that there is no clear diagnostic imaging marker that offers a reliable differential diagnosis between the different forms of Lewy body diseases (PD, PDD, or DLB) or that could facilitate tracking of disease progression.

Neuroimaging seems to be an obvious method which allows obtaining additional information on brain structure, changes, and functioning. The development of imaging methods or other objective measures to supplement clinical criteria is needed. However, a method which would accurately facilitate diagnosis of DLB prior to death is still being searched.

2. Imaging in Dementia with Lewy Bodies

Neuroimaging seems to be a promising method in dementia studies. Both structural imaging research and functional imaging research have been performed in DLB patients [25]. Most imaging studies on DLB have used standard structural magnetic resonance imaging (MRI). Also, other MRI techniques, such as tensor-diffusion imaging to visualize fiber tracts, MRI spectroscopy to visualize *in vivo* metabolism, and magnetization transfer ratios to visualize fine structural damage, have been studied in DLB patients [26].

The main structural imaging finding assumed as characteristic change in the DLB cases is the relative preservation of hippocampal and medial temporal lobe, a feature that is important in its differentiation from AD. White matter lesions are equally frequent in DLB and AD and together with cortical pathology may influence the severity of cognitive impairment.

The detailed description of findings in neuroimaging studies in DLB and the role of different MRI based techniques is covered in the excellent paper by Watson et al. [23].

Functional examination of the brain tissue is available with 18F-fluorodeoxyglucose positron emission tomography (FDG-PET) or single photon emission computed tomography (SPECT) and both have clinical utility for the differential diagnosis of dementia [27]. Occipital hypometabolism in PET and hypoperfusion in SPECT were observed in DLB, while temporal lobe perfusion is relatively preserved [28]. Intense research was done for visualizing brain neurotransmitter's abnormalities in DLB, especially in the dopaminergic system [29] and reduced dopamine transporter levels in DLB as shown with [123I]FP-CIT-SPECT currently appear to be the most reliable and valid biomarker of disease [30]. ^{123}I-MIBG myocardial scintigraphy may have an important position in differential diagnosis between DLB and other dementias and for that purpose it was included into the diagnostic criteria of DLB [7].

Neurochemical studies have shown a pronounced reduction in the cholinergic activity in DLB, even greater than in AD brains. Investigation of brain metabolites changes is challenging in the context of neuropathological and neurochemical findings [31].

3. Proton Magnetic Resonance Spectroscopy (^{1}H-MRS)

Proton magnetic resonance spectroscopy (^{1}H-MRS) provides a noninvasive method of assessing an *in vivo* biochemistry of brain tissue. ^{1}H-MRS using standard or research-dedicated magnetic resonance imaging devices allows making measurements of chemical levels within the brain by measuring the signal originating from protons attached to key biomolecules. The neurochemistry is defined on a regional basis by acquiring a radiofrequency signal with chemical shift from one or many volumes or voxels. The result of ^{1}H-MRS examination is a spectrum and up to 80 brain metabolites and flux rates can be distinguished within the spectrum [36]. The signal indicating particular compound is localized on a horizontal scale (chemical shift), and their relative metabolite concentration is determined from the metabolite's peak height. The brain proton spectrum includes metabolite peaks for 5 important compounds: N-acetylaspartate (NAA), creatine (Cr), choline (Cho), myo-inositol (mI), and glutamine/glutamate (Glx). Peaks of lipids and lactate are not observed in healthy brain, and therefore their absorptions are not visible within normal spectrum. Both have diagnostic value in cases of brain diseases. NAA is regarded as a marker of neuronal integrity and is reduced in neuronal dysfunction or loss. Creatine is a marker of general metabolism and is assumed to be relatively constant. Therefore, a peak of Cr is often applied as an internal reference level and is used for ratio's calculation. Choline is a metabolic marker of membrane density and integrity. Myo-inositol is mainly present in the glial cells and is considered as a glial marker. Finally, glutamine/glutamate metabolism occurs in neurons and glial cells and plays a role in detoxification and regulation of neurotransmitters. Reduction of glutamine/glutamate (Glx) may reflect glial cell or axonal impairment. The detailed description of MRS technique basics is covered excellently elsewhere [37–41].

Among all dementia types, ^{1}H-MRS was firstly used in the studies on AD and MCI. Both decreased N-acetylaspartate

Table 1: 1H-MRS studies in DLB (modified after Watson et al. [23]).

Author and reference	Subjects	Area (voxel of interest)	Metabolite ratios in DLB cases			
			NAA/Cr	Cho/Cr	Glx/Cr	mI/Cr
Molina et al. (2002) [32]	CTL ($n = 11$) vs DLB ($n = 12$)	WM: centrum semiovale	↓	↓	↓↔	NA
		GM: parasagittal parietal cortex	↔	↔	↔	NA
Kantarci et al. (2004) [33]	CTL ($n = 206$) vs DLB ($n = 20$) vs AD ($n = 121$)	Right and left posterior cingulated gyrus and inferior precunei	↔	↑↔	↔	↔
Magierski et al. (2004) [34]	CTL ($n = 8$) vs DLB ($n = 12$) vs AD ($n = 12$)	Centrum semiovale, occipital grey matter and temporal lobes	↓	NA	NA	↔
Xuan et al. (2008) [35]	CTL ($n = 8$) vs DLB ($n = 8$)	Bilateral hippocampi	↓	↔	NA	NA

↔: Unchanged; ↓: reduced; ↑: increased; NA: not applicable; CTL: controls; AD: Alzheimer's disease; DLB: dementia with Lewy bodies; WM: white matter; GM; grey matter.

(NAA) and increased myo-inositol in the occipital, temporal, parietal, and frontal regions as well as in whole brain of AD patients were found [42, 43] and changes were detectable even at the early stages of the disease. ^{1}H-MRS examination was used for identifying MCI, distinguishing between MCI and normal controls [44, 45] and result of examination was evaluated as a predictor of clinical conversion of MCI to AD dementia based on clinical followup [46, 47]. The most current paper on MRS in MCI, summarizing 29 papers and providing meta-analysis of data, was published by Tumati et al. last year [48].

Proton magnetic resonance spectroscopy was used for determination profile of brain metabolites in DLB, but limited published data of ^{1}H-MRS are available in DLB patients in comparison to AD or MCI. Only 4 original papers including DLB cases were identified and all of them are described later (see Table 1). Cause of this lacking research in DLB cases is complex and not fully understood. Among all, duration of examination with 1.5T MRI scanner seems difficult and not feasible in many DLB patients. Brain atrophy, cognitive fluctuation, psychotic symptoms, and motor artefacts due to Parkinsonian features in particular are the reasons for difficulties in ^{1}H-MRS studies in DLB subjects.

The first ^{1}H-MRS study in DLB subjects was published in 2002. Molina et al. [32] examined white matter from the left centrum semiovale and grey matter from the midline parietal region in DLB patients and age-matched healthy controls. Investigators made an attempt to acquire spectra from the temporal lobe and basal ganglia. These measurements were unsuccessful due to lack of proper magnetic homogeneity in those regions in almost all patients and many of the healthy controls. Authors reported significantly lower mean NAA/Cr, Glx1/Cr, and Cho/Cr ratios in the white matter. No significant differences in the grey matter were found. Finally, authors concluded that the large overlap between the spectroscopic profiles of DLB patients and healthy subjects limits usefulness of this method in the differentiation procedure.

We have performed pilot study to evaluate the feasibility of proton magnetic resonance spectroscopy in DLB and so far results were published in part as a conference poster only [34]. Primarily, 22 subjects meeting the Consortium on DLB International Workshop Criteria for probable DLB were evaluated. DLB patients represented different dementia stages, so the DLB group was not homogeneous. Finally, 15 DLB subjects and 14 patients meeting DSM-IV criteria for AD were included and final results are described below. Seven DLB subjects were excluded because they were severely demented and uncooperative, even during clinical assessment. Eleven healthy control subjects participated in the study.

The subjects included in the study underwent general medical, neurological, psychiatric, and neuropsychological investigations. The clinical assessment included vital signs, the mini-mental state examination, clinical dementia rating (CDR), the clock drawing test, Hachinski ischemic scale, the motor section of the unified Parkinson's disease rating scale (UPDRS), the memory-orientation-concentration test of Blessed, the neuropsychiatric inventory (NPI), and the activities of daily living (ADL). The neuropsychological assessment consisted of the evaluation of short-term memory (forward and backward digit span), episodic memory (10-items word list), semantic memory (Boston naming test, letter, and category fluency tests), perceptual and spatial abilities (WAIS-R block designs subtest, Rey complex figure), and abstractive reasoning (WAIS-R similarities subtest). Diagnostic criteria were applied and AD and DLB groups were selected on the basis of clinical and neuropsychological assessment. Control subjects were recruited in the group of patients' relatives. Volunteers underwent psychiatric and neuropsychological investigations. None of the participating control subjects had any neurological or somatic diseases. All demented patients in this study had an informant who provided an adequate clinical history.

All patients and volunteers were examined using a 1.5 T MR scanner with a head coil. We performed MRI in T1 weighted images, in three orthogonal planes without administration of paramagnetic contrast medium. These images were used for voxel positioning. ^{1}H-MRS was performed using short echo time SVS STEAM sequence: TE 20 ms and TR 2000 ms. Volumes of interest (VOI, voxel) were positioned in the parietal white matter, occipital grey matter, and temporal lobe separately. The raw data were then evaluated automatically with the protocols available in

the Magnetom Vision Plus—Siemens software. The relative signal intensities of the main metabolites were obtained by manual and semiautomated approximations of the spectra chosen from the volumes of interest. The ratios of the metabolites relative signal intensities in the group of healthy volunteers were evaluated separately for the brain parietal white matter, occipital grey matter and temporal lobe. These ratios were used as a reference to determine the metabolite changes occurring in patients with DLB and AD.

In our study, ^{1}H-MRS scans acquiring in 3 localizations was successful in 5 DLB, 7 AD patients and 7 control subjects. Five DLB subjects were uncooperative during scanning so measurement was ineffective in all localizations. Examination of the temporal lobe failed because of movement artefacts in 2 AD patients. ^{1}H-MRS scans acquiring was successful in the centrum semiovale in all AD and control subjects and 9 DLB patients. Measurement of metabolites in the occipital lobe was successful in all AD and control subjects and 10 DLB patients. Attempts were made to acquire proton spectra from the temporal lobes. These measurements were unsuccessful due to voxel localization problems associated with large brain atrophy in this region in 5 AD and 4 DLB patients and 4 volunteers. Examination of the occipital lobe and white matter failed in the more impaired subjects. This group had higher NPI (OL: $P = 0.013$ and WM: $P = 0.044$, resp.) and UPDRS (OL: $P = 0.001$ and WM: $P = 0.003$, resp.) than the group with successful examination.

In our study, temporal lobe scanning was unsuccessful in 21 cases; the reasons for difficulties were uncooperativeness in 5 DLB cases, movement artefacts in 2 AD and 1 DLB subjects, and pronounced brain atrophy in the examined region in 5 AD and 4 DLB patients and 4 controls. Movement artefacts were caused by various factors, primarily by Parkinsonism of DLB subjects. Features of Parkinsonism are generally mild to moderate in DLB but usually start unanimously with dementia. Bradykinesia, rigidity and falls are common, while resting tremor could be absent. Rigidity makes it very difficult to lie on the back for a long time. The structure of the examination procedure is probably the second cause of movement artefacts. The temporal lobe was examined following the examination of centrum semiovale and occipital region, which might have caused patients fatigue and inability to remain motionless. The complete procedure is 40 minute long and could be exhausting for the demented subjects. Moreover, uncooperativeness of DLB subjects could be a consequence of fluctuations of cognition.

Unsuccessful scanning of the temporal lobe in our study was caused by considerable brain atrophy in the examined region in 5 AD and 4 DLB patients and 4 volunteers. Different patterns of brain atrophy were described by Burton et al. [49]. They observed regional grey matter loss bilaterally in the temporal and frontal lobes and insular cortex of DLB patients compared to control subjects. Comparison of dementia groups showed preservation of the medial temporal lobe, hippocampus, and amygdala in DLB relative to AD.

We have not found any correlation between unsuccessful temporal lobe scanning and any analysed variable (cognitive impairment, NPI score, and UPDRS score). Excessive asymptomatic brain atrophy could account for this finding. It was also seen in the control group, where we have found the atrophy of the temporal lobe without clinical impairment during neuropsychological assessment. Parkinsonism and behavioural disturbances made scanning of the centrum semiovale and occipital lobe difficult, without negative effect on the temporal lobe examination. The assessment of centrum semiovale and occipital lobe in DLB patients was more difficult than in AD and control groups.

Kantarci et al. [33] evaluated ^{1}H-MRS metabolite ratio changes in common dementias (AD, DLB, FTLD, and vascular dementia (VaD)) with respect to normal subjects within standard voxels covering right and left posterior cingulate gyri and inferior precunei. The study showed a number of differences in the ^{1}H-MRS metabolites profiles and it will be discussed in detail below. NAA/Cr ratio lower than normal in patients with AD, FTLD, and VaD was reported. They found lower NAA/Cr ratio in AD and FTLD cases than in DLB patients. mI/Cr ratio was higher in patients with AD and FTLD than in normal subjects. In patients with AD, FTLD, and DLB higher Ch/Cr ratio was found when compared to normal subjects. No metabolite differences between patients with AD and FTLD or between patients with DLB and VaD were found. mI/Cr ratio was higher in patients with AD and FTLD than VaD. Moreover, mI/Cr was higher in patients with FTLD than DLB too. The only measurement that was different from normal in patients with DLB was the Cho/Cr ratio. Authors concluded that they found decreased level of NAA/Cr in dementias characterized by neuron loss (AD, FTLD, and VaD). As it could be expected, mI/Cr levels were increased in dementias associated with gliosis (AD and FTLD). Finally, Cho/Cr levels were elevated in dementias with a profound cholinergic deficit (AD and DLB). In discussion the authors stated that the elevation of Cho/Cr in AD and DLB patients is not completely understood and requires further research. It can be linked to decrease of Cho/Cr levels with cholinergic agonist treatment in AD, so they suggested that Cho/Cr levels could be a biomarker of therapeutic efficacy in AD and DLB drug trials.

Xuan et al. [35] assumed that the decrease of NAA in hippocampus was found in studies of AD patients, so the same result may be found in DLB patients. DLB patients showed statistically significant reduction in NAA/Cr ratios in left hippocampus when compared to controls. Cho/Cr ratios of DLB subjects did not differ from those of the control group. NAA/Cr ratios of DLB patients in right hippocampus were also significantly lower than controls. Similarly to the left side, Cho/Cr ratios in right hippocampus of DLB patients did not differ from those of the control group. Authors concluded that their data show relatively decrease of N-acetylaspartate in the hippocampus of patients with early- or intermediate-stage DLB.

Another interesting aspect of ^{1}H-MRS examination is prognostic value of changes in brain metabolic concentrations. Attempts for selecting MCI cases who will convert to DLB or AD were made. Fayed et al. [50] described group of MCI cases ($n = 119$) who were examined with ^{1}H-MRS at the baseline visit and were monitored through followup. After

the followup period (a mean period of 29 months; range 17–44), 54 patients converted to dementia (AD, $n = 49$; DLB, $n = 5$). Metabolites ratios were compared, but they did not find differences in NAA/Cr ratio or Cho/Cr ratios between patients with DLB and patients with other types of MCI or AD. In contrast, Zhang et al. [51] reported that decreased NAA/Cr ratio in the posterior cingulate gyri characterized patients with MCI who progressed to AD and distinguished them from MCI patients who progressed to DLB. So they concluded that ^{1}H-MRS may be a useful adjunct in early differential diagnosis of AD and DLB in patients with MCI.

Some data were published in the field of proton spectroscopy in Parkinson's disease dementia. As it was stated above, PDD and DLB share many clinical and neuropsychological features. So it could be challenging to compare results of DLB and PDD studies made with ^{1}H-MRS technique. Maybe it will be possible to confirm or reject assumption that clinicians are able to separate PDD and DLB mostly by the "one-year rule" of dementia onset. In other words, maybe the ^{1}H-MRS spectrum is a candidate for winning the title of noninvasive and precise biomarker.

So far, significantly decreased level of NAA in the occipital region in the PDD group compared to the PD and control groups was found [52]. Significantly, lower NAA/Cr ratio of the posterior cingulate in PDD cases when compared with controls and nondemented PD patients was also found in study by Griffith et al. [53]. Authors observed no abnormalities in Cho/Cr or mI/Cr ratios of PDD cases [53], but changes were visible when comparison of AD and controls was done [54]. Significantly reduced NAA/Cr ratio and significantly increased Cho/Cr ratio and mI/Cr ratio of posterior cingulate in AD cases when compared to controls were described. Moreover, patients with PDD exhibited significantly reduced NAA/Cr and Glu/Cr ratios compared with controls. Glu/Cr ratio was also significantly reduced in PDD cases compared with AD. The findings suggest that reduced NAA/Cr of the posterior cingulate could be used as a marker for dementia in patients with PD, authors said in conclusion [53].

Interestingly, changes in metabolites correlated with different aspects of clinical status of PDD and PD cases. The correlation between NAA/Cr ratio and mental status of patients with PD and patients with PDD was observed [53] and NAA values correlated with neuropsychological performance but not with severity of motor impairment [52]. Lately, similar metabolic and clinical findings were described by Pagonabarraga et al. [55] who examined spectrum of PD patients (cognitively intact cases, patients with mild cognitive impairment, and cases with dementia). They have analyzed the relative importance of temporal lobe defects versus executive impairment in the progression to dementia in PD by using ^{1}H-MRS of the hippocampus and dorsolateral prefrontal cortex. NAA concentrations in the right dorsolateral prefrontal cortex were significantly decreased in PD cases with MCI when compared to cognitively intact PD cases. NAA concentrations were also significantly decreased in the left hippocampus of PDD cases when compared to PD patients with MCI. Similarly to previous studies, decrease of NAA was correlated with neuropsychological results.

4. Conclusions

Many authors focused their research or papers on differential diagnosis in dementia. As it was said in the introduction exact diagnosis is essential for many purposes. At this moment there are so many similarities and only some differences between DLB and PDD, both Lewy body diseases. Attempts were done for establishing biomarkers with CSF examination [56, 57], neuroimaging, and neurochemistry [58].

Proton magnetic resonance spectroscopy (^{1}H-MRS) provides a noninvasive method of assessing an *in vivo* tissue biochemistry. ^{1}H-MRS using standard or research-dedicated magnetic resonance imaging devices does not need any injection of contrast substances, and the price of evaluation is comparable with regular MRI examination (few times lower than PET scanning). ^{1}H-MRS seems to be a promising method of brain research and was intensively applied in many neurological disorders, including AD cases. Studies in DLB and PDD were also performed but are limited in number. To our knowledge, papers with head-to-head comparison of DLB and PDD cases are lacking and there is a need for further studies. Honestly speaking this could be challenging due to difficulties described earlier.

Last but not least, differential diagnosis is essential at the beginning of treatment and at early clinical presentation. At early phase of dementing illness it is easier, and in some cases it is possible at this time only to make differential diagnosis based on clinical and neuropsychological evaluation. Within the course of dementia major symptoms disappear, additional symptoms occur (for example, seizures or Parkinsonism), and AD may mimic Lewy body diseases. Neuropathological verification of clinical diagnosis has the best value. It would be perfect for differential diagnosis and for understanding of the nature of DLB to perform ^{1}H-MRS examination at MCI stage, follow the cases to the point of dementia diagnosis, and verify diagnosis postmortem.

Abbreviations

DLB: Dementia with Lewy Bodies
AD: Alzheimer's disease
PDD: Parkinson's disease dementia
MCI: Mild cognitive impairment
CTL: Controls
FTLD: Frontotemporal lobar degeneration
VaD: Vascular dementia
^{1}H-MRS: Proton magnetic resonance spectroscopy
MRI: Magnetic resonance imaging
PET: Positron emission tomography
SPECT: Single photon emission computed tomography
NAA: N-acetylaspartate
Cho: Choline compound
Cr: Creatine and phosphocreatine
mI: Myo-inositol
Glx: Glutamate-glutamine complex
Ppm: Parts per million.

Conflict of Interests

The authors declare that there is no conflict of interests regarding the publication of this paper.

Acknowledgments

This work was conducted within the framework of Healthy Aging Research Centre, Medical University of Lodz (supported by grant from European Union, Framework Programme 7). The authors thank all of the colleagues who contributed in our study (Arkadiusz Rotkiewicz, M.D., Ph.D.; Witold Gajewicz, M.D., Ph.D.; Iwona Karlinska, M.S. (Psych), Ph.D.; Ludomir Stefanczyk, M.D., Ph.D.; and Iwona Kloszewska M.D., Ph.D.) and who gave their time and expertise to review the paper (Adam Wysokiński, M.D., Ph.D.).

References

[1] I. G. McKeith, J. Mintzer, D. Aarsland, and D. Burn, "International psychogeriatric association expert meeting on DLB.: dementia with Lewy bodies," *The Lancet Neurology*, vol. 3, no. 1, pp. 19–28, 2004.

[2] G. M. Halliday, J. L. Holton, T. Revesz, and D. W. Dickson, "Neuropathology underlying clinical variability in patients with synucleinopathies," *Acta Neuropathologica*, vol. 122, no. 2, pp. 187–204, 2011.

[3] W. J. Schulz-Schaeffer, "The synaptic pathology of α-synuclein aggregation in dementia with Lewy bodies, Parkinson's disease and Parkinson's disease dementia," *Acta Neuropathologica*, vol. 120, no. 2, pp. 131–143, 2010.

[4] I. G. McKeith, R. H. Perry, A. F. Fairbairn, S. Jabeen, and E. K. Perry, "Operational criteria for senile dementia of Lewy body type (SDLT)," *Psychological Medicine*, vol. 22, no. 4, pp. 911–922, 1992.

[5] I. G. McKeith, D. Galasko, K. Kosaka et al., "Consensus guidelines for the clinical and pathologic diagnosis of dementia with Lewy bodies (DLB): report of the consortium on DLB international workshop," *Neurology*, vol. 47, no. 5, pp. 1113–1124, 1996.

[6] I. G. McKeith, E. K. Perry, and R. H. Perry, "Report of the second dementia with Lewy body international workshop: diagnosis and treatment," *Neurology*, vol. 53, no. 5, pp. 902–905, 1999.

[7] I. G. McKeith, D. W. Dickson, J. Lowe et al., "Diagnosis and management of dementia with Lewy bodies: third report of the DLB consortium," *Neurology*, vol. 65, no. 12, pp. 1863–1872, 2005.

[8] C. F. Lippa, J. E. Duda, M. Grossman et al., "DLB and PDD boundary issues: diagnosis, treatment, molecular pathology, and biomarkers," *Neurology*, vol. 68, no. 11, pp. 812–819, 2007.

[9] L. F. Morra and P. J. Donovick, "Clinical presentation and differential diagnosis of dementia with Lewy bodies: a review," *International Journal of Geriatric Psychiatry*, vol. 29, no. 6, pp. 569–576, 2014.

[10] M. M. Williams, C. Xiong, J. C. Morris, and J. E. Galvin, "Survival and mortality differences between dementia with Lewy bodies vs Alzheimer disease," *Neurology*, vol. 67, no. 11, pp. 1935–1941, 2006.

[11] R. Magierski, I. Kłoszewska, and T. M. Sobów, "The influence of vascular risk factors on the survival rate of patients with dementia with Lewy bodies and Alzheimer disease," *Neurologia i Neurochirurgia Polska*, vol. 44, no. 2, pp. 139–147, 2010.

[12] H. Hanyu, T. Sato, K. Hirao, H. Kanetaka, H. Sakurai, and T. Iwamoto, "Differences in clinical course between dementia with Lewy bodies and Alzheimer's disease," *European Journal of Neurology*, vol. 16, no. 2, pp. 212–217, 2009.

[13] B. Hu, L. Ross, J. Neuhaus et al., "Off-label medication use in frontotemporal dementia," *American Journal of Alzheimer's Disease & other Dementias*, vol. 25, no. 2, pp. 128–133, 2010.

[14] M. F. Mendez, J. S. Shapira, A. McMurtray, and E. Licht, "Preliminary findings? Behavioral worsening on donepezil in patients with frontotemporal dementia," *American Journal of Geriatric Psychiatry*, vol. 15, no. 1, pp. 84–87, 2007.

[15] M. Rolinski, C. Fox, I. Maidment, and R. McShane, "Cholinesterase inhibitors for dementia with Lewy bodies, Parkinson's disease dementia and cognitive impairment in Parkinson's disease," *Cochrane Database of Systematic Reviews*, vol. 14, no. 3, 2012.

[16] K. A. Wesnes, I. G. Mckeith, R. Ferrara et al., "Effects of rivastigmine on cognitive function in dementia with lewy bodies: a randomised placebo-controlled international study using the Cognitive Drug Research computerised assessment system," *Dementia and Geriatric Cognitive Disorders*, vol. 13, no. 3, pp. 183–192, 2002.

[17] I. McKeith, T. del Ser, P. Spano et al., "Efficacy of rivastigmine in dementia with Lewy bodies: a randomised, double-blind, placebo-controlled international study," *The Lancet*, vol. 356, no. 9247, pp. 2031–2036, 2000.

[18] M. Satoh, H. Ishikawa, K. Meguro, M. Kasuya, H. Ishii, and S. Yamaguchi, "Improved visual hallucination by donepezil and occipital glucose metabolism in dementia with lewy bodies: the Osaki-Tajiri project," *European Neurology*, vol. 64, no. 6, pp. 337–344, 2010.

[19] C. Ballard, J. Grace, I. McKeith, and C. Holmes, "Neuroleptic sensitivity in dementia with lewy bodies and Alzheimer's disease," *The Lancet*, vol. 351, no. 9108, pp. 1032–1033, 1998.

[20] I. McKeith, A. Fairbairn, R. Perry, P. Thompson, and E. Perry, "Neuroleptic sensitivity in patients with senile dementia of Lewy body type," *British Medical Journal*, vol. 305, no. 6855, pp. 673–678, 1992.

[21] D. Aarsland, R. Perry, J. P. Larsen et al., "Neuroleptic sensitivity in Parkinson's disease and parkinsonian dementias," *Journal of Clinical Psychiatry*, vol. 66, no. 5, pp. 633–637, 2005.

[22] K. Johnell, D. Religa, and M. Eriksdotter, "Differences in drug therapy between dementia disorders in the swedish dementia registry: a nationwide study of over 7,000 patients," *Dementia and Geriatric Cognitive Disorders*, vol. 35, no. 5-6, pp. 239–248, 2013.

[23] R. Watson, A. M. Blamire, and J. T. O'Brien, "Magnetic resonance imaging in lewy body dementias," *Dementia and Geriatric Cognitive Disorders*, vol. 28, no. 6, pp. 493–506, 2009.

[24] A. C. Vernon, C. Ballard, and M. Modo, "Neuroimaging for Lewy body disease: is the in vivo molecular imaging of α-synuclein neuropathology required and feasible?" *Brain Research Reviews*, vol. 65, no. 1, pp. 28–55, 2010.

[25] S. Minoshima, N. L. Foster, E. C. Petrie, R. L. Albin, K. A. Frey, and D. E. Kuhl, "Neuroimaging in dementia with Lewy bodies: metabolism, neurochemistry, and morphology," *Journal of Geriatric Psychiatry and Neurology*, vol. 15, no. 4, pp. 200–209, 2002.

[26] A. Rongve, D. Aarsland, and C. Ballard, "Current perspectives in dementia with Lewy bodies," *Aging Health*, vol. 2, no. 3, pp. 461–472, 2006.

[27] C. M. Davison and J. T. O'Brien, "A comparison of FDG-PET and blood flow SPECT in the diagnosis of neurodegenerative dementias: a systematic review," *International Journal of Geriatric Psychiatry*, vol. 29, no. 6, pp. 551–561, 2014.

[28] K. Lobotesis, J. D. Fenwick, A. Phipps et al., "Occipital hypoperfusion on SPECT in dementia with Lewy bodies but not AD," *Neurology*, vol. 56, no. 5, pp. 643–649, 2001.

[29] N. Sinha, M. Firbank, and J. T. O'Brien, "Biomarkers in dementia with Lewy bodies: a review," *International Journal of Geriatric Psychiatry*, vol. 27, no. 5, pp. 443–453, 2012.

[30] L. Warr and Z. Walker, "Identification of biomarkers in Lewy-body disorders," *Quarterly Journal of Nuclear Medicine and Molecular Imaging*, vol. 56, no. 1, pp. 39–54, 2012.

[31] M. A. Piggott, J. Owens, J. O'Brien et al., "Muscarinic receptors in basal ganglia in dementia with Lewy bodies, Parkinson's disease and Alzheimer's disease," *Journal of Chemical Neuroanatomy*, vol. 25, no. 3, pp. 161–173, 2003.

[32] J. A. Molina, J. M. García-Segura, J. Benito-León et al., "Proton magnetic resonance spectroscopy in dementia with Lewy bodies," *European Neurology*, vol. 48, no. 3, pp. 158–163, 2002.

[33] K. Kantarci, R. C. Petersen, B. F. Boeve et al., "1H MR spectroscopy in common dementias," *Neurology*, vol. 63, no. 8, pp. 1393–1398, 2004.

[34] R. Magierski, A. Rotkiewicz, W. Gajewicz et al., "P4.017 Proton magnetic resonance spectroscopy(1HMRS) in the evaluation of brain metabolites changes in dementia with Lewy bodies and Alzheimer's disease," *European Neuropsychopharmacology*, vol. 14, supplement 3, pp. S329–S330, 2004.

[35] X. Xuan, M. Ding, and X. Gong, "Proton magnetic resonance spectroscopy detects a relative decrease of N-acetylaspartate in the hippocampus of patients with dementia with Lewy bodies," *Journal of Neuroimaging*, vol. 18, no. 2, pp. 137–141, 2008.

[36] A. Lin, B. D. Ross, K. Harris, and W. Wong, "Efficacy of proton magnetic resonance spectroscopy in neurological diagnosis and neurotherapeutic decision making," *NeuroRx*, vol. 2, no. 2, pp. 197–214, 2005.

[37] A. J. Ross and P. S. Sachdev, "Magnetic resonance spectroscopy in cognitive research," *Brain Research Reviews*, vol. 44, no. 2-3, pp. 83–102, 2004.

[38] Y. Rosen and R. E. Lenkinski, "Recent advances in magnetic resonance neurospectroscopy," *Neurotherapeutics*, vol. 4, no. 3, pp. 330–345, 2007.

[39] D. P. Soares and M. Law, "Magnetic resonance spectroscopy of the brain: review of metabolites and clinical applications," *Clinical Radiology*, vol. 64, no. 1, pp. 12–21, 2009.

[40] J. R. Alger, "Quantitative proton magnetic resonance spectroscopy and spectroscopic imaging of the brain: a didactic review," *Topics in Magnetic Resonance Imaging*, vol. 21, no. 2, pp. 115–128, 2010.

[41] J. M. N. Duarte, H. Lei, V. Mlynárik, and R. Gruetter, "The neurochemical profile quantified by in vivo ^{1}H NMR spectroscopy," *NeuroImage*, vol. 61, no. 2, pp. 342–362, 2012.

[42] M. J. Valenzuela and P. Sachdev, "Magnetic resonance spectroscopy in AD," *Neurology*, vol. 56, no. 5, pp. 592–598, 2001.

[43] A. Falini, M. Bozzali, G. Magnani et al., "A whole brain MR spectroscopy study from patients with Alzheimer's disease and mild cognitive impairment," *NeuroImage*, vol. 26, no. 4, pp. 1159–1163, 2005.

[44] J. M. G. Santos, D. Gavrila, C. Antúnez et al., "Magnetic resonance spectroscopy performance for detection of dementia, Alzheimer's disease and mild cognitive impairment in a community-based survey," *Dementia and Geriatric Cognitive Disorders*, vol. 26, no. 1, pp. 15–25, 2008.

[45] T. Wang, S. Xiao, X. Li et al., "Using proton magnetic resonance spectroscopy to identify mild cognitive impairment," *International Psychogeriatrics*, vol. 24, no. 1, pp. 19–27, 2012.

[46] K. Kantarci, S. D. Weigand, R. C. Petersen et al., "Longitudinal 1H MRS changes in mild cognitive impairment and Alzheimer's disease," *Neurobiology of Aging*, vol. 28, no. 9, pp. 1330–1339, 2007.

[47] J. Walecki, M. Barcikowska, J. B. Ćwikła, and T. Gabryelewicz, "N-acetylaspartate, choline, myoinositol, glutamine and glutamate (glx) concentration changes in proton MR spectroscopy (1H MRS) in patients with mild cognitive impairment (MCI)," *Medical Science Monitor*, vol. 17, no. 12, pp. MT105–MT111, 2011.

[48] S. Tumati, S. Martens, and A. Aleman, "Magnetic resonance spectroscopy in mild cognitive impairment: systematic review and meta-analysis," *Neuroscience and Biobehavioral Reviews*, vol. 37, no. 10, part 2, pp. 2571–2586, 2013.

[49] E. J. Burton, G. Karas, S. M. Paling et al., "Patterns of cerebral atrophy in Dementia with Lewy bodies using voxel-based morphometry," *NeuroImage*, vol. 17, no. 2, pp. 618–630, 2002.

[50] N. Fayed, J. Dávila, A. Oliveros, J. Castillo, and J. J. Medrano, "Utility of different MR modalities in mild cognitive impairment and its use as a predictor of conversion to probable dementia," *Academic Radiology*, vol. 15, no. 9, pp. 1089–1098, 2008.

[51] B. Zhang, T. Ferman, B. Boeve et al., "MRS differentiates MCI patients who progress to dementia with Lewy bodies and Alzheimer's disease," *Alzheimer's & Dementia*, vol. 9, no. 4, supplement, p. P37, 2013.

[52] C. Summerfield, B. Gómez-Ansón, E. Tolosa et al., "Dementia in Parkinson disease: a proton magnetic resonance spectroscopy study," *Archives of Neurology*, vol. 59, no. 9, pp. 1415–1420, 2002.

[53] H. R. Griffith, J. A. den Hollander, O. C. Okonkwo, T. O'Brien, R. L. Watts, and D. C. Marson, "Brain N-acetylaspartate is reduced in Parkinson disease with dementia," *Alzheimer Disease and Associated Disorders*, vol. 22, no. 1, pp. 54–60, 2008.

[54] H. R. Griffith, J. A. den Hollander, O. C. Okonkwo, T. O'Brien, R. L. Watts, and D. C. Marson, "Brain metabolism differs in Alzheimer's disease and Parkinson's disease dementia," *Alzheimer's and Dementia*, vol. 4, no. 6, pp. 421–427, 2008.

[55] J. Pagonabarraga, B. Gómez-Ansón, R. Rotger et al., "Spectroscopic changes associated with mild cognitive impairment and dementia in Parkinson's disease," *Dementia and Geriatric Cognitive Disorders*, vol. 34, no. 5-6, pp. 312–318, 2012.

[56] M. Bibl, B. Mollenhauer, H. Esselmann et al., "CSF amyloid-β-peptides in Alzheimer's disease, dementia with Lewy bodies and Parkinson's disease dementia," *Brain*, vol. 129, no. part 5, pp. 1177–1187, 2006.

[57] L. Parnetti, P. Tiraboschi, A. Lanari et al., "Cerebrospinal fluid biomarkers in Parkinson's disease with dementia and dementia with Lewy bodies," *Biological Psychiatry*, vol. 64, no. 10, pp. 850–855, 2008.

[58] K. K. Johansen, L. R. White, S. B. Sando, and J. O. Aasly, "Biomarkers: Parkinson disease with dementia and dementia with Lewy bodies," *Parkinsonism and Related Disorders*, vol. 16, no. 5, pp. 307–315, 2010.

Hindawi Publishing Corporation
BioMed Research International
Volume 2014, Article ID 473250, 11 pages
http://dx.doi.org/10.1155/2014/473250

Research Article

Side of Limb-Onset Predicts Laterality of Gray Matter Loss in Amyotrophic Lateral Sclerosis

Qiuli Zhang,[1] Cuiping Mao,[1] Jiaoting Jin,[2] Chen Niu,[1] Lijun Bai,[3] Jingxia Dang,[2] and Ming Zhang[1]

[1] *Department of Medical Imaging, First Affiliated Hospital, Medical College Xi'an Jiaotong University, 277 West Yanta Road, Xi'an, Shaanxi 710061, China*
[2] *Department of Neurology, First Affiliated Hospital Medical College Xi'an Jiaotong University, 277 West Yanta Road, Xi'an, Shaanxi 710061, China*
[3] *The Key Laboratory of Biomedical Information Engineering, Ministry of Education and Department of Biomedical Engineering, School of Life Science and Technology, Xi'an Jiaotong University, No. 28, Xianning West Road, Xi'an, Shaanxi 710049, China*

Correspondence should be addressed to Jingxia Dang; jxdang2000@126.com and Ming Zhang; profzmmri@gmail.com

Received 26 February 2014; Accepted 3 June 2014; Published 1 July 2014

Academic Editor: Lin Ai

Conflicting findings have been reported regarding the lateralized brain abnormality in patients with amyotrophic lateral sclerosis (ALS). In this study, we aimed to investigate the probable lateralization of gray matter (GM) atrophy in ALS patients. We focused on the relationship between the asymmetry in decreased GM volume and the side of disease onset in patients with limb-onset. Structural imaging evaluation of normalized atrophy (SIENAX) and voxel-based morphometry (VBM) were used to assess differences in global and local brain regions in patients with heterogeneous body onset and subgroups with different side of limb-onset. We found global brain atrophy and GM losses in the frontal and parietal areas in each patient group as well as left predominant GM losses in the total cohort. The intriguing findings in subgroup analyses demonstrated that the motor cortex in the contralateral hemisphere of the initially involved limb was most affected. We also found that regional brain atrophy was related to disease progression rate. Our observations suggested that side of limb-onset can predict laterality of GM loss in ALS patients and disease progression correlates with the extent of cortical abnormality.

1. Introduction

Amyotrophic lateral sclerosis (ALS) is a fatal disease characterized by the degeneration of upper and lower motor neurons, leading to hyperreflexia, spasticity, muscle weakness, and fasciculation [1]. Increasing evidence from clinical, pathological, and genetic studies has characterized ALS as a multisystem degeneration on the continuum with frontotemporal dementia (FTD) [1, 2]. The high prevalence of cognitive and behavioral impairments, even at times as severe as frank dementia, is now considered as another crucial feature in ALS [2–4].

The application of advanced neuroimaging techniques in detecting cortical abnormality has revealed compelling findings that match well with clinical manifestations and pathological abnormalities in ALS [5, 6]. For instance, the findings of focal morphological changes within the motor homunculus are consistent with the nature of focal onset and motor phenotype heterogeneity in ALS [7, 8]. Additionally, when comparing patients with pure motor syndromes with those with cognition or behavior dysfunction, the concurrent atrophy in motor cortex and frontal and/or temporal regions provides convincing insight into the relation between clinical profiles and the underlying pathological impairments *in vivo* [9–11].

However, inconsistent findings have also been reported in ALS [6]. Amongst these, the important and common finding of asymmetry or unilateral predominant structural

and functional abnormality has not been comprehensively investigated. First, asymmetrical symptom onset is a well-established clinical feature in early stage of ALS, which may imply a lateralized brain pathology [12, 13]. Furthermore, intra- and inter-hemisphere asymmetry as a distinctive feature for differential diagnosis in other neurodegenerative diseases and subtypes of FTD [14–16], together with the finding that ALS and FTD may share similar degeneration pattern [17, 18], point to the fact that asymmetry may contribute to the heterogeneity of clinical presentations in ALS as well. Emerging evidence has suggested that the function of the frontal lobe, which was often involved in ALS, is divergent among hemispheres of the brain [19–22]. Therefore, on the basis of "prion-like" or network-based propagation [14, 23–25], the involvement of specific frontal areas adjacent to or functional linked with motor cortex in different hemisphere could be associated with divergent clinical profiles. For example, damage to the left hemisphere would prone to induce language deficits [26] while damage to the right hemisphere may produce attention or emotional disturbances along with disease progression [19, 20], all of which were observed clinically in the diverse ALS population [4, 18, 27]. Therefore, the existence of asymmetrical brain pathology may be the key for understanding the widely heterogeneous clinical features, as the case in FTD.

Nevertheless, lateralized structural changes are not thought to be a notable aspect in ALS [6, 28–30]. In addition, inconsistent reports on the unilateral predominated brain atrophy also skew our understanding of the neurological impairments in ALS. Specifically, some studies concluded rightward degeneration based on pronounced gray matter (GM) loss or functional abnormality in the right hemisphere [31–35]. While other studies confronted the unilateral predominant atrophy as a separate clinical constellation or a specific group effect [36–41].

Among these, only a few studies have examined the asymmetry issue by measuring the relationship between lateralized brain metabolic ratio changes and clinical presentations or separating patients based on the laterality of limb-onset. These studies suggested that the lateralization of clinical syndromes mostly corresponds to brain abnormalities in the contralateral hemisphere [39–41]. However, the contralateral hemisphere of the lateralized clinical presentation or side of syndrome defect was unclear, because the variable spreading pattern [42] and diminished asymmetry of clinical presentation as the disease progresses will make the lateralized clinical presentation in these former studies [39, 40] differ with the laterality of limb-onset in later study [41]. Therefore, combining with the correlation between region of onset and the characteristics of neuron loss in the lower motor neurons [43], it is critical to define the lateralization of syndrome according to the sidedness of onset, as suggested by Zhang et al. [41].

Here we aimed to explore lateralization or asymmetrical GM loss in ALS patients and establish the relationship between the sides of limb defect at disease onset with imaging findings to help clarify the neurologic basis of the various motor syndromes in ALS. Optimized and reliable voxel-based morphometry (VBM) and Structural imaging evaluation of normalized atrophy (SIENAX) were used in the following analyses to identify regional and gross changes. First, all patients with heterogeneous body part defects at disease onset were compared with normal controls to assess whether there is a unilateral GM abnormality. Then subgroup analyses were conducted on patients with unilateral homogenous side of limb-onset with their respective normal controls to investigate for GM loss patterns in each group. Based on the previous findings [7, 8, 13, 41, 43], we hypothesize that amongst patients with homogenous side of disease onset, the prominent GM abnormality will be located primarily in the contralateral hemisphere to the initially involved limbs.

2. Materials and Methods

2.1. Subjects. Forty-three patients (27 males, 32 to 71 years old) from October 2011 to August 2013 with either a definite or probable diagnosis of sporadic ALS, according to the revised EI Escorial criteria, were enrolled in this study [30]. Based on the body part affected at disease onset, 36 patients were defined as limb-onset and 7 patients were bulbar-onset. Of the 36 patients with limb-onset, 20 patients presented with right side syndromes at onset (16 upper extremity, 4 lower extremity), and 16 patients present with left limb involvement (12 upper extremity, 4 lower extremity). Disease severity (full score = 40) and disease progression (40-ALSFRS/disease duration (months)) were assessed with the ALS functional rating scale (ALSFRS) [31]. In addition, 43 age- and gender-matched control subjects (27 males, ranged 30–74 years) were recruited. To minimize confounding factors caused by non-ALS-related alterations of the brain, patients with current or history of any of the listed conditions below were excluded (brain injury, trauma, epilepsy, vascular disease, psychiatric illness, or other systemic diseases). All 86 patients enrolled were right handed and had a Mini-Mental State Exam (MMSE) score of ≥26 [32]. Written consent was obtained for all subjects and this study was approved by the Research Ethics Committee of the First Affiliated Hospital of Medical College of Xi'an Jiaotong University.

2.2. Study Design. Composite study population included 43 ALS patients and 43 normal controls. Subgroup analyses were composed of (1) twenty patients with right limb-onset and their age- and gender-matched healthy controls and (2) sixteen patients with left limb-onset and their age- and gender-matched healthy controls. The seven patients with bulbar-onset were not included in subgroup analyses due to small sample size and potential reduction in statistical power.

2.3. Imaging Acquisition. All imaging data were acquired using a 3T MR system (General Electric, Signal HDxt, Milwaukee, WI, USA) equipped with an eight-channel head-coil; a high resolution T_1-weighted image was acquired for global and local brain regions measurements. Acquisition parameters are as follows: 3D T_1 fast spoiled gradient echo sequence; repetition time (TR) = 10.8 ms; echo time (TE) = 4.8 ms; slice orientation, parallel with the anterior and posterior commissure line; matrix = 256 × 256; field of

view = 256 mm × 256 mm; slice thickness = 1 mm; no gap; and 140 continuous slices were acquired, covering the whole brain. Routine T_2 weighted images, implemented with propeller sequences, are as follows: TR = 4680 ms; TE = 105.2 ms; field of view = 256 mm × 256 mm; slice thickness = 5 mm. T_1 weighted images are as follows: TR = 2928 ms; TE = 22 ms; slice thickness = 5 mm. Routine T_1 and T_2 weighted images were used to get rid of subjects with obvious cerebral disease such as stroke or severe infarction. The scan lasted for approximately 8 minutes.

2.4. Statistical Analysis. Statistical analysis was performed with the Statistical Package for Social Sciences for Windows (Version 13; SPSS, Chicago, Illinois). The normality of data was statistically examined by using the Kolmogorov-Smirnoff tests. Group differences of demographic characteristics including age, gender, and clinical measurements, as well as tissue specific volume calculated by SIENAX, were tested by using independent two-sample Student's *t*-test, chi-square test, and analysis of covariance, as appropriate.

Parametric or nonparametric correlations, as well as partial correlation analyses, were performed to assess the relationship between volume of specific tissue-type and other MR imaging and clinical measurements, as appropriate.

2.5. Global Brain Measurements. Normalized global and tissue-type volume for head size were calculated with cross-sectional software tool—SIENAX, part of FSL [44, 45] (Version 2.6; FMRIB software library, http://fsl.fmrib.ox.ac.uk/fsl/fslwiki/SIENA). More precisely, extracted brain from single subject's whole-head input data was estimated by removing skull images [46] and was then used to affine-registered to MNI152 space [47, 48]. Subsequently, the volumetric scaling factor determined by the skull image in registration step was used to assess normalized tissue-specific volume, after tissue segmentation with partial volume estimation using FAST4 [49]. Consequently, for each subject, normalized volumes of the GM volume (NGMV), neocortical volume (NCV), and WM volume (NWMV) were obtained. Brain parenchyma fraction (BPF) was also assessed.

2.6. Regional Brain Atrophy Evaluation. Regional GM comparisons between all the groups were assessed using the optimized VBM tools, FSL-VBM (http://fsl.fmrib.ox.ac.uk/fsl/fslwiki/FSLVBM) [50, 51], from the FMRIB Software Library. Firstly, for each individual dataset, brain extracted tools were used to remove nonbrain tissues [46]. The FAST4 was then carried out for tissue-type segmentation [49]. The resulting GM partial volume images were aligned to MNI152 standard space using FLIRT [47, 48], followed optionally by nonlinear registration using FNIRT [52, 53]. A left-right symmetric study-specific GM template was averaged from the total number of subjects' gray-matter-segmented native images, both in whole group and subgroups analyses, which were then nonlinearly reregistered. In order to correct for local expansion or contraction, the registered partial volume images were modulated by dividing by the Jacobian of the warp field. The modulated segmented images were finally smoothed with an isotropic Gaussian kernel with a sigma of 3 mm.

Table 1: Summary of clinical characteristics between patients with ALS and normal controls in whole group analysis.

	NC (n = 43)	ALS (n = 43)	P
Age	51.8 ± 9.4	53.5 ± 9.0	0.389
Male, n	26	26	1
MMSE	28.8 ± 1.1	28.2 ± 1.9	0.054
ALSFRS	n/a	30.1 ± 6.6	—
Disease duration (months)	n/a	16.9 ± 16.5	—
Disease progression rate	n/a	0.98 ± 1.03	—

NC: normal controls; MMSE: Mini-Mental Status Evaluation; disease progression rate = (40-ALSFRS)/disease duration. n/a: not applicable.

Differences in the distribution of GM between patients and controls were examined by using permutation-based nonparametric testing, correcting for multiple comparisons by implementing threshold-free cluster enhancement (TFCE) [54].

In the total and subgroup analyses, age and total brain volume (the sum of NGMV, NWMV, and normalized cerebrospinal fluid) were used as nonexplanatory covariates in the general linear model.

The significance threshold was set at $P < 0.05$ (family-wise error (FWE) corrected) for whole group analysis. In subgroup analysis, statistical map was derived from an uncorrected voxel level threshold at $P < 0.001$, which did not survive after FWE correction. Only clusters comprising more than 20 adjacent voxels were included.

2.7. Correlation Analysis. In order to further evaluate the clinical relevance in whole brain tissue-specific measurements and regional GM density, we performed correlation analyses. Regional GM density was extracted over the clusters identified in the groups' analyses, according to its anatomical components. Clinical variables mainly include disease severity assessment—ALSFRS, disease duration, and disease progression rate.

3. Results

3.1. Demographic, Clinical Characteristics. In whole group analysis, there were no significant differences in age, gender, and MMSE score between 43 patients with sporadic ALS and 43 healthy controls (Table 1). In subgroup analysis, although age, gender, and MMSE score did not differ in patients with right and left limb-onset compared with controls, patients with right limb-onset were significantly older and presented with a less ALSFRS score (Table 2).

3.2. Normalized Global and Tissue-Specific Measurements. Because the normalized volume of tissue-specific measurements was strongly age-related, the r values between age and global measurements range from −0.259 for NWMV to −0.589 for BPF (all of the correlations were statistically significant at $P < 0.05$). We compared group differences both

Table 2: Summary of clinical characteristics between patients with ALS and normal controls in subgroups.

	R_limb-onset ($n = 20$)	R_NC ($n = 20$)	P^1	L_limb-onset ($n = 16$)	L_NC ($n = 16$)	P^2	P^3
Age	57.5 ± 8.1 (55.8 ± 8.0)[a]	56.0 ± 6.4	0.520	48.4 + 9.7 (47.4 ± 9.9)[a]	50.6 ± 9.0	0.515	0.005 0.008[a]
Male, n	14	14	1	9	9	1	0.307
MMSE	27.5 ± 2.1	28.8 ± 1.2	0.051	28.9 ± 1.6	29.2 ± 1.0	0.508	0.055
ALSFRS	27.7 ± 6.6	n/a	—	32.3 ± 6.3	n/a	—	0.043
Disease duration (months)	20.9 ± 20.8	n/a	—	13.8 ± 6.9	n/a	—	0.239
Disease progression rate	1.12 ± 0.88	n/a	—	0.66 ± 0.62	n/a	—	0.088

R_NC: normal controls corresponding to patients with right limb-onset; L_NC: normal controls corresponding to patients with left limb-onset. [a]Mean age of disease onset in patients with right and left limb-onset and corresponding P value.
P^1 represents the statistical differences in ALS patients with right limb-onset and corresponding normal controls. P^2 represents the statistical differences in ALS patients with left limb-onset and corresponding normal controls. P^3 represents the statistical differences in subgroups between ALS patients with right and left limb-onset.

Table 3: Global-brain volumetric measurements in total group of patients with ALS and normal controls by SIENAX.

	NC	ALS	P^1	P^2
BPF	0.97 ± 0.01	0.96 ± 0.01	0.009	0.000
NCV (mm^3)	584.0 ± 34.6	558.7 ± 30.2	0.001	0.000
NGMV (mm^3)	737.7 ± 46.4	699.4 ± 105.9	0.016	0.004
NWMV (mm^3)	697.0 ± 38.2	675.9 ± 30.1	0.006	0.004

BPF: brain parenchyma fraction; NCV: normalized neocortex volume; NGMV: normalized gray matter volume; NWMV: normalized white matter volume.
P^1: P value in total group analysis between patients with ALS and normal controls, by using two-sample t-test.
P^2: P value in total group analysis between patients with ALS and normal controls, by using analysis of covariance, with age as covariate.

before and after adjusting with age. In whole group analysis, we found reduced NCV, NGMV, NWMV, and BPF in patients with ALS (Table 3 and Figure 1). In subgroup analysis, significant group differences including NGMV, NWMV, NCV, and BPF were found between patients with right limb-onset and normal controls (Table 4 and Figure 1). In patients with left limb-onset, only BPF was found statistically smaller than those in normal controls after correcting age (Table 4 and Figure 1).

3.3. Regional GM Losses in Total and Subgroup Analysis. In total group analysis, prominent GM volume reductions were found in the left frontal and parietal cortices including the precentral gyri, superior frontal gyri, supplementary motor areas, and postcentral gyri ($P < 0.05$, FWE corrected) (Table 5 and Figure 2).

In subgroup comparisons, patients with right limb-onset showed decreased GM volume in the bilateral precentral gyri, left superior frontal gyri, supplementary motor areas, and postcentral gyri compared with normal controls ($P < 0.001$, uncorrected) (Table 6 and Figure 2). GM losses in patients with left limb-onset were mainly located in the bilateral precentral gyri, right superior frontal gyri, supplementary motor areas, postcentral gyri, bilateral supramarginal gyri, parietal operculum, and angular gyri in the left side ($P < 0.001$, uncorrected) (Table 7 and Figure 3).

3.4. Relationships between Neuroimaging and Clinical Outcomes in Whole Group and Subgroup Patients. No statistically significant relations were found between normalized global measurements and clinical profiles, both in whole group and subgroup patients before and after correcting for age.

Correlation analyses in the whole group comparison found a positive correlation between the GM density in the left postcentral gyri and disease severity score—ALSFRS ($r = 0.38$, $P = 0.012$). In patients with right limb-onset, we found that disease progression rate was negatively related with GM density in the right precentral gyri ($r = -0.515$, $P = 0.020$) (Figure 4). There was no statistical significant relationship between clinical features of patients and neuroimaging features in patients with left limb-onset.

4. Discussion

In this study, we found global and local brain region atrophy in patients with ALS. Additionally, BPF was a sensitive biomarker in assessing global brain atrophy. Regional brain atrophy profile in each patient group demonstrated that GM loss was primarily but not exclusively in the primary motor, premotor, and supplementary motor areas in the frontal lobes and associated with variable parietal lobes involvement. Interestingly, unilateral dominant GM losses in patients with heterogeneous body-onset in total group were mainly determined by patients with right limb-onset. Furthermore, subgroup analyses have implied that motor cortex in the contralateral hemisphere of the initially involved limb was most affected. Lastly, compared with left limb-onset patients, the age at disease onset were much older in patients with right limb-onset, who also presented with more severe disease disability.

4.1. Demographics and Clinical Findings. In contrast to left limb-onset patients, older age and lower ALSFRS were found in patients with right limb-onset ($P = 0.005$, 0.043, resp.). To verify whether the difference of age was caused by the

Table 4: Global-brain volumetric measurements in ALS patients with right or left limb-onset and respective normal controls by SIENAX.

	R_NC	R_limb-onset	P^1	L_NC	L_limb-onset	P^2
BPF	0.97 ± 0.007	0.96 ± 0.009	0.000	0.974 ± 0.006	0.971 ± 0.005	0.016
NCV (mm^3)	576.90 ± 34.04	551.37 ± 28.93	0.008	588.46 ± 35.43	566.68 ± 25.80	0.053
NGMV (mm^3)	726.61 ± 44.80	699.30 ± 39.59	0.042	746.02 ± 45.15	680.55 ± 167.20	0.113
NWMV (mm^3)	703.38 ± 38.84	663.01 ± 28.44	0.001	694.24 ± 39.67	685.97 ± 27.15	0.402

P^1, P^2: P value in subgroup analysis between patients with right or left limb-onset and respective normal controls, by using analysis of covariance, adjusted for age.

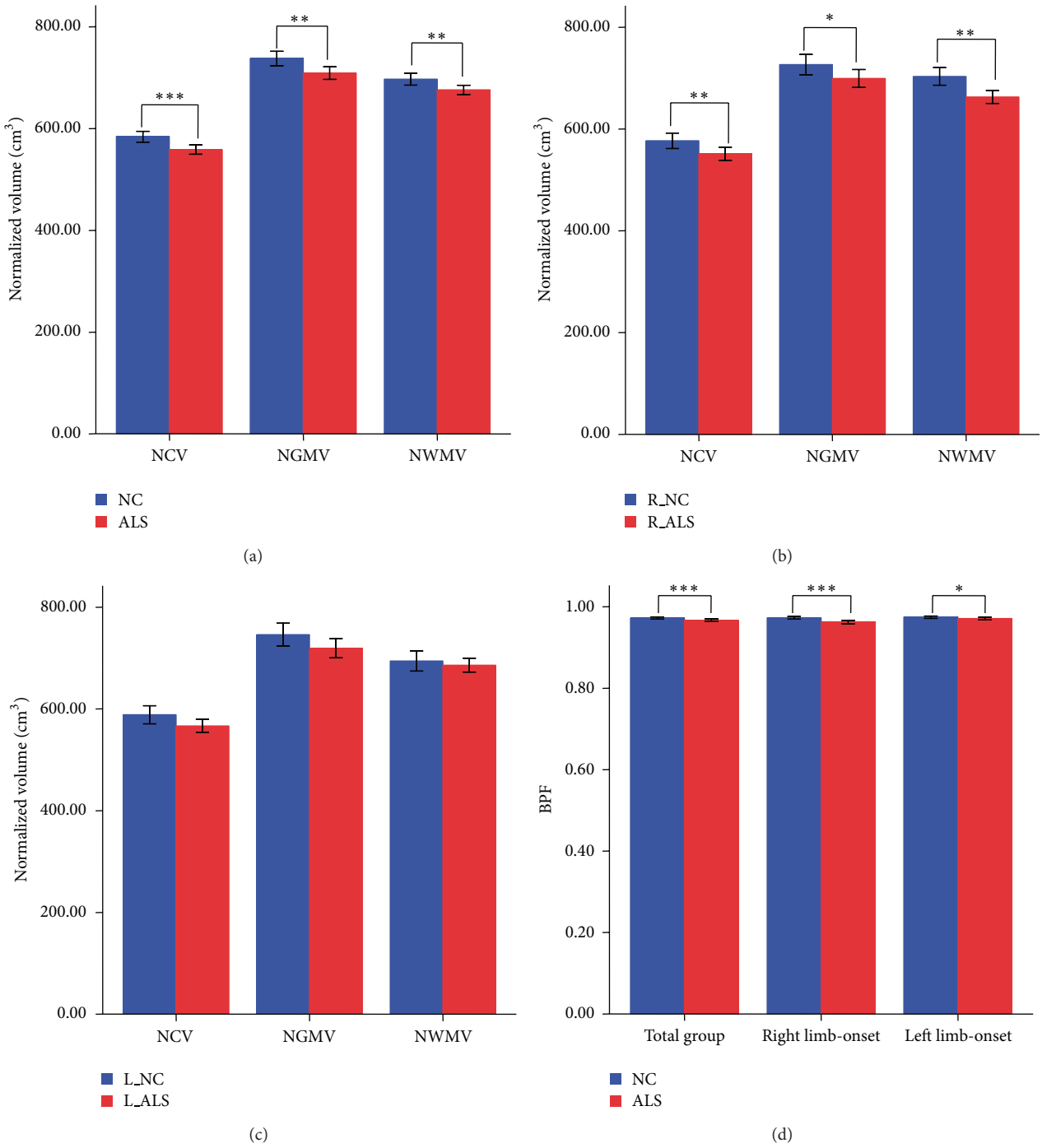

Figure 1: Global volumetric measurements comparisons in total group ((a), (d)) and subgroups between ALS patients with right limb-onset ((b), (d)), patients with left limb-onset ((c), (d)), and corresponding normal controls. $^{***}P < 0.001$; $^{**}P < 0.01$; $^{*}P < 0.05$.

Table 5: Brain areas with reduced GM volume in total group between ALS patients and normal controls ($P < 0.05$, FWE-corrected).

Brain anatomical regions	BA region	MNI coordinates of peak voxels (mm)			Cluster size	T value	P value
		X	Y	Z			
L_precentral gyri	4	−26	−24	62	450	4.85	0.0132
		−24	−22	58		4.80	0.0136
L_superior frontal gyri	6	−8	−8	72	124	4.79	0.0144
L_supplementary motor areas	6	−8	−10	70	28	4.50	0.015
L_postcentral gyri	3	−36	−26	54	60	4.25	0.0196

L: left; BA: Brodmann areas.

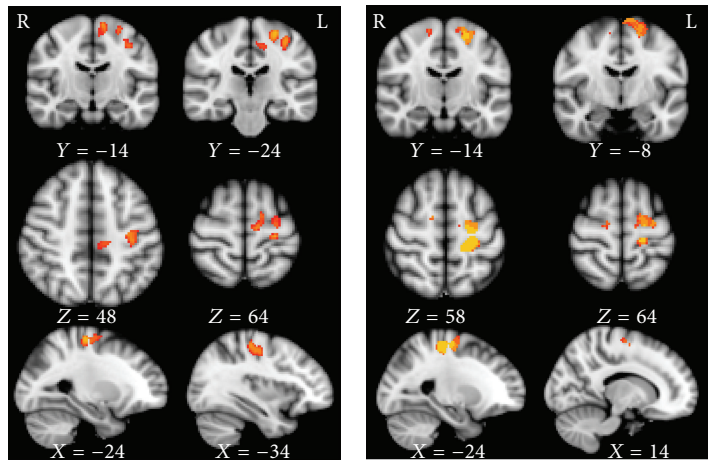

(a) (b)

Figure 2: (a) GM losses in total group analysis between ALS patients and normal controls ($P < 0.05$, FWE-corrected). (b) GM losses in subgroup analysis between ALS patients with right limb-onset and corresponding normal controls ($P < 0.001$, uncorrected).

discrepancy of age at disease onset or derived from variable disease durations (see Table 2), we further compared age at disease onset between the two subgroups. Interestingly, we did find that patients with left limb-onset were much younger at disease onset in our study compared to those with right limb-onset (Table 2, $P = 0.008$). Additionally, patients with right limb-onset who were significantly older had lower ALSFRS scores indicating that a more advanced disease severity is potentially linked with age, a negative predictor for prognosis [44]. However, the questionnaire of ALSFRS in our study and widely used revised-ALSFRS are insufficient to make appropriate and advisable assessing of functional disability caused by nondominant hand [13, 55]. This is particularly relevant since more than half of the patients presented with upper limb dysfunction at disease onset in right and left limb-onset subgroups (16/20, 12/16, resp.). Therefore, we thought it was not adequate to speculate that the ALSFRS in patients with left limb was truly higher because of biased functional disability assessments in our right-hand dominant patients' cohorts. However, even though our results were consistent with Rule et al. regarding the differences in the mean age and ALSFRS-R score between patients with right and left side of body impairments, which was not statistically significant [38], this interesting inference should be further verified with a larger sample of patients.

4.2. Global Atrophy in ALS. Global brain atrophy in ALS patients, as indicated in our study with reduced NCV, NGMV, NWMV, and BPF, had been revealed in several previous studies [11, 32, 36, 56, 57]. Amongst these, decreased BPF can be found even in the absence of obvious brain parenchyma volume loss suggesting that BPF may be a more sensitive biomarker than other measurements in assessing global brain atrophy [32, 58]. This in fact proved to be the case in our study in which the subgroup comparison only showed decreased BPF in patients with left limb-onset, all of whom did not show remarkable gray or white matter volume loss. Consistent with the obvious regional GM loss in later studies, there were reduced NCV and NGMV. Unlike the global measurements mentioned above, decreased NWMV had been found in some studies [56, 57], but not others [11, 32]. We speculated that this discrepancy is the result of the highly heterogeneous study cohorts and methodological sensitivities. When using more advanced methods such as in Rajagopalan et al., studies indeed confirmed white matter abnormality in ALS [59]. The differences between global indexes in patients with right and left limb-onset implied that global atrophy was more prevalent in older patients when compared with age-matched healthy controls. In addition, this is partially relevant with the context of our findings that global brain atrophy measurements are strongly age-related, as well as the hypothesis

Table 6: Brain areas with reduced GM volume in ALS patients with right limb-onset and corresponding normal controls ($P < 0.001$, uncorrected).

Brain anatomical regions	BA region	MNI coordinates of peak voxels (mm)			Cluster size	T value	P value
		X	Y	Z			
L_precentral gyri	4, 6	−20	−30	58	337	4.56	0.0002
		−16	−30	60		4.52	
		−26	−26	58		4.42	
L_superior frontal gyri	6	−12	−8	70	208	4.55	0.0006
		−16	−6	68		4.49	
L_supplementary motor areas	6	−4	−8	72	20	3.22	0.0004
L_postcentral gyri	3	−20	−34	58	74	4.45	0.0002
R_precentral gyri	4	14	−12	62	48	3.59	0.0006

L: left; R: right.

Table 7: Brain areas with reduced GM volume in ALS patients with left limb-onset and corresponding normal controls ($P < 0.001$, uncorrected).

Brain anatomical regions	BA region	MNI coordinates of peak voxels (mm)			Cluster size	T value	P value
		X	Y	Z			
R_precentral gyri	4, 6	10	−18	48	89	4.07	0.0008
R_superior frontal gyri	6	14	−2	62	209	3.70	0.0008
R_supplementary motor areas	6	12	−6	58	28	3.42	0.0002
R_postcentral gyri	3	36	−28	42	33	4.09	0.0008
R_supramarginal gyri	40	62	−40	22	26	2.12	0.0002
L_precentral gyri	4, 6	−34	−14	54	111	3.56	0.0004
L_parietal opercular		−52	−38	20	28	3.92	0.0002
L_supramarginal gyri	40	−54	−46	18	93	3.42	0.0002
L_angular gyri	39	−44	−52	12	48	3.36	0.0004

L: left; R: right.

suggested by Mezzapesa et al. that ALS pathology enhanced normal aging [32].

4.3. Regional and Lateralized GM Loss in Whole and Subgroup Analysis. We found regional brain atrophy of the motor cortex particularly in the frontal lobe and postcentral gyri, supramarginal gyri, angular gyri, and parietal operculum in the parietal lobe, all consistent with previous findings [9, 11, 21, 22, 60–63]. All of these regions participated in motor performance or motor imagery [64] and GM losses in these regions reflected dysfunctions of both motor performance and motor imagery in ALS [37]. We suggested that atrophy in premotor and supplementary motor areas in each group extended the feature of focal onset in primary motor cortex to other motor related areas in the frontal areas [7, 8]. These findings and additional GM abnormalities in parietal areas are consistent with the longitudinal findings performed by Verstraete et al, suggesting that neurodegeneration begins with primary motor cortex and extends to secondary motor cortex in the frontal and parietal lobes [63]. However, in our subgroup analysis, we uncovered an intriguing pattern that the more extensive GM losses were found in patients with left limb-onset compared to those in patients with right limb-onset. This finding may be due to the fact that general widespread GM abnormalities are often associated with greater disease disability, but it certainly warrants further investigation to clarify whether disease disability assessed by ALSFRS in patients with left limb-onset was artificially higher as we discussed above. Another possibility that deserves further study is that patients with left limb-onset may represent the ALS patients who were younger than 45 years old at the time of disease onset and characterized in prevalent upper motor neuron involvements, thus, leading to widespread GM abnormalities [65]. These profound differences between the right limb and left limb-onset subgroups in their clinical features and GM losses are intriguing and require further exploration.

Except for the aforementioned regional anatomical abnormal, the main finding in our study was that motor cortex in the contralateral hemisphere of the initially involved limb was the most heavily affected region. This was consistent with and supplemented the findings in Zhang et al. [41] and the pathological findings [13]. In addition, according to the pattern of GM loss in total cohorts and patients with right

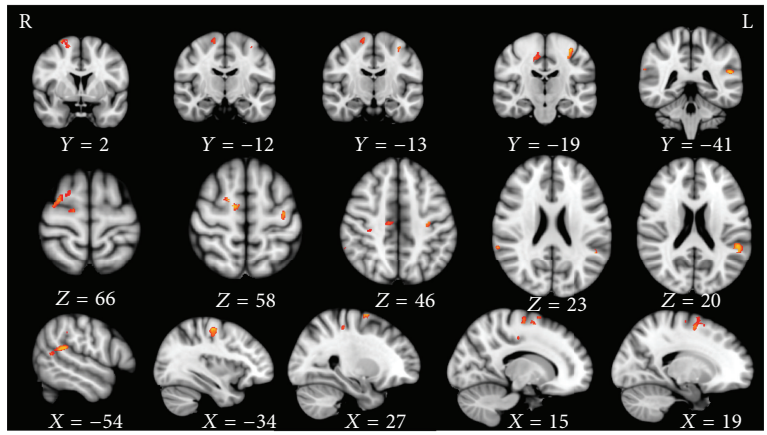

Figure 3: GM losses in subgroup analysis between ALS patients with left limb-onset and corresponding normal controls ($P < 0.001$, uncorrected).

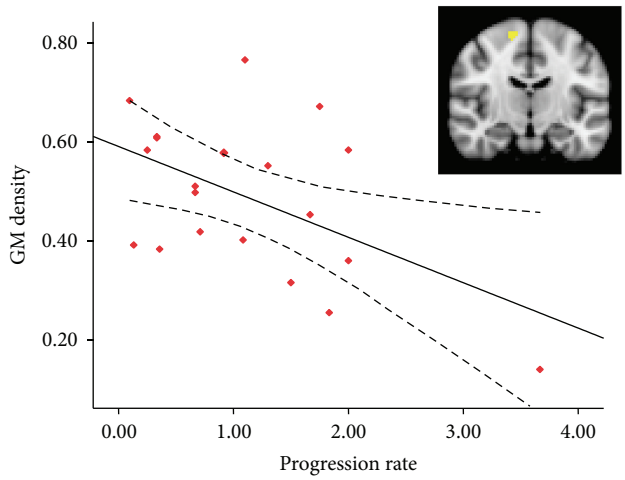

Figure 4: GM density in the right precentral gyri showed a negative correlation with disease progression rate ($r = -0.505$, $P = 0.020$).

limb-onset, we suggested that GM loss in the whole group population was mainly reflective of the abnormalities caused by the subpopulation of patients with right limb-onset. These findings indicated to us that it was noteworthy to take clinical profiles into account when interpreting cortical abnormality in group level, especially in those with heterogeneous backgrounds. Furthermore, the macroscopic signatures of GM atrophy in subgroup comparisons suggested that, when comparing with patients with left limb-onset, right limb-onset is more likely to have language deficits which was as common as executive dysfunction in ALS [27]. This may be a consequence of the susceptibility of Broca's areas (Brodmann areas 44, 45) in the left inferior frontal cortex to prion-like contiguous spread from the motor cortex or through network-based structural white matter connections [23, 26]. This pathological basis associated with more common right hand deficits [66] may explain the high prevalence of language deficits as well as the proved high sensitivity of the verbal frequency in assessing executive deficits in ALS [27]. Meanwhile, among patients with left limb-onset, abnormal GM in the right motor cortex may be easily accompanied with more extensive frontal impairments in the ipsilateral side and may induce behavioral dysfunction [14, 15]. Additionally, the proportion of cognitive and/or behavioral impairments was strongly associated with the different progression rates among individuals, which may mean that patients with fast disease progression may be more prone to show cognition or behavioral dysfunction in cross-sectional study and vice versa. But these inferences need to be confirmed by the cognitive screening and longitudinal evaluations.

In addition, one must keep in mind that the unilateral predominant cortical abnormality determined by the side of limb-onset does not tell the whole story. Along with the temporal evolution of disease, ALS does eventually involve other limbs symmetrically and the presenting of GM loss in the ipsilateral hemisphere of the initially involved limb may reduce this asymmetry, as indicated in our subgroup analysis. More than 18/20 and 9/16 of patients presented with contralateral upper and/or lower limb dysfunction in patients with right and left limb-onset, respectively. Moreover, the association of cognitive or behavioral impairments in ALS and their variability [4, 15], as well as heterogeneous disease progression rate in individual ALS patients, will increase or reduce the asymmetry dominated by motor symptoms and add to the complexity of this disease.

4.4. Correlation Analysis between Clinical Variables and MR Findings. In the whole group comparisons, we found a positive correlation between the GM density in the left postcentral gyri and ALSFRS. We inferred that such correlation would be found in a less heterogeneous patient group with right limb-onset because the differences in whole group comparisons were mainly derived from disease related effects in this group. Nevertheless, congruous with other studies, this relation was only found in pooled patients with different clinical profiles [7, 8].

Meanwhile, a negative relationship between GM density in the right precentral gyri and disease progression rate was

found in patients with right limb-onset. Warren et al. have hypothesized that the involvement of longer-range connections corresponds with rapid spread in contrast to slower spread caused by involvement of clustered connections [14]. Compared with ipsilateral frontal and parietal areas adjacent to precentral gyri, GM losses in the contralateral hemisphere were relatively remote areas and represented rapid disease progression. In previous studies, it has been suggested that the involvement of the temporal lobe can be a marker for more rapid disease progression [28]. In addition, several longitudinal studies have implied that, compared with the disassociation between rapidly progressive clinical profiles and less or nonprogressive deterioration of primary motor cortex, the extensive involvements of motor function or cognitive, behavioral related brain regions were remarkable in the follow-up [28, 67]. In sum, we proposed that the correlation between GM density in the right precentral gyri and disease progression rate indicated that the relatively distant region from the initial onset regions—the left precentral gyri in patients with right limb-onset in our study—was involved later when disease progressed. Thus, along with temporal evolution of the disease, faster disease progression will present with more areas involved and relate with the extent of cortical abnormality in the disease course. This finding may present a novel hypothesis to explain the changing pattern of remote brain regions involvement with disease progression rate as described in previous findings. In addition, we propose that the lack of relation between abnormal brain regions and clinical variables in patients with left limb-onset might be caused by inadequate disease disability assessments that would also result in a less accurate disease progression rate.

4.5. Limitations. There are several limitations in this study. Firstly, patients with bulbar-onset were not included in the subgroups and this therefore made it impossible to evaluate the distinguished features of brain abnormal in these patients. Secondly, several studies confirm that ALS patients with large scales of cognitive and behavioral impairments were associated with different vulnerability of specific genetic mutations that were not considered in this study. Lastly, lack of fully exploring of cognitive domains and mutant genetic screening in our patients is fundamental deficit and limited us and made us unable to further clarify the brain atrophy profiles and asymmetries.

5. Conclusions

In this study, we found global and regional brain atrophy in patients with ALS. The topographic characteristics of subgroup analysis further indicated that the motor cortex in the contralateral hemisphere of the initially involved limb was most affected with relatively sparing of the ipsilateral brain. The unilateral dominant topography of brain changes implied that the clinical profiles of patients with different side of limb-onset might become divergent, particularly focusing on the extramotor syndromes, as disease progresses. The unexpected findings of demographic and clinical discrepancy between patients with right or left limb-onset also highlight a novel distinct feature of ALS, which deserves further exploration.

Conflict of Interests

There are no competing interests to disclose.

Acknowledgments

This paper is supported by the National Natural Science Foundation of China (Grant nos. 81371530 and 81371630), the Shaanxi science and technology program (Grant no. 2014K11-02-01-04), the Fundamental Research Funds for the Central Universities, the Beijing Nova program (Grant no. Z111101054511116), and the Beijing Natural Science Foundation (Grant no. 4122082).

References

[1] W. Robberecht and T. Philips, "The changing scene of amyotrophic lateral sclerosis," *Nature Reviews Neuroscience*, vol. 14, no. 4, pp. 248–264, 2013.

[2] M. R. Turner, O. Hardiman, M. Benatar et al., "Controversies and priorities in amyotrophic lateral sclerosis," *The Lancet Neurology*, vol. 12, no. 3, pp. 310–322, 2013.

[3] S. Byrne, M. Elamin, P. Bede et al., "Cognitive and clinical characteristics of patients with amyotrophic lateral sclerosis carrying a C9orf72 repeat expansion: a population-based cohort study," *The Lancet Neurology*, vol. 11, no. 3, pp. 232–240, 2012.

[4] J. Phukan, M. Elamin, P. Bede et al., "The syndrome of cognitive impairment in amyotrophic lateral sclerosis: a population-based study," *Journal of Neurology, Neurosurgery & Psychiatry*, vol. 83, no. 1, pp. 102–108, 2012.

[5] M. R. Turner, F. Agosta, P. Bede, V. Govind, D. Lulé, and E. Verstraete, "Neuroimaging in amyotrophic lateral sclerosis," *Biomarkers in Medicine*, vol. 6, no. 3, pp. 319–337, 2012.

[6] P. Bede and O. Hardiman, "Lessons of ALS imaging: pitfalls and future directions—a critical review," *NeuroImage: Clinical*, vol. 4, pp. 436–443, 2014.

[7] P. Bede, A. Bokde, M. Elamin et al., "Grey matter correlates of clinical variables in amyotrophic lateral sclerosis (ALS): a neuroimaging study of ALS motor phenotype heterogeneity and cortical focality," *Journal of Neurology, Neurosurgery and Psychiatry*, vol. 84, no. 7, pp. 766–773, 2013.

[8] C. Schuster, E. Kasper, J. Machts et al., "Focal thinning of the motor cortex mirrors clinical features of amyotrophic lateral sclerosis and their phenotypes: a neuroimaging study," *Journal of Neurology*, vol. 260, no. 11, pp. 2856–2864, 2013.

[9] D. J. Irwin, C. T. McMillan, J. Brettschneider et al., "Cognitive decline and reduced survival in C9orf72 expansion frontotemporal degeneration and amyotrophic lateral sclerosis," *Journal of Neurology, Neurosurgery and Psychiatry*, vol. 84, no. 2, pp. 163–169, 2013.

[10] P. Lillo, E. Mioshi, J. R. Burrell, M. C. Kiernan, J. R. Hodges, and M. Hornberger, "Grey and white matter changes across the amyotrophiclateral sclerosis-frontotemporal dementia continuum," *PLoS ONE*, vol. 7, no. 8, Article ID e43993, 2012.

[11] J. L. Chang, C. Lomen-Hoerth, J. Murphy et al., "A voxel-based morphometry study of patterns of brain atrophy in ALS and ALS/FTLD," *Neurology*, vol. 65, no. 1, pp. 75–80, 2005.

[12] M. Sabatelli, A. Conte, and M. Zollino, "Clinical and genetic heterogeneity of amyotrophic lateral sclerosis," *Clinical Genetics*, vol. 83, no. 5, pp. 408–416, 2013.

[13] Y. Mochizuki, T. Mizutani, and T. Takasu, "Amyotrophic lateral sclerosis with marked neurological asymmetry: clinicopathological study," *Acta Neuropathologica*, vol. 90, no. 1, pp. 44–50, 1995.

[14] J. D. Warren, J. D. Rohrer, J. M. Schott, N. C. Fox, J. Hardy, and M. N. Rossor, "Molecular nexopathies: a new paradigm of neurodegenerative disease," *Trends in Neurosciences*, vol. 36, no. 10, pp. 561–569, 2013.

[15] J. D. Rohrer, T. Lashley, J. M. Schott et al., "Clinical and neuroanatomical signatures of tissue pathology in frontotemporal lobar degeneration," *Brain*, vol. 134, no. 9, pp. 2565–2581, 2011.

[16] M. Hornberger, S. Wong, R. Tan et al., "In vivo and post-mortem memory circuit integrity in frontotemporal dementia and Alzheimer's disease," *Brain*, vol. 135, no. 10, pp. 3015–3025, 2012.

[17] S. C. Ling, M. Polymenidou, and D. W. Cleveland, "Converging mechanisms in ALS and FTD: disrupted RNA and protein homeostasis," *Neuron*, vol. 79, no. 3, pp. 416–438, 2013.

[18] P. Lillo, S. Savage, E. Mioshi, M. C. Kiernan, and J. R. Hodges, "Amyotrophic lateral sclerosis and frontotemporal dementia: a behavioural and cognitive continuum," *Amyotrophic Lateral Sclerosis*, vol. 13, no. 1, pp. 102–109, 2012.

[19] G. A. Miller, L. D. Crocker, J. M. Spielberg, Z. P. Infantolino, and W. Heller, "Issues in localization of brain function: the case of lateralized frontal cortex in cognition, emotion, and psychopathology," *Frontiers in Integrative Neuroscience*, vol. 7, no. 2, pp. 1–9, 2013.

[20] Y. Iturria-Medina, A. P. Fernández, D. M. Morris et al., "Brain hemispheric structural efficiency and interconnectivity rightward asymmetry in human and nonhuman primates," *Cerebral Cortex*, vol. 21, no. 1, pp. 56–67, 2011.

[21] S. Tsermentseli, P. N. Leigh, and L. H. Goldstein, "The anatomy of cognitive impairment in amyotrophic lateral sclerosis: more than frontal lobe dysfunction," *Cortex*, vol. 48, no. 2, pp. 166–182, 2012.

[22] F. Trojsi, M. R. Monsurr, F. Esposito, and G. Tedeschi, "Widespread structural and functional connectivity changes in amyotrophic lateral sclerosis: insights from advanced neuroimaging research," *Neural Plasticity*, vol. 2012, Article ID 473538, 13 pages, 2012.

[23] M. Polymenidou and D. W. Cleveland, "The seeds of neurodegeneration: prion-like spreading in ALS," *Cell*, vol. 147, no. 3, pp. 498–508, 2011.

[24] T. Kanouchi, T. Ohkubo, and T. Yokota, "Can regional spreading of amyotrophic lateral sclerosis motor symptoms be explained by prion-like propagation?" *Journal of Neurology, Neurosurgery and Psychiatry*, vol. 83, no. 7, pp. 739–745, 2012.

[25] W. W. Seeley, R. K. Crawford, J. Zhou, B. L. Miller, and M. D. Greicius, "Neurodegenerative diseases target large-scale human brain networks," *Neuron*, vol. 62, no. 1, pp. 42–52, 2009.

[26] F. Pulvermüller and L. Fadiga, "Active perception: sensorimotor circuits as a cortical basis for language," *Nature Reviews Neuroscience*, vol. 11, no. 5, pp. 351–360, 2010.

[27] L. J. Taylor, R. G. Brown, S. Tsermentseli et al., "Is language impairment more common than executive dysfunction in amyotrophic lateral sclerosis?" *Journal of Neurology, Neurosurgery and Psychiatry*, vol. 84, no. 5, pp. 494–498, 2013.

[28] E. Verstraete, J. H. Veldink, J. Hendrikse, H. J. Schelhaas, M. P. van den Heuvel, and L. H. van den Berg, "Structural MRI reveals cortical thinning in amyotrophic lateral sclerosis," *Journal of Neurology, Neurosurgery & Psychiatry*, vol. 83, no. 4, pp. 383–388, 2012.

[29] L. Thivard, P. Pradat, S. Lehéricy et al., "Diffusion tensor imaging and voxel based morphometry study in amyotrophic lateral sclerosis: relationships with motor disability," *Journal of Neurology, Neurosurgery and Psychiatry*, vol. 78, no. 8, pp. 889–892, 2007.

[30] M. Grossman, C. Anderson, A. Khan, B. Avants, L. Elman, and L. McCluskey, "Impaired action knowledge in amyotrophic lateral sclerosis," *Neurology*, vol. 71, no. 18, pp. 1396–1401, 2008.

[31] F. Agosta, E. Pagani, M. A. Rocca et al., "Voxel-based morphometry study of brain volumetry and diffusivity in amyotrophic lateral sclerosis patients with mild disability," *Human Brain Mapping*, vol. 28, no. 12, pp. 1430–1438, 2007.

[32] D. M. Mezzapesa, A. Ceccarelli, F. Dicuonzo et al., "Whole-brain and regional brain atrophy in amyotrophic lateral sclerosis," *American Journal of Neuroradiology*, vol. 28, no. 2, pp. 255–259, 2007.

[33] Z. Chen and L. Ma, "Grey matter volume changes over the whole brain in amyotrophic lateral sclerosis: a voxel-wise meta-analysis of voxel based morphometry studies," *Amyotrophic Lateral Sclerosis*, vol. 11, no. 6, pp. 549–554, 2010.

[34] M. Cosottini, I. Pesaresi, S. Piazza et al., "Structural and functional evaluation of cortical motor areas in Amyotrophic Lateral Sclerosis," *Experimental Neurology*, vol. 234, no. 1, pp. 169–180, 2012.

[35] A. Meoded, J. Y. Kwan, T. L. Peters et al., "Imaging findings associated with cognitive performance in primary lateral sclerosis and amyotrophic lateral sclerosis," *Dementia and Geriatric Cognitive Disorders Extra*, vol. 3, no. 1, pp. 233–250, 2013.

[36] J. Kassubek, A. Unrath, H. J. Huppertz et al., "Global brain atrophy and corticospinal tract alterations in ALS, as investigated by voxel-based morphometry of 3-D MRI," *Amyotrophic Lateral Sclerosis*, vol. 6, no. 4, pp. 213–220, 2005.

[37] A. Poujois, F. C. Schneider, I. Faillenot et al., "Brain plasticity in the motor network is correlated with disease progression in amyotrophic lateral sclerosis," *Human Brain Mapping*, vol. 34, no. 10, pp. 2391–2401, 2012.

[38] R. R. Rule, N. Schuff, R. G. Miller, and M. W. Weiner, "Gray matter perfusion correlates with disease severity in ALS," *Neurology*, vol. 74, no. 10, pp. 821–827, 2010.

[39] W. Block, F. Träber, S. Flacke, F. Jessen, C. Pohl, and H. Schild, "In-vivo proton MR-spectroscopy of the human brain: assessment of N-acetylaspartate (NAA) reduction as a marker for neurodegeneration," *Amino Acids*, vol. 23, no. 1–3, pp. 317–323, 2002.

[40] C. Pohl, W. Block, J. Karitzky et al., "Proton magnetic resonance spectroscopy of the motor cortex in 70 patients with amyotrophic lateral sclerosis," *Archives of Neurology*, vol. 58, no. 5, pp. 729–735, 2001.

[41] Y. Zhang, N. Schuff, S. C. Woolley et al., "Progression of white matter degeneration in amyotrophic lateral sclerosis: a diffusion tensor imaging study," *Amyotrophic Lateral Sclerosis*, vol. 12, no. 6, pp. 421–429, 2011.

[42] G. M. Gargiulo-Monachelli, F. Janota, M. Bettini, C. L. Shoesmith, M. J. Strong, and R. E. P. Sica, "Regional spread pattern predicts survival in patients with sporadic amyotrophic lateral sclerosis," *European Journal of Neurology*, vol. 19, no. 6, pp. 834–841, 2012.

[43] J. Ravits, P. Laurie, Y. Fan, and D. H. Moore, "Implications of ALS focality," *Neurology*, vol. 68, no. 19, pp. 1576–1582, 2007.

[44] S. M. Smith, Y. Zhang, M. Jenkinson et al., "Accurate, robust, and automated longitudinal and cross-sectional brain change analysis," *NeuroImage*, vol. 17, no. 1, pp. 479–489, 2002.

[45] S. M. Smith, M. Jenkinson, M. W. Woolrich et al., "Advances in functional and structural MR image analysis and implementation as FSL," *NeuroImage*, vol. 23, supplement, 1, pp. S208–S219, 2004.

[46] S. M. Smith, "Fast robust automated brain extraction," *Human Brain Mapping*, vol. 17, no. 3, pp. 143–155, 2002.

[47] M. Jenkinson and S. Smith, "A global optimisation method for robust affine registration of brain images," *Medical Image Analysis*, vol. 5, no. 2, pp. 143–156, 2001.

[48] M. Jenkinson, P. Bannister, M. Brady, and S. Smith, "Improved optimization for the robust and accurate linear registration and motion correction of brain images," *NeuroImage*, vol. 17, no. 2, pp. 825–841, 2002.

[49] Y. Zhang, M. Brady, and S. Smith, "Segmentation of brain MR images through a hidden Markov random field model and the expectation-maximization algorithm," *IEEE Transactions on Medical Imaging*, vol. 20, no. 1, pp. 45–57, 2001.

[50] C. D. Good, I. S. Johnsrude, J. Ashburner, R. N. A. Henson, K. J. Fristen, and R. S. J. Frackowiak, "A voxel-based morphometric study of ageing in 465 normal adult human brains," in *Proceedings of the 5th IEEE EMBS International Summer School on Biomedical Imaging*, June 2002.

[51] J. Ashburner and K. J. Friston, "Voxel-based morphometry—the methods," *NeuroImage*, vol. 11, no. 6, pp. 805–821, 2000.

[52] J. L. R. Andersson, M. Jenkinson, and S. Simth, "Non-linear optimisation," FMRIB TR07JA1, 2007.

[53] J. L. R. Andersson, M. Jenkinson, and S. Smith, "Non-linear registration, aka Spatial normalisation," FMRIB Technical Report TR07JA2, 2007.

[54] S. M. Smith and T. E. Nichols, "Threshold-free cluster enhancement: addressing problems of smoothing, threshold dependence and localisation in cluster inference," *NeuroImage*, vol. 44, no. 1, pp. 83–98, 2009.

[55] J. M. Cedarbaum, N. Stambler, E. Malta et al., "The ALSFRS-R: a revised ALS functional rating scale that incorporates assessments of respiratory function," *Journal of the Neurological Sciences*, vol. 169, no. 1-2, pp. 13–21, 1999.

[56] C. Ellis, J. Suckling, E. Amaro et al., "Volumetric analysis reveals corticospinal tract degeneration and extramotor involvement in ALS," *Neurology*, vol. 57, no. 9, pp. 1571–1578, 2001.

[57] S. Abrahams, L. H. Goldstein, J. Suckling et al., "Frontotemporal white matter changes in amyotrophic lateral sclerosis," *Journal of Neurology*, vol. 252, no. 3, pp. 321–331, 2005.

[58] G. Tedeschi, F. Trojsi, A. Tessitore et al., "Interaction between aging and neurodegeneration in amyotrophic lateral sclerosis," *Neurobiology of Aging*, vol. 33, no. 5, pp. 886–898, 2012.

[59] V. Rajagopalan, Z. Liu, D. Allexandre et al., "Brain white matter shape changes in Amyotrophic Lateral Sclerosis (ALS): a fractal dimension study," *PLoS ONE*, vol. 8, no. 9, Article ID e73614, 2013.

[60] A. d' Ambrosio, A. Gallo, F. Trojsi et al., "Frontotemporal cortical thinning in amyotrophic lateral sclerosis," *American Journal of Neuroradiology*, vol. 35, no. 2, pp. 304–310, 2014.

[61] M. Elamin, P. Bede, S. Byrne et al., "Cognitive changes predict functional decline in ALS: a population-based longitudinal study," *Neurology*, vol. 80, no. 17, pp. 1590–1597, 2013.

[62] P. Lillo, E. Mioshi, J. R. Burrell, M. C. Kiernan, J. R. Hodges, and M. Hornberger, "Grey and white matter changes across the amyotrophic lateral sclerosis-frontotemporal dementia continuum," *PLoS ONE*, vol. 7, no. 8, Article ID e43993, 2012.

[63] E. Verstraete, J. H. Veldink, L. H. van den Berg, and M. P. van den Heuvel, "Structural brain network imaging shows expanding disconnection of the motor system in amyotrophic lateral sclerosis," *Human Brain Mapping*, vol. 35, no. 4, pp. 1351–1361, 2014.

[64] T. Hanakawa, I. Immisch, K. Toma, M. A. Dimyan, P. Van Gelderen, and M. Hallett, "Functional properties of brain areas associated with motor execution and imagery," *Journal of Neurophysiology*, vol. 89, no. 2, pp. 989–1002, 2003.

[65] M. R. Turner, J. Barnwell, A. Al-Chalabi, and A. Eisen, "Young-onset amyotrophic lateral sclerosis: historical and other observations," *Brain*, vol. 135, no. 9, pp. 2883–2891, 2012.

[66] M. R. Turner, P. Wicks, C. A. Brownstein et al., "Concordance between site of onset and limb dominance in amyotrophic lateral sclerosis," *Journal of Neurology, Neurosurgery and Psychiatry*, vol. 82, no. 8, pp. 853–854, 2011.

[67] F. Agosta, M. L. Gorno-Tempini, E. Pagani et al., "Longitudinal assessment of grey matter contraction in amyotrophic lateral sclerosis: a tensor based morphometry study," *Amyotrophic Lateral Sclerosis*, vol. 10, no. 3, pp. 168–174, 2009.

Hindawi Publishing Corporation
BioMed Research International
Volume 2014, Article ID 524096, 5 pages
http://dx.doi.org/10.1155/2014/524096

Research Article

Corticospinal Tract Change during Motor Recovery in Patients with Medulla Infarct: A Diffusion Tensor Imaging Study

Dongdong Rong,[1,2] Miao Zhang,[1,2] Qingfeng Ma,[3] Jie Lu,[1,2] and Kuncheng Li[1,2]

[1] *Department of Radiology, Xuanwu Hospital of Capital Medical University, Beijing 100053, China*
[2] *Beijing Key Laboratory of Magnetic Resonance Imaging and Brain Informatics, Beijing 100053, China*
[3] *Department of Neurology, Xuanwu Hospital of Capital Medical University, Beijing 100053, China*

Correspondence should be addressed to Kuncheng Li; kuncheng.li@gmail.com

Received 25 February 2014; Accepted 29 April 2014; Published 25 May 2014

Academic Editor: Lijun Bai

Diffusion tensor imaging (DTI) and tractography (DTT) provide a powerful vehicle for investigating motor recovery mechanisms. However, little is known about these mechanisms in patients with medullary lesions. We used DTI and DTT to evaluate three patients presenting with motor deficits following unilateral medulla infarct. Patients were scanned three times during 1 month (within 7, 14, and 30 days after stroke onset). Fractional anisotropy (FA) values were measured in the medulla, cerebral peduncle, and internal capsule. The three-dimensional corticospinal tract (CST) was reconstructed using DTT. Patients 1 and 2 showed good motor recovery after 14 days, and the FA values of their affected CST were slightly decreased. DTTs demonstrated that the affected CST passed along periinfarct areas and that tract integrity was preserved in the medulla. Patient 3 had the most obvious decrease in FA values along the affected CST, with motor deficits of the right upper extremity after 30 days. The affected CST passed through the infarct and was disrupted in the medulla. In conclusion, DTI can detect the involvement and changes of the CST in patients with medulla infarct during motor recovery. The degree of degeneration and spared periinfarct CST compensation may be an important motor recovery mechanism.

1. Introduction

Lateral medulla infarction occurs fairly infrequently in neurology clinical practice. Patients often present with limited neurologic deficits and, on occasion, hemiparesis accompanies medulla infarction. The corticospinal tract (CST) is the major neuronal pathway that mediates voluntary movements in humans. Many studies have elucidated the motor recovery mechanisms following ischemic stroke associated with the integrity of the CST. However, most previous studies have focused on the corona radiata and pontine lesions. Little is known about the motor recovery mechanisms in patients with medullary infarction.

Magnetic resonance imaging (MRI) plays an important role in the diagnosis and treatment of acute stroke. With the advent of diffusion-weighted imaging (DWI) techniques, small infarctions occurring in the medulla can be more easily identified. Furthermore, diffusion tensor imaging (DTI) can evaluate the degree of fiber damage in stroke affecting the CST. Diffusion tensor tractography (DTT), derived from DTI, allows for visualization of the architecture and integrity of the CST in three dimensions and can assess white matter tracts, such as the CST, at the subcortical level. The validity and reliability of DTT for CST have been demonstrated in previous studies [1–5]. In this study, we report three patients who showed hemiparesis due to isolated unilateral medulla infarct. We used DTI to investigate the involvement and change of the CST during motor recovery.

2. Materials and Methods

2.1. Participants. Three right-handed patients with isolated unilateral medulla infarct (a 55-year-old man, a 54-year-old man, and a 74-year-old woman) were recruited for this study. The study protocol was approved by the local Institutional

Table 1: Patient demographic and clinical data.

Patient	Sex/age	Symptoms	FM			BI		
			<7 d	14 d	30 d	<7 d	14 d	30 d
1	M/55	R hemiparesis	98.5	100	100	95	100	100
2	M/54	L hemiparesis	97	100	100	98	100	100
3	F/74	R hemiplegia	36.4	70.5	83.3	50	80	85

M = male; F = female; L = left; R = right; FM, Fugl-Meyer; BI, Barthel index.

Review Board and written informed consent was obtained from all participants.

We recruited the three stroke patients using the following enrollment criteria: having first-onset stroke and manifested motor deficits, fully obtained admission history (within 7 days after onset of symptoms), single infarction confined to the medulla identified on MRI, and no other concomitant brain lesion or previous infarcts. The exclusion criteria were as follows: contraindications for MRI, unclear onset of symptoms, lesions outside the medulla, recurrence infarction during followup, deafness and/or blindness, aphasia, or a visual field deficit. All patients were scanned three times during a period of 1 month (within days 7, 14, and 30 after stroke onset).

2.2. MRI Data Acquisition. MRI scanning was performed on a 3.0-Tesla whole-body scanner (Trio Tim, Siemens). Traditional axial T1-weighted (TR 155 ms/TE 2.81 ms), fast-spin echo T2-weighted imaging (TR 3830 ms/TE 98 ms), FLAIR (TR 8500 ms/TE 87 ms), and DWI (TR 3000 ms/TE 91 ms; $b = 0$, 500 and 1000 s/mm^2) were performed. The DTI acquisition parameters were as follows: TR 8000 ms/TE 83 ms, NEX = 1, matrix 128 × 128, field of view 24 × 24 cm, $b = 0$, 700 s/mm^2, and a slice thickness of 2 mm without a gap. We acquired 64 contiguous slices parallel to the anterior commissure-posterior commissure line.

2.3. DTI Data Postprocessing. DTI data were transferred to a work station (Multi-Modality Work Place, Siemens Healthcare) for processing. Circular regions of interest (ROI) were symmetrically drawn on axial slices on the left and right sides along the pyramidal tract pathway at three levels: the medulla, cerebral peduncle, and posterior limb of the internal capsule along the CST. To include only the CST region, the ROI size was set between 30 mm^2 and 35 mm^2 voxels. FA values for each ROI were obtained by averaging all voxels within the ROI. The FA ratio (rFA) between the infarct ipsilateral and contralateral side was calculated (rFA = $FA_{\text{ipsilateral side}}/FA_{\text{contralateral side}}$) in each patient. The three-dimensional CST was reconstructed using Siemens software. For fiber tracking of the CST, two ROIs were manually placed on two-dimensional transverse color-coded directional FA images. The upper ROI was placed on the posterior limb of the internal capsule and the lower ROI was placed on the lower pons. Only the fibers passing through both ROIs were displayed and designated as the CST. The thresholds of the tracking termination were 0.2 for the FA and 45° for the angle between two contiguous eigenvectors. The three-dimensional fiber tracts were then superimposed on axial DWI.

2.4. Clinical Evaluation. During each visit, behavioral assessments were performed by clinicians. The Fugl-Meyer (FM) scale and Barthel index (BI) were measured to evaluate the patient's motor deficits. All three patients showed some motor function recovery at the time of the third DTI scan (1 month after onset).

3. Results

3.1. Clinical Data. The demographics and the evolution of motor function from baseline and throughout the 30 days of recovery in the three patients are summarized in Table 1. Patient 1 suffered from a left dorsolateral medullary infarction presenting with moderate right hemiparesis. Patient 2 had a smaller infarct in the right dorsolateral medullary with mild left hemiparesis. Both patients 1 and 2 had generally excellent motor recovery without disability (FM and BI score of 100) after 14 days. Patient 3 had an infarct of the left ventral medulla and deficits of the right upper extremity remaining after 30 days (FM score of 83.3 and BI score of 85).

3.2. Fractional Anisotropy. Table 2 shows the dynamic changes in the FA values of the infarct on the ipsilateral and contralateral sides of the CST from day 7 to day 30 in all three patients. Compared with the matched regions on the contralateral side, the FA values in the medulla, cerebral peduncle, and internal capsule on the infarct side all slightly decreased across the three time points. Of the three patients, patient 3 had the most obvious decrease in rFA values. The rFA values of the medulla decreased from 0.849 to 0.734 during the 30 days. In patients 1 and 2, the rFA values of the CST showed a slight decline but always stayed above 0.92.

3.3. Diffusion Tensor Tractography. The DTTs for the CSTs of the unaffected hemispheres in the patients originated from the primary sensorimotor cortex and then descended along the known CST pathway. The CST descended from the affected hemisphere traveling via the anterior areas (patients 1 and 2) just around the infarct on the first DTT (Figures 1 and 2). The integrity of the CST was preserved around the infarct, just slightly compressed. On the followup DTTs, the CSTs of the affected hemisphere passed through the same respective spared periinfarct areas in these two patients. However, the left CST descended from the affected hemisphere traveling

Table 2: FA Values of corticospinal tract in the patients with medullary infarction.

Patient		Medulla			Cerebral peduncle			Internal capsule		
		<7 d	14 d	30 d	<7 d	14 d	30 d	<7 d	14 d	30 d
1	Ipsi	0.528 ± 0.217	0.546 ± 0.042	0.557 ± 0.163	0.744 ± 0.107	0.688 ± 0.118	0.799 ± 0.119	0.729 ± 0.080	0.701 ± 0.043	0.700 ± 0.024
	Contra	0.544 ± 0.152	0.554 ± 0.158	0.577 ± 0.088	0.758 ± 0.124	0.695 ± 0.053	0.811 ± 0.012	0.740 ± 0.046	0.736 ± 0.022	0.721 ± 0.035
	rFA	0.971	0.986	0.965	0.982	0.990	0.985	0.985	0.952	0.971
2	Ipsi	0.646 ± 0.131	0.622 ± 0.208	0.655 ± 0.221	0.784 ± 0.011	0.827 ± 0.066	0.775 ± 130.1	0.793 ± 0.027	0.798 ± 0.022	0.768 ± 0.076
	Contra	0.695 ± 0.169	0.651 ± 0.167	0.684 ± 0.013	0.801 ± 0.042	0.857 ± 0.051	0.799 ± 0.056	0.806 ± 0.114	0.863 ± 0.054	0.807 ± 0.101
	rFA	0.9300	0.955	0.958	0.979	0.965	0.970	0.984	0.925	0.951
3	Ipsi	0.331 ± 0.093	0.404 ± 0.061	0.441 ± 0.082	0.767 ± 0.050	0.736 ± 0.032	0.773 ± 0.060	0.774 ± 0.069	0.769 ± 0.107	0.781 ± 0.086
	Contra	0.390 ± 0.110	0.536 ± 0.106	0.601 ± 0.299	0.832 ± 0.043	0.852 ± 0.083	0.868 ± 0.071	0.780 ± 0.080	0.778 ± 0.092	0.786 ± 0.120
	rFA	0.849	0.754	0.734	0.922	0.864	0.891	0.992	0.988	0.994

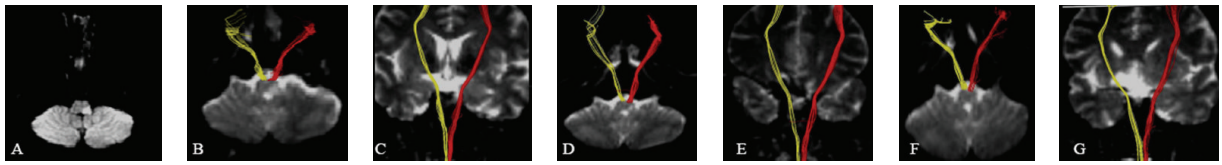

(a) (b) (c) (d) (e) (f) (g)

Figure 1: (a) Diffusion weighted imaging showed an infarct in the left dorsolateral medulla on day 3 after onset; (b)–(g) diffusion tensor tractography showed axial and coronary corticospinal tract ((b)–(c) on day 3; (d)-(e) on day 14; (f)-(g) on day 30). Red for the infarct side; yellow for the contralateral side. The integrity of the corticospinal tract was preserved around the infarct.

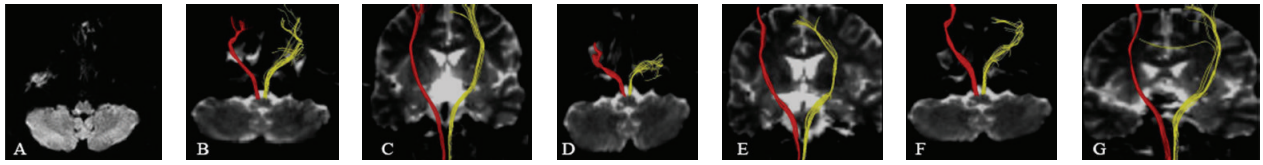

(a) (b) (c) (d) (e) (f) (g)

Figure 2: (a) Diffusion weighted imaging showed an infarct in the right dorsolateral medulla on day 5 after onset; (b)–(g) diffusion tensor tractography showed axial and coronary corticospinal tract ((b)-(c) on day 5; (d)-(e) on day 14; (f)-(g) on day 30). Red for the infarct side; yellow for the contralateral side. The integrity of the corticospinal tract was preserved around the infarct.

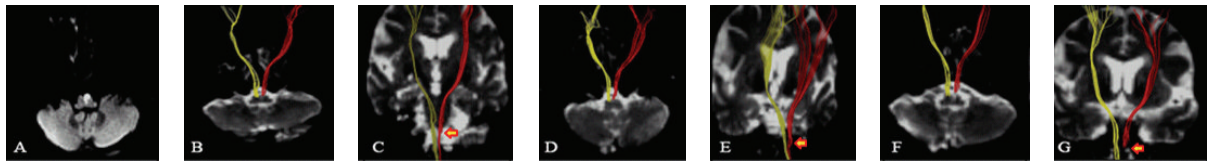

(a) (b) (c) (d) (e) (f) (g)

Figure 3: (a) Diffusion weighted imaging showed an infarct in the left ventral medulla on day 4 after onset; (b)–(g) diffusion tensor tractography showed axial and coronary corticospinal tract ((b)-(c) on day 4; (d)-(e) on day 14; (f)-(g) on day 30). Red for the infarct side; yellow for the contralateral side. The corticospinal tract was mostly interrupted by the infarct (arrow).

via the anterolateral around the infarct on the first DTT in patient 3 (Figure 3). The affected CST was partly disrupted below the medulla infarct. At day 14, the affected tracts were mostly interrupted by the infarct.

4. Discussion

In this study, we investigated the motor recovery mechanism in patients with unilateral medullary infarction who showed motor recovery after the onset of hemiparesis. The results revealed the deterioration of the CST associated with the motor outcome in patients. Differential patterns of recovery were found in the three patients. The main reason that the patients presented good motor recovery can be explained by the slight decline in the FA values and the maintenance of the integrity of the ipsilateral CST. The patients had shown severe paralysis of the right upper extremity at the onset of stroke; motor function recovered slowly over 1 month. The study suggests that the patients had poor motor outcomes in the affected extremities for the following reasons. First, low FA values were found in the affected CST compared with contralateral tracts. Second, DTTs demonstrated that a majority of the fiber tracts in the affected medulla were damaged.

We found that the FA values in the medulla, cerebral peduncle, and internal capsule on the infarct side all decreased across the three scan times. The size of medulla is small. Therefore the unilateral infarction and edema of medulla may affect bilateral corticospinal tract. The FA values in the medulla, cerebral peduncle, and internal capsule were found decreased on both sides. In patient 3, the ventral medulla infarction was relatively large, so the FA values decreased more obvious. In patients 1 and 2, the FA values of the affected CST showed a slight decline, although the fiber was spared. Patient 3 had the most obvious decrease in FA values along the affected CST and the rFA values of the medulla decreased from 0.849 to 0.734 during the 30 days. Because the blood supply to the internal capsule and cerebral peduncle differs from those in the medulla, our findings cannot be explained by ischemia. Previous studies reported that the FA reduction reflects deterioration of axonal integrity leading to axonal loss and Wallerian degeneration (WD) [6, 7]. Compared with conventional MRI imaging, such as that with T2 and FLAIR sequences, FA values are an early marker of axonal degeneration. In addition, several

longitudinal studies of DTI in patients with cerebral infarction demonstrated WD of the pyramidal tract. Therefore, the changes in the FA values in the medulla and along the CST in our study were due to axonal injury and WD. The mechanism of retrograde secondary damage in the cerebral peduncle and internal capsule is consistent with that of anterograde WD.

Our study confirms that DTT can provide important clues to the spatial relationship between infarcts and the CST in stroke patients. Therefore, it can be used to predict motor outcomes. The affected CST descended running via the anterior areas just around the infarct on DTTs in patients 1 and 2. The integrity of the CST was preserved. The motor recovery could be attributed to periinfarct spared CST or the resolution of the transient edema around the lesion. In patient 3, the affected CST was partly disrupted and the motor function slowly recovered. Thus, CST integrity plays an important role during the recovery of motor function. Previous studies have suggested that motor function can be controlled well only by a part of the CST [8]. In this study, it seems that patients' motor function was controlled via the spared periinfarct CST, also in the medulla. However, patients with more CST involvement tend to have poorer prognosis. So far, many studies on the state of the CST or motor recovery mechanisms at the subcortical level have been reported [9–12]. However, to our knowledge, only one study has used DTI to investigate patients with medulla infarct [13]. Jang et al. reported one patient whose motor functions of the affected extremities rapidly recovered to a normal state over the 4 months following stroke onset. The integrity of the CST was shown to be spared in the anterior portion of the medulla infarct using DTT.

In conclusion, we demonstrated that DTI could detect the involvement of and changes in the CST in patients with medulla infarct during motor recovery. The degree of degeneration and the spared periinfarct CST compensation may be an important mechanism of motor recovery. However, this present study is admittedly limited because only three patients were involved. Therefore, our findings need to be further verified in studies with larger case numbers and combined DTI and functional MRI techniques.

Conflict of Interests

The authors declare that they have no conflict of interests.

References

[1] S. Mori and J. Zhang, "Principles of diffusion tensor imaging and its applications to basic neuroscience research," *Neuron*, vol. 51, no. 5, pp. 527–539, 2006.

[2] Y. Assaf and O. Pasternak, "Diffusion tensor imaging (DTI)-based white matter mapping in brain research: a review," *Journal of Molecular Neuroscience*, vol. 34, no. 1, pp. 51–61, 2008.

[3] M. Møller, J. Frandsen, G. Andersen, A. Gjedde, P. Vestergaard-Poulsen, and L. Østergaard, "Dynamic changes in corticospinal tracts after stroke detected by fibretracking," *Journal of Neurology, Neurosurgery and Psychiatry*, vol. 78, no. 6, pp. 587–592, 2007.

[4] P. Mukherjee, "Diffusion tensor imaging and fiber tractography in acute stroke," *Neuroimaging Clinics of North America*, vol. 15, no. 3, pp. 655–665, 2005.

[5] C. Wang, G. T. Stebbins, D. L. Nyenhuis et al., "Longitudinal changes in white matter following ischemic stroke: a three-year follow-up study," *Neurobiology of Aging*, vol. 27, no. 12, pp. 1827–1833, 2006.

[6] Z. Liang, J. Zeng, C. Zhang et al., "Progression of pathological changes in the middle cerebellar peduncle by diffusion tensor imaging correlates with lesser motor gains after pontine infarction," *Neurorehabilitation and Neural Repair*, vol. 23, no. 7, pp. 692–698, 2009.

[7] G. Thomalla, V. Glauche, M. A. Koch, C. Beaulieu, C. Weiller, and J. Röther, "Diffusion tensor imaging detects early Wallerian degeneration of the pyramidal tract after ischemic stroke," *NeuroImage*, vol. 22, no. 4, pp. 1767–1774, 2004.

[8] J.-W. Park, S. H. Kim, Y. W. Kim et al., "Motor control via spared peri-infarct corticospinal tract in patients with pontine infarct," *Journal of Computer Assisted Tomography*, vol. 32, no. 1, pp. 159–162, 2008.

[9] C. Lai, S. Z. Zhang, H. M. Liu et al., "White matter tractography by diffusion tensor imaging plays an important role in prognosis estimation of acute lacunar infarctions," *The British Journal of Radiology*, vol. 80, no. 958, pp. 782–789, 2007.

[10] S. H. Jang, "Prediction of motor outcome for hemiparetic stroke patients using diffusion tensor imaging: a review," *NeuroRehabilitation*, vol. 27, no. 4, pp. 367–372, 2010.

[11] S. H. Jang, "A review of motor recovery mechanisms in patients with stroke," *NeuroRehabilitation*, vol. 22, no. 4, pp. 253–259, 2007.

[12] R. Lindenberg, V. Renga, L. L. Zhu, F. Betzler, D. Alsop, and G. Schlaug, "Structural integrity of corticospinal motor fibers predicts motor impairment in chronic stroke," *Neurology*, vol. 74, no. 4, pp. 280–287, 2010.

[13] S. H. Jang, D. S. Yang, and J. Lee, "Preservation of the integrity of the corticospinal tract in a patient with medulla infarct," *The American Journal of Physical Medicine and Rehabilitation*, vol. 88, no. 3, pp. 256–258, 2009.

Hindawi Publishing Corporation
BioMed Research International
Volume 2014, Article ID 846830, 7 pages
http://dx.doi.org/10.1155/2014/846830

Research Article

Dysfunction of Affective Network in Post Ischemic Stroke Depression: A Resting-State Functional Magnetic Resonance Imaging Study

Peiyao Zhang,[1] Qin Xu,[2] Jianping Dai,[1] Jun Wang,[3,4] Ning Zhang,[5] and Yuejia Luo[3,4]

[1] *Department of Neuroradiology, Beijing Tiantan Hospital, Capital Medical University, No. 6 Tiantanxili, Dongcheng District, Beijing 100050, China*
[2] *Centre for Studies of Psychological Application, Key Laboratory of Mental Health and Cognitive Science of Guangdong Province, School of Psychology, South China Normal University, Guangzhou, China*
[3] *State Key Laboratory of Cognitive Neuroscience and Learning & IDG/McGovern Institute for Brain Research, Beijing Normal University, 19 Xinjiekouwai Street, Haidian District, Beijing 100875, China*
[4] *Center for Collaboration and Innovation in Brain and Learning Sciences, Beijing Normal University, 19 Xinjiekouwai Street, Haidian District, Beijing 100875, China*
[5] *Department of Neurology, Beijing Tiantan Hospital, Capital Medical University, No. 6 Tiantanxili, Dongcheng District, Beijing 100050, China*

Correspondence should be addressed to Jianping Dai; lyfx1228@sohu.com and Jun Wang; jun_wang@bnu.edu.cn

Received 25 January 2014; Revised 27 April 2014; Accepted 29 April 2014; Published 14 May 2014

Academic Editor: Lijun Bai

Objective. Previous studies have demonstrated that stroke characteristics and social and psychological factors jointly contribute to the development of poststroke depression (PSD). The purpose of this study was to identify altered functional connectivity (FC) of the affective network (AN) in patients with PSD and to explore the correlation between FC and the severity of PSD. *Materials and Methods*. 26 PSD patients, 24 stroke patients without depression, and 24 age-matched normal controls underwent the resting-state functional MRI (fMRI) scanning. The bilateral anterior cingulated cortices (ACCs) were selected as regions of interest (ROIs). FC was calculated and compared among the three groups. The association between FC and Hamilton Depression Rate Scale (HDRS) scores of PSD group was investigated. *Results*. The FC of the AN was disrupted in PSD patients compared to stroke patients without depression and normal controls. Moreover, the left orbital part of inferior frontal gyrus which indicated altered FC was significantly correlated with HDRS scores in PSD patients. *Conclusions*. Dysfunction of the affective network may be one of the reasons of the development of PSD.

1. Introduction

Stroke is one of the most common causes of human death [1]. Large-scale stroke survivors suffer from poststroke depression (PSD), which not only hinders recovery but also increases the risk of death significantly [2, 3]. Some studies involving the determinants of PSD have focused on infarction characteristics, including location, size, volume, and white matter lesions, while other studies have proposed that the course of PSD seemed to be dependent on psychosocial factors, such as personality, disability, and social support [4–7]. However, few studies have been conducted to determine the relationship between the risk of PSD and brain lesions or other correlative factors [8–10]. Due to different definitions of depression, the duration of disease, measurement methods, and patient sampling, the pathogenesis of PSD is controversial [6, 9, 10].

In recent years, resting-state functional MRI (fMRI) provided a powerful framework for detecting the mechanism underlying cognitive disorders [11, 12]. The first study of resting-state functional connectivity (FC) showed that spontaneous low-frequency fluctuations in blood oxygen level-dependent (BOLD) signals were exhibited in a sensorimotor network when the brain was in a resting state [13]. FC was

considered as the temporal correlation of spontaneous fluctuations in anatomically separated, but functionally related brain regions, and these brain regions were comprised of some specific networks [14]. The most widely explored network is the default mode network (DMN) [15–18].

Moreover, another neural functional network, the affective network (AN), was also detected in a task-related functional MRI study of mood disorders [19–21]. The AN consists of the prefrontal cortex, amygdala, insula, ventral striatum, hippocampus, and anterior cingulate cortex and was associated with emotional activity and modulation [22–25].

We hypothesized that FC in patients with PSD is different from stroke patients without depression and normal controls and the dysfunction of the AN in patients with PSD is associated with the severity of depression. Thus, the objective of this study is to compare FC of the AN among three groups (PSD, stroke without depression, and normal control groups) and to determine the difference between each group. The bilateral anterior cingulate cortices (ACCs) were selected as the region of interest (ROI) in the AN. The correlation between altered FC in PSD patients and severity of depression was also explored.

2. Methodology

2.1. Subjects. This prospective study was accepted by the local Ethics Committee of Beijing Tiantan Hospital of Capital Medical University. All the subjects signed the written informed consent before participation.

In this study, 50 patients (40–75 years of age) who had their first time ischemic stroke were recruited from the Department of Neurology at Beijing Tiantan Hospital of Capital Medical University between January 2010 and April 2013, including 26 PSD patients (6 females) and 24 stroke patients without depression (5 females). Twenty-four age-matched healthy volunteers were also enrolled as normal control (NC) group (6 females). All the subjects were right-handed.

Patients with PSD were selected consecutively on the basis of the following inclusion criteria: (a) MRI findings of cerebral stroke were confirmed by two senior radiologists; (b) all patients were evaluated by two psychiatrists for depression using the Diagnostic and Statistical Manual of Mental Disorders (DSM-IV, fourth edition); (c) Hamilton Depression Rating Scale (HDRS) 17-item [26] scores >7 were performed to evaluate the depression severity; (d) duration of illness <2 weeks; and (e) patients had experienced their first ischemic stroke and were medication-free.

The inclusion criteria of stroke patients without depression were as follows: (a) diagnosis of stroke performed by two senior radiologists; (b) no depression according to DSM-IV; (c) HDRS 17-item [26] scores <7; (d) duration of illness <2 weeks; and (e) patients having their first ischemic stroke.

Normal controls were referred when they met the following criteria: (a) T2-flair showed no white matter disease; (b) no depression according to DSM-IV; and (c) HDRS scores <7.

Exclusion criteria for all subjects were as follows: (a) other psychiatric diseases, including substance abuse or dependence; (b) other neurological diseases such as dementia; (c) medical disorders impairing cognitive function; (d) a family history of serious psychiatric or neurological illness in first-degree relatives; (e) cerebral hemorrhage or brain trauma; and (f) other contraindications to MR scanning.

2.2. MRI Scan Protocol. The MRI scan was performed on a Siemens 3.0T Trio MRI scanner using a standard quadrature head coil. All subjects underwent structural imaging sessions including acquisition of a scout scan with three orthogonal slices, followed by a coarse 3D sagittal T1-weighted magnetization-prepared rapid gradient echo (mp-rage) sequence (176 slices; thickness/gap = 1.0/0 mm; repetition time [TR] = 1900 ms; echo time [TE] = 2.13 ms; flip angle = 9°; matrix 256 × 256; field of view [FOV] = 256 × 256 mm^2) over the whole brain to automatically compute fMRI slice tilts and offsets that optimize whole-brain coverage parallel to the anterior-posterior commissure plane. The scanning time was 8 minutes. Resting-state functional images were acquired using an echo-planar imaging sequence as follows: TR = 2000 ms; TE = 30 ms; flip angle = 90°; slices = 31; thickness/gap = 3/1 mm; matrix 64 × 64; FOV = 200 × 200 mm^2. The scanning time was 8 minutes. During the resting-state scanning, all the subjects were instructed to be quiet with their eyes closed and not to think about anything in particular. A sponge mat was used to limit head movement.

2.3. Data Analysis. The raw data were preprocessed using SPM8 soft package (http://www.fil.ion.ucl.ac.uk/). With respect to the equilibrium and subject adaptability, the first 10 images of each subject were discarded. Therefore, 230 images for each subject were sequentially put into the following preprocessing procedures. All subjects in this study met the criteria of the head motion less than 3 mm of translation and 3° of rotation in any direction. After motion correction, the images were spatially normalized into standard MNI space and resampled to 3 × 3 × 3 mm^3, then spatially smoothed with a 4 × 4 × 4 mm^3 full width at half-maximum Gaussian kernel. After that, a low-pass frequency filter ($0.01 < f < 0.08$ Hz) was applied to reduce physiologic high frequency noise. All the procedures were performed using the REST package (http://www.restfmri.net/forum/).

2.4. ROI Selection. The bilateral ACCs were extracted and combined as one ROI as these areas were defined by previous studies in depressive patients [19, 27]. In the current study, the bilateral ACCs were extracted from the automated anatomical labeling [28] atlas from MRIcro software (http://www.cabiatl.com/mricro/) (Figure 1). Using seed ROI analysis, a seed reference time course was obtained by averaging the time series over the voxels in the bilateral ACCs. Pearson's correlation analysis was carried out between the seed reference and the whole brain in a voxel-wise manner, with the global mean time course, the white matter mean time course, the cerebrospinal fluid mean time course, and the six head motion parameters as nuisance covariates. Then the correlation coefficients were converted to z-scores by applying Fisher's r-to-z transformation $\{z = 0.5 \ln[(1+r)/(1-r)]\}$.

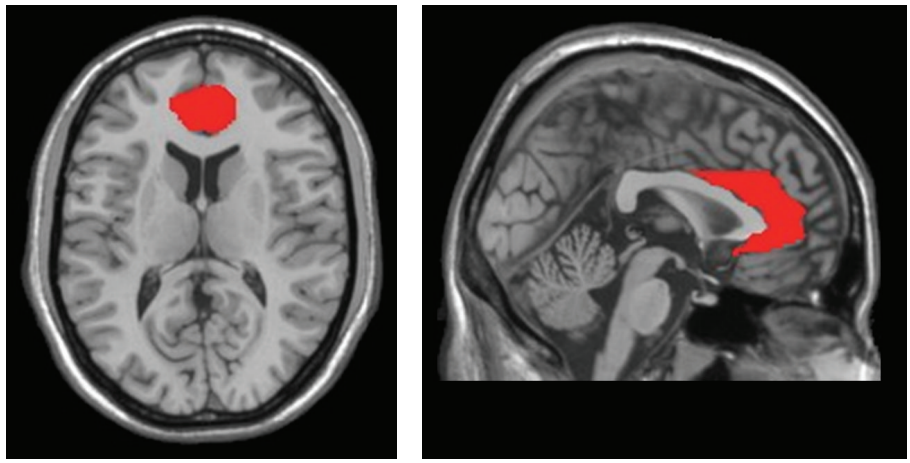

(a) (b)

Figure 1: The bilateral ACCs (red region) in axial view (a) and sagital view (b) were extracted from the automated anatomical labeling atlas implemented in MRIcro software. The bilateral ACCs were combined as one-seed region of interest (ROI).

Table 1: Demographic and clinical characteristic of the samples.

	PSD (n = 26)	Stroke (n = 24)	NC (n = 24)
Age	56.4 ± 10.2	60.2 ± 9.8	57.1 ± 9.5
Gender			
Male	20	19	18
Female	6	5	6
HDRS score	12.5 ± 3.87	—	—
Disease period (day)	9.92 ± 2.77	9.62 ± 2.72	—

HDRS: Hamilton Depression Rating Scale. Unless otherwise indicated, data are expressed as the mean ± SD. NC: normal control.

2.5. Statistical Analysis. In this study, one-way analysis of variance (ANOVA) was carried out to detect comparison of FC across the three groups. Voxels with $P < 0.01$ and cluster size ≥18 voxels were considered significantly different between groups, which corresponds to $P < 0.01$ after correction for multiple comparisons using Monte Carlo simulation (AlphaSim in REST software [http://www.restfmri.net/forum/]). After that, a two-sample post hoc t test analyses were performed between each pair of groups (PSD versus stroke, PSD versus NC, and stroke versus NC) to further confirm the between-group differences. Voxels with $P < 0.01$ and cluster size ≥18 voxels were considered significantly different, corresponding to corrected $P < 0.05$ as determined by AlphaSim.

To investigate the relationship between the altered FCs and depression, correlation analyses were performed between the mean z-scores of the clusters which showed significant differences among the three groups and the HDRS scores in the PSD group (significant level was $P \leq 0.05$) using SPSS7 software.

3. Result

3.1. Subjects. The detailed information of demographic and clinical characteristics of all participants is shown in Table 1. The age, gender, and disease period showed no significant differences among the three groups of subjects.

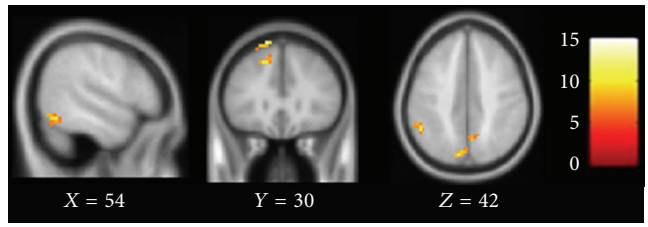

Figure 2: Brain regions which show altered connectivity with ACC among PSD, stroke, and NC groups. Images were thresholded at $F = 4.91$ ($P < 0.01$, corrected by AlphaSim).

3.2. MRI Image Analysis. By using one-way ANOVA, a significant difference of connection with the seed region was revealed among the three groups.

The brain regions which had altered connectivity with ACC in the comparison between the PSD group and two other groups, including the right triangular part of the inferior frontal gyrus ($F = 8.6$, df = 2, and $P < 0.01$) and the left orbital part of inferior frontal gyrus ($F = 4.01$, df = 2, and $P < 0.01$; Figures 2 and 3).

Further investigation on the detailed differences of FC in the three groups was performed using a *post hoc t* test ($P < 0.01$, cluster size ≥18 was considered significant (Table 2, Figure 4)).

The FC of the left inferior temporal gyrus, left orbital part of the inferior frontal gyrus, and right triangular part

Table 2: Brain regions show different FC with ACC between two groups.

Regions	BA	Cluster size	Maximal t-score	Primary peak location (MNI)		
PSD versus Stroke						
Positive						
ITG.L	21	33	3.27	−45	3	−36
ORBinf.L		35	4.01	−42	30	−6
IFGtriang.R		21	4.18	36	24	26
Negative	none	none	none	none	none	none
PSD versus NC						
Positive						
ITG.R	37	42	3.15	51	−63	−15
IFGtriang.L		105	4.15	−48	27	12
ORBinf.L		66	4.01	−42	30	−6
ORBsup.L		32	4.12	−12	57	−9
MFG.L	10	66	3.92	−39	48	6
IFGtriang.R		34	3.64	36	24	26
Negative						
PCUN.L	7	30	−3.03	−9	−61	34
MTG.L		22	−3.84	−57	−63	3
Strokes versus NC						
Negative						
TPOsup.L		18	−3.12	−30	6	−24

Significant level of $P < 0.01$, cluster size ≥ 18 with AlphaSim correction for multiple comparisons, $^{*}P < 0.05$; NC: normal control; BA: Broadman area; MNI: Montreal Neurological Institute spatial array coordinates; ITG: inferior temporal gyrus; ORBinf.: inferior frontal gyrus, orbital part; IFGtriang.: inferior frontal gyrus, triangular part; ORBsup.: superior frontal gyrus, orbital part; STG: superior temporal gyrus; MFG: middle frontal gyrus; ANG: angular gyrus; SFG: superior frontal gyrus; PCUN: precuneus; MTG: middle temporal gyrus; TPOsup.: superior temporal gyrus; L: left; R: right.

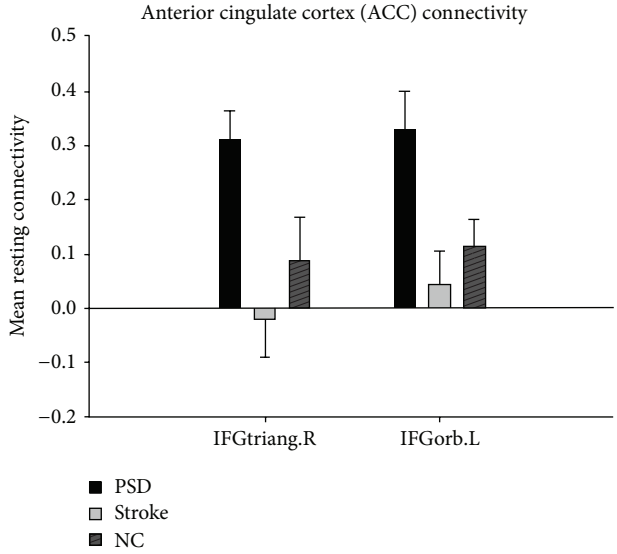

Figure 3: Comparison of PSD, stroke, and NC groups for mean resting connectivity between bilateral ACC and IFGtriang.R and IFGorb.L.

of the inferior frontal gyrus was increased with the ACC in the PSD group compared with the stroke group (Figure 4(a)). Furthermore, additional brain regions, including the right inferior temporal gyrus, the left triangular part of the inferior frontal gyrus, the left orbital part of the superior frontal gyrus, and the left middle frontal gyrus had increased FC with the ACC, while the left precuneus and left middle temporal gyrus showed reduced FC with the ACC, existed in the PSD group compared with the NC group (Figure 4(b)). Decreased FC of the left superior temporal gyrus existed in comparison with the stroke and NC groups (Figure 4(c)).

3.3. Correlation Analysis. Moreover, the FC between the significantly altered clusters (Figure 2) and the seed ROI were computed and then correlated with the HDRS scores of the PSD group ($P \leq 0.05$). We found that the FC between the left orbital part of the inferior frontal gyrus and ACC was positively correlated with the HDRS scores ($r = 0.39$, $P = 0.05$; Figure 5).

4. Discussion

The key finding in this study was that FC of the AN in PSD was altered compared to the stroke and NC groups. Moreover, the altered FC was associated with the HDRS scores in PSD patients. As a result, these findings may support a strong association between the AN impairments and the risk of developing PSD in the subacute phase of stroke.

In the current study, the right inferior temporal gyrus, bilateral triangular part of the inferior frontal gyrus, left orbital part of the inferior frontal gyrus, left orbital part of the

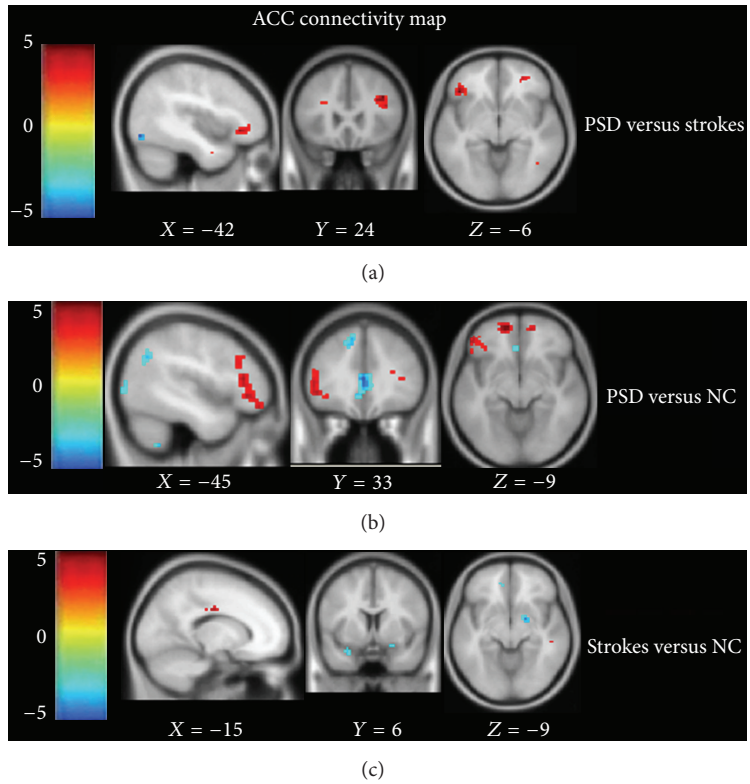

FIGURE 4: (a)–(c) Comparison of connectivity maps with ACC between two groups. (a) Intergroup difference between PSD and stroke groups; (b) intergroup difference between PSD and NC groups; (c) intergroup difference between stroke and NC groups. The threshold of the images was at $t = 2.42$, $P < 0.01$, corrected by AlphaSim, $^{*}P < 0.05$.

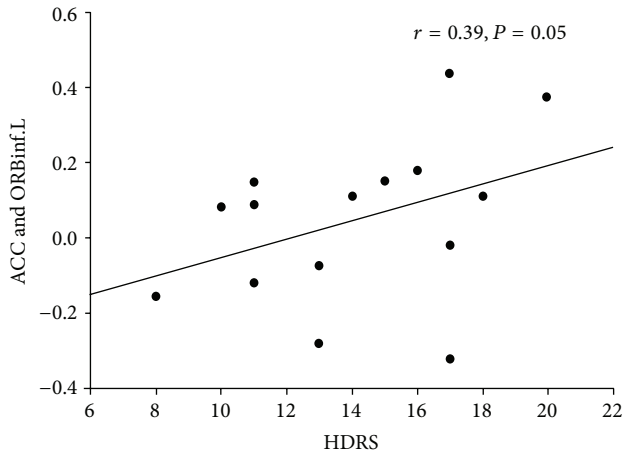

FIGURE 5: Plots displaying the correlation between the FC (mean z-scores) and the HDRS scores in the left orbital part of the inferior frontal gyrus (ORBinf.L) in the PSD patients. HDRS, Hamilton Depression Rating Scale.

superior frontal gyrus, and left middle frontal gyrus showed increased FC with ACC between PSD and NC while the left precuneus and left middle temporal gyrus showed decreased FC with the ACC. The altered regions in PSD compared to stroke were included in the comparison between PSD and NC, except the left inferior temporal gyrus, which showed increased FC with the ACC. Comparing the stroke and NC groups, the left superior temporal gyrus, which showed reduced FC, was absent in the comparison between the PSD and NC. These results suggest that impaired FC of the AN may be related to the development of PSD.

The brain regions which indicated increased FC in the current study were mainly found in the bilateral frontal lobes, which are associated with emotion regulation [29]. The results of the current study are consistent with previous studies, showing that increased FC of right inferior frontal gyrus was found in an affective-related network of depressed patients [30]. Additionally Sheline et al. [27] also suggested that ACC indicated increased FC with bilateral dorsomedial prefrontal cortex. This similarity between PSD and depression may contribute to depressive symptoms which exist both in PSD and depressive patients. A previous study has also reported that the inferior frontal gyrus is implicated in dealing with emotional distraction [31]. Later, another research reported that the inferior frontal gyrus of major depressive patients indicated deactivation in coping with emotional distraction [32]. Accordingly, the increased FC of the bilateral inferior frontal gyrus in the current study may suggest that there is a trend towards inhibition of emotional replication in PSD patients. Furthermore, Cullen et al. [33] found that superior temporal gyrus showed reduced FC with subgenual ACC in adolescence with major depressive disorder. The current study implies a similar finding as

decreased FC was shown in the left middle temporal gyrus. Both PSD and depression patients appear to have decreased FC in the temporal lobe, but in different locations. This may suggest that PSD differs from depression. On the other hand, Anand et al. discovered that the FC of bilateral dorsomedial thalamus, amygdala, and left pallidostriatum with ACC was reduced in depressed patients [19]. And the study for patients with bipolar disorder (BDM) and unipolar major depression (MDD) once again proved that depression caused altered FC of bilateral dorsomedial thalamus and amygdala [21]. However, no identical region with them has been found in the present study. The divergence in the present findings from previous studies may be have partly resulted from the difference in illness duration, stages of depressive severity, and the selection of ROI. Nevertheless, to some extent, it may also confirm that PSD is different from depression.

In the current study the correlation between altered FC and HDRS scores has also been detected. The increased FC between the left orbital part of the inferior frontal gyrus and ACC was associated with the severity of depression. Altered FC of the right inferior frontal gyrus, which was considered to be involved in affective processing, has been demonstrated in MDD patients [30]. Zhou et al. [34] suggested that the FC between the left dorsolateral prefrontal cortex and the right middle/superior frontal gyrus was correlated with the HDRS score. Another study suggested that there was an association between left frontal impairment and the severity of depression in affective PSD patients [35]. These results were consistent with our findings and may confirm the speculation that FC impairment of the AN was associated with PSD. However, although the association between frontal FC damage and severity of depression was indicated both in previous studies and in the current study, the specific location was different. Moreover, there was a negative correlation between the left hippocampus and HDRS scores, while the positive correlation was found between the left caudate nucleus and HDRS scores [36]. These differences may be due to the differences in samples, selection of ROI, and depression severity but may also confirm that PSD is different from depression.

The limitations of this study were that the lesion location, volume and correlation with the altered FC were not considered. These additional studies such as comparing the lesion characteristics between the PSD and stroke patients without depression groups will be performed in the future studies. In the previous study, the central coordinates of ROIs were based on the task-related state fMRI study for depressive patients [28]. In the present study, a task-related state fMRI study was not performed because of the subacute phase of the stroke patients.

5. Conclusion

In this study, altered FC of brain regions which belongs to the AN has been found in PSD patients, and significant differences also have been found between PSD and stroke without depression patients according to the AN. Furthermore, altered FC is correlated with HDRS scores in PSD patients. From these findings we can infer that the dysfunction of the AN may be one of the causes of PSD.

Conflict of Interests

The authors declare that they have no conflict of interests regarding to the publication of this paper.

Funding

The paper was funded by State Key Program of National Natural Science of China (Grant no. 30930031).

Acknowledgments

The authors thank Yuzhi Shi for her help with patient recruitment and clinical evaluation. They thank all the volunteers and patients for their participation in the study.

References

[1] American Heart Association, "Stroke—1989. Recommendations on stroke prevention, diagnosis, and therapy. Report of the WHO task force on stroke and other cerebrovascular disorders," vol. 20, no. 10, pp. 1407–1431, 1989.

[2] L. Snaphaan, M. Rijpkema, I. Van Uden, G. Fernández, and F.-E. De Leeuw, "Reduced medial temporal lobe functionality in stroke patients: a functional magnetic resonance imaging study," *Brain*, vol. 132, no. 7, pp. 1882–1888, 2009.

[3] A. Jaillard, B. Naegele, S. Trabucco-Miguel, J. F. LeBas, and M. Hommel, "Hidden dysfunctioning in subacute stroke," *Stroke*, vol. 40, no. 7, pp. 2473–2479, 2009.

[4] R. J. Davidson, D. A. Lewis, L. B. Alloy et al., "Neural and behavioral substrates of mood and mood regulation," *Biological Psychiatry*, vol. 52, no. 6, pp. 478–502, 2002.

[5] G. M. S. Nys, M. J. E. van Zandvoort, H. B. van der Worp et al., "Early cognitive impairment predicts long-term depressive symptoms and quality of life after stroke," *Journal of the Neurological Sciences*, vol. 247, no. 2, pp. 149–156, 2006.

[6] S. K. Bhogal, R. Teasell, N. Foley, and M. Speechley, "Lesion location and poststroke depression: systematic review of the methodological limitations in the literature," *Stroke*, vol. 35, no. 3, pp. 794–802, 2004.

[7] W. K. Tang, Y. K. Chen, J. Y. Lu et al., "Cerebral microbleeds and symptom severity of post-stroke depression: a magnetic resonance imaging study," *Journal of Affective Disorders*, vol. 129, no. 1–3, pp. 354–358, 2011.

[8] A. J. Carson, S. MacHale, K. Allen et al., "Depression after stroke and lesion location: a systematic review," *The Lancet*, vol. 356, no. 9224, pp. 122–126, 2000.

[9] M. Santos, E. Kövari, G. Gold et al., "The neuroanatomical model of post-stroke depression: towards a change of focus?" *Journal of the Neurological Sciences*, vol. 283, no. 1-2, pp. 158–162, 2009.

[10] A. Singh, N. Herrmann, and S. E. Black, "The importance of lesion location in poststroke depression: a critical review," *Canadian Journal of Psychiatry*, vol. 43, no. 9, pp. 921–927, 1998.

[11] M. Greicius, "Resting-state functional connectivity in neuropsychiatric disorders," *Current Opinion in Neurology*, vol. 21, no. 4, pp. 424–430, 2008.

[12] Z. Wang, C. Yan, C. Zhao et al., "Spatial patterns of intrinsic brain activity in mild cognitive impairment and alzheimer's disease: a resting-state functional MRI study," *Human Brain Mapping*, vol. 32, no. 10, pp. 1720–1740, 2011.

[13] B. Biswal, F. Z. Yetkin, V. M. Haughton, and J. S. Hyde, "Functional connectivity in the motor cortex of resting human brain using echo-planar MRI," *Magnetic Resonance in Medicine*, vol. 34, no. 4, pp. 537–541, 1995.

[14] M. De Luca, C. F. Beckmann, N. De Stefano, P. M. Matthews, and S. M. Smith, "fMRI resting state networks define distinct modes of long-distance interactions in the human brain," *NeuroImage*, vol. 29, no. 4, pp. 1359–1367, 2006.

[15] M. D. Greicius, K. Supekar, V. Menon, and R. F. Dougherty, "Resting-state functional connectivity reflects structural connectivity in the default mode network," *Cerebral Cortex*, vol. 19, no. 1, pp. 72–78, 2009.

[16] R. N. Spreng, R. A. Mar, and A. S. N. Kim, "The common neural basis of autobiographical memory, prospection, navigation, theory of mind, and the default mode: a quantitative meta-analysis," *Journal of Cognitive Neuroscience*, vol. 21, no. 3, pp. 489–510, 2009.

[17] R. Bluhm, P. Williamson, R. Lanius et al., "Resting state default-mode network connectivity in early depression using a seed region-of-interest analysis: decreased connectivity with caudate nucleus," *Psychiatry and Clinical Neurosciences*, vol. 63, no. 6, pp. 754–761, 2009.

[18] S. Lassalle-Lagadec, I. Sibon, B. Dilharreguy, P. Renou, O. Fleury, and M. Allard, "Subacute default mode network dysfunction in the prediction of post-stroke depression severity," *Radiology*, vol. 264, no. 1, pp. 218–224, 2012.

[19] A. Anand, Y. Li, Y. Wang et al., "Activity and connectivity of brain mood regulating circuit in depression: a functional magnetic resonance study," *Biological Psychiatry*, vol. 57, no. 10, pp. 1079–1088, 2005.

[20] A. Anand, Y. Li, Y. Wang et al., "Antidepressant effect on connectivity of the mood-regulating circuit: an fMRI study," *Neuropsychopharmacology*, vol. 30, no. 7, pp. 1334–1344, 2005.

[21] A. Anand, Y. Li, Y. Wang, M. J. Lowe, and M. Dzemidzic, "Resting state corticolimbic connectivity abnormalities in unmedicated bipolar disorder and unipolar depression," *Psychiatry Research—Neuroimaging*, vol. 171, no. 3, pp. 189–198, 2009.

[22] G. Bush, P. Luu, and M. I. Posner, "Cognitive and emotional influences in anterior cingulate cortex," *Trends in Cognitive Sciences*, vol. 4, no. 6, pp. 215–222, 2000.

[23] M. L. Phillips, W. C. Drevets, S. L. Rauch, and R. Lane, "Neurobiology of emotion perception II: implications for major psychiatric disorders," *Biological Psychiatry*, vol. 54, no. 5, pp. 515–528, 2003.

[24] H. S. Mayberg, M. Liotti, S. K. Brannan et al., "Reciprocal limbic-cortical function and negative mood: converging PET findings in depression and normal sadness," *The American Journal of Psychiatry*, vol. 156, no. 5, pp. 675–682, 1999.

[25] W. C. Drevets, J. Savitz, and M. Trimble, "The subgenual anterior cingulate cortex in mood disorders," *CNS Spectrums*, vol. 13, no. 8, pp. 663–681, 2008.

[26] M. Hamilton, "A rating scale for depression," *Journal of Neurology, Neurosurgery, and Psychiatry*, vol. 23, pp. 56–62, 1960.

[27] Y. I. Sheline, J. L. Price, Z. Yan, and M. A. Mintun, "Resting-state functional MRI in depression unmasks increased connectivity between networks via the dorsal nexus," *Proceedings of the National Academy of Sciences of the United States of America*, vol. 107, no. 24, pp. 11020–11025, 2010.

[28] N. Tzourio-Mazoyer, B. Landeau, D. Papathanassiou et al., "Automated anatomical labeling of activations in SPM using a macroscopic anatomical parcellation of the MNI MRI single-subject brain," *NeuroImage*, vol. 15, no. 1, pp. 273–289, 2002.

[29] R. L. Buckner, J. R. Andrews-Hanna, and D. L. Schacter, "The brain's default network: anatomy, function, and relevance to disease," *Annals of the New York Academy of Sciences*, vol. 1124, pp. 1–38, 2008.

[30] I. M. Veer, C. F. Beckmann, M. J. van Tol et al., "Whole brain resting-state analysis reveals decreased functional connectivity in major depression," *Frontiers in Systems Neuroscience*, vol. 4, article 41, 2010.

[31] F. Dolcos, P. Kragel, L. Wang, and G. McCarthy, "Role of the inferior frontal cortex in coping with distracting emotions," *NeuroReport*, vol. 17, no. 15, pp. 1591–1594, 2006.

[32] L. Wang, K. S. LaBar, M. Smoski et al., "Prefrontal mechanisms for executive control over emotional distraction are altered in major depression," *Psychiatry Research—Neuroimaging*, vol. 163, no. 2, pp. 143–155, 2008.

[33] K. R. Cullen, D. G. Gee, B. Klimes-Dougan et al., "A preliminary study of functional connectivity in comorbid adolescent depression," *Neuroscience Letters*, vol. 460, no. 3, pp. 227–231, 2009.

[34] Y. Zhou, C. Yu, H. Zheng et al., "Increased neural resources recruitment in the intrinsic organization in major depression," *Journal of Affective Disorders*, vol. 121, no. 3, pp. 220–230, 2010.

[35] S. Hama, H. Yamashita, M. Shigenobu et al., "Post-stroke affective or apathetic depression and lesion location: left frontal lobe and bilateral basal ganglia," *European Archives of Psychiatry and Clinical Neuroscience*, vol. 257, no. 3, pp. 149–152, 2007.

[36] J. Zhang, J. Wang, Q. Wu et al., "Disrupted brain connectivity networks in drug-naive, first-episode major depressive disorder," *Biological Psychiatry*, vol. 70, no. 4, pp. 334–342, 2011.

Hindawi Publishing Corporation
BioMed Research International
Volume 2014, Article ID 148465, 8 pages
http://dx.doi.org/10.1155/2014/148465

Research Article

Depressive Symptoms in Multiple Sclerosis from an In Vivo Study with TBSS

Yujuan Shen,[1] Lijun Bai,[2] Ying Gao,[1] Fangyuan Cui,[1] Zhongjian Tan,[3] Yin Tao,[2] Chuanzhu Sun,[2] and Li Zhou[1]

[1] *Department of Neurology, Dongzhimen Hospital Affiliated to Beijing University of Chinese Medicine, Beijing 100700, China*
[2] *The Key Laboratory of Biomedical Information Engineering, Ministry of Education, Department of Biomedical Engineering, School of Life Science and Technology, Xi'an Jiaotong University, Xi'an 710049, China*
[3] *Department of MRI Scanning, Dongzhimen Hospital Affiliated to Beijing University of Chinese Medicine, Beijing 100700, China*

Correspondence should be addressed to Lijun Bai; bailj4152615@gmail.com and Li Zhou; zhouljk7211@163.com

Received 21 February 2014; Revised 5 April 2014; Accepted 8 April 2014; Published 4 May 2014

Academic Editor: Lin Ai

Clinically significant depression can impact up to 50% of patients with multiple sclerosis (MS) over a course of their life time, which is associated with an increased morbidity and mortality. In our study, fifteen relapsing-remitting MS (RRMS) patients and 15 age- and gender-matched normal controls were included. Diffusion tensor imaging (DTI) was acquired by employing a single-shot echo planar imaging sequence on a 3.0 T MR scanner and fractional anisotropy (FA) was performed with tract-based spatial statistics (TBSS) approach. Finally, widespread WM and GM abnormalities were observed in RRMS patients. Moreover, the relationships between the depressive symptoms which can be measured by Hamilton depression rating scale (HAMD) as well as clinical disabilities measured by the expanded disability status scale (EDSS) and FA changes were listed. There was a positive relation between EDSS and the FA changes in the right inferior parietal lobule, while negative relation was located in the left anterior cingulate cortex and hippocampus. Also a positive relation between HAMD and FA changes was found in the right posterior middle cingulate gyrus, the right hippocampus, the left hypothalamus, the right precentral gyrus, and the posterior cingulate which demonstrated a link between the depressive symptoms and clinically relevant brain areas in RRMS patients.

1. Introduction

Multiple sclerosis (MS) is an autoimmune disease of the central nervous system (CNS) characterized by inflammation, demyelination, and neurodegeneration [1] and it is the most common cause of neurological disability among young adults, affecting approximately one in 1,000 individuals in Europe and North America [2]. Affective disorders are common and disabling conditions in MS. Clinically significant depression can affect up to 50% of patients with MS over the course of their lifetime and it is associated with an increased morbidity and mortality [3]. Also disability is a common symptom in MS patients [4]. The factors responsible for mood disturbances in MS are still controversial: a psychological reaction to a progressively disabling and unpredictable disease may be a relevant contributor while reactive mechanisms alone are probably not sufficient to account for the high prevalence and wide spectrum of depression.

Brain magnetic resonance imaging (MRI) lesions are highly associated with depression in MS [5, 6]. Neuroimaging studies in patients with MS have revealed associations between brain abnormalities and depression. The study by Pujol et al. [7] using axial spin echo sequence investigated three major anatomic divisions (basal, medial, and lateral) of the frontotemporal WM. They found that depressive score was significantly correlated with lesion load (LL) of the left accurate fasciculus region; in particular lesions in this area accounted for 17% of depressive score variance. Another MRI study including 95 consecutive MS patients, of which 19% of the patients met the criteria for depression, reported that the severity of depression was correlated with right frontal

lobule and with right temporal brain atrophy; furthermore, T1 lesions in the superior parietal and superior frontal regions predicted depression in MS patients [8].

Ordinary MRI tests could sensitively display MS lesions; however they lack pathological specifications [9]. Researchers have proved that the concealing injuries existed in MS patients while the outcomes of ordinary MRI displayed normal [10] (i.e., the micropathology alteration exists and its DTI data changes also) [11, 12]. DTI enables the random diffusional motion of water molecules to be measured, thus providing metrics such as mean diffusivity (MD) and FA in order to allow quantification of the size and geometry of water-filled spaces [13] and provide complete pathology message of brain tissues. In the past few years, DTI studies have been widely applied to the CNS of MS and optical neuromyelitis, and they have demonstrated a powerful means to early diagnosis and patient's condition monitoring.

Previous DTI studies generally adopted region of interest based analysis which needs specially prior information. Considering that MS may involve wide range of axonal degeneration, the whole brain analysis may be an optical method and lead to improved sensitivity and specificity to the disease and its related clinical impairments. Methods on the structural changes of WM fiber tracts in current research are mainly including hand-painted region of interest (ROI), voxel-based analysis (VBA), and TBSS, in which VBA is the most common research method. But for the anisotropic larger DTI image space, the registration accuracy is not high by VBA method which will lead to a certain difference based on the research results for the DTI images when different researchers are in view of the same kind of neurological diseases. However, TBSS analysis method aims at the main problem of image space registration rate, modifying from the registration rate algorithm, and makes the registration rate improved. So we chose TBSS as the analysis method. TBSS, adopting skeletonized processing ideas, projects individual fiber bundle FA value onto average FA bundle skeleton templates and accomplishes the justification of different subject fabric without taking standardization and smoothing [14] and thus significantly improves group comparison fidelity.

In the present study, we aimed at exploring global microstructural changes in MS and defining which changes are particularly affected by the disease such as the EDSS and HAMD scores and inquiring the relationships between FA values and HAMD as well as EDSS.

2. Materials and Methods

2.1. Subjects. In this study, we recruited the 15 patients who suffered from RRMS and were treated in Dongzhimen hospital in-patient or out-patient department from January 2012 to November 2013. All patients were in line with the revised McDonald criteria [15] and classification standard. The inclusion criteria were (1) participants were in the remission stage, who had no acute attack and did not have an exacerbation of their MS during the last month; (2) they were not currently taking any glucocorticosteroid medication; (3) their medication and treatment had no obvious adjustment recently and all of them had no history of serious psychiatric illness or neurologic disease other than MS; (4) Chinese was the primary language of all the participants; (5) the right-handed subjects according to the modified Edinburgh Handedness Questionnaire [16] were included. Those participants who had contraindications to MRI, poor quality of the images acquired, or showed one or more gadolinium-enhancing lesions (GEL) on baseline MRI were excluded to avoid effects of edema and inflammation on DTI measures [17]. Fifteen age- and sex-matched right-handed healthy subjects were used as a control group.

2.2. Clinical Assessments. For every participant, sex, age, onset age, disease duration, first onset symptoms, and recurrent symptoms variables were obtained while healthy controls' age and gender were also collected. A single neurologist assessed patients' disability using the EDSS [18] at the day of the neuropsychological assessment. All subjects were clinically evaluated by means of HAMD by themselves and two highly trained doctors on the same day prior to scanning. In this study, we used the HAMD 24 version and the criteria were as follows: total score $t < 8$ was divided into normal, 8–20 might suffer from depression, 20–35 was a depressive patient certainly, and >35 suffered from the severe depression.

2.3. MRI Acquisition. In the study, high-resolution brain MRI was acquired by using 2 pulse sequences on a 3T Signa scanner (Verio, Siemens AG, Erlangen, Germany) with an 8-channel head coil. The following sequences were acquired in a single session: (1) functional EPI oriented parallel to the AC-PC line and covering the whole brain to obtain sagittal sequence (repetition time (TR) = 2,000 ms, echo time (TE) = 30 ms, matrix = 64 mm × 64 mm, and field of view (FOV) = 225 mm × 225 mm), 36 slices, 3.5 mm thick, and no gap; (2) 3D magnetization-prepared rapid acquisition gradient echo (MPRAGE) sequence with 176 coronary, 1 mm slices, and 0 mm gap (TR = 2,700 ms, TE = 2.97 ms, flip angle = 7°, matrix = 256 mm × 256 mm, FOV = 250 mm × 250 mm, and voxel size= 1 mm × 1 mm × 1 mm); (3) T2-weighted image with a fast-spin echo sequence in the axial plane (TR = 6,000 ms, TE = 94 ms, matrix = 320 mm × 320 mm, and FOV = 220 mm × 220 mm), 25 slices, 4 mm thick, and no gap; (4) T2-Flair weighted image (TR = 8,800 ms, TE = 82 ms, flip angle = 150°, matrix = 256 mm × 256 mm, and FOV = 240 mm × 240 mm). DTI data acquisition was acquired with an axial single-shot echo planar spin echo sequence with 30 gradient directions (TR = 18,000 ms, TE = 94 ms, matrix = 160 mm × 160 mm, FOV = 256 mm × 256 mm, $b = 0$ and 1,000), 80 slices, 1.5 mm thick, and no gap. Image data processing was performed on a Linux workstation using Jim 5.0 software (Xinapse System, Leicester, UK; http://www.xinapse.com/), the Functional MRI of the Brain (FMRIB) software library (FSL) 4.1 package (FMRIB Image Analysis Group, Oxford, UK; http://www.fmrib.ox.ac.uk/fsl/), MATLAB 7.0 (MathWorks, Natick, Massachusetts, USA), and the Statistical Parametric Mapping 8 (SPM8) software (Wellcome Department of Cognitive Neurology, London, UK; http://www.fil.ion.ucl.ac.uk/spm/).

2.4. DTI Analysis. Diffusion data were preprocessed and analyzed using tools from the Oxford University Centre for FMRIB software library (FSL version 4.1). First, the b0 image of each subject was skull-stripped using the brain extraction tool. The data was corrected for subject motion and eddy-current induced geometrical distortions, and the diffusion sensitizing gradients ("bvecs") were rotated to correct for motion. Using FDT, the diffusion tensor model was fit to the data, from which FA images were calculated.

For TBSS, all subjects' FA data was registered to a common space (the FA158 MNI space template) using a combination of affine and nonlinear registration. A mean FA image was created and eroded to a skeleton and threshold at FA > 0.25. Each subject's aligned FA data was then projected onto this skeleton and the resulting alignment-invariant representation of the central trajectory of WM pathways was used for voxel-wise statistical analysis (Randomize, 5000 permutations). The contrast TBI < controls was examined using threshold free cluster enhancement (TFCE), with correction for multiple comparisons at $P < 0.05$.

2.5. Statistical Analysis. The Statistical Package of Social Sciences (17.0; SPSS Inc., Chicago, IL) software was used to carry out the statistical analysis. All values were reported as mean ± standard deviation (SD) or median (range) as appropriate. Differences between groups were tested using paired t-test for continuous and categorical variables, respectively. Correlations among global DTI measures and between global MRI values and clinical scores (EDSS and HAMD) were analyzed by univariate analysis (Pearson's correlation coefficient) after correction for age, and results corrected for multiple comparisons were needed.

3. Results

3.1. Demographic and Clinical Characteristics. In our study, fifteen patients (4 males and 11 females) were obtained according to the inclusion and exclusion criteria, who were aged from 19 to 57 years (37.53 ± 11.57). The disease duration of these patients ranged from 2 to 34 years (7.27 ± 8.55), onset age was from 13 to 53 years (30 ± 11.62), and the median EDSS score was 2 (range from 0 to 4). We also recruited 15 sex- and age-matched healthy volunteers who were aged from 23 to 60 years (36.67 ± 12.60) and had no history of physical illness or psychiatric disorder, and their nervous system examination was normal as the control group. A paired t-test was served to assess between-group differences of age between controls and patients ($P = 0.407 > 0.05$).

3.2. Clinical Rating Scales. In our research, patients and healthy controls (HC) were valued clinically by EDSS and HAMD. EDSS scores in patients ranged from 0 to 4 (1.73 ± 1.36), and in HC EDSS scores were all 0. HAMD scores in patients were from 1 to 35 (12.80 ± 11.620), while in HC they were from 0 to 14 (5.07 ± 3.918). Our study showed that there was a significant difference in HAMD score ($P = 0.046 < 0.05$) between patients and HC. And among the 15 patients there were 9 people whose HAMD score was greater than or equal to 8, accounting for 60%.

3.3. TBSS Analysis. Quantitative comparison for TBSS analysis demonstrated widespread statistically significant differences in FA values ($P < 0.05$, corrected for multiple comparisons), and FA values in all patients were lower compared with control subjects. Areas of reduced FA were seen widely in the GM and WM, such as the frontal lobe, limbic system, occipital lobe, temporal lobe, and parietal lobe. In particular, the main differences were located in bilateral corpus callosum, inferior parietal lobule, precentral gyrus, postcentral gyrus, superior frontal gyrus, cingulate gyrus, cerebellar lingual, declive, culmen, fastigium, dentate nucleus, parahippocampal gyrus, hippocampus, precuneus, basal ganglia, hypothalamus, insula, thalamus, fusiform gyrus, superior and transverse temporal gyrus, and the left middle temporal gyrus. Regional increases in the FA values of patients were not found. Compared with HC, the main lesions of the reduced FA value which has statistical differences and voxel were listed in Tables 1 and 2.

3.4. Correlation between Diffusion Parameters (FA) and Clinical Scores. Significant correlations were found between FA and EDSS in some lesions of WM and GM: the right inferior parietal lobule of WM ($r = 0.6307$, $P = 0.0117$), the left anterior cingulate ($r = -0.5505$, $P = 0.0335$), and hippocampus ($r = -0.5143$, $P = 0.0498$) of GM.

We also found the significant correlations between FA and HAMD in some lesions of WM and GM: the right posterior middle cingulate gyrus ($r = 0.6265$, $P = 0.0124$), hippocampus ($r = 0.5742$, $P = 0.0252$), and the left hypothalamus ($r = 0.5357$, $P = 0.0396$) of GM; the right precentral gyrus ($r = 0.6575$, $P = 0.0077$), cingulate gyrus ($r = -0.5959$, $P = 0.091$), and posterior cingulate ($r = 0.5742$, $P = 0.0258$) of WM.

R statistics (http://www.r-project.org/) analysis providing Spearman correlation coefficients values and their statistical significance were reported in Table 3 and shown in Figures 1 and 2.

4. Discussion

In our work, the patients' onset age was from 13 to 53 years and the sex ratio (female to male) was 2.75. This result suggested that MS tends to appear in the young and middle aged females which was consistent with most of the previous studies [19, 20]. The statistical difference of HAMD score ($P = 0.046 < 0.05$) between patients and HC was obvious, and among the 15 patients there were 9 people whose HAMD score was greater than or equal to 8, accounting for 60%. This result indicated that MS patients had a high incidence of depressive symptoms which was supported by the previous literature study [21].

DTI, as a new technology, which developed on the basis of diffusion weighted imaging (DWI) and could display brain WM fiber bundle and its direction in vivo noninvasively, is mainly used to evaluate the structural integrity of the microstructure, water molecules isotropic and anisotropic diffusion movement, and so forth. The results of DTI manifested the damage lesions mainly by the measures of FA values

Table 1: The areas of FA value significantly reduced in GM by TBSS analysis.

		Talairach			t value	V mm^3
		X	Y	Z		
Limbic system						
ACG	L	−3	31	15	3.846	65
BA24	R	3	26	19	5.182	159
ACG	L	−3	4	−6	3.543	44
BA25	R	7	16	−8	3.238	45
PCG	L	14	−50	8	3.135	122
BA29/30	R	−5	−60	9	2.002	39
MCG	L	−20	−16	38	2.999	113
BA24	R	18	−3	45	4.299	250
PMCG	L	−18	−43	28	3.307	62
BA31	R	19	−43	37	4.761	102
Amygdala	L	−19	−6	−19	3.355	48
	R	19	−6	−18	2.113	81
Hippocampus	L	−30	−36	−6	2.948	35
	R	33	−14	−18	3.682	97
Subcortical						
Putamen	L	−22	−9	9	4.632	217
	R	23	−7	11	3.981	200
Thalamus	L	−5	−9	13	3.947	143
Cerebellum						
CL	L	−4	−46	−15	4.041	60
	R	3	−48	−18	2.968	32
Culmen	L	−1	−54	−14	4.073	1204
	R	14	−41	−18	4.317	894
Declive	L	−1	−55	−14	3.875	363
	R	3	−55	−11	4.160	152

and decreased FA values could indicate a result of demyelination processes [22]. In the present study, we found that all the patients presented attenuated FA values when compared with HC. Similar results could be seen in some recent studies [23, 24]. Our data also confirmed that abnormalities in all the patients involved both WM and GM damage, which was consistent with many researches [13, 25, 26]. And our imaging data indicated that the lesions in WM of patients were mainly located in bilateral frontal lobe, limbic lobe, parietal lobe, occipital lobe, temporal lobe, corpus callosum, and sublobar while in GM the numerous lesions were primarily located in the limbic, sublobar, and cerebellum. In some previous researches, lesion was seen not only in the neocortex (especially in the cingulate cortex) [25, 27] but also in the GM of the thalamus, hypothalamus, cerebellum [27], basal ganglia [27, 28], and hippocampus [27, 29]. Audoin et al. [30] have reported that GM atrophy is associated with the bilateral insula, orbitofrontal cortices, internal and inferior temporal regions, thalamus, caudate nuclei, lenticular nuclei, cerebellum, and the posterior cingulate cortex. According to our result, it was roughly consistent with these previous studies.

However, most previous works adopted regional analysis, studying only certain parts of the brain, such as the normal appearing WM (NAWM) and GM (NAGM) [31], or the cerebellum [32], thalamus [33], and corpus callosum [34, 35]. Different from these reports, we studied WM and GM of the whole brain to find out the lesions by using a relatively new analysis method—TBSS. Hence, our research showed wider range of the lesions and this study could more fully state the distribution characteristics of the lesion site in the patients' brain DTI.

In this work, we adopted HAMD as evaluation index of psychological function and the relationships between FA value of the lesions in WM and GM of the entire brain and the HAMD scores in patients were explored. We investigated that HAMD scores were positively correlated with FA values in the left hypothalamus, right posterior middle cingulate gyrus and hippocampus of GM, the right precentral gyrus, and posterior cingulate of WM. These results told us that depressive symptoms were mainly negatively associated with the degree of demyelinating lesions in limbic system and frontal lobe, which had been reported in the previous paper [36]. Gobbi et al. [37] reported that depression in MS is linked to the atrophy of cortical regions located in the bilateral frontal lobes. Feinstein et al. [31] found that depressed subjects had a higher hypointense lesion volume in the right medial inferior frontal region, while having a smaller NAWM

Table 2: The areas of FA value significantly reduced in WM by TBSS analysis.

		Talairach			t value	V mm^3
		X	Y	Z		
Limbic system						
ACG	L	−7	24	−4	4.655	158
BA24	R	15	18	23	4.275	318
CG	L	−15	−33	35	5.154	1561
	R	19	−28	34	4.884	1798
PHG	L	−22	−18	−13	4.989	663
BA28/36	R	19	−41	2	5.884	654
PCG	L	−11	−56	6	2.974	125
BA29/30	R	14	−53	14	4.149	253
Subcortical						
	IH	−1	−16	24	2.889	63
CC	L	−3	13	20	3.917	1180
	R	13	−29	25	6.924	1068
Insula	L	−38	−43	20	3.899	123
BA13	R	39	−41	19	4.562	107
Frontal lobe						
CG	L	−17	15	36	3.727	38
PrG	L	−25	−17	50	2.299	30
BA4	R	37	−10	26	2.836	55
CC	L	−11	20	18	3.835	207
	R	13	19	20	3.922	146
Parietal						
IPL	L	−42	−42	25	3.559	135
	R	38	−42	26	4.286	110
Precuneus	L	−21	−59	32	4.402	435
BA31	R	19	−42	44	5.347	271

BA: Brodmann area; ACG: anterior cingulate gyrus; CG: cingulate gyrus; PCG: posterior cingulate gyrus; MCG: middle cingulate gyrus; PMCG: posterior middle cingulate gyrus; CC: corpus callosum; IPL: inferior parietal lobule; PrG: precentral gyrus; DLPFC: dorsolateral prefrontal cortex; AG: angular gyrus; CL: cerebellar lingual; IH: interhemispheric; PHG: parahippocampal gyrus.

Table 3: Significant correlations (Spearman correlation coefficients) between diffusion parameters (FA) and clinical scores.

CRS and correlated lesions		R value	P value
EDSS (GM)			
ACC	L	−0.5505*	0.0335
Hippocampus	L	−0.5143*	0.0498
EDSS (WM)			
IPL		0.6307*	0.0117
HAMD (GM)			
pMCC	R	0.6265*	0.0124
Hippocampus	R	0.5742*	0.0252
Hypothalamus	L	0.5357*	0.0396
HAMD (WM)			
PrG	R	0.6575*	0.0077
CG	R	−0.5959	0.0910
PCC	R	0.5724*	0.0258

*Significant correlation, $P < 0.05$.
R: right, L: left, CRS: clinical rating scales, ACC: anterior cingulate cortex, IPL: inferior parietal lobule, pMCC: posterior middle cingulate cortex, PrG: precentral gyrus, CG: cingulate gyrus, and PCC: posterior cingulate cortex.

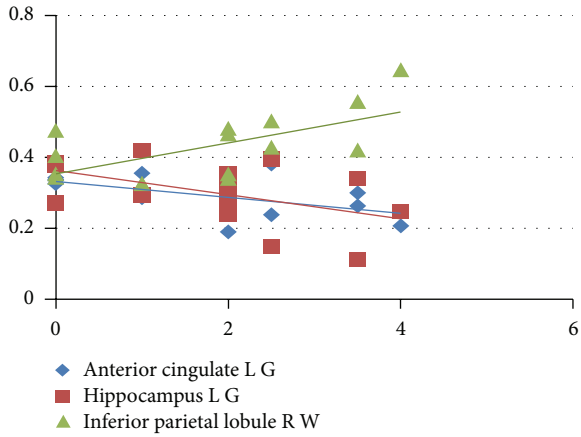

Figure 1: The correlation between EDSS and MRI lesion in GM and WM.

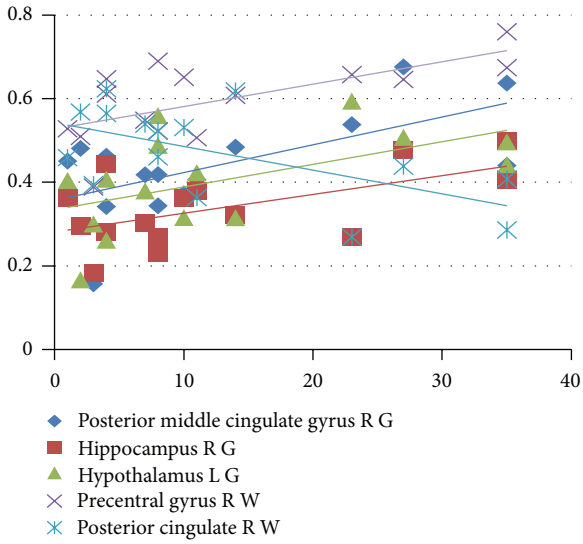

Figure 2: The correlation between HAMD and MRI lesion in GM and WM. R: right, L: left, G: GM, and W: WM.

volume in the left superior frontal region and lower FA in the left anterior temporal NAWM and NAGM regions, respectively. The cause may be that frontal lobe and limbic system are relevant to human's affect, memory, and learning. Once these functions defected, depression would occur in patients. Besides, we also found the negative correlations between FA and HAMD in cingulate gyrus, which was never found before. The mechanism is unknown, and the ongoing compensatory cerebral process at work in the MS brain attempting to maintain an euthymic state which was found by functional MRI (fMRI) [38] may be correlated with it.

EDSS is regarded as the evaluation index of the neurologic deficits and many papers have studied the relationship between FA value of the lesions and EDSS score. Some suggested that there was no correlation [33, 39, 40], while some showed that there was a positive correlation between them: EDSS was positively correlated with FA value of the normal appear thalamus ($r = 0.66$, $P = 0.045$) [41], caudate ($r = 0.444$, $P < 0.01$), and thalamus ($r = 0.362$, $P < 0.05$) [42] and was slightly negatively correlated with the atrophy of the right cerebellum ($r = -0.37$, $P = 0.0027$) [30]. However, one paper showed that it was strongly negatively associated with some lesions ($r = -0.82$, $P = 0.013$) [23]. But the cause of the negative correlation between EDSS and the degree of demyelination still needs further investigations. For the pathological changes in this relationship, according to Tedeschi et al. [43] and Hofstetter et al. [44], GM atrophy is associated with MS clinical disability. Routinely detectable cortical lesions are related to physical disability [45]. And Ciccarelli et al. [46] have reported that, in patients with RRMS, there was a strong correlation between EDSS score and FA in both supratentorial and infratentorial NAWM. Gorgoraptis et al. [39] found that smaller paracentral cortex volume was associated with worse walking ability, as measured by the TWT. One research showed that either the NAWM FA or the GM volume in each of these regions correlated with disability [47, 48]. Studies from DTI features of RRMS patients show that GM atrophy is a better indicator of disability progression than WM atrophy or accumulation of lesion burden [49–52]. In our study, EDSS is strongly correlated with FA value in the right inferior parietal lobule of WM positively and the left anterior cingulate and hippocampus of GM negatively in patients. Anterior cingulate cortex (ACC), including Brodmann 24, 25, and 32 area, which is located in the medial area of frontal lobe, can monitor the ongoing goal orientation behavior, provide signals in response to conflict or mistakes, and allocate the attentive resources effectively in related brain regions according to the requirements of the current task processing, and therefore it may be a senior regulatory structure in the executive function neural network [53], while hippocampus is responsible for learning and memory. Considering the functions of the damage regions in human, we all agreed that once these functions disappear this may lead to clinical disability in patients with MS.

However, our study has some limitations. First, this research only recruited the MS patients who were in remission and did not include patients who were in the acute stage as a control group for the related pathology study. Second, we conducted a cross-sectional study only, not for long-time follow-up observations. Third, in our work some appearances cannot be explained just with our present knowledge and findings. For instance, EDSS was negatively correlated with the degree of demyelination in the right inferior parietal lobule of WM and the further causes of the positive relationship between HAMD and FA in the lesions. For further study, we will expand the scope of the study population, conduct longitudinal observation on the basis of the study, and further analyze the relationships between the lesions and clinical scores.

5. Conclusions

In conclusion, our study used TBSS analysis method for the whole brain DTI of RRMS patients who were in remission and a large amount of information was provided for multiple areas of the brain GM and WM in pathological changes. The characteristics of the various lesion areas and

the relationships between the clinical scores of MS patients were discussed in this paper, providing the possible mechanisms for the pathogenesis of MS. In addition, we had shown that GM damage could explain clinical depression and disability better than WM. These findings were important for our understanding of MS and for future clinical trial design. And TBSS can be useful in future studies with other MS patient samples to provide an unbiased localization of damage and generate location-specific hypotheses.

Conflict of Interests

There are no competing interests.

Authors' Contribution

Yujuan Shen and Fangyuan Cui contributed equally to this work.

Acknowledgments

This study was supported by the National Natural Science Foundation of China (Grant no. 81071217, no. 81371630), the Fundamental Research Funds for the Central Universities, the Beijing Nova Program (Grant no. Z111101054511116), 2011 Beijing University of Chinese Medicine subject project independently (Grant no. 2011JYBZZJS-014), and the Beijing Natural Science Foundation (Grant no. 4122082).

References

[1] E. M. Frohman, M. K. Racke, and C. S. Raine, "Medical progress: multiple sclerosis—the plaque and its pathogenesis," *New England Journal of Medicine*, vol. 354, no. 9, pp. 942–955, 2006.

[2] M. Pugliatti, S. Sotgiu, and G. Rosati, "The worldwide prevalence of multiple sclerosis," *Clinical Neurology and Neurosurgery*, vol. 104, no. 3, pp. 182–191, 2002.

[3] A. Feinstein, "Multiple sclerosis and depression," *Multiple Sclerosis*, vol. 17, no. 11, pp. 1276–1281, 2011.

[4] M. Coenen, B. Basedow-Rajwich, N. König, J. Kesselring, and A. Cieza, "Functioning and disability in multiple sclerosis from the patient perspective," *Chronic Illness*, vol. 7, no. 4, pp. 291–310, 2011.

[5] R. Bakshi, D. Czarnecki, Z. A. Shaikh et al., "Brain MRI lesions and atrophy are related to depression in multiple sclerosis," *NeuroReport*, vol. 11, no. 6, pp. 1153–1158, 2000.

[6] A. Feinstein, "Neuropsychiatric syndromes associated with multiple sclerosis," *Journal of Neurology*, vol. 254, no. 2, pp. 73–76, 2007.

[7] J. Pujol, J. Bello, J. Deus, J. L. Marti-Vilalta, and A. Capdevila, "Lesions in the left arcuate fasciculus region and depressive symptoms in multiple sclerosis," *Neurology*, vol. 49, no. 4, pp. 1105–1110, 1997.

[8] M. Zorzon, R. de Masi, D. Nasuelli et al., "Depression and anxiety in multiple sclerosis. A clinical and MRI study in 95 subjects," *Journal of Neurology*, vol. 248, no. 5, pp. 416–421, 2001.

[9] Y. Miki, R. I. Grossman, J. K. Udupa et al., "Relapsing-remitting multiple sclerosis: longitudinal analysis of MR images—lack of correlation between changes in T2 lesion volume and clinical findings," *Radiology*, vol. 213, no. 2, pp. 395–399, 1999.

[10] Y. Ge, R. I. Grossman, J. K. Udupa, J. S. Babb, L. J. Mannon, and J. C. McGowan, "Magnetization transfer ratio histogram analysis of normal-appearing gray matter and normal-appearing white matter in multiple sclerosis," *Journal of Computer Assisted Tomography*, vol. 26, no. 1, pp. 62–68, 2002.

[11] W. Rashid, A. Hadjiprocopis, C. M. Griffin et al., "Diffusion tensor imaging of early relapsing-remitting multiple sclerosis with histogram analysis using automated segmentation and brain volume correction," *Multiple Sclerosis*, vol. 10, no. 1, pp. 9–15, 2004.

[12] S. D. Roosendaal, J. J. G. Geurts, H. Vrenken et al., "Regional DTI differences in multiple sclerosis patients," *NeuroImage*, vol. 44, no. 4, pp. 1397–1403, 2009.

[13] M. Rovaris, F. Agosta, E. Pagani, and M. Filippi, "Diffusion tensor MR imaging," *Neuroimaging Clinics of North America*, vol. 19, no. 1, pp. 37–43, 2009.

[14] D. K. Jones, X. A. Chitnis, D. Job et al., "What happens when nine different group analyze the same DT-MRI data set using voxel-based methods," *Proceedings of the International Society for Magnetic Resonance in Medicin*, vol. 15, article 74, 2007.

[15] C. H. Polman, S. C. Reingold, and G. Edan, "Diagnostic criteria for multiple sclerosis: 2005 revisions to the 'McDonald Criteria'," *Annals of Neurology*, vol. 58, pp. 840–846, 2005.

[16] R. C. Oldfield, "The assessment and analysis of handedness: the Edinburgh inventory," *Neuropsychologia*, vol. 9, no. 1, pp. 97–113, 1971.

[17] E. Sbardella, N. Petsas, F. Tona et al., "Assessing the correlation between grey and white matter damage with motor and cognitive impairment in multiple sclerosis patients," *PLoS ONE*, vol. 8, Article ID e63250, 2013.

[18] J. F. Kurtzke, "Rating neurologic impairment in multiple sclerosis: an expanded disability status scale (EDSS)," *Neurology*, vol. 33, no. 11, pp. 1444–1452, 1983.

[19] K. Jefferies, "The neuropsychiatry of multiple sclerosis," *Advances in Psychiatric Treatment*, vol. 12, no. 3, pp. 214–220, 2006.

[20] B. Reipert, "Multiple sclerosis: a short review of the disease and its differences between men and women," *Journal of Men's Health and Gender*, vol. 1, no. 4, pp. 334–340, 2004.

[21] K. Gottberg, U. Einarsson, S. Fredrikson, L. Von Koch, and L. W. Holmqvist, "A population-based study of depressive symptoms in multiple sclerosis in Stockholm county: association with functioning and sense of coherence," *Journal of Neurology, Neurosurgery and Psychiatry*, vol. 78, no. 1, pp. 60–65, 2007.

[22] S.-K. Song, S.-W. Sun, W.-K. Ju, S.-J. Lin, A. H. Cross, and A. H. Neufeld, "Diffusion tensor imaging detects and differentiates axon and myelin degeneration in mouse optic nerve after retinal ischemia," *NeuroImage*, vol. 20, no. 3, pp. 1714–1722, 2003.

[23] M. Onu, A. Roceanu, U. Sboto-Frankenstein et al., "Diffusion abnormality maps in demyelinating disease: correlations with clinical scores," *European Journal of Radiology*, vol. 81, no. 3, pp. e386–e391, 2012.

[24] K. Erb, G. Bohner, L. Harms et al., "Olfactory function in patients with multiple sclerosis: a diffusion tensor imaging study," *Journal of the Neurological Sciences*, vol. 316, no. 1-2, pp. 56–60, 2012.

[25] M. Filippi and M. A. Rocca, "MR imaging of gray matter involvement in multiple sclerosis: implications for understanding disease pathophysiology and monitoring treatment efficacy," *American Journal of Neuroradiology*, vol. 31, no. 7, pp. 1171–1177, 2010.

[26] A. Kutzelnigg, C. F. Lucchinetti, C. Stadelmann et al., "Cortical demyelination and diffuse white matter injury in multiple sclerosis," *Brain*, vol. 128, no. 11, pp. 2705–2712, 2005.

[27] J. J. Geurts and F. Barkhof, "Grey matter pathology in multiple sclerosis," *The Lancet Neurology*, vol. 7, no. 9, pp. 841–851, 2008.

[28] I. E. C. Ormerod, D. H. Miller, W. I. McDonald et al., "The role of NMR imaging in the assessment of multiple sclerosis and isolated neurological lesions. A quantitative study," *Brain*, vol. 110, no. 6, pp. 1579–1616, 1987.

[29] S. D. Roosendaal, B. Moraal, H. Vrenken et al., "In vivo MR imaging of hippocampal lesions in multiple sclerosis," *Journal of Magnetic Resonance Imaging*, vol. 27, no. 4, pp. 726–731, 2008.

[30] B. Audoin, W. Zaaraoui, F. Reuter et al., "Atrophy mainly affects the limbic system and the deep grey matter at the first stage of multiple sclerosis," *Journal of Neurology, Neurosurgery and Psychiatry*, vol. 81, no. 6, pp. 690–695, 2010.

[31] A. Feinstein, P. O'Connor, N. Akbar, L. Moradzadeh, C. J. M. Scott, and N. J. Lobaugh, "Diffusion tensor imaging abnormalities in depressed multiple sclerosis patients," *Multiple Sclerosis*, vol. 16, no. 2, pp. 189–196, 2010.

[32] V. M. Anderson, C. A. M. Wheeler-Kingshott, K. Abdel-Aziz et al., "A comprehensive assessment of cerebellar damage in multiple sclerosis using diffusion tractography and volumetric analysis," *Multiple Sclerosis*, vol. 17, no. 9, pp. 1079–1087, 2011.

[33] F. Tovar-Moll, I. E. Evangelou, A. W. Chiu et al., "Thalamic involvement and its impact on clinical disability in patients with multiple sclerosis: a diffusion tensor imaging study at 3T," *American Journal of Neuroradiology*, vol. 30, no. 7, pp. 1380–1386, 2009.

[34] Y. Zhou, M. P. Milham, X.-N. Zuo et al., "Functional homotopic changes in multiple sclerosis with resting-state functional MR imaging," *American Journal of Neuroradiology*, vol. 34, pp. 1180–1187, 2013.

[35] T. Sigal, M. Shmuel, D. Mark, H. Gil, and A. Anat, "Diffusion tensor imaging of corpus callosum integrity in multiple sclerosis: correlation with disease variables," *Journal of Neuroimaging*, vol. 22, no. 1, pp. 33–37, 2012.

[36] P. V. Rabins, B. R. Brooks, and P. O'Donnell, "Structural brain correlates of emotional disorder in multiple sclerosis," *Brain*, vol. 109, no. 4, pp. 585–597, 1986.

[37] C. Gobbi, M. Rocca, and G. Riccitelli, "Influence of the topography of brain damage on depression and fatigue in patients with multiple sclerosis," *Multiple Sclerosis*, vol. 20, no. 2, pp. 192–201.

[38] L. Passamonti, A. Cerasa, M. Liguori et al., "Neurobiological mechanisms underlying emotional processing in relapsing-remitting multiple sclerosis," *Brain*, vol. 132, no. 12, pp. 3380–3391, 2009.

[39] N. Gorgoraptis, C. A. M. Wheeler-Kingshott, T. M. Jenkins et al., "Combining tractography and cortical measures to test system-specific hypotheses in multiple sclerosis," *Multiple Sclerosis*, vol. 16, no. 5, pp. 555–565, 2010.

[40] S. Temel, H. D. Kekligkoglu, G. Vural et al., "Diffusion tensor magnetic resonance imaging in patients with multiple sclerosis and its relationship with disability," *Neuroradiology Journal*, vol. 26, pp. 3–17, 2013.

[41] K. M. Hasan, I. S. Walimuni, H. Abid et al., "Multimodal quantitative magnetic resonance imaging of thalamic development and aging across the human lifespan: implications to neurodegeneration in multiple sclerosis," *Journal of Neuroscience*, vol. 31, no. 46, pp. 16826–16832, 2011.

[42] S. Hannoun, F. Durand-Dubief, C. Confavreux et al., "Diffusion tensor-MRI evidence for extra-axonal neuronal degeneration in caudate and thalamic nuclei of patients with multiple sclerosis," *American Journal of Neuroradiology*, vol. 8, pp. 1363–1368, 2012.

[43] G. Tedeschi, L. Lavorgna, P. Russo et al., "Brain atrophy and lesion load in a large population of patients with multiple sclerosis," *Neurology*, vol. 65, no. 2, pp. 280–285, 2005.

[44] L. Hofstetter, Y. Naegelin, L. Filli et al., "Progression in disability and regional grey matter atrophy in Relapsing-remitting multiple sclerosis," *Multiple Sclerosis*, 2013.

[45] A. Mike, B. I. Glanz, P. Hildenbrand et al., "Identification and clinical impact of multiple sclerosis cortical lesions as assessed by routine 3T MR imaging," *American Journal of Neuroradiology*, vol. 32, no. 3, pp. 515–521, 2011.

[46] O. Ciccarelli, D. J. Werring, C. A. M. Wheeler-Kingshott et al., "Investigation of MS normal-appearing brain using diffusion tensor MRI with clinical correlations," *Neurology*, vol. 56, no. 7, pp. 926–933, 2001.

[47] L. V. Zollinger, T. H. Kim, K. Hill, E. K. Jeong, and J. W. Rose, "Using diffusion tensor imaging and immunofluorescent assay to evaluate the pathology of multiple sclerosis," *Journal of Magnetic Resonance Imaging*, vol. 33, no. 3, pp. 557–564, 2011.

[48] A. Giorgio, J. Palace, H. Johansen-Berg et al., "Relationships of brain white matter microstructure with clinical and MR measures in relapsing-remitting multiple sclerosis," *Journal of Magnetic Resonance Imaging*, vol. 31, no. 2, pp. 309–316, 2010.

[49] E. Fisher, J.-C. Lee, K. Nakamura, and R. A. Rudick, "Gray matter atrophy in multiple sclerosis: a longitudinal study," *Annals of Neurology*, vol. 64, no. 3, pp. 255–265, 2008.

[50] L. K. Fisniku, D. T. Chard, J. S. Jackson et al., "Gray matter atrophy is related to long-term disability in multiple sclerosis," *Annals of Neurology*, vol. 64, no. 3, pp. 247–254, 2008.

[51] D. Horakova, J. L. Cox, E. Havrdova et al., "Evolution of different MRI measures in patients with active relapsing-remitting multiple sclerosis over 2 and 5 years: a case-control study," *Journal of Neurology, Neurosurgery and Psychiatry*, vol. 79, no. 4, pp. 407–414, 2008.

[52] G. Tedeschi, D. Dinacci, M. Comerci et al., "Brain atrophy evolution and lesion load accrual in multiple sclerosis: a 2-year follow-up study," *Multiple Sclerosis*, vol. 15, no. 2, pp. 204–211, 2009.

[53] M. S. Gazzaniga, R. B. Ivry, and G. R. Mangun, *Cognitive Neuroscience: The Biology of the Mind*, W. W. Norton & Company, New York, NY, USA, 2nd edition, 2002.

Hindawi Publishing Corporation
BioMed Research International
Volume 2014, Article ID 920902, 7 pages
http://dx.doi.org/10.1155/2014/920902

Research Article

Selective Changes of Resting-State Brain Oscillations in aMCI: An fMRI Study Using ALFF

Zhilian Zhao,[1,2] Jie Lu,[1,2] Xiuqin Jia,[1,2] Wang Chao,[1,2] Ying Han,[3] Jianping Jia,[3] and Kuncheng Li[1,2]

[1] *Department of Radiology, Xuanwu Hospital of Capital Medical University, Beijing 100053, China*
[2] *Beijing Key Laboratory of Magnetic Resonance Imaging and Brain Informatics, Beijing 100053, China*
[3] *Department of Neurology, Xuanwu Hospital of Capital Medical University, Beijing 100053, China*

Correspondence should be addressed to Kuncheng Li; kuncheng.li@gmail.com

Received 28 January 2014; Accepted 11 March 2014; Published 14 April 2014

Academic Editor: Lijun Bai

Mild cognitive impairment (MCI) refers to a transitional state between normal aging and dementia and is a syndrome with cognitive decline greater than expected for an individual's age and educational level. As a subtype of MCI, amnestic mild cognitive impairment (aMCI) most often leads to Alzheimer's disease. This study aims to elucidate the altered brain activation in patients with aMCI using resting-state functional magnetic resonance. We observed Frequency-dependent changes in the amplitude of low-frequency fluctuations in aMCI patients ($n = 20$), and normal subjects ($n = 18$). At the same time, we took gray matter volume as a covariate. We found that aMCI patients had decreased amplitude of low-frequency fluctuation signal in left superior temporal gyrus, right middle temporal gyrus, right inferior parietal lobe, and right postcentral gyrus compared to the control group. Specially, aMCI patients showed increased signal in left superior and middle frontal gyrus. Our results suggested that increased activation in frontal lobe of aMCI patients may indicate effective recruitment of compensatory brain resources. This finding and interpretation may lead to the better understanding of cognitive changes of aMCI.

1. Introduction

The concept of mild cognitive impairment (MCI) refers to subjects who experience cognitive impairments but who are not demented [1]. MCI is a syndrome with cognitive decline greater than expected for an individual's age and educational level but not interfering notably with activities of daily living. The prevalence of MCI is about 15% in adults older than 65 years and more than half of MCI patients progress to dementia within 5 years. The common outcome of nonamnestic MCI is frontotemporal dementia or dementia with Lewy bodies. Patients with the amnestic subtype of MCI (aMCI) have an annual conversion rate of 6–25% to Alzheimer's disease (AD). As such, aMCI has been regarded as a prodromal stage of AD [2–6]. Over the past decade, significant progress has been accomplished in our understanding of its epidemiology, risk factors, natural history, and treatment. Although there remain some controversies surrounding MCI, it is increasingly recognized that MCI should be handled as a clinically defined condition. Because the standard diagnostic procedure of aMCI primarily relies on neuropsychological examinations, there is strong demand to develop neuroimaging techniques as reliable surrogate MCI markers. Whereas structural MRI provides important diagnostic and prognostic information, fMRI remains promising as an imaging marker of MCI, including aMCI.

Recently, low-frequency fluctuations (LFF) fMRI has gained increased attention based on observations using fMRI approaches and direct current coupled electroencephalographic scalp recordings [7–9]. Spatially organized and temporally coherent fluctuations in the low-frequency range (0.01–0.1 Hz) have been at the center of attention, as the BOLD signal displays a spatial structure similar to task function-related activation [10–12].

Most studies of resting-state functional magnetic resonance imaging (fMRI) have applied the temporal correlation

in the time courses to study the functional connectivity between different brain regions. Biswal and coworkers have shown that spontaneous low-frequency (<0.08 Hz) fluctuation (LFF) is highly synchronous among motor cortices [10]. Recently, resting-state synchronization has also been investigated in patients [13–16] and in healthy subjects [17–19]. The power of (LFF) may also be used as a biomarker to assess cerebral spontaneous activity [20]. ALFF is defined as the total power within the frequency range between 0.01 and 0.1 Hz. Our study aims to evaluate the ALFF signal in reflecting cerebral physiological states in aMCI patients and healthy subjects. We evaluate whether the ALFF abnormalities in aMCI have similar distribution pattern as independent component analysis (ICA) approach [21]. Several studies had shown grey matter loss in aMCI or MCI [22–25] and regional brain atrophy may lead to artificial reduction in low-frequency fluctuation [26]. In order to directly test our hypothesis and improve the statistical strength, we took gray matter volume as a covariate.

2. Materials and Methods

2.1. Study Population. Thirty-eight right-handed subjects were recruited. Participants were divided into two groups based on their clinical profiles: twenty participants were classified as aMCI patients and the other eighteen as healthy controls. Patients were recruited from a memory clinic at the Department of Neurology and healthy controls were recruited from a community investigation of epidemiological research. Informed consent was approved by the Medical Research Ethics Committee of Xuanwu Hospital and obtained from all subjects. Prior to resting-state fMRI scanning, examination of each subject included medical history, neurological examination, informant interview, neuropsychological assessment 4 including mini-mental state examination (MMSE), clinical dementia rating (CDR), activity of daily living scale, Hachinski ischemic scale, Hamilton rating scale for depression, auditory verbal learning test (AVLT), structural MRI, and standard laboratory tests.

aMCI diagnosis was established according to the criteria for amnestic MCI [5, 6]. To be diagnosed as having MCI, patients had to fulfill the following criteria: (a) impaired memory performance on a normalized objective verbal memory test, (b) recent history of symptomatic worsening in memory, (c) normal or near-normal performance on global cognitive tests [mini-mental state examination (MMSE) score > 24] as well as on activities of daily living scale, (d) global rating of 0.5 on the CDR scale, with a score of at least 0.5 on the memory domain, and (e) absence of dementia. Stroke, psychiatric diseases, drug abuse, moderate to serious hypertension, and systematic diseases were ruled out. Memory complaints or neurological deficiencies were not observed in the healthy controls with normal conventional brain MR imaging and an MMSE score ≥ 28. Demographics and neuropsychological findings of aMCI patients and healthy elderly are shown in Table 1. Demographics of aMCI patients and healthy controls, including age, sex, and education years, were matched between the two groups.

Table 1: Demographics and neuropsychological findings of aMCI patients and healthy elderly.

	aMCI patient ($n = 20$)	Healthy elderly ($n = 18$)
Age	65.11 ± 9.92	66.81 ± 7.43
Female/male	12/8	10/8
Education (y)	11.84 ± 3.32	12.02 ± 2.93
MMSE	25.21 ± 2.24	29.31 ± 1.22
AVLT, learning A1	7.22 ± 1.73	3.95 ± 1.82
AVLT, learning A2	9.39 ± 2.73	5.15 ± 1.42
AVLT, learning A3	10.94 ± 2.15	6.05 ± 2.54
AVLT, delayed recall A4	11.33 ± 2.52	4.75 ± 3.51
AVLT, recognition A5	13.06 ± 1.80	7.80 ± 3.53
CDR	0.5	0

The age of participants was equally distributed between the two diagnostic groups ($t = 2.06$, $P = 0.57$, two-sample two-tailed t-test) with similar medians and ranges. However, the groups were significantly different with regard to MMSE scores and AVLT scores ($P < 0.001$, two-sample two-tailed t-test).

2.2. Data Acquisition. MRI data were collected on a 3T scanner (Siemens, Trio, Erlangen, Germany), with an eight-channel receiver coil. Subjects were instructed to keep their eyes closed and to refrain from initiating goal-directed, attention-demanding activity during the scanning sessions, and resting-state fMRI was acquired. fMRI was acquired using gradient echo planner imaging (EPI) for a 6 min and 20 s period, resulting in a total of 124 volumes (repetition time (TR)/echo time (TE) = 3000/30 ms, flip angle = 90°, field of view (FOV) = 256 × 256 mm^2, matrix size = 64 × 64, 28 slices, slice thickness = 4 mm, and 0 mm interslice gap). A T_1WI anatomical dataset was obtained from each subject using a magnetization-prepared rapid acquisition gradient echo sequence (TR/TE = 1900/2.2 ms, inversion time (TI) = 900 ms, flip angle = 9°, FOV = 256 × 256 mm^2, matrix size = 224 × 256, 176 slices, voxel size = 1 × 1 × 1 mm^3). According to the inclusion criteria, T_2WI and FLAIR scans were reviewed to exclude the presence of remarkable macroscopic brain abnormalities.

2.3. Voxel-Based Morphometry Data Processing. Structural MRI data analysis was performed using an optimized VBM protocol (http://dbm.neuro.uni-jena.de/vbm/) under SPM5 (http://www.fil.ion.ucl.ac.uk/spm/), which included slice timing, motion correction, spatial normalization, and smoothing.

Images were segmented into grey matter, white matter, and cerebral spinal fluid (CSF) [27]. The images were then normalized to the Montreal Neurological Institute (MNI) template, and then the parameters were applied to normalize individual T_1 images separately. The fully normalized images were once again segmented into grey matter, white matter, and CSF. The normalized and modulated white matter and

gray matter images were smoothed using a 4 mm × 4 mm × 4 mm full-width half-maximum (FWHM) Gaussian kernel for subsequent statistical analysis. Then, the grey matter volume of the aMCI patients and the normal controls was calculated. The result was also entered into the following statistical analysis to examine the effects of GM atrophy on the functional results.

2.4. Resting-State fMRI Data Processing and Statistics. Functional MRI data were processed using the statistical parametric mapping (SPM5, http://www.fil.ion.ucl.ac.uk/spm/), which included slice timing, motion correction, and spatial normalization. ALFF analysis was performed by using resting-state fMRI data analysis toolkit (http://resting-fmri.sourceforge.net/). The procedure for calculating the ALFF is similar to the previous studies [20, 28]. The filtered time series was transformed to a frequency domain with a fast Fourier transform (FFT) (parameters: taper percent = 0, FFT length = shortest) and the power spectrum was then obtained. The square root was thus calculated at each frequency of the power spectrum and the averaged square root was obtained across 0.01–0.08 Hz at each voxel. This averaged square root was taken as the ALFF. For standardization purposes, the ALFF of each voxel was divided by the global mean ALFF value within a brain mask, which was obtained from the intersection of the brain of all subjects' T_1 images. The analysis included the grey matter as a covariate. A two-sample t-test was performed to test the ALFF difference between aMCI patients and normal controls. Voxels with a corrected P value < 0.01 (single voxel threshold of $P < 0.05$ and cluster size 540 mm^3, using the AlphaSim program with parameters: FWHM = 8 mm, with mask) were considered significant.

3. Results

3.1. Demography and Neuropsychological Test. Demographic characteristics and neuropsychological scores were shown in Table 1. There were no significant differences between the two groups in gender, age, and years of education, but the MMSE and AVLT (auditory verbal learning test) scores were significantly different ($P < 0.05$) between the two groups.

3.2. Brain Regions of Decreased Gray Matter Volume between the Two Groups. To assess possible causes of reduced functional activity, we analyzed our data for structural differences between both study groups. The aMCI patients showed widespread reduction in gray matter volume in the right uncus, the bilateral inferior, superior, and middle frontal gyrus, the bilateral medial temporal gyrus, the left inferior temporal gyrus, the left superior temporal gyrus, the right superior parietal gyrus, and the left middle occipital gyrus ($P < 0.001$, corrected) (Figures 1 and 2, Table 2). Some of these areas did overlap with those regions found to be altered in the patient group using ALFF.

3.3. Whole Brain Functional Alteration Data: The Between-Group Differences. Figure 2 shows the statistical map resulting from comparison of the changes of ALFF in different brain areas in healthy elderly versus aMCI patients. ALFF was higher in controls than patients in left superior temporal gyrus, right middle temporal gyrus, right inferior parietal lobe, and right postcentral gyrus. ALFF was significantly higher in patients than controls in left superior, middle frontal gyrus (see Figure 2 and Table 3).

Table 2: Areas of gray matter loss in aMCI patients compared with healthy controls.

	Region	BA	Voxels	MNI			T-score
				x	y	z	
NC-MCI	Left MTG	35	23	−18	−27	−24	5.26
	Right MTG	30	14	15	−33	−12	4.05
	Left MOG	34	12	−9	−3	−24	3.93
	Right MFG	37	12	60	−45	−9	3.79
	Right uncus	44	12	63	6	21	3.75
	Left IFG	10	10	−30	51	−3	3.32
	Right SFG	22	14	60	6	3	3.26

*MTG: medial temporal gyrus; MOG: middle occipital gyrus; MFG: middle frontal gyrus; IFG: inferior frontal gyrus; SFG: superior frontal gyrus.

4. Discussion

In the current study, we reported abnormal ALFF in aMCI patients compared to healthy controls. ALFF was higher in controls than patients in the left superior temporal gyrus, right middle temporal gyrus, right inferior parietal lobe, and right postcentral gyrus. Patients had higher ALFF than controls in left superior, middle frontal gyrus. Thus, our data suggested that there are abnormalities in LFOs in aMCI patients. The current findings add to a literature suggesting abnormalities of neural synchrony in aMCI and extend these findings to the LFO domain.

The reduced LFO in the IPL and the temporal gyrus is consistent with previous studies of aMCI. More recently, functional imaging studies have suggested that memory processes are subserved by a set of distributed, large-scale neural networks. Specific regions of the default network are selectively vulnerable to early amyloid deposition in AD. The lateral parietal and temporoparietal areas are involved in the default network [29]. Using ICA, [21] found that right inferior parietal lobule exhibited decreased functional activity in aMCI compared to normal control, and [30] found reduced activity in the patient group in bilateral superior parietal lobes. Previous studies have demonstrated that some regions constitute a structurally and functionally connected neuronal network that supports the default function of the human brain. The IPL is one of the brain regions that constitute the major posterior extent of the default mode network (DMN). Reduced right IPL activity indicated impaired memory functional system in aMCI patients. Episodic memory function is severely affected in AD and is also the key early marker for prodromal stages such as MCI [31]. This may suggest that the aMCI is prodromal stage of AD.

Table 3: Resting-state activities in controls and aMCI patients (amplitude of low-frequency fluctuations).

Condition	Connected regions	BA	Cluster	t-score	Coordinates (MNI)		
NC-MCI	Left superior temporal gyrus	22	37	3.10	−45	−3	−3
				2.69	−45	6	−6
	Right middle temporal gyrus	21	16	2.85	60	−42	0
				2.67	63	−48	6
	Right inferior parietal lobe	40	16	2.577	51	−42	60
	Right postcentral gyrus	20		2.303	51	−33	60
	Right inferior parietal lobe	40		2.131	42	−45	57
MCI-NC	Left middle frontal gyrus	10	28	4.148	−36	57	−12
	Left superior frontal gyrus	11		3.577	−30	57	−3
				2.43	−24	63	−3

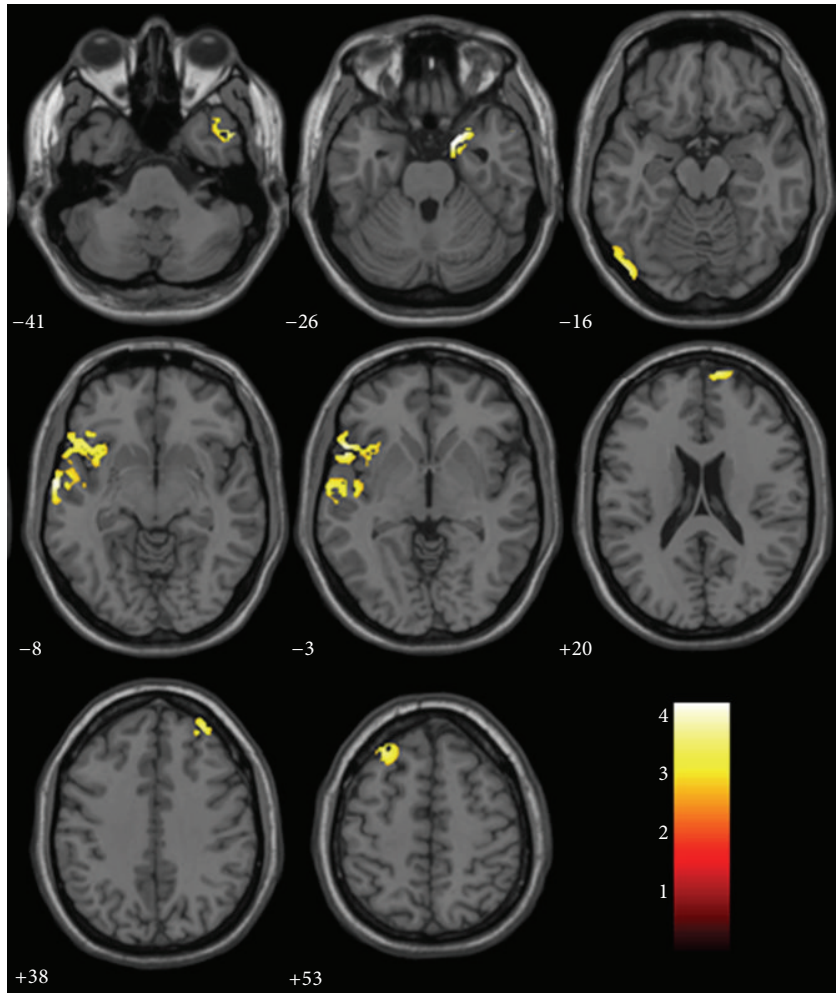

Figure 1: VBM analysis showed brain regions of significant reduction of gray matter volume in aMCI patients relative to controls on axial position images. Reader's right is subjects' right.

An interesting finding of the present study is that, in aMCI without motor clinical impairment, LFOs abnormalities occur also in the motor system, mainly in right postcentral gyrus. The abnormal change in motor system may resemble those described for the cognitive network. Recent evidence indicates that part of classical motor areas may have nonmotor cognitive functions in addition to the well-known motor functions [32]. It is well known that the parietal cortex, which has extensive connections with regions of the frontal lobes, where it sends rich sensory information for movement control, is involved in the elaboration of somatosensory inputs and in movement preparation and planning [33].

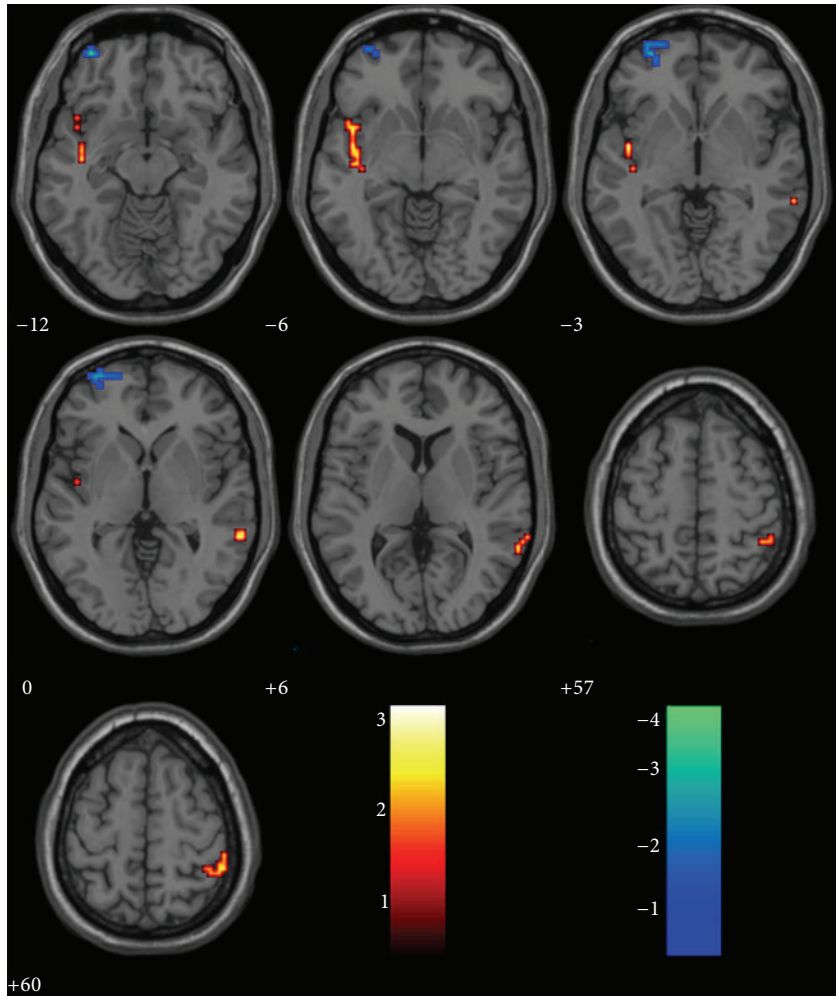

Figure 2: Decreased and increased activity in aMCI patients shown in axial projection compared to the healthy elder. Hot: NC-aMCI (decreased); winter: aMCI-NC (increased).

These results may suggest an overactivation of selected areas of the sensorimotor network. However, there may be other explanations that we have not known. More work needs to be done to study the role of the postcentral gyrus in the aMCI patients.

The areas of increased amplitude in patients are mainly located in left frontal regions previously associated with abnormal function in this disorder. The frontal cortices are key regions involved in human memory processing [21, 34]. This is consistent with the assumption that AD and MCI patients may be able to use additional neural resources in prefrontal regions to compensate for losses in cognitive function [21, 35, 36]. Critically, activity in this network of regions was correlated with the ability of the patients to perform the tasks accurately. Patients who had more activity in bilateral prefrontal areas were better able to perform tasks of semantic and episodic memory [35, 37]. However, it still remains unclear whether these alterations may be compensatory to maintain memory performance in the setting of early AD pathology or instead represent evidence of excitotoxicity and impending neuronal failure.

There were several limitations in the current study that need to be addressed. First, the education years among the aMCI subjects we selected were large, between 0 (illiteracy) and 19; this may have confounding effects on the results; in future studies we would group our subjects across their education with more aMCI patients. Second, the subjects were instructed to keep their eyes closed during the resting scan; subjects may have looked at something subconsciously and we did not obtain such behavioral data, or some subjects sleep during the examination. Previous studies have suggested that the alpha power is related to different resting conditions 13 [38, 39]. Future studies would benefit from the use of eye tracking or visual monitoring equipment during the resting-state session.

5. Conclusions

In conclusion, we have demonstrated ALFF differences in aMCI patients using functional MRI method. This resting-state fMRI study suggests that the abnormal spontaneous

activity of these regions may indicate the underlying pathophysiology of aMCI. Research is ongoing to determine if these early alterations will serve as sensitive predictors of clinical decline and, eventually, as markers of aMCI progress to AD.

Conflict of Interests

The authors declare that there is no conflict of interests regarding the publication of this paper.

Acknowledgment

This work was partially supported by the Natural Science Foundation of China, Grant nos. 30930029 and 30970823.

References

[1] H. H. Feldman and C. Jacova, "Mild cognitive impairment," *American Journal of Geriatric Psychiatry*, vol. 13, no. 8, pp. 645–655, 2005.

[2] D. A. Bennett, R. S. Wilson, J. A. Schneider et al., "Natural history of mild cognitive impairment in older persons," *Neurology*, vol. 59, no. 2, pp. 198–205, 2002.

[3] K. Blennow, M. J. de Leon, and H. Zetterberg, "Alzheimer's disease," *The Lancet*, vol. 368, no. 9533, pp. 387–403, 2006.

[4] C. DeCarli, "Mild cognitive impairment: prevalence, prognosis, aetiology, and treatment," *The Lancet Neurology*, vol. 2, no. 1, pp. 15–21, 2003.

[5] R. C. Petersen, G. E. Smith, S. C. Waring, R. J. Ivnik, E. G. Tangalos, and E. Kokmen, "Mild cognitive impairment: clinical characterization and outcome," *Archives of Neurology*, vol. 56, no. 3, pp. 303–308, 1999.

[6] R. C. Petersen, R. Doody, A. Kurz et al., "Current concepts in mild cognitive impairment," *Archives of Neurology*, vol. 58, no. 12, pp. 1985–1992, 2001.

[7] C. Demanuele, C. J. James, and E. J. Sonuga-Barke, "Distinguishing low frequency oscillations within the 1/f spectral behaviour of electromagnetic brain signals," *Behavioral and Brain Functions*, vol. 3, article 62, 2007.

[8] M. D. Fox and M. E. Raichle, "Spontaneous fluctuations in brain activity observed with functional magnetic resonance imaging," *Nature Reviews Neuroscience*, vol. 8, no. 9, pp. 700–711, 2007.

[9] X.-N. Zuo, A. Di Martino, C. Kelly et al., "The oscillating brain: complex and reliable," *NeuroImage*, vol. 49, no. 2, pp. 1432–1445, 2010.

[10] B. Biswal, F. Z. Yetkin, V. M. Haughton, and J. S. Hyde, "Functional connectivity in the motor cortex of resting human brain using echo-planar MRI," *Magnetic Resonance in Medicine*, vol. 34, no. 4, pp. 537–541, 1995.

[11] M. D. Fox, A. Z. Snyder, J. L. Vincent, M. Corbetta, D. C. Van Essen, and M. E. Raichle, "The human brain is intrinsically organized into dynamic, anticorrelated functional networks," *Proceedings of the National Academy of Sciences of the United States of America*, vol. 102, no. 27, pp. 9673–9678, 2005.

[12] V. Kiviniemi, T. Starck, J. Remes et al., "Functional segmentation of the brain cortex using high model order group PICA," *Human Brain Mapping*, vol. 30, no. 12, pp. 3865–3886, 2009.

[13] S.-J. Li, Z. Li, G. Wu, M.-J. Zhang, M. Franczak, and P. G. Antuono, "Alzheimer disease: evaluation of a functional MR imaging index as a marker," *Radiology*, vol. 225, no. 1, pp. 253–259, 2002.

[14] M. D. Greicius, G. Srivastava, A. L. Reiss, and V. Menon, "Default-mode network activity distinguishes Alzheimer's disease from healthy aging: evidence from functional MRI," *Proceedings of the National Academy of Sciences of the United States of America*, vol. 101, no. 13, pp. 4637–4642, 2004.

[15] Z. Wang, C. Yan, C. Zhao et al., "Spatial patterns of intrinsic brain activity in mild cognitive impairment and alzheimer's disease: a resting-state functional MRI study," *Human Brain Mapping*, vol. 32, no. 10, pp. 1720–1740, 2011.

[16] Y. Han, J. Wang, Z. Zhao et al., "Frequency-dependent changes in the amplitude of low-frequency fluctuations in amnestic mild cognitive impairment: a resting-state fMRI study," *NeuroImage*, vol. 55, no. 1, pp. 287–295, 2011.

[17] D. Cordes, V. M. Haughton, K. Arfanakis et al., "Frequencies contributing to functional connectivity in the cerebral cortex in "resting-state" data," *American Journal of Neuroradiology*, vol. 22, no. 7, pp. 1326–1333, 2001.

[18] M. J. Lowe, B. J. Mock, and J. A. Sorenson, "Functional connectivity in single and multislice echoplanar imaging using resting-state fluctuations," *NeuroImage*, vol. 7, no. 2, pp. 119–132, 1998.

[19] V. Kiviniemi, J.-H. Kantola, J. Jauhiainen, and O. Tervonen, "Comparison of methods for detecting nondeterministic BOLD fluctuation in fMRI," *Magnetic Resonance Imaging*, vol. 22, no. 2, pp. 197–203, 2004.

[20] H. Yang, X.-Y. Long, Y. Yang et al., "Amplitude of low frequency fluctuation within visual areas revealed by resting-state functional MRI," *NeuroImage*, vol. 36, no. 1, pp. 144–152, 2007.

[21] Z. Qi, X. Wu, Z. Wang et al., "Impairment and compensation coexist in amnestic MCI default mode network," *NeuroImage*, vol. 50, no. 1, pp. 48–55, 2010.

[22] M. Bozzali, M. Filippi, G. Magnani et al., "The contribution of voxel-based morphometry in staging patients with mild cognitive impairment," *Neurology*, vol. 67, no. 3, pp. 453–460, 2006.

[23] G. Chételat, B. Landeau, F. Eustache et al., "Using voxel-based morphometry to map the structural changes associated with rapid conversion in MCI: a longitudinal MRI study," *NeuroImage*, vol. 27, no. 4, pp. 934–946, 2005.

[24] A. Hämäläinen, S. Tervo, M. Grau-Olivares et al., "Voxel-based morphometry to detect brain atrophy in progressive mild cognitive impairment," *NeuroImage*, vol. 37, no. 4, pp. 1122–1131, 2007.

[25] L. Rami, B. Gómez-Anson, G. C. Monte, B. Bosch, R. Sánchez-Valle, and J. L. Molinuevo, "Voxel based morphometry features and follow-up of amnestic patients at high risk for Alzheimer's disease conversion," *International Journal of Geriatric Psychiatry*, vol. 24, no. 8, pp. 875–884, 2009.

[26] Y. He, L. Wang, Y. F. Zang et al., "Regional coherence changes in the early stages of Alzheimer's disease: a combined structural and resting-state functional MRI study," *NeuroImage*, vol. 35, no. 2, pp. 488–500, 2007.

[27] J. Talairach and P. Tournoux, *Co-Planar Stereotaxic Atlas of the Human Brain*, Thieme Medical, New York, NY, USA, 1987.

[28] Y. F. Zang, Y. He, C. Z. Zhu et al., "Altered baseline brain activity in children with ADHD revealed by resting-state functional MRI," *Brain & Development*, vol. 29, no. 2, pp. 83–91, 2007.

[29] R. L. Buckner, "Memory and executive function in aging and ad: Multiple factors that cause decline and reserve factors that compensate," *Neuron*, vol. 44, no. 1, pp. 195–208, 2004.

[30] C. Sorg, V. Riedl, M. Muhlau et al., "Selective changes of resting-state networks in individuals at risk for Alzheimer's disease," *Proceedings of the National Academy of Sciences of the United States of America*, vol. 104, no. 47, pp. 18760–18765, 2007.

[31] L. A. Rabin, N. Paré, A. J. Saykin et al., "Differential memory test sensitivity for diagnosing amnestic mild cognitive impairment and predicting conversion to Alzheimer's disease," *Neuropsychology, Development, and Cognition. B, Aging, Neuropsychology and Cognition*, vol. 16, no. 3, pp. 357–376, 2009.

[32] T. Hanakawa, M. Honda, N. Sawamoto et al., "The role of rostral Brodmann area 6 in mental-operation tasks: an integrative neuroimaging approach," *Cerebral Cortex*, vol. 12, no. 11, pp. 1157–1170, 2002.

[33] G. Rizzolatti, L. Fogassi, and V. Gallese, "Parietal cortex: from sight to action," *Current Opinion in Neurobiology*, vol. 7, no. 4, pp. 562–567, 1997.

[34] R. L. Buckner, J. R. Andrews-Hanna, and D. L. Schacter, "The brain's default network: anatomy, function, and relevance to disease," *Annals of the New York Academy of Sciences*, vol. 1124, pp. 1–38, 2008.

[35] C. L. Grady, A. R. McIntosh, S. Beig, M. L. Keightley, H. Burian, and S. E. Black, "Evidence from functional neuroimaging of a compensatory prefrontal network in Alzheimer's disease," *The Journal of Neuroscience*, vol. 23, no. 3, pp. 986–993, 2003.

[36] L. Wang, Y. Zang, Y. He et al., "Changes in hippocampal connectivity in the early stages of Alzheimer's disease: evidence from resting state fMRI," *NeuroImage*, vol. 31, no. 2, pp. 496–504, 2006.

[37] A. L. Bokde, M. Karmann, C. Born et al., "Altered brain activation during a verbal working memory task in subjects with amnestic mild cognitive impairment," *Journal of Alzheimer's Disease*, vol. 21, no. 1, pp. 103–118, 2010.

[38] B. Feige, K. Scheffler, F. Esposito, F. Di Salle, J. Hennig, and E. Seifritz, "Cortical and subcortical correlates of electroencephalographic alpha rhythm modulation," *Journal of Neurophysiology*, vol. 93, no. 5, pp. 2864–2872, 2005.

[39] Q. Zou, X. Long, X. Zuo et al., "Functional connectivity between the thalamus and visual cortex under eyes closed and eyes open conditions: a resting-state fMRI study," *Human Brain Mapping*, vol. 30, no. 9, pp. 3066–3078, 2009.

Hindawi Publishing Corporation
BioMed Research International
Volume 2014, Article ID 237437, 7 pages
http://dx.doi.org/10.1155/2014/237437

Review Article

Role of PET and SPECT in the Study of Amyotrophic Lateral Sclerosis

Angelina Cistaro,[1,2,3] Vincenzo Cuccurullo,[4] Natale Quartuccio,[5] Marco Pagani,[3,6] Maria Consuelo Valentini,[7] and Luigi Mansi[4]

[1] *Positron Emission Tomography Centre IRMET S.p.A., Euromedic Inc., V. O. Vigliani 89/A, 10136 Turin, Italy*
[2] *PET Pediatric AIMN InterGroup, V. O. Vigliani 89/A, 10136 Turin, Italy*
[3] *Institute of Cognitive Sciences and Technologies, National Research Council, Piazzale Aldo Moro 7, 00185 Rome, Italy*
[4] *Nuclear Medicine Unit, Department of Clinical and Experimental Internistic "F. Magrassi, A. Lanzara", Seconda Università di Napoli, Vico Luigi de Crecchio 16, 80138 Naples, Italy*
[5] *Nuclear Medicine Unit, Department of Biomedical Sciences and of Morphological and Functional Images, University of Messina, Via Consolare Valeria 1, 98125 Messina, Italy*
[6] *Department of Nuclear Medicine, Karolinska University Hospital, Solnavägen 1, Solna, 171 77 Stockholm, Sweden*
[7] *Department of Neuroradiology, San Giovanni Battista-OIRM-S.Anna-CTO Hospital, Via Cherasco 15, 10126 Turin, Italy*

Correspondence should be addressed to Angelina Cistaro; a.cistaro@irmet.com

Received 5 February 2014; Accepted 13 March 2014; Published 10 April 2014

Academic Editor: Fan-Rong Liang

Amyotrophic lateral sclerosis has been defined as a "heterogeneous group of neurodegenerative syndromes characterized by progressive muscle paralysis caused by the degeneration of motor neurons allocated in primary motor cortex, brainstem, and spinal cord." A comprehensive diagnostic workup for ALS usually includes several electrodiagnostic, clinical laboratory and genetic tests. Neuroimaging exams, such as computed tomography, magnetic resonance imaging and spinal cord myelogram, may also be required. Nuclear medicine, with PET and SPECT, may also play a role in the evaluation of patients with ALS, and provide additional information to the clinicians. This paper aims to offer to the reader a comprehensive review of the different radiotracers for the assessment of the metabolism of glucose (FDG), the measurement of cerebral blood flow (CBF), or the evaluation of neurotransmitters, astrocytes, and microglia by means of newer and not yet clinically diffuse radiopharmaceuticals.

1. Nuclear Medicine as Functional and/or Molecular Imaging in the Study of Nervous System

The living being is composed of biomolecules in dynamic equilibrium between them in the definition of the so-called homeostasis, which represents the physiology [1]. The disease can be considered the alteration of this system, being the representation of an imbalance which is expressed initially as functional impairment, sometimes reversible [2]. However, beside the possibility of a return to normal condition, there is the risk of further evolution towards an alteration that may become apparent at the morphostructural level [3].

There is therefore a gradation in the progress of the disease that can be identified according to a timeline that shows the morphostructural modification as a late event, preceded by functional alteration [4]. Consequently, functional imaging, that is, the representation of pathophysiological alterations, may be more precocious in the early detection of disease with respect to a diagnostic imaging based on morphostructural premises [5]. Furthermore functional imaging has a greater capacity in assessing the prognosis and the relationship with the therapy in the individual patient, being pathophysiological changes a better predictor of the evolution of the disease and/or the effectiveness of therapeutic action [6].

In diagnostic imaging even more interesting is the possibility of studying the molecular mechanisms that underlie the disease, allowing the representation of the initial pathological alteration [7]. Without dwelling on technical insights, there

are two basic systems of study: Single Photon Emission Tomography (SPECT), which creates images using single gamma radiations emitted by gamma-emitting radionuclides, and Positron Emission Tomography (PET), which displays images resulting from double gamma photons in coincidence, which derive from annihilation of positrons [5]. Both devices may be integrated within the so-called hybrid machines, which have made possible a technological revolution that has given and continues to bear fruits even in the clinical setting [8]. Recently another promising hybrid device, PET/MRI, was developed. PET/MRI represents an exciting novel imaging option for oncological as well as neurological applications [9].

In nuclear medicine, it is possible to obtain a large number of radioactive probes and then "trace" multiple functions and molecular mechanisms in the body [7]. Through them, it is possible to acquire sensitive and precise information, which creates the basis for investigating the earliest levels of disease, resulting in favourable therapeutic implications [5]. Though the primary role in clinical diagnosis, the functional information has however to be integrated by the morphostructural one [10]. In this way, it is at first possible to increase the diagnostic accuracy, better understanding and delineating the limits of normal and pathological anatomical structures, with a significant improvement either in sensitivity and specificity [11]. Furthermore, because of their better spatial resolution and/or of the different presuppositions underlying the image, morphostructural techniques, such as CT, MRI, and US, may also detect abnormalities that are not visible with a functional study [11].

The clinical analysis of neurological diseases with nuclear medicine is at the present connected with three main categories of radiotracers studying (1) perfusion, (2) metabolism, and (3) receptors [5].

Among all used radiotracers, the most important is still the first among those proposed, namely, the F-18 fluorodeoxyglucose (FDG), which traces the metabolism of glucose. Currently, being mainly used for oncologic applications [12, 13], PET-FDG has a clinical interest also in nonneoplastic pathologies, in particular in inflammatory diseases [14]. Furthermore, FDG plays an important role also in the evaluation of neurological diseases, first of all in dementia [15].

Among the most interesting applications of this method in the brain, there is certainly that, related to Amyotrophic Lateral Sclerosis (ALS), which is the subject of this paper. Together with FDG, further information in ALS may be acquired using radiotracers measuring cerebral blood flow (CBF) or newer and not yet clinically diffuse radiopharmaceuticals, as those allowing the evaluation of neurotransmitters, astrocytes, and microglia [16].

2. Amyotrophic Lateral Sclerosis

Amyotrophic Lateral Sclerosis (ALS), also known as Charcot, Lou Gehrig, or motor neuron's disease, has been defined as a "heterogeneous group of neurodegenerative syndromes characterized by progressive muscle paralysis caused by the degeneration of motor neurons allocated in primary motor cortex, brainstem, and spinal cord" [17]. The disease was identified in 1874 by JM Charcot as "a degenerative process involving neurons in the anterior horns of the spinal cord and in motor nuclei of brainstem" [18]. ALS affects not only motor neurons but also their nonneural neighbours, including astrocytes and microglia, whose involvement amplifies the initial damage and drives disease progression and spread [19]. The main clinical variants of ALS include Primary Muscular Atrophy (PMA), Primary Lateral Sclerosis (PLS), and Progressive Bulbar Palsy (PBP) [19].

Being currently still unknown aetiology, many etiopathogenetic hypotheses have been made for ALS. Mutations in several genes have been demonstrated to be linked to ALS, Cu/Zn superoxide dismutase (SOD1), TAR DNA-binding protein (TARDBP), the gene encoding the TAR DNA-binding protein 43—TDP-43, the fused in sarcoma/translocated in liposarcoma (FUS/TLS) protein, and chromosome 9 open reading frame 72 gene (C9ORF72) being the most important [20]. Other mutated genes involved in ALS are PFN1, OPTN, VCP, UBQLN2, ANG, FIG4, DCTN1, and CHMP2B [20]. Furthermore ALS has been related to (1) effect of exotoxins, which would lead to an excessive stimulation of glutaminergic postsynaptic NMDA and AMPA receptors; (2) oxidative stress, with accumulation of reactive oxygen; (3) mitochondrial dysfunction, with morphological and biochemical abnormalities. Among the factors involved are also included the alteration of the axonal transport, the deposit of aggregates of proteic neurofilaments, the dysfunction of glial cells, and the deficit of neurotropic factors [19].

With regard to the possibility of a role of genetic factors, it should be remembered that the disease is expressed in 90% of cases as sporadic form, being identified as a familiar disease, with autosomal dominant inheritance, in less than 10% of patients. Being a little more frequent in males (M/F = 1.3), ALS has an average age of onset at 55–65 years. The incidence is 1.5–2.7 and the prevalence is 2.7–7.4 per 100,000 inhabitants/year. Progression and severity can vary greatly from one patient to another. The mortality rate is 1.54–2.55 per 100,000 patients, with a median survival of 3–5 years. The main cause of death is the failure of the respiratory muscles [21].

3. Diagnostic Workup of ALS

ALS is a very difficult disease to diagnose and at the present there is no test or procedure to confirm without any doubt the final diagnosis [22]. More frequently, clinical suspicion emerges through a careful clinical examination, repeated over time by an expert neurologist, and a series of diagnostic tests to rule out other possible disorders justifying clinical symptoms. According to ALS Association (fighting Lou Gehrig's disease) a comprehensive diagnostic workup has to include most, if not all, of the following procedures [21]:

(i) electrodiagnostic tests including conventional electromyography (EMG), nerve conduction studies, transcranial magnetic stimulation, central motor conduction studies, and quantitative electromyography

(ii) neuroimaging including computed tomography (CT) scanning or magnetic resonance imaging (MRI) of the brain and spinal cord myelogram of cervical spine,

(iii) clinical laboratory tests which will include muscle enzymes (serum creatine kinase (unusual above ten times upper limit of normal), ALT, AST, and LDH), serum creatinine (related to loss of skeletal muscle mass), hypochloremia, increased bicarbonate (related to advanced respiratory compromise), and elevated CSF protein (uncommonly more than 100 mg/dL)

(iv) muscle and/or nerve biopsy,

(v) genetic testing.

The clinical role of diagnostic imaging, mainly interpreted by MRI, is mainly individuated in excluding alternative diseases, being nontypical and/or difficult to be detected diagnostic signs univocally defining ALS. Being this disease strictly connected with the motor neuron, the pathological damage should be evidenced exclusively at the level of the motor cortex and/or at the level of the subcortical structures involved in the motor system [21].

The currently most used diagnostic criteria for ALS are those of El Escorial World Federation of Neurology [23], which divide ALS into 5 diagnostic categories: clinically definite ALS, clinically probable ALS, clinically probable-laboratory supported ALS, and clinically possible ALS (Table 1).

4. Glucose Metabolism and Cerebral Blood Flow in ALS Patients

Either glucose metabolism or cerebral blood flow is similarly reduced in patients with ALS [24–29]. Surprisingly, since first studies with FDG PET performed in early 80's [30] in patients with upper motor neuron signs compared to age-matched control subjects, a decreased activity was observed not only in the motor primary and accessory medial motor cortex, but also at level of parietal and occipital lobes, being spared visual areas.

A frontal lobe dysfunction was also demonstrated in non-demented ALS patients by Abrahams et al. [31], measuring cerebral blood flow (rCBF) with PET. The study was based on an activation paradigm of executive frontal lobe function (verbal fluency), which contrasted with rCBF during word generation and word repetition. A PET scan was performed in groups of age matched individuals constituted by patients with ALS, respectively, affected (ALSi = impaired) or not (ALSu = unimpaired) with a cognitive impairment, both compared with healthy controls. The ALSi subjects displayed significantly impaired activation in cortical and subcortical regions including the dorsolateral prefrontal cortex, lateral premotor cortex, medial prefrontal and premotor cortices, and insular cortex bilaterally and the anterior thalamic nuclear complex. Although the three groups showed matched word generation performance on the scanning paradigm, the ALSu group displayed a relatively unimpaired pattern of activation. These results are in agreement with an extramotor neuronal involvement in some non-demented ALS patients that develops probably along a thalamo-frontal association pathway.

Dalakas et al. [24], using FDG PET, observed that in patients with upper motor neuron signs, the mean cortical Regional Cerebral Metabolic Rate of Glucose Consumption (rCMRGlc) was significantly lower than in normal subjects. Moreover, subsequent reduction in the rCMRGlc, in agreement with the clinical worsening, was observed in 3 out of the 4 patients who underwent repeated PET scan. Conversely, a normal or near-normal rCMRGlc was seen throughout the brain in ALS patients with disease confined to lower motor neurons and in 3 subjects with lower motor neuron disease, depending from old paralytic poliomyelitis. As already observed in cerebellar diaschisis [32], these data demonstrate that a hypometabolism may be seen in a structurally normal cortex, in case of functionally altered neurons neurologically connected with dead and/or dedifferentiated cells. Hatazawa et al. [25] reported a more detailed regional analysis concerning almost the same population studied by Dalakas, also including the evaluation of the motor-sensory cortex at higher levels than used earlier. A brain size correction was added to avoid differences in measured activity depending on brain size, but not from hypometabolism. In this more detailed analysis, a generalized reduction of FDG's uptake was shown in patients with both upper and lower motor neuron disease that was greatest in the motor-sensory cortex and putamen. The motor-sensory deficit was strongly correlated with length of disease, and a marked sequential reduction was seen in the four patients who repeated a PET study. In this paper, a right-left asymmetry in the population described above and a normal or near normal FDG uptake in the four ALS patients without upper motor neuron involvement were also reported. In 2007, the correlation of the extent of cortical lesions with the intensity of motor dysfunction in ALS patients, measured by the ALS functional rating scale score (ALSFRS), has been also studied by Habert et al. [33], who evaluated cerebral perfusion using SPECT with 99mTc-ECD and a statistical parametric mapping (SPM) method. A positive correlation between the degree of involvement of the motor functions and the perfusion decrease of the cerebral cortex was demonstrated. Analyzing the ALSFRS subscores, the cortical involvement was important for lower limbs score, moderate for bulbar score, and below the level of statistical significance for the respiratory and upper limb scores. An asymmetric hypoperfusion, because of a major involvement of the right hemisphere, was seen mainly in the lateral premotor cortex, the insula, and the cingulate cortex.

5. Different Patterns of Glucose Metabolism in ALS Patients

Using PET-FDG, different patterns of hypometabolism have been observed when the motor neuron disease (MND) coexists with Frontotemporal Dementia (FTD). Comparing patients with FTD and MND with subjects affected with FTD alone Jeong et al. [34] demonstrated that the patients with FTD/MND showed glucose hypometabolism only in the frontal area, whereas most patients with FTD had hypometabolism in the frontal and temporal areas. Furthermore, in case of FTD/MND, a more symmetric pattern of hypometabolism with respect to patients with FTD alone was showed. To better understand the FDG distribution in patients with FTD, Jeong performed also an SPM analysis

Table 1: ALS diagnostic categories according to the El Escorial World Federation of Neurology diagnostic criteria.

Clinically definite ALS	Defined on clinical evidence alone by the presence of UMN, as well as LMN signs, in three regions
Clinically probable ALS	Defined on clinical evidence alone by UMN and LMN signs in at least two regions with some UMN signs necessarily rostral to (above) the LMN signs.
Clinically probable-laboratory-supported ALS	Defined when clinical signs of UMN and LMN dysfunction are in only one region, or when UMN signs alone are present in one region, and LMN signs defined by EMG criteria are present in at least two limbs, with proper application of neuroimaging and clinical laboratory protocols to exclude other causes.
Clinically possible ALS	Defined when clinical signs of UMN and LMN dysfunction are found together in only one region or UMN signs are found alone in two or more regions; or LMN signs are found rostral to UMN signs and the diagnosis of clinically probable-laboratory-supported ALS cannot be proven by evidence on clinical grounds in conjunction with electrodiagnostic, neurophysiologic, neuroimaging, or clinical laboratory studies. Other diagnoses must have been excluded to accept a diagnosis of clinically possible ALS

in comparison with normal controls [35]. A significant hypometabolism was identified in extensive prefrontal areas, cingulate gyri, anterior temporal regions, and the left inferior parietal lobule and less relevant in the bilateral insula and uncus, left putamen and globus pallidus, and medial thalamic structures. Frontal hypometabolism was more frequently prominent in the left hemisphere than in the right.

Cistaro et al. [36] studied with FDG PET 32 patients with ALS, of either bulbar ($n = 13$) or spinal ($n = 19$) onset, compared by SPM with 22 subjects taken as controls. Patients with spinal onset had significantly higher scores in a neuropsychological test assessing verbal fluency compared with patients with bulbar onset. In this study an unprecedented evidence of relatively increased metabolism in the amygdalae, midbrain, and pons was observed in ALS patients as compared with control subjects, possibly due to local activation of astrocytes and microglia. Highly significant relative decreases in metabolism were found in large frontal and parietal regions in the bulbar onset patients as compared with the spinal onset subjects and the controls, suggesting a differential metabolic and neuropsychological state between the two conditions.

Data of Cistaro et al. [36] are in agreement with an increased metabolism along the course of the cerebral spinal fluid (CSF), at level of pons and midbrain. The hypermetabolism could depend on a colonization of the pyramidal tract by active astrocytes and/or microglia. Interestingly a reduced fractional anisotropy has been observed in the pons and along the CSF in patients who underwent either PET or fMRI [37]. With respect to the hypometabolism observed in patients with a bulbar onset, our results support the presence of an extramotory involvement in ALS which may interest dorsolateral and prefrontal cortex. Conversely, a normal or near normal frontoparietal FDG uptake has been observed in ALS patients with a spinal onset.

In 2014, Cistaro et al. performed another study, valuating the FDG PET profile of 15 patients with familial ALS carrying the GGGGCC hexanucleotide repeat expansion in the C9ORF72 gene and comparing them with a group of 12 patients with ALS and comorbid frontotemporal dementia (FTD) without the C9ORF72 expansion (ALS-FTD), a group of 30 cognitively normal patients and 40 normal controls. The authors demonstrated that, among the 4 groups, patients carrying the C9ORF72 mutation show a more extensive involvement of the central nervous system, with significant hypometabolism in the anterior and posterior cingulate cortex, insula, caudate, and thalamus, the left frontal and superior temporal cortex, and hypermetabolism in the midbrain, bilateral occipital cortex, globus pallidus,, and left inferior temporal cortex [38].

6. Microglia Involvement in ALS Patients

The explanation of subcortical hypermetabolic areas as a possible consequence of a colonization by active astrocytes and/or microglia is in agreement with the new view of FDG's cerebral uptake, which changed in the last decades [39]. It has been demonstrated that glucose is not consumed exclusively by neurons and that glucose consumption does not directly reflect only neural activity [40]. In this respect, the importance of astrocytes in glutamate-driven glucose metabolism and regulation has been highlighted [40], supporting the indication that also cells other than neurons are involved in FDG's uptake.

The evidence of widespread cerebral microglial activation in amyotrophic lateral sclerosis may be further understood reading the paper by Turner et al. [41], who reported an experience with [11C](R)-PK1l195, a ligand for the peripheral benzodiazepine binding site, expressed by activated microglia. The PET study has been performed in ten ALS patients and 14 healthy controls. Significantly increased binding was found in motor cortex, pons, dorsolateral prefrontal cortex, and thalamus in the ALS patients, with significant correlation between binding in the motor cortex and the burden of upper motor neuron signs clinically evident. This paper supports the interest for the development of therapeutic strategies in ALS aimed at inflammatory pathways. Favourable results have already been obtained in experimental models where an increased survival has been observed in animals when treated with anti-inflammatory drugs. To demonstrate the relevance of astrocytosis in ALS, Johansson et al. [42] utilized [11C](L)-deprenyl-D2, which

binds to the enzyme MAO-B, primarily located in astrocytes. An increased uptake of deuterium-substituted [11C](L)-deprenyl PET was demonstrated in pons and white matter of seven patients with ALS, compared with seven healthy control subjects.

7. Evaluation of ALS Patients with PET Receptor Studies

An original study has been published by Lloyd et al. [43], who evaluated extramotor involvement in ALS, using as PET radiotracer the [(11)C]flumazenil (FMZ), a benzodiazepine GABA(A) marker. The study was performed in seventeen nondemented patients with clinically definite or probable ALS compared with seventeen normal controls. The analysis was based on SPM maps, derived to localize changes in regional flumazenil volumes of distribution (FMZVD), which correlate closely with receptor density. Relative FMZVD was significantly decreased in the ALS group in the prefrontal cortex, parietal cortex, visual association cortex, and left motor/premotor cortex. A relative reduction in FMZVD was also present, though less evident, in the left ventrolateral and dorsolateral prefrontal cortex, Broca's area, and the right temporal and right visual association cortex. These data are in agreement with a cerebral dysfunction in ALS which involves not only the motor cortex, but also premotor and extramotor areas, particularly in the prefrontal regions. A more recent study using [11C]flumazenil (FMZ) PET has been performed by Turner et al. [44], who focalized their interest in patients with ALS, also including subjects who presented the "D90A" SOD1 mutation. The mutations of the superoxide dismutase-1 (SOD1) gene are associated with five to ten percent cases of ALS. Between them, the "D90A" mutation individuate a unique phenotype, characterized by a markedly slower disease progression, with a mean survival of 14 years, probably dependent on the relative sparing of inhibitory cortical neuronal circuits. The study has been based on the comparison of results obtained in twenty-four sporadic ALS (sALS), 10 homozygous D90A patients, and two subjects homozygous for the D90A mutation, but without symptoms or signs ("presymptomatic", psD90A), with those achieved in 24 age-matched normal controls. While in sALS a decreased uptake has been observed within premotor regions, motor cortex, and posterior motor association areas; in the homD90A group the reduction was concentrated in the left frontotemporal junction and anterior cingulate gyrus. In the two psD90A subjects, a small focus of reduced uptake was seen at the left frontotemporal junction, therefore showing a pattern similar to the one observed in the clinically affected patients. No statistically significant association between the reduction in cortical FMZ binding and revised Amyotrophic Lateral Sclerosis Functional Rating Scale (ALSFRS) was demonstrated in sALS patients, whereas the upper motor neuron (UMN) score correlated with widespread and marked cortical decreases over the dominant hemisphere. Conversely, in the D90A group, the decreased in FMZ uptake was strongly statistically associated with ALSFRS-R, rather than the UMN score, being also related to the disease's duration.

To evaluate the possible interest of dopaminergic radiotracers in ALS, Takahashi et al. [45] utilized F-18 fluorodopa in 16 patients with sporadic ALS and without extrapyramidal disease, compared with age-matched controls. A significant progressive fall in fluorodopa uptake was observed in 3 patients with ALS of long duration.

The possible interest of radiotracers of serotonin was inquired by Turner et al. [41], who performed PET with [11C]-WAY100635 PET, a sensitive marker of in vivo 5-HT1A receptor binding, in ALS patients compared with controls. An SPM analysis evidenced a striking and widespread decrease in cerebral 5-HT1A binding in ALS patients compared with controls in both motor and extramotor regions, with the most marked changes in frontotemporal regions. Their hypothesis was that these findings reflect widespread damage to cortical pyramidal neurones that express 5-HT1A receptors, although a purely functional change in receptor binding cannot be excluded.

8. Conclusion

In the older definition ALS is considered as a disease exclusively characterized by preferential loss of motor neurons in the motor cortex, brainstem, and spinal cord, that is, by a pathological involvement exclusively of the motor system. Although they do not have yet been included in the clinical scenario, PET and SPECT may give interesting information in these patients, having capability to trace many important pathophysiological and biochemical targets involved in the disease. The greatest advantage achievable by molecular imaging is in individuating early functional alterations, preceding the morphostructural evidence, better explaining clinical symptoms, as those connected with a frontal dementia, and helping to define a prognostic stratification. At the present, clinical information may be mainly acquired using PET-FDG. Important data, to be utilized as premise to a therapeutic strategy based on inflammation as a target, could be achieved with radiotracers allowing to detect astrocytosis. Finally, having been demonstrated a possible role of fMRI in detecting alterations in fractional anisotropy, at level of subcortical structures, very intriguing perspectives could be associated with the diffusion of PET-MRI hybrid machines, allowing obtaining simultaneously, together with the morphostructural information, functional data acquirable either with PET or fMRI.

Conflict of Interests

The authors declare that there is no conflict of interests regarding the publication of this paper.

References

[1] W. B. Cannon, "Organization for physiological homeostasis," *Physiological Reviews*, vol. 9, pp. 399–431, 1929.

[2] M. Ereshefsky, "Defining "health" and " disease"," *Studies in History and Philosophy of Science C :Studies in History and Philosophy of Biological and Biomedical Sciences*, vol. 40, no. 3, pp. 221–227, 2009.

[3] S. P. Jackson and J. Bartek, "The DNA-damage response in human biology and disease," *Nature*, vol. 461, no. 7267, pp. 1071–1078, 2009.

[4] L. Mansi, "Ich bin ein Molekularmediziner (how much CT and nuclear medicine in molecular CT?)," *European Journal of Nuclear Medicine and Molecular Imaging*, vol. 36, no. 3, pp. 531–532, 2009.

[5] G. L. Cascini, V. Cuccurullo, O. Tamburrini, A. Rotondo, and L. Mansi, "Peptide imaging with somatostatin analogues: more than cancer probes," *Current Radiopharmaceuticals*, vol. 6, pp. 36–40, 2013.

[6] A. Cistaro, N. Quartuccio, S. Vesco et al., "Positron emission tomography," *Ophthalmology*, vol. 119, pp. 1496–1497, 2012.

[7] S. L. Kitson, V. Cuccurullo, T. S. Moody, and L. Mansi, "Radionuclide antibody-conjugates, a targeted therapy towards cancer," *Current Radiopharmaceuticals*, vol. 6, pp. 57–71, 2013.

[8] M. Benadiba, G. Luurtsema, L. Wichert-Ana, C. A. Buchpigel, and G. Busatto Filho, "New molecular targets for PET and SPECT imaging in neurodegenerative diseases," *Revista Brasileira De Psiquiatria*, vol. 34, pp. S125–S136, 2012.

[9] L. Mansi, A. Ciarmiello, and V. Cuccurullo, "PET/MRI and the revolution of the third eye," *European Journal of Nuclear Medicine and Molecular Imaging*, vol. 39, pp. 1519–1524, 2012.

[10] V. Cuccurullo, G. L. Cascini, O. Tamburrini, A. Rotondo, and L. Mansi, "Bone metastases radiopharmaceuticals: an overview," *Current Radiopharmaceuticals*, vol. 6, pp. 41–47, 2013.

[11] V. Cuccurullo, G. L. Cascini, and L. Mansi, "Structural, pathophysiological and clinical aspects of diagnostic imaging in breast recurrence: the breast after treatment," *The Quarterly Journal of Nuclear Medicine and Molecular Imaging*, vol. 57, pp. 322–331, 2013.

[12] A. Cistaro, N. Quartuccio, A. Mojtahedi et al., "Prediction of 2 years-survival in patients with stage I and II non-small cell lung cancer utilizing (18)F-FDG PET/CT SUV quantification," *Radiology and Oncology*, vol. 47, pp. 219–223, 2013.

[13] N. Quartuccio, G. Treglia, M. Salsano et al., "The role of Fluorine-18-Fluorodeoxyglucose positron emission tomography in staging and restaging of patients with osteosarcoma," *Radiology and Oncology*, vol. 47, pp. 97–102, 2013.

[14] A. Cistaro, N. Quartuccio, L. Mansi, A. Signore, M. Dolci, and G. Treglia, "The role of positron emission tomography in Inflammatory bowel disease," *European Journal of Inflammation*, vol. 10, pp. 251–256.

[15] S. Morbelli, R. Perneczky, A. Drzezga et al., "Metabolic networks underlying cognitive reserve in prodromal Alzheimer disease: a European Alzheimer disease consortium project," *Journal of Nuclear Medicine*, vol. 54, pp. 894–902, 2013.

[16] G. Giovacchini, F. Squitieri, M. Esmaeilzadeh, A. Milano, L. Mansi, and A. Ciarmiello, "PET translates neurophysiology into images: a review to stimulate a network between neuroimaging and basic research," *Journal of Cellular Physiology*, vol. 226, no. 4, pp. 948–961, 2011.

[17] A. Chiò, G. Logroscino, O. Hardiman et al., "Prognostic factors in ALS: a critical review," *Amyotrophic Lateral Sclerosis*, vol. 10, no. 5-6, pp. 310–323, 2009.

[18] L. P. Rowland, "How amyotrophic lateral sclerosis got its name: the clinical-pathologic genius of Jean-Martin Charcot," *Archives of Neurology*, vol. 58, no. 3, pp. 512–515, 2001.

[19] L. C. Wijesekera and P. N. Leigh, "Amyotrophic lateral sclerosis," *Orphanet Journal of Rare Diseases*, vol. 4, no. 1, article 3, 2009.

[20] A. E. Renton, A. Chiò, and B. J. Traynor, "State of play in amyotrophic later al sclerosis genetics," *Nature Neuroscience*, vol. 17, pp. 17–23, 2014.

[21] S. Sathasivam, "Motor neurone disease: clinical features, diagnosis, diagnostic pitfalls and prognostic markers," *Singapore Medical Journal*, vol. 51, no. 5, pp. 367–373, 2010.

[22] V. Silani, S. Messina, B. Poletti et al., "The diagnosis of amyotrophic lateral sclerosis," *Archives Italiennes de Biologie*, vol. 149, no. 1, pp. 5–27, 2011.

[23] P. G. Ince, J. Lowe, and P. J. Shaw, "Amyotrophic lateral sclerosis: current issues in classification, pathogenesis and molecular pathology," *Neuropathology and Applied Neurobiology*, vol. 24, no. 2, pp. 104–117, 1998.

[24] M. C. Dalakas, J. Hatazawa, R. A. Brooks, and G. Di Chiro, "Lowered cerebral glucose utilization in amyotrophic lateral sclerosis," *Annals of Neurology*, vol. 22, no. 5, pp. 580–586, 1987.

[25] J. Hatazawa, R. A. Brooks, M. C. Dalakas, L. Mansi, and G. Di Chiro, "Cortical motor-sensory hypometabolism in amyotrophic lateral sclerosis: a PET study," *Journal of Computer Assisted Tomography*, vol. 12, no. 4, pp. 630–636, 1988.

[26] B. P. Drayer, "Imaging of the aging brain. Part I: normal findings," *Radiology*, vol. 166, no. 3, pp. 785–796, 1988.

[27] A. C. Ludolph, K. J. Langen, M. Regard et al., "Frontal lobe function in amyotrophic lateral sclerosis: a neuropsychologic and positron emission tomography study," *Acta Neurologica Scandinavica*, vol. 85, no. 2, pp. 81–89, 1992.

[28] K. Ishikawa, H. Nagura, T. Yokota, and H. Yamanouchi, "Signal loss in the motor cortex on magnetic resonance images in amyotrophic lateral sclerosis," *Annals of Neurology*, vol. 33, no. 2, pp. 218–222, 1993.

[29] Z. Shiozawa, K. Shindo, E. Ohta, K. Ohushi, M. Nagamatsu, and T. Nagasaka, "A concise overview of recent breakthroughs in imaging of ALS," *Amyotrophic Lateral Sclerosis*, vol. 1, no. 2, pp. S3–S6, 2000.

[30] L. Mansi, M. C. Dalakas, G. DiChiro et al., "Evaluation of cerebral glucose metabolism in patients with amyotrophic lateral sclerosis (ALS) by [18F]-fluorodeoxyglucose (FDG) and positron emission tomography (PET)," *Journal of Nuclear Medicine*, vol. 24, article P21, 1983.

[31] S. Abrahams, L. H. Goldstein, J. J. M. Kew et al., "Frontal lobe dysfunction in amyotrophic lateral sclerosis: a PET study," *Brain*, vol. 119, no. 6, pp. 2105–2120, 1996.

[32] N. J. Patronas, G. Di Chiro, and B. H. Smith, "Depressed cerebellar glucose metabolism in supratentorial tumors," *Brain Research*, vol. 291, no. 1, pp. 93–101, 1984.

[33] M.-O. Habert, L. Lacomblez, P. Maksud, G. E. L. Fakhri, J.-F. Pradat, and V. Meininger, "Brain perfusion imaging in amyotrophic lateral sclerosis: extent of cortical changes according to the severity and topography of motor impairment," *Amyotrophic Lateral Sclerosis*, vol. 8, no. 1, pp. 9–15, 2007.

[34] Y. Jeong, K. C. Park, S. S. Cho et al., "Pattern of glucose hypometabolism in frontotemporal dementia with motor neuron disease," *Neurology*, vol. 64, no. 4, pp. 734–736, 2005.

[35] Y. Jeong, S. S. Cho, J. M. Park et al., "18F-FDG PET findings in frontotemporal dementia: an SPM analysis of 29 patients," *Journal of Nuclear Medicine*, vol. 46, no. 2, pp. 233–239, 2005.

[36] A. Cistaro, M. C. Valentini, A. Chiò et al., "Brain hypermetabolism in amyotrophic lateral sclerosis: a FDG PET study in ALS of spinal and bulbar onset," *European Journal of Nuclear Medicine and Molecular Imaging*, vol. 39, no. 2, pp. 251–259, 2012.

[37] G. Carrara, C. Carapelli, F. Venturi et al., "A distinct MR imaging phenotype in amyotrophic lateral sclerosis: correlation between T1 magnetization transfer contrast hyperintensity along the corticospinal tract and diffusion tensor imaging analysis,"

American Journal of Neuroradiology, vol. 33, no. 4, pp. 733–739, 2012.

[38] A. Cistaro, M. Pagani, A. Montuschi et al., "The metabolic signature of C9ORF72-related ALS: FDG PET comparison with nonmutated patients," *European Journal of Nuclear Medicine and Molecular Imaging*, 2014.

[39] S. Sestini, A. Castagnoli, and L. Mansi, "The new FDG brain revolution: the neurovascular unit and the default network," *European Journal of Nuclear Medicine and Molecular Imaging*, vol. 37, no. 5, pp. 913–916, 2010.

[40] S. Sestini, "Genetic studies of diseases: the neural basis of functional neuroimaging signal with positron and single-photon emission tomography," *Cellular and Molecular Life Sciences*, vol. 64, no. 14, pp. 1778–1784, 2007.

[41] M. R. Turner, A. Cagnin, F. E. Turkheimer et al., "Evidence of widespread cerebral microglial activation in amyotrophic lateral sclerosis: an [11C](R)-PK11195 positron emission tomography study," *Neurobiology of Disease*, vol. 15, no. 3, pp. 601–609, 2004.

[42] A. Johansson, H. Engler, G. Blomquist et al., "Evidence for astrocytosis in ALS demonstrated by [11C](l)-deprenyl-D2 PET," *Journal of the Neurological Sciences*, vol. 255, no. 1-2, pp. 17–22, 2007.

[43] C. M. Lloyd, M. P. Richardson, D. J. Brooks, A. Al-Chalabi, and P. N. Leigh, "Extramotor involvement in ALS: PET studies with the GABA(A) ligand [11C]flumazenil," *Brain*, vol. 123, no. 11, pp. 2289–2296, 2000.

[44] M. R. Turner, A. Hammers, A. Al-Chalabi et al., "Distinct cerebral lesions in sporadic and "D90A" SOD1 ALS: studies with [11C]flumazenil PET," *Brain*, vol. 128, no. 6, pp. 1323–1329, 2005.

[45] H. Takahashi, B. J. Snow, M. H. Bhatt, R. Peppard, A. Eisen, and D. B. Calne, "Evidence for a dopaminergic deficit in sporadic amyotrophic lateral sclerosis on positron emission scanning," *The Lancet*, vol. 342, no. 8878, pp. 1016–1018, 1993.

Hindawi Publishing Corporation
BioMed Research International
Volume 2014, Article ID 915026, 7 pages
http://dx.doi.org/10.1155/2014/915026

Clinical Study

Hypothalamus-Anchored Resting Brain Network Changes before and after Sertraline Treatment in Major Depression

Rui Yang,[1,2,3] Hongbo Zhang,[2,4] Xiaoping Wu,[1,3] Junle Yang,[1,3] Mingyue Ma,[1,3] Yanjun Gao,[1,3] Hongsheng Liu,[1,3] and Shengbin Li[2,4]

[1] *The Affiliated Xi'an Central Hospital of Medical College of Xi'an Jiaotong University, Xi'an 710003, China*
[2] *Key Laboratory of Environment and Gene Related Diseases, Ministry of Education, Xi'an Jiaotong University, Xi'an 710061, China*
[3] *Xi'an Central Hospital, Xi'an 710003, China*
[4] *Key Laboratory of Health Ministry for Forensic Science, Xi'an Jiaotong University, Xi'an 710061, China*

Correspondence should be addressed to Shengbin Li; forensicslee@163.com

Received 26 January 2014; Revised 12 February 2014; Accepted 13 February 2014; Published 20 March 2014

Academic Editor: Lijun Bai

Sertraline, one of the oldest antidepressants, remains to be the most efficacious treatment for depression. However, major depression disorder (MDD) is characterized by altered emotion processing and deficits in cognitive control. In cognitive interference tasks, patients with MDD have shown excessive hypothalamus activity. The purpose of this study was to examine the effects of antidepressant treatment (sertraline) on hypothalamus-anchored resting brain circuitry. Functional magnetic resonance imaging was conducted on depressed patients ($n = 12$) both before and after antidepressant treatment. After eight weeks of antidepressant treatment, patients with depression showed significantly increased connectivity between the hypothalamus and dorsolateral prefrontal cortex, orbitofrontal cortex, anterior cingulate cortex, insula, putamen, caudate, and claustrum. By contrast, decreased connectivity of the hypothalamus-related areas was primarily located in the inferior frontal gyrus, medial frontal gyrus, cingulated gyrus, precuneus, thalamus, and cerebellum. After eight weeks of antidepressant therapy, 8 out of the 12 depressed subjects achieved 70% reduction or better in depressive symptoms, as measured on the Hamilton depression rating scale. Our findings may infer that antidepressant treatment can alter the functional connectivity of the hypothalamus resting brain to achieve its therapeutic effect.

1. Introduction

Depression is the commonest psychiatric disorder. It is the most disabling medical condition, in terms of years lost to disability, and it is predicted that depression will be the foremost contributor to the worldwide burden of disease by 2030 [1]. Depression is characterized by a profoundly negative view of the world, oneself, and the future [2], and this negative world view has been associated with negative biases in attention, interpretation, and memory [3]. In clinical settings, the depression is often misdiagnosed especially without a history of mania [4], leading to inadequate treatment, increased medical costs, and poor outcomes [5–7]. A recent upsurge of interest has been directed toward developing both diagnostic and prognostic biomarkers that can aid to diagnose which individuals are relatively more likely to progress clinically.

Previous studies using structural MRI have already revealed abnormalities in various brain areas and significant changes in the amygdala volume in adults suffering from depression and mood disorders [8]. The affective network largely consists of the prefrontal cortex as well as subcortical and allocortical brain structures such as the thalamus, amygdala, basal ganglia, and hippocampus. Studies probing this system demonstrated reduced frontal-subcortical connectivity in depression [9], which is thought to reflect impaired cognitive regulation of mood. Therefore, in particular functional MRI (fMRI), studies of the neural mechanisms of depression have shifted from those highlighting focal regions of abnormal brain functions to those focusing on the dysfunctional brain connectivity between spatially distinct brain regions. Resting state fMRI reflects the neuronal baseline activity of the brain, representing the state of the human

brain without goal-directed neuronal action and external input [10], and the resting state functional connectivity in the blood oxygenation level-dependent signal during rest corresponds to consistent functionally relevant resting state networks (RSNs) [11]. With the benefit of its easy control and good acceptance, the resting state fMRI has received increasing attention for studying unipolar depression [12]. Some previous studies have observed increased connectivity within the default mode (DMN) network in depressed patients, and, interestingly, heightened DMN connectivity is also associated with depressive rumination [13, 14].

The hypothalamus is a subcortical region with roughly 4 cm^3 neuronal tissue in human brain [15] located at the third ventricle, rostroventral to the thalamus. It consisted of several subareas embedded cytoarchitectonically distinguishable and proved to be functionally distinct with some functional overlaps [16]. Previous studies have demonstrated the involvement of hypothalamic nuclei in wide range of tasks including cognitive, behavioural, and visceral processes [17–21]. The hypothalamo-pituitary-adrenal (HPA) system constructs a common pathway in the mediation of the stress response. Cortisol normally exerts a negative feedback to shut down the stress response when facing the threat, acting upon the levels of the pituitary and hypothalamus. In addition, stimulation by corticosteroids can be exerted at the level of the amygdala, the prefrontal cortex, and the brain stem (locus coeruleus), interfering with HPA activity and stress effects on memory [22–24]. A large part of the environmental and genetic risk factors for depression appear to correlate with increased HPA-axis activity in adulthood. When patients or animals in models for depression are treated with antidepressants and electroconvulsive therapy or when patients show spontaneous remission, the HPA-axis function returns to normal [25]. Although antidepressant agents have been largely used for the treatment of major depressive disorder (MDD), the neurobiological mechanisms of their efficacy remains poorly understood [26–30]. Moreover, patients often present different clinical results: patients with fewer depressive episodes can achieve a rapid remission while others present with prolonged, remittent, or refractory illness [31–34]. In this respect, evaluating the brain functional antidepressant effects will allow a better understanding of the pathogenesis of MDD and its response to antidepressant treatment.

In the present study, we aimed to explore the effects of antidepressant treatment (sertraline) on functional connectivity network in unipolar depression while using the hypothalamus as the seed region. To address this question, we conducted a functional magnetic resonance imaging study of depression patients both before and after antidepressant treatment while they performed a resting scanning. We hypothesized that depression patients after medication would present increased, relative to their premedicated state.

2. Materials and Methods

2.1. Patients. Twelve major depression patients (7 males) participated in this study. This study was conducted at Xi'an Central Hospital. Each subject underwent a screening evaluation involving structured clinical interviews and assessments by trained clinicians and semistructured medical and psychiatric interviews with the study psychiatrist (K.L.P.). All subjects were characterized with the (1) structured clinical interview for DSM-IV; (2) Hamilton depression rating scale (HDRS). Table 1 details the demographic and clinical characteristics of the subjects. All subjects had no history of head injury, organic mental disorders, alcohol or drug abuse, serious physical illness, or other mental illness. During the treatment, they were free of other treatments with psychiatric medications. None of the females were currently pregnant or lactating. All subjects provided written informed consent, and the study was approved by both local hospital institutional review boards. Head structural magnetic resonance imaging (MRI) results were evaluated by a single neuroimaging physician who was blinded to the experimental groups, and no obvious structural abnormalities were found.

Table 1: Demographic and clinical characteristics of the subjects.

	Depression group	
	Mean	SD
Age (years)	34.91	12.16
Duration (years)	4.04	3.14
Height (cm)	168.3	6.54
Weight (kg)	79.51	9.96
Hamilton depression (before)	24.08	4.40
Hamilton depression (after)	5.83	2.32

2.2. Sertraline Treatment. Treatment consisted of the sertraline in a fixed-dosing design over 8 weeks (50–100 mg/day). Patients were evaluated at weeks 1 and 8 by the study psychiatrist (K.L.P.) in medication management sessions to assess symptom change and adverse events, with the target dose of 50–100 mg/day; clinical response was measured with the HDRS. Although we did not measure sertraline blood levels, the study psychiatrist and staff inquired about missed doses and conducted a pill count to confirm the subject report. No subject in the study ever missed more than 2 consecutive daily doses over the course of the 8-week study, and no subject regularly (>3 times) missed the dose.

2.3. Data Acquisition. The MR images were acquired with a 1.5 Tesla GE Excite MRI system (GE Health care Milwaukee, WI, USA). A foam pillow and a band across the forehead were used to fix the head. Resting state functional images were acquired with a single shot gradient recalled echo planar imaging sequence. The sequence covered the whole brain, axial view, parallel to the to the AC-PC line collected to cover the whole brain.

In AC-PC line, TR = 2500 ms, TE = 35 ms, resolution = 64 × 64, field of view (FOV) = 240 mm × 240 mm, flip angle = 90°, slice thickness = 3 mm without gap, 36 slices. A set of T1-weighted high-resolution structural images were collected using a 3D Fast SPGR sequence for anatomical localization.

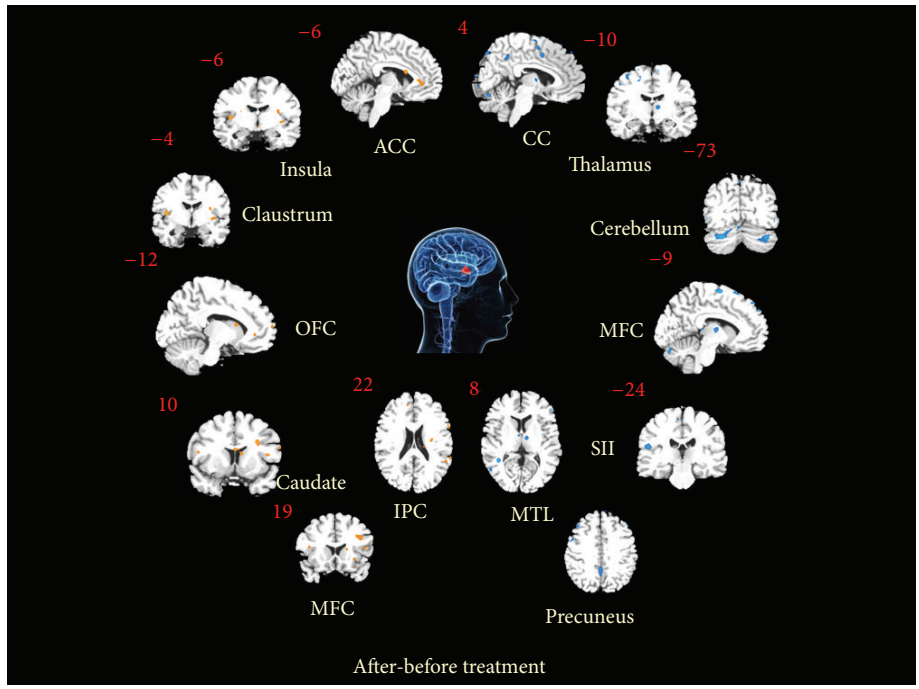

Figure 1: Both the increased and decreased hypothalamus-related functional connectivity resting brain networks after 8-week sertraline treatment for major depression ($P < 0.01$, FDR corrected).

TR = 10.6 ms, TE = 4.8 ms, field of view (FOV) = 256 mm × 256 mm, flip angle = 15°, in-plane resolution = 1 mm × 1 mm, slice thickness: 1 mm without gap, 128 slices. All subjects were asked to remain relaxed without being engaged in any mental tasks. They were also instructed to keep their eyes closed but not fell asleep.

2.4. Image Preprocessing. All preprocessing steps were carried out using statistical parametric mapping (SPM5, http://www.fil.ion.ucl.ac.uk/spm/). Functional images were preprocessed using sinc interpolation for slice scan time correction, trilinear sinc interpolation for alignment (motion correction) of functional volumes, and high-pass temporal filtering to 1 Hz to remove slow drifts in the data. The image data were further processed with spatial normalization based on the MNI space and resampled at 2 mm × 2 mm × 2 mm. Resting data were also filtered using a band pass filter (0.01~0.08 Hz) to reduce low-frequency drift and high-frequency noise. Finally, the functional images were spatially smoothed with a 6 mm full width at half maximum (FWHM) Gaussian kernel. All resting state functional images were preprocessed using statistical parametric mapping 5 (SPM5) and included motion correction, normalization, and smoothing.

2.5. Functional Connectivity Analysis. For each subject, the "seeding" time courses of the hypothalamus were, respectively, cross-correlated with all low-pass filtered voxels to generate functional connectivity maps within each of the three conditions. The resulting correlation coefficient t-maps were normalized and corrected to roughly standard normal distributions using methods previously described. The normality of the distribution was then tested using Kurtosis tests ($P < 0.001$, corrected). The maps of each individual were entered into one-sample t-tests, respectively, to determine whether group data was significantly different from zero. For visualization, all connectivity results were transformed into the Talairach stereotactic space and overlaid on MRIcro (http://www.mccauslandcenter.sc.edu/CRNL/) for presentation purposes. All resulting t-maps were then cluster-filtered to remove correlations involving less than three contiguous voxels and then superimposed on high-resolution anatomical images using a $P < 0.001$ cut-off threshold (FDR, corrected).

3. Results

Due to excessive head movement during scanning, imaging data from 2 patients were excluded and consequently a total of 10 participants were included in this study. Their demographic data and psychological scores are listed in Table 1. After eight weeks of antidepressant therapy, 8 out of the 12 depressed subjects achieved 70% reduction or better in depressive symptoms, as measured on the HDRS scale. Seven showed 50–70% improvement, and the remaining four showed 59–68% reductions. Thus, in our sample, approximately two-third of the sample showed very significant improvements in symptoms, and all patients responded at least partially to the treatment.

Our results show that sertraline treatment has a larger impact on the hypothalamus-related brain networks for major depression patients (shown in Figure 1 and Table 2, $P < 0.005$, FWE corrected). After treatment, the hypothalamus

Table 2: Significant changes in hypothalamus-related connectivity network derived from after versus before medication ($P < 0.001$, FDR corrected).

(a) Increased

		Talairach			t value	Voxels
		x	y	z		
Frontal						
DLPFC BA/44	R	48	16	10	3.08	44
OFC BA/10	R	8	38	−7	2.25	44
SFG BA/8	R	14	39	48	2.33	22
Precentral gyrus BA/44	R	44	12	9	3.20	20
Limbic						
ACC BA/24	R	6	31	0	2.76	45
Hippocampus	R	33	−14	−18	3.23	16
Subcortical						
Insula BA/13	R	42	12	10	2.61	43
Putamen	R	24	8	−2	2.09	28
Caudate	R	8	10	11	3.57	82
Claustrum	R	32	−3	13	2.54	25
Temporal						
STG BA/22	R	63	−40	20	2.37	27
Parietal						
IPL BA/40	R	55	−44	22	2.40	38
SG BA/40	R	57	−37	30	2.33	24

(b) Decreased

		Talairach			t value	Voxels
		x	y	z		
Frontal						
IFG BA 47	L	53	17	−6	−2.87	54
IFG BA 9	R	−53	11	31	−2.35	427
Precentral gyrus	L	−49	−8	43	−2.29	16
MFC BA 6/8	R	6	−1	61	−2.98	144
SFG BA 6	L	−2	28	54	−2.86	112
	R	8	−1	63	−3.04	152
Limbic						
Cingulate gyrus	L	−6	6	40	−2.63	155
BA 32	R	4	10	40	−2.32	88
Temporal cortex	L					
MTL BA/37	R	−53	−66	7	−2.48	48
Parietal cortex						
Precuneus	L	−4	−73	50	−2.68	137
BA 7	R	4	−44	45	−2.19	37
Subcortical						
Thalamus	L	−4	−4	4	−2.34	30
	R	8	−9	8	−2.75	28
Cerebellum						
Declive	L	−16	−82	−16	−3.46	455
	R	36	−75	−21	−3.07	290
Uvula	L	−28	−71	−23	−3.19	111
	R	34	−63	−25	−3.24	110

Abbreviations: BA: Brodmann area; DLPFC: dorsolateral prefrontal cortex; OFC: orbitofrontal cortex; SFG: superior frontal gyrus; ACC: anterior cingulate cortex; STG: superior temporal gyrus; IPL: inferior parietal lobule; SG: supramarginal gyrus; IFG: inferior frontal gyrus; MFC: medial frontal cortex; MTL: medial temporal lobule.

showed prominently enhanced functional connectivity with the frontal cortex (mainly located in the dorsolateral prefrontal cortex, DLPFC; orbitofrontal cortex, OFC; superior frontal gyrus, SFG; and precentral gyrus), limbic system (anterior cingulate cortex, ACC; hippocampus), subcortical areas (insula, putamen, caudate, and claustrum), temporal lobe (superior temporal gyrus, STG), parietal (inferior parietal lobule, IPL; supramarginal gyrus, SG).

By contrast, sertraline treatment can also attenuate functional connectivity anchored by the hypothalamus for major depression patients. These areas were mainly located in the frontal cortex (inferior frontal gyrus, IFG; medial frontal gyrus, MFG; and superior frontal gyrus, SFG), limbic system (cingulated gyrus), temporal cortex (middle temporal gyrus, MTG), parietal cortex (precuneus), subcortical area (thalamus), and cerebellum (declive and uvula).

4. Discussion

The major finding of this study is that sertraline treatment exhibited larger impacts on the modulation of the hypothalamus-related functional connectivity brain network for major depression patients. These associations may be partially verified by the promotion of depression degree. As expected, depression degree showed significant differences after sertraline treatment. Our findings contribute to the growing evidence that sertraline treatment may be a beneficial effect on the depression patients and it mainly involved prefrontal-limbic-hypothalamus pathways. To our knowledge, this is the first in vivo magnetic resonance imaging study to demonstrate sertraline treatment impact on the hypothalamus-related resting brain network in depression patients.

Major depressive disorder is characterized by disruptions in executive control, linked to abnormal DLPFC function. The DLPFC plays an important role in working memory and other aspects of executive function [35, 36]. Previous studies have demonstrated structural changes in the prefrontal regions in major depressive disorder subjects, including decreases in cortical thickness and neural size, together with reductions in neural and glial density [37]. In the study by Thomas et al., ischemia in the white matter of DLPFC was found in subjects with late-life depression [38] and lends support to the "vascular depression" hypothesis [39, 40]. Results from these studies associate depression with abnormally low levels of DLPFC activity [41, 42]. Our findings were consistent with studies linking the DLPFC with depression and further proved that sertraline treatment can effectively improve the functional connectivity between hypothalamus and DLPFC.

The major physiological response to stress involves activations of neuroendocrine systems, mainly through the hypothalamus-pituitary-adrenal (HPA) axis.

Emotional stimuli always reach the HPA axis via the amygdala and descending pathways from the forebrain. The amygdala exerts excitatory control over the hypothalamus to stimulate the HPA axis, which, via increased cortisol levels, acts in a positive feedback manner to further stimulate

the amygdala [43]. By contrast, the hippocampus exerts inhibitory control over the HPA axis, and hippocampus acts in a negative feedback manner to inhibit the HPA axis. This is crucial for limiting the activity of the HPA axis, since that, without it, the positive feedback loop via the amygdala would cause the system to run out of control [44–46]. Descending negative feedback over the HPA axis is also exerted at the level of the dorsomedial prefrontal cortex (PFC) and the prelimbic cortex [47] so activation of these areas by emotional self-regulation can also improve the control over the HPA axis. Our results were consistent with the inference that sertraline treatment can effectively improve the functional connectivity between the hypothalamus and hippocampus.

The functional role of the cingulate cortex—and specifically the ACC—in depression is well described [48]. Our data shows significant enhancement of functional connectivity between the hypothalamus and ACC. This region is also a key component of the default mode network [49]. Abnormal resting state functional connectivity of these same regions has been described in depression [13]. Previous work using DTI data shows that connectivity in the cingulate portion of the cingulate bundle has structural changes with depression at baseline and also has an impact on remission [50]. The OFC has extensive connections with the limbic system, including the cingulate cortex [51]. The presence of enhanced functional connectivity with the hypothalamus in both ACC and the OFC supports the notion that sertraline treatment can improve the damages on these regions.

Another intriguing research is the decreased functional connectivity between the hypothalamus and cerebellum (located in the posterior part). The cerebellum generally accepts the information from temporal lobe, prefrontal lobe, and cingulated gyrus and these areas have exerted controls on the cognitive and emotional regulation [52]. It is also emphasized that the involvement of the cerebellum in cognitive and emotional controls and proposed the concept of the cerebellar cognitive affective syndrome, which usually refers from the affective bluntness and depression to affective disorder, and finally appears in execution, visual, spatial and language dysfunction [53]. Our results proved that the hypothalamus may project attenuated influence on the cerebellum after the sertraline treatment.

Limitations of this study include potential bias given that only small samples were included in the current study. Further study will include much larger sample patients and verify our hypothesis. Other factors not included in this analysis, such as age of onset, illness duration, and prior antidepressant use, may influence the hypothalamus-related resting brain network in depression. In addition, and perhaps most critical, was a lack of data on medication history. Since the majority of subjects had long-term depression (average episode duration = 4.04 years), they were likely to have taken antidepressants prior to study baseline; this prior medication use would likely have had a greater influence on functional brain networks than would concurrent medications, if any relationship exists. These factors should be addressed in future studies.

Conflict of Interests

The authors declare that there is no conflict of interests regarding the publication of this paper.

Authors' Contribution

Rui Yang and Hongbo Zhang contribute equally to this work.

Acknowledgment

This work was supported by the Natural Science Foundation of Shaanxi Province (2012JM4028).

References

[1] WHO, *The Global Burden of Disease: 2004 Update*, WHO, 2008.

[2] A. T. Beck, *Depression: Causes and Treatment*, University of Pennsylvania Press, Philadelphia, Pa, USA, 1967.

[3] A. Mathews and C. MacLeod, "Cognitive vulnerability to emotional disorders," *Annual Review of Clinical Psychology*, vol. 1, pp. 167–195, 2005.

[4] G. Parker, "Classifying depression: should paradigms lost be regained?" *American Journal of Psychiatry*, vol. 157, no. 8, pp. 1195–1203, 2000.

[5] J. Houenou, J. Frommberger, S. Carde et al., "Neuroimaging-based markers of bipolar disorder: evidence from two meta-analyses," *Journal of Affective Disorders*, vol. 132, no. 3, pp. 344–355, 2011.

[6] P. E. Keck Jr, R. C. Kessler, and R. Ross, "Clinical and economic effects of inrecognized or inadequately treated bipolar disorder," *Journal of Psychiatric Practice*, vol. 14, supplement 2, pp. 31–38, 2008.

[7] C. L. Bowden, "Strategies to reduce misdiagnosis of bipolar depression," *Psychiatric Services*, vol. 52, no. 1, pp. 51–55, 2001.

[8] V. Lorenzetti, N. B. Allen, A. Fornito, and M. Yücel, "Structural brain abnormalities in major depressive disorder: a selective review of recent MRI studies," *Journal of Affective Disorders*, vol. 117, no. 1-2, pp. 1–17, 2009.

[9] A. Anand, Y. Li, Y. Wang et al., "Activity and connectivity of brain mood regulating circuit in depression: a functional magnetic resonance study," *Biological Psychiatry*, vol. 57, no. 10, pp. 1079–1088, 2005.

[10] M. L. Schölvinck, A. Maier, F. Q. Ye, J. H. Duyn, and D. A. Leopold, "Neural basis of global resting-state fMRI activity," *Proceedings of the National Academy of Sciences of the United States of America*, vol. 107, no. 22, pp. 10238–10243, 2010.

[11] J. S. Damoiseaux, S. A. R. B. Rombouts, F. Barkhof et al., "Consistent resting-state networks across healthy subjects," *Proceedings of the National Academy of Sciences of the United States of America*, vol. 103, no. 37, pp. 13848–13853, 2006.

[12] C.-H. Liu, X. Ma, X. Wu et al., "Resting-state abnormal baseline brain activity in unipolar and bipolar depression," *Neuroscience Letters*, vol. 516, no. 2, pp. 202–206, 2012.

[13] M. D. Greicius, B. H. Flores, V. Menon et al., "Resting-state functional connectivity in major depression: abnormally increased contributions from subgenual cingulate cortex and thalamus," *Biological Psychiatry*, vol. 62, no. 5, pp. 429–437, 2007.

[14] Y. I. Sheline, J. L. Price, Z. Yan, and M. A. Mintun, "Resting-state functional MRI in depression unmasks increased connectivity

between networks via the dorsal nexus," *Proceedings of the National Academy of Sciences of the United States of America*, vol. 107, no. 24, pp. 11020–11025, 2010.

[15] M. A. Hofman and D. F. Swaab, "The human hypothalamus: comparative morphometry and photoperiodic influences," *Progress in Brain Research*, vol. 93, pp. 133–149, 1992.

[16] R. Nieuwenhuys, J. Voogd, and C. van Huijzen, "Diencephalon: hypothalamus," in *The Human Central Nervous System: A Synopsis and Atlas*, pp. 289–336, Springer, Berlin, Germany, 4th edition, 2008.

[17] S. M. Strakowski, M. P. DelBello, and C. M. Adler, "The functional neuroanatomy of bipolar disorder: a review of neuroimaging findings," *Molecular Psychiatry*, vol. 10, no. 1, pp. 105–116, 2005.

[18] M. E. Sublette, M. A. Oquendo, and J. J. Mann, "Rational approaches to the neurobiologic study of youth at risk for bipolar disorder and suicide," *Bipolar Disorders*, vol. 8, no. 5, pp. 526–542, 2006.

[19] D. A. Cousins, K. Butts, and A. H. Young, "The role of dopamine in bipolar disorder," *Bipolar Disorders*, vol. 11, no. 8, pp. 787–806, 2009.

[20] J. L. Price and W. C. Drevets, "Neurocircuitry of mood disorders," *Neuropsychopharmacology*, vol. 35, no. 1, pp. 192–216, 2010.

[21] D. F. Swaab, "Hypothalamic involvement in psychiatric disorders," in *Handbook of Clinical Neurology*, M. J. Aminoff, F. Boller, and D. F. Swaab, Eds., vol. 80 of *The Human Hypothalamus: Basic and Clinical Aspects*, pp. 248–272, Elsevier, Amsterdam, 2003.

[22] G. L. Quirarte, B. Roozendaal, and J. L. Mcgaugh, "Glucocorticoid enhancement of memory storage involves noradrenergic activation in the basolateral amygdala," *Proceedings of the National Academy of Sciences of the United States of America*, vol. 94, no. 25, pp. 14048–14053, 1997.

[23] B. Roozendaal, "Stress and memory: opposing effects of glucocorticoids on memory consolidation and memory retrieval," *Neurobiology of Learning and Memory*, vol. 78, no. 3, pp. 578–595, 2002.

[24] E. Fuchs, B. Czéh, M. H. P. Kole, T. Michaelis, and P. J. Lucassen, "Alterations of neuroplasticity in depression: the hippocampus and beyond," *European Neuropsychopharmacology*, vol. 14, no. 5, pp. S481–S490, 2004.

[25] C. B. Nemeroff, "The corticotropin-releasing factor (CRF) hypothesis of depression: new findings and new directions," *Molecular Psychiatry*, vol. 1, no. 4, pp. 336–342, 1996.

[26] H. K. Manji, J. A. Quiroz, J. Sporn et al., "Enhancing neuronal plasticity and cellular resilience to develop novel, improved therapeutics for difficult-to-treat depression," *Biological Psychiatry*, vol. 53, no. 8, pp. 707–742, 2003.

[27] P. Brambilla, J. Perez, F. Barale, G. Schettini, and J. C. Soares, "GABAergic dysfunction in mood disorders," *Molecular Psychiatry*, vol. 8, no. 8, pp. 721–737, 2003.

[28] P. Brambilla, A. Cipriani, M. Hotopf, and C. Barbui, "Side-effect profile of fluoxetine in comparison with other SSRIs, tricyclic and newer antidepressants: a meta-analysis of clinical trial data," *Pharmacopsychiatry*, vol. 38, no. 2, pp. 69–77, 2005.

[29] M. Sala, F. Coppa, C. Cappucciati et al., "Antidepressants: their effects on cardiac channels, QT prolongation and Torsade de Pointes," *Current Opinion in Investigational Drugs*, vol. 7, no. 3, pp. 256–263, 2006.

[30] H. Verdoux, M. Tournier, and B. Bégaud, "Pharmacoepidemiology of psychotropic drugs: examples of current research challenges on major public health issues," *Epidemiologia e Psichiatria Sociale*, vol. 18, no. 2, pp. 107–113, 2009.

[31] M. B. Keller, P. W. Lavori, T. I. Mueller et al., "Time to recovery, chronicity, and levels of psychopathology in major depression: a 5-year prospective follow-up of 431 subjects," *Archives of General Psychiatry*, vol. 49, no. 10, pp. 809–816, 1992.

[32] A. Cipriani, P. Brambilla, T. Furukawa et al., "Fluoxetine versus other types of pharmacotherapy for depression," *Cochrane Database of Systematic Reviews*, no. 4, Article ID CD004185, 2005.

[33] S. Patten, A. Cipriani, P. Brambilla, M. Nosè, and C. Barbui, "International dosage differences in fluoxetine clinical trials," *Canadian Journal of Psychiatry*, vol. 50, no. 1, pp. 31–38, 2005.

[34] M. Slade, M. Amering, and L. Oades, "Recovery: an international perspective," *Epidemiologia e Psichiatria Sociale*, vol. 17, no. 2, pp. 128–137, 2008.

[35] T. S. Braver, J. D. Cohen, L. E. Nystrom, J. Jonides, E. E. Smith, and D. C. Noll, "A parametric study of prefrontal cortex involvement in human working memory," *NeuroImage*, vol. 5, no. 1, pp. 49–62, 1997.

[36] M. D'Esposito, B. R. Postle, and B. Rypma, "Prefrontal cortical contributions to working memory: evidence from event-related fMRI studies," *Experimental Brain Research*, vol. 133, no. 1, pp. 3–11, 2000.

[37] G. Rajkowska, J. J. Miguel-Hidalgo, J. Wei et al., "Morphometric evidence for neuronal and glial prefrontal cell pathology in major depression," *Biological Psychiatry*, vol. 45, no. 9, pp. 1085–1098, 1999.

[38] A. J. Thomas, R. Perry, R. N. Kalaria, A. Oakley, W. McMeekin, and J. T. O'Brien, "Neuropathological evidence for ischemia in the white matter of the dorsolateral prefrontal cortex in late-life depression," *International Journal of Geriatric Psychiatry*, vol. 18, no. 1, pp. 7–13, 2003.

[39] G. S. Alexopoulos, B. S. Meyers, R. C. Young, T. Kakuma, D. Silbersweig, and M. Charlson, "Clinically defined vascular depression," *American Journal of Psychiatry*, vol. 154, no. 4, pp. 562–565, 1997.

[40] K. R. R. Krishnan, J. C. Hays, and D. G. Blazer, "MRI-defined vascular depression," *American Journal of Psychiatry*, vol. 154, no. 4, pp. 497–501, 1997.

[41] F. Biver, S. Goldman, V. Delvenne et al., "Frontal and parietal metabolic disturbances in unipolar depression," *Biological Psychiatry*, vol. 36, no. 6, pp. 381–388, 1994.

[42] I. I. Galynker, J. Cai, F. Ongseng, H. Finestone, E. Dutta, and D. Serseni, "Hypofrontality and negative symptoms in major depressive disorder," *Journal of Nuclear Medicine*, vol. 39, no. 4, pp. 608–612, 1998.

[43] S. Duvarci and D. Pare, "Glucocorticoids enhance the excitability of principal basolateral amygdala neurons," *Journal of Neuroscience*, vol. 27, no. 16, pp. 4482–4491, 2007.

[44] L. Jacobson and R. Sapolsky, "The role of the hippocampus in feedback regulation of the hypothalamic-pituitary-adrenocortical axis," *Endocrine Reviews*, vol. 12, no. 2, pp. 118–134, 1991.

[45] J. P. Herman, C. M. F. Prewitt, and W. E. Cullinan, "Neuronal circuit regulation of the hypothalamo-pituitary-adrenocortical stress axis," *Critical Reviews in Neurobiology*, vol. 10, no. 3-4, pp. 371–394, 1996.

[46] C. Belzung and E. Billette de Villemeur, "The design of new antidepressants: canformal models help? A first attempt using

a model of the hippocampal controlover the HPA-axis based on a review from the literature," *Behavioural Pharmacology*, vol. 21, no. 8, pp. 677–689, 2010.

[47] Y. M. Ulrich-Lai and J. P. Herman, "Neural regulation of endocrine and autonomic stress responses," *Nature Reviews Neuroscience*, vol. 10, pp. 397–409, 2009.

[48] W. C. Drevets, J. Savitz, and M. Trimble, "The subgenual anterior cingulate cortex in mood disorders," *CNS Spectrum*, vol. 13, no. 8, pp. 663–681, 2008.

[49] M. D. Greicius, "Functional connectivity in the resting brain: a network analysis of the default mode hypothesis," *Proceedings of the National Academy of Sciences of the United States of America*, vol. 100, no. 1, pp. 253–258, 2003.

[50] M. S. Korgaonkar, "Loss of white matter integrity in major depressive disorder: evidence using tract-based spatial statistical analysis of diffusion tensor imaging," *Human Brain Mapping*, vol. 32, no. 12, pp. 2161–2171, 2011.

[51] D. Ongür and J. L. Price, "The organization of networks within the orbital and medial prefrontal cortex of rats, monkeys and humans," *Cerebral Cortex*, vol. 10, no. 3, pp. 206–219, 2000.

[52] F. A. Middleton and P. L. Strick, "Cerebellar projections to the prefrontal cortex of the primate," *Journal of Neuroscience*, vol. 21, pp. 700–712, 2001.

[53] J. D. Schmahmann, "Disorders of the cerebellum: ataxia, dysmetria of thought, and the cerebellar cognitive affective syndrome," *Journal of Neuropsychiatry & Clinical Neurosciences*, vol. 16, pp. 367–378, 2004.

Hindawi Publishing Corporation
BioMed Research International
Volume 2014, Article ID 785039, 22 pages
http://dx.doi.org/10.1155/2014/785039

Review Article

A Survey of FDG- and Amyloid-PET Imaging in Dementia and GRADE Analysis

Perani Daniela,[1] Schillaci Orazio,[2] Padovani Alessandro,[3] Nobili Flavio Mariano,[4] Iaccarino Leonardo,[1] Della Rosa Pasquale Anthony,[5] Frisoni Giovanni,[6] and Caltagirone Carlo[7]

[1] *Nuclear Medicine Department, Vita-Salute San Raffaele University, San Raffaele Hospital and Division of Neuroscience, San Raffaele Scientific Institute, Via Olgettina 60, 20132 Milan, Italy*
[2] *Nuclear Medicine Department, University of Rome "Tor Vergata" and IRCCS Neuromed, 86077 Pozzilli, Italy*
[3] *Department of Medical and Experimental Sciences, Unit of Neurology, Brescia University, 25123 Brescia, Italy*
[4] *Department of Neuroscience Ophthalmology and Genetics, University of Genoa, 16132 Genoa, Italy*
[5] *IBFM-CNR, Via F.lli Cervi 93, Segrate, 20090 Milan, Italy*
[6] *IRCCS Centro San Giovanni di Dio Fatebenefratelli, and Memory Clinic and LANVIE, Laboratory of Neuroimaging of Aging, University Hospitals and University of Geneva, 1225 Geneva, Switzerland*
[7] *University of Rome Tor Vergata and IRCSS S. Lucia, 00142 Rome, Italy*

Correspondence should be addressed to Perani Daniela; perani.daniela@hsr.it

Received 10 October 2013; Accepted 29 January 2014; Published 19 March 2014

Academic Editor: Yong He

PET based tools can improve the early diagnosis of Alzheimer's disease (AD) and differential diagnosis of dementia. The importance of identifying individuals at risk of developing dementia among people with subjective cognitive complaints or mild cognitive impairment has clinical, social, and therapeutic implications. Within the two major classes of AD biomarkers currently identified, that is, markers of pathology and neurodegeneration, amyloid- and FDG-PET imaging represent decisive tools for their measurement. As a consequence, the PET tools have been recognized to be of crucial value in the recent guidelines for the early diagnosis of AD and other dementia conditions. The references based recommendations, however, include large PET imaging literature based on visual methods that greatly reduces sensitivity and specificity and lacks a clear cut-off between normal and pathological findings. PET imaging can be assessed using parametric or voxel-wise analyses by comparing the subject's scan with a normative data set, significantly increasing the diagnostic accuracy. This paper is a survey of the relevant literature on FDG and amyloid-PET imaging aimed at providing the value of quantification for the early and differential diagnosis of AD. This allowed a meta-analysis and GRADE analysis revealing high values for PET imaging that might be useful in considering recommendations.

1. Introduction

In Western countries, during the last century, the elderly population (over 65) has almost triplicated and in the next fifty years it will represent almost 35% of the total population. Along with ageing, dementia will become not only a dramatic clinical entity, but also a serious socio-economic issue, given that patients diagnosed with this devastating disease will likely increase by 50% by 2030.

However, the 2011 World Alzheimer Report (http://www.alz.co.uk/research/world-report) has underlined that only a percentage ranging between 20 and 50% of dementia cases are identified and recognized in the early stages, that is, at least half of the population of dementia patients suffering do not receive a complete diagnostic workup since disease onset.

This diagnostic delay gives rise to a so-called "treatment gap" between early stages of the disease and a formal

diagnosis which can then trigger necessary care and organized support ameliorating the patient's quality of life along with that of caregivers and family members. Clinical diagnosis *per se* has limited accuracy and requires the presence of cognitive symptoms, while biomarkers that are specific for AD-related pathologic phenomena would allow more accurate diagnosis when patients are in the prodromal or even preclinical stage of the disease, a period that is generally held to be the best intervention time for AD, at least at present days. PET allows the investigation of both the measurements of cerebral glucose metabolism by ^{18}F-2-fluoro-2-deoxy-D-glucose (FDG) and the Aβ amyloid deposition through specific molecular imaging techniques involving radiopharmaceuticals binding to amyloid. In the last decades, PET evidence for functional and molecular changes in neurodegenerative diseases has been largely shown [1–4]. In Alzheimer's disease (AD), within the two major classes of biomarkers now identified, biomarkers of disease state (i.e., biomarkers of amyloid β [Aβ] accumulation) and biomarkers of disease stage (i.e., biomarkers of neuronal injury), amyloid-PET, and FDG-PET imaging represent critical and decisive tools. PET imaging is now recognized of value to the early diagnosis and to clearly support the final diagnosis of AD [5–8]. Revisions of the NINCDS-ADRDA diagnostic criteria of AD [5, 9], as well as the new National Institute of Aging-Alzheimer Association criteria of MCI due to AD [6] have been proposed, positing that individuals with memory impairment who are positive for AD biomarkers have a high likelihood of having AD pathology. The corollary is that biomarker positive MCI patients frequently progress to dementia. Crucially, when both Abeta and neuronal injury biomarkers are negative, the dementia is unlikely to be attributable to AD pathology [1, 10–12].

The references based recommendations rely on sensitivity and specificity of the PET methods derived by the imaging literature that is based either on parametric approaches or on visual method that greatly depends on the observer's experience and lacks a clear cut-off between normal and pathological findings.

On the other hand, PET neuroimaging research has focused on the development of tools improving either detection of people at higher risk of dementia or early diagnosis of Alzheimer disease (AD) [13–16]. These methods improve the accuracy for the diagnosis of AD and prediction of progression from mild cognitive impairment to AD dementia [17–23]. Noteworthy, markers of amyloidosis and neurodegeneration are currently being used as outcomes in proof-of-concept drug studies [24].

The sensitivity and specificity of the PET methods indeed greatly depends on the use of quantification methods [15, 25, 26]. For example, FDG-PET can be assessed using software that analyses the pattern of tracer uptake voxel-wise by comparing the subject's scan with a reference data set of normal ageing, allowing a better recognition of the patterns of hypometabolism compared with visual interpretation [15, 17, 27].

The same is true for measurements of amyloid load using PET [25, 28, 29]. In AD, it has been shown that quantification or parametric measurements of amyloid load are fundamental since they allow cut off scores for a better differentiation between normal subjects, preclinical AD, and AD individuals [21, 22, 30]. In addition, due to the demonstration between group and intersubject variability, quantification of amyloid load would be crucial for multicentre studies and therapy monitoring. A real problem exists, whether a dichotomous readout such as that of amyloid-PET scans will be used (or misused) in the diagnostic procedures. It needs to be prevented a positive amyloid scan to become a *de facto* diagnosis of AD. Semiautomated (such as standardized uptake value ratio (SUVR)) or automated semiquantitative measures (such as using SPM-based protocols) will have the advantage of being operator independent. Semiquantitative or quantitative measures require thresholds for positivity/negativity. Thresholds include information on risk to develop dementia for subthreshold degrees of amyloid positivity. Semiquantitative or quantitative measures might in the future discriminate "accumulators" from "nonaccumulators," distinction that in normal persons could predict the development of MCI as a prodromal step to full blown AD [31]. Finally, it has to be highlighted that, today, the rationale for the use of PET biomarkers in prodromal AD diagnosis is that biomarkers change over decades before full-blown AD dementia develops [32].

Aim of this paper was to provide a survey of the specific PET literature based on the above considerations, with a meta-analysis and a GRADE analysis on FDG- and amyloid-PET imaging in the early and differential diagnosis of Alzheimer disease.

This survey was based indeed on restricted inclusion criteria of the relevant literature, namely,

(1) only articles published since 2001 which retain high quality 3D PET scans and control to an optimal degree any methodological shortcoming;

(2) for FDG-PET, only studies employing voxel-based analysis techniques (such as SPM, Neurostat, and AD t-sum) with statistical parametric mapping procedures that can provide unbiased, statistically defined measures of brain abnormality in the individual brain toward a reference control population throughout the whole brain;

(3) specifically to amyloid-PET, only articles reporting quantification or parameterization of β-amyloid deposition (in AD, MCI subjects, and normal controls) either with short half-life ^{11}C-labeled ligands (^{11}C PIB) and ^{18}F-labeled tracers (^{18}F-AV-45 Florbetapir, ^{18}F-BAY94-9172 Florbetaben, and the ^{11}C-PiB derivative ^{18}F-GE-067 Flutemetamol).

In addition, we included a descriptive analysis of the related literature reporting differences in the levels of sensitivity and specificity for the standard visual FDG-PET scan or dichotomous readout based amyloid-PET with respect to parametric or semiquantitative analysis [33–35].

1.1. Premises on FDG-PET Imaging Studies. ^{18}F-Fluorodeoxyglucose-PET (^{18}F-FDG) is used to measure cerebral

metabolic rate of glucose that is considered an index of synaptic functionality and density [36]. It has been widely used for various purposes, ranging from early diagnosis to differential diagnosis of dementias [3, 4]. There is substantial agreement about its effectiveness for diagnosis of dementia mainly for the typical hypometabolism patterns associated with the different neurodegenerative conditions (see [16]). Hypometabolism in AD has showed a very peculiar pattern since the emergence of early PET evidences [37, 38] recently defined in detail as involving parietal and temporal regions, precuneus, posterior cingulate cortex, medial temporal cortex, and structures (like hippocampus) [10, 14, 39–41]. Cerebral map of glucose metabolism can be visually inspected by experienced raters to evaluate possible neurodegenerative patterns. Despite the potential of visual inspection, modern techniques for quantification of FDG uptake are now widely used, and have been demonstrated to improve diagnosis accuracy and readability of hypometabolism patterns [33]. Statistical parametric mapping (SPM) produces unbiased smoothed and regularized images that allow a comparison between a single patient and a control group to define functionally abnormal regions. ^{18}F-FDG has been otherwise widely used to differentiate AD from non-AD dementias like DLB or FTLD spectrum. In a landmark study, Minoshima and coworkers [42] reported that relying on occipital cortex metabolism produced a sensitivity of 90% and a specificity of 80% in discriminating AD versus DLB, using autopsy pathology as reference. Similarly, Foster et al. [33] showed that ^{18}F-FDG can help discriminate between AD versus FTLD spectrum with 97% sensitivity and 86% specificity (93% accuracy). Importantly, studies have been also underlying that an absence of peculiar hypometabolism patterns may exclude a diagnosis of dementia [1].

As a matter of fact, hippocampal hypometabolism, a crucial marker of AD, is often missed, particularly in voxel-based analysis using smoothing procedure. As suggested in literature [41], by using manual region-of-interest-based (ROI) analytical methods and MRI/PET coregistration methods, the temporal medial dysfunction should be highlighted. In addition, even if has to be clarified, the method-related nature of this MRI/PET inconsistency, using coronal and/or sagittal dimensions (anterior-posterior) instead of axial orientation (inferior-superior) may at least partially overcome this "hippocampal issue," as this formation is smaller in axial view rather than in coronal or sagittal [41].

It appears that the normalization and smoothing procedures of SPM package tool that is necessary to minimize between individual inhomogeneity in brain shape and dimension may mask reduced uptake in small structures, such as the hippocampus. Moreover, spatial resolution of PET systems is best in superficial cortical areas close to the detectors while it is worst in midline and medial structures far from the detectors. Lastly, a pathophysiological explanation admits that the high synaptic density at posterior temporal-parietal association cortex and limbic cortex makes it easier to detect glucose hypometabolism in these regions as compared to the MTL structures which are rich in cell bodies but relatively poorer in synaptic density [43].

Furthermore, another florid field of research regards longitudinal studies to predict MCI-AD conversion and therefore early diagnosis of AD. Different techniques (MRI, PET, CSF, and clinical evaluation) have been extensively compared, and even though combined predictors are now considered the best solution, it has widely reported a major role (namely, in sensitivities, specificities, and prediction accuracy) of the PET [44–47].

1.2. Premises on Amyloid-PET Imaging Studies. β-amyloid plaques are a hallmark of AD and can be found in moderate to high number in cortical gray matter in all cases of AD and develop many years before the onset of dementia. The amyloid theory postulates that amyloid accumulation is the main causative event leading to synaptic and neuronal degeneration and subsequent gray matter atrophy [31]. This hypothesis is supported by the evidence that the soluble form of β-amyloid in equilibrium with the soluble β-amyloid found in plaques is potentially neurotoxic though the time interval between the deposition of β-amyloid and the beginning of a neurodegenerative process that still remains unclear [48].

In contrast, Aβ plaques are not found in frontotemporal dementia (FTD) or pure vascular dementia [12]. The amyloid hypothesis is still debated and several arguments point against amyloid as a main pathogenic factor in AD pathology [49]. Whatever the role of amyloid is, whether causative or merely an epiphenomenon, all patients with AD have an increased brain amyloid load. Therefore, the development of imaging tools for the detection and quantification of amyloid deposition is of particular relevance for the confirmation or exclusion of AD, the distinction of AD from other dementias, and its early diagnosis [50].

The first tracer for amyloid was developed at the University of Pittsburgh through modification of thioflavin T; a fluorescent dye used to identify plaques in brain tissue specimen [51] that was given the name Pittsburgh compound B (^{11}C-PiB). ^{11}C-PiB was found to bind to the amyloid in the classic (i.e., neuritic) plaques of AD, which are distributed around the degenerating neuritis. ^{11}C-PiB could label β-amyloid in living brains, and it was used in patients suffering from AD since the earliest investigations [52]. It lacks specificity to these classic plaques, as it also binds to diffuse amyloid plaques that can be found in a substantial proportion of healthy elderly and are not specific for AD [53]. Further, PiB binds to cerebrovascular amyloid in cerebral amyloid angiopathy (CAA), mainly in posterior parietal and occipital cortex. As such, PiB cannot be regarded as a specific marker of AD-amyloidosis but rather of brain amyloidosis more in general.

Leinonen et al. [54] evaluated ^{11}C-PiB uptake findings in AD patients with and without typical AD neuropathological lesions in frontal cortical biopsy specimens. The authors found a significantly higher PiB uptake in the frontal, parietal, and lateral temporal cortices and striatum in patients with Aβ aggregates in the frontal cortex compared with those without notable Aβ aggregates in the brain biopsy specimen. Moreover, the patients with the highest Aβ load in

the biopsy specimen had also the highest ^{11}C-PiB uptake in PET imaging.

Several authors investigated the diagnostic accuracy of AD by means of ^{11}C-PiB PET as unique imaging method or in combination with other measures (usually FDG-PET or volumetric MRI) and mainly using clinical criteria as reference test. For example, by comparing ^{18}F-FDG to ^{11}C-PiB PET scan, Lowe et al. [55] obtained a similar diagnostic accuracy in early cognitive impairment, but ^{11}C-PiB PET scan allowed a better discrimination between amnestic MCI and nonamnestic MCI, thus demonstrating that amyloid deposition occurs before cerebral metabolic dysfunction.

Devanand et al. [56] found that ^{11}C-PiB binding potential (BP) analysis slightly outperformed regional cerebral metabolic rate for cerebral glucose analysis of FDGPET images in discriminating AD patients from healthy controls (HC).

Similarly, [34] demonstrated the higher sensitivity of ^{11}C-PiB BP analysis in discriminating AD from FTD patients. Other two studies, comparing ^{18}F-FDG-PET and ^{11}C-PiB PET, have concluded that they give complementary information for the early diagnosis and followup of patients with dementia [57, 58]. This is a central issue, since dissociation between metabolic reduction and amyloid deposition has been also shown. In particular, in a 3 and 5 years of follow-up study on MCI and AD patients, Kadir and coworkers found that fibrillar amyloid load progressively increased in MCI patients and was followed by more stable level in clinical AD patients, whereas glucose metabolism started to decline early in MCI patients and became more pronounced in advanced clinical stage [59]. Also, the mismatch between the two imaging modalities was shown in a study investigating the effects of phenserine treatment on glucose metabolism and amyloid load in 20 AD patients [60].

A number of longitudinal studies have argued for the role of ^{11}C-PiB tracer in predicting conversion from MCI to AD. For example, it has been shown that, compared to nonconverting MCI patients and healthy controls (HC), MCI patients that converted to AD at clinical followup displayed significantly higher ^{11}C-PiB retention, at levels comparable to that of AD patients [61]. Okello et al. [21] found that the 50% of MCI patients showing a positive ^{11}C-PiB uptake at baseline converted to overt AD at 1-year followup and had greater ^{11}C-PiB retention than nonconverter patients. Similarly, in a 2-year follow-up study, Koivunen and colleagues [62], measuring ^{11}C-PiB retention in MCI and control subjects, showed that MCI patients who converted to AD had greater ^{11}C-PiB retention in several brain areas, including cingulum, frontal and temporal cortices, putamen, and caudate.

Now, it is widely accepted that ^{11}C-PiB PET can provide a quantitative representation of fibrillar deposition amyloid-beta deposition in the brain. Therefore, it is of the utmost importance to develop quantitative methods of amyloid-PET data analysis and that such methods can be standardized and applied across centers.

Analyses of PET images for the quantification of Aβ deposition have been done both qualitatively (e.g., visual analysis of tracer uptake) and quantitatively. In this latter case, analysis of tracer retention requires normalization of the uptake values, to allow inter- and intrasubject comparisons. The standard uptake value ratio (SUVR) normalizes the uptake values to the mean uptake value within a region containing nonspecific binding, usually the cerebellar grey matter. Another method, for example, based on distribution volume ratios (DVRs) and their combination with arterial plasma input, metabolite correction, or references tissue models may yield different results [63].

The interrater reliability of manual and automated ROI delineation for ^{11}C-PiB PET imaging was recently assessed for the detection of early amyloid deposition in human brain [64]. Despite methodological differences in the manual and automated approaches, the analysis revealed good agreement in primary cortical areas and the cerebellar reference region for SUV and SUVR outcomes. These data are important because a reliable methodology is needed for the detection of low levels of amyloid deposition on a cross-sectional basis and small changes in amyloid deposition on a longitudinal basis and also to enable valid definition of amyloid positivity thresholds and determination of relationships between *in vivo* PET imaging and postmortem assessments of amyloid-beta load.

A new noninvasive efficient graphical approach, called the relative equilibrium-based (RE) graphical plot, has been developed for tracer kinetics analysis, with equilibrium relative to input function; this method has been recently used to improve and simplify two of the most common approaches for ^{11}C-PiB PET quantification [65]. In this paper, results from theoretical analysis were confirmed by 78 PET studies of nondemented older adults, indicating that the RE plot could improve pixel wise quantification of amyloid-beta burden when compared with 2 frequently used methods like the Logan plot and the SUVR.

In the majority of ^{11}C-PiB PET studies, the cerebellum has been chosen as a reference region. However, because cerebellar amyloid may be present in genetic AD, cerebral amyloid angiopathy and prion diseases, whether the pons could be used as an alternative reference region for the analysis of ^{11}C-PIB binding in AD has been evaluated [66]. The findings of the study in 12 sporadic AD patients, 10 age-matched controls, and 3 other subjects (2 with presymptomatic presenilin-1 mutation carriers and one probable familial AD) suggest that that the target-to-pons ratio for the analysis of ^{11}C PIB images has low test-retest variability and high reproducibility and can be used as a simplified method of quantification when the cerebellum as a reference is not appropriate.

The definition of a cutoff that separates individuals with no significant amyloid-beta deposition from those in which deposition has begun is crucial for the clinical acceptance of ^{11}C-PiB PET. In a cohort of older subjects in which the separation between PiB positive and PiB negative subjects was not so distinct, the application of visual read and quantitative approaches optimized the identification of early amyloid-beta deposition [26].

In addition to ^{11}C-PiB, other ^{18}F-labeled tracers have been developed and investigated. Flutemetamol (GE-067) is

the 3′-fluoro-derivative of PiB, whereas florbetaben (BAY-94-9172, AV-1) and florbetapir (AV-45) are stilbene and styrylpyridine derivatives, which exhibit high affinity binding for fibrillary amyloid. Flutemetamol kinetic analysis of tracer binding showed reliable quantification by use of relative standardized uptake value ratios with the cerebellar cortex as a reference region, and data acquisition for this analysis requires only 20 min scanning and is feasible in a standard clinical setting [67]. Florbetaben and florbetapir are chemically closely related compounds but the former has slower kinetics, resulting in a longer imaging acquisition time (for stable uptake up to 130 min after injection), in comparison with Flutemetamol (90 min) and Florbetapir (60 min) [68].

In a recent PET study using ^{18}F-Florbetapir with 74 HC and 29 AD patients with terminal disease, demonstrated a high correlation between *in-vivo* tracer uptake and the presence of β-amyloid at autopsy, as well as 96% sensitivity and 100% specificity in distinguishing HC from AD, thus suggesting that ^{18}F-Florbetapir PET provides an accurate and reliable assessment of amyloid burden [69]. A large study pooling data from the 4 registered phases I and II trials of florbetapir PET imaging, confirmed the ability of florbetapir uptake analysis to characterize amyloid levels in clinically probable AD, MCI, and HC groups using both continuous and binary quantitative measures of amyloid burden [70].

2. Methods

2.1. Study Inclusion Criteria. The general inclusion criteria for relevant research studies were the following:

(i) articles had to be published in a peer-review scientific journal;

(ii) studies reporting sensitivity and specificity measures in relation to a histopathological or clinical diagnosis of neurodegenerative diseases;

(iii) studies including large cohorts of subjects (see Table 1: early diagnosis FDG: range 20–395; Table 2: differential diagnosis FDG: range 45–297; Table 3: early diagnosis amyloid: range 13–107);

(iv) studies investigating the prediction of mild cognitive impairment (MCI) to Alzheimer's disease (AD) conversion that retrospectively analyzed the initial characteristics of those who were progressive and those who remained stable.

2.1.1. Specifically to FDG-PET. (i) Only articles published since 2001 were considered, which retain high quality by controlling to an optimal degree both clinical and methodological shortcomings.

(ii) Only studies employing voxel-based analysis techniques (such as SPM, Neurostat, and AD t-sum) with statistical parametric mapping procedures can provide unbiased, statistically defined measures of brain abnormality throughout the whole brain on a voxel-by-voxel basis; the basic procedure in voxel-based analysis involves the spatial normalization and smoothing of each individual's PET scan to an anatomically defined standard brain reference volume (the template or atlas volume) in the stereotactic space. This enables voxel-by-voxel statistical comparison of the ^{18}F-FDG pattern in the individual brain toward a reference control population. FDG uptake in each voxel must be previously normalized to the average uptake of a reference region, since without arterial blood sampling or other validated quantification methods, the standard PET procedure does not allow true quantitative measurements of glucose consumption. The reference region can change; the "default" reference region in SPM is the whole brain while Neurostat allows choosing among the whole brain, the cerebellum, and the thalamus. By changing the reference region, the results of parametric mapping may change as well. Final agreement on the region to be used is still lacking; the choice of whole brain tends to reduce sensitivity because the hypometabolic voxels are included in the average, while the cerebellum tends to increase sensitivity because it is less affected by neurodegeneration in AD. Taking in mind these limitations and that they do not allow true quantitative estimation of glucose metabolism but rather of glucose metabolism distribution, all these procedures result in an observer-independent mapping of regional abnormalities of glucose metabolism.

2.1.2. Specifically to Amyloid-PET. (i) Only articles reporting parameterization of β-amyloid deposition in patients with AD, MCI and normal controls either with short half-life ^{11}C-labeled ligands ^{11}C PIB and ^{18}F-labeled tracers (^{18}F-AV-45 Florbetapir, ^{18}F-BAY94-9172 Florbetaben, and ^{18}F-GE-067 Flutemetamol). Articles reporting quantification with other β-amyloid compounds have been excluded when (a) there was uncertainty about the selectiveness of the binding to amyloid plaques (e.g., ^{11}C BF-227) or (b) utilization of recently released compounds still needing for a systematic evaluation (e.g., ^{18}F-AZ4694, namely, NAV4694).

(ii) Furthermore, only articles using quantification methods such as distribution volume ratio (DVR) or standardized volume uptake ratio (SUVR) were included in the analysis. Similar to FDG-PET, to calculate the uptake without blood sampling, results are shown as ratios with a reference region, usually cerebellum (even though utilization of pons is currently debated [66] see also *Pet Amyloid Imaging studies paragraph*). Obviously the change of reference region can affect the results, but as a final agreement is lacking, this is up to the authors to rely on the affinity of the different compounds for multiple reference regions. As regards SUVR, to discriminate between "amyloid positive" and "amyloid negative" burdens (as well as between "low" and "high" retention), authors have been applying cut-off scores, usually obtained by control groups (like in [71] or using values reported in literature i.e., [72] for ^{11}C-PIB PET or [73] for ^{18}F-Florbetapir). Therefore, manipulating cut-off scores can heavily affect results, leading to radically different groups' characterization. Despite these variations in the methodology of amyloid quantification, automated algorithms can fairly discriminate between different patterns of retention, in an observer-independent fashion, leading to important advantages in clinical practice and diagnosis.

Table 1: Summary of included 18F-FDG-PET for early diagnosis and conversion prediction, with LHR, increase in LHR+, GRADE, and population.

Authors	Population	Method	Cohort investigated	Follow-up (months)	Sensitivity	Specificity	LHR+	Increase in the LHR+	Quality of evidence (GRADE)
Arnáiz et al., 2001 [79]	20MCI	ROI	20	36	0.67	0.82	3.72	Small	L
*Herholz et al., 2002 [27]	110 HC; 395 pAD	AD t-sum	395	—	0.93	0.93	13.29	Large	M
Mosconi et al., 2004 [80]	37 MCI	SPM	37	12	1	0.9	10.00	Moderate	M
Drzezga et al., 2005 [82]	30 MCI	SPM + Minoshima	30	16	0.92	0.89	8.36	Moderate	M
Anchisi et al., 2005 [17]	48 aMCI	SPM	48	12	0.929	0.824	5.28	Moderate	M
*Haense et al., 2009a [84]	89 AD; 102 HC	AD t-sum	89	—	0.83	0.78	3.77	Small	L
*Haense et al., 2009b [84]	237 AD; 37 HC	AD t-sum	237	—	0.78	0.94	13.00	Large	M
Yuan et al., 2009 [20]	280 MCI	Meta-analysis	280	14.25	0.888	0.849	5.88	Moderate	M
*Landau et al., 2010 [85]	85 MCI; 97 AD; 102 HC	SPM + ROI	97	—	0.82	0.7	2.73	Small	L
Brück et al., 2013 [86]	22 MCI	SPM + ROI	22	24	0.87	0.78	3.95	Small	L
*Arbizu et al., 2013 [87]	80 HC; 36 MCIc; 85 MCIs; 67 AD	Automated voxel-based analytical method	67	—	0.818	0.86	5.84	Moderate	M

Total number of patients and healthy controls considered in the study. Method: quantitative method applied in the study. Cohort investigated: number of patients considered for sensitivity and specificity estimations. Followup: duration of observational period (for early diagnosis study). Sensitivity and specificity: results of the study. LHR+: likelihood ratio. Increase in the LHR+: increase in the probability of the likelihood of the disease. GRADE: results of GRADE evaluation. Quality of evidence was evaluated based on LHR+ values, LHR+ increase probability, and size of the sample included.

Abbreviations: pAD: probable Alzheimer's disease; MCI: mild cognitive impairment; aMCI: amnestic mild cognitive impairment; MCIc: MCI converters; MCIs: MCI stable; HC: healthy controls.

*Studies including early diagnosis of AD.

Table 2: Summary of the included PET studies for differential diagnosis, with LHR+, increase of the LHR+, and GRADE.

Authors	Population	Method	Cohort investigated	Sensitivity	Specificity	LHR+	Increase in the LHR+	Quality of evidence (GRADE)
Minoshima et al., 2001 [42]	AD + LBD	Minoshima	74	0.9	0.8	4.50	Small	L
Gilman et al., 2005 [88]	AD + LBD	VOI lCMRglc	45	0.643	0.652	1.85	Minimal	VL
Foster et al., 2007 [33]	AD + FTD	Minoshima	45	0.732	0.976	30.50	Large	M
Mosconi et al., 2008a [89]	AD + FTD	Minoshima	297	0.99	0.65	2.83	Small	L
Mosconi et al., 2008b [89]	AD + LBD	Minoshima	226	0.99	0.71	3.41	Small	L
Mosconi et al., 2008c [89]	AD + HC	Minoshima	199	0.99	0.98	49.50	Large	M
Mosconi et al., 2008d [89]	FTD + LBD	Minoshima	125	0.71	0.65	2.03	Small	L

Population: different dementias considered in the diagnosis. Method: quantitative method applied in the study. Cohort investigated: number of patients considered for sensitivity and specificity estimations in the discrimination. Sensitivity and specificity: results of the study data show potential of discrimination. LHR+: likelihood ratio. Increase in the LHR+: increase in the probability of the likelihood of the disease. GRADE: results of GRADE evaluation. Quality of evidence was evaluated based on LHR+ values, LHR+ increase probability, and size of the sample included.
Abbreviations: AD: Alzheimer's disease; LBD: Lewy body dementia; FTD: frontotemporal dementia; HC: healthy controls.

Table 3: Summary of the included amyloid-PET studies included with LHR and GRADE analysis.

Authors	Population	Method	Cohort investigated	Follow-up months	Sens.	Spec.	LHR+	Increase in the LHR+	Quality of evidence (GRADE)
Barthel et al., 2011 [96, 97]	81 AD; 69 HC	ROI SUVR analysis	81	—	0.85	0.91	9.44	Moderate	M
Rabinovici et al., 2011 [34]	62 AD; 45 FTD	ROI DVR analysis	107	12	0.89	0.83	5.24	Moderate	M
Rostomian et al., 2011 [58]	42 AD; 31 FTD	ROI DVR analysis	73	16	0.905	0.84	5.66	Moderate	M
Rowe et al., 2008 [93]	15 AD; 5 FTD; 15 HC	SUVR analysis	20	12	1	0.9	10.00	Moderate	L
Villemagne et al., 2011 [12]	30 AD; 20 MCI; 32 HC; 11 FTD; 7 LBD; 5 PD; 4 VaD	SUVR analysis	30	—	0.97	0.84	6.06	Moderate	M
Clark et al., 2012 [102]	5 MCI; 29 AD; 12 HC; 13 ODD	SUVR analysis	47	24	0.97	0.99	97.00	Large	M
Camus et al., 2012 [29]	13 AD; 12 MCI; 21 HC	SUVR + Visual	13	—	0.923	0.905	9.72	Moderate	VL
Koivunen et al., 2011 [62]	29 MCI; 13 HC	PiB retention analysis	29	24	0.94	0.42	1.62	Minimal	VL
Mosconi et al., 2009 [19]	31 MCI	ROI ratio SPM	31	32.16	0.93	0.76	3.88	Small	L
Forsberg et al., 2010 [100]	37 mild AD; 21 MCI	ROI ratio SPM	58	33	1	0.71	3.45	Small	L
Jack et al., 2010 [46]	53 MCI	DVR	53	20.4	0.83	0.46	1.54	Minimal	VL
Wolk et al., 2009 [101]	23 MCI	DVR SPM	23	21	1	0.56	2.27	Small	L

Population: total number of patients and healthy controls considered in the study. Method: quantitative method applied in the study. Cohort investigated: number of patients considered for sensitivity and specificity estimations. Followup: duration of observational period (for early diagnosis study). Sensitivity and specificity: results of the study. LHR+: likelihood ratio. Increase in the LHR+: increase in the probability of the likelihood of the disease. GRADE: results of GRADE evaluation. Quality of evidence was evaluated based on LHR+ values, LHR+ increase probability, and size of the sample included.
Abbreviations: AD: Alzheimer's disease; FTD: frontotemporal dementia; MCI: mild cognitive impairment; ODD: other dementia; LBD: Lewy body dementia; VaD: vascular dementia; HC: healthy controls.

2.2. Meta-Analysis and GRADE Analysis

2.2.1. GRADE Evaluation. Scientific evidences available regarding each of the tests (^{18}F-FDG-PET or amyloid-PET) for the early and differential diagnosis of AD, as well as for MCI conversion prediction, are graded in terms of Level of Confidence (LoC: VL = very low, L = low, M = moderate, and H = high), as reported by GRADE system [74–76]. Tables 1, 2, and 3 show the level of confidence ratings assigned to the studies reviewed in this paper, indicating that none of the studies was rated high whereas most studies were rated moderate to low.

It is to be mentioned that according to the GRADE system, the best way to assess any "diagnostic strategy" is randomized controlled trials in which investigators randomize patients to experimental or control diagnostic approaches in order to provide high quality evidence of test accuracy for the development of recommendations about diagnostic testing.

Both the clinical context and complex implementation of brain FDG or amyloid-PET protocols, however, paralleled with ethical issues raised by the degree of invasiveness of both procedures, are not comparable to randomized trials or many observational studies in which the alternative diagnostic test has been carried out in order to establish high quality of evidence or clear differences in patient important outcomes based on GRADE framework.

Furthermore, it must be acknowledged that the results of FDG- or amyloid-PET diagnostic approaches do not have nothing to do with effective treatments (as the usual GRADE evaluative study set); however, they may have a significant positive impact in terms of patient outcomes, such as reducing the treatment gap between AD pathological onset and diagnosis of the disease, thus improving ability to plan which can be considered analogous to an effective patient treatment [77]; the correct diagnostic inclusion of patients in pharmacological trials [78], the appropriate family context, and behavior induced by the diagnosis are very useful in supporting pharmacological and cognitive remediation approaches.

Notwithstanding the here selected criteria for investigations employing FDG- or amyloid-PET brain imaging have been rated only as "low" or "moderate" quality evidence for recommendations about diagnostic procedures in a GRADE system, we have to consider that there will be great indirect benefits for their "patient-outcome" (i.e., test accuracy in terms of sensitivity and specificity). Assessing the directness of evidence supporting the use of a diagnostic test requires judgments about the relationship between test results and patient-important consequences, therefore in this paper a severe challenge arose in the attempt to apply GRADE to two crucial questions about FDG- or amyloid-PET as accurate, valid and powerful diagnostic tests, for (1) the early diagnosis and (2) the differential diagnosis of AD.

Guyatt et al. [76] stated that "GRADE will disappoint those who hope for a framework that eliminates disagreements in interpreting evidence and in deciding on the best among alternative courses of action. Although the GRADE system makes judgments about quality of evidence and strength of recommendations in a more systematic and transparent manner, it does not eliminate the need for judgments."

That is, applying a GRADE system in a PET functional and molecular imaging evaluation for diagnosis can be accepted due to the high value for low and moderate results in such a setting.

In this survey, we performed three different meta-analyses for evaluating the accuracy and effectiveness of diagnostic tests (i.e., FDG or amyloid), in order to make a judgment about quality of evidence (GRADE) on the early or differential diagnosis and for conversion prediction of dementia in our population. Given that the sensitivity of a test shows the proportion of patients with the disease (i.e., AD) whom the test classifies as positive while the specificity shows the proportion without the disease (i.e., no neurodegenerative disease) whom the test classifies as negative, we computed the positive likelihood ratio for each study included in the three meta-analyses, (i.e., FDG-PET or amyloid-PET imaging in the early diagnosis of Alzheimer disease and FDG-PET in the differential diagnosis of Alzheimer disease) which combines information from sensitivity and specificity and gives an indication of how much the odds of disease change based on a positive or a negative result (i.e., accuracy). For example, a positive likelihood ratio of 10 means that a positive test result is ten times more likely in a diseased subject than in a healthy person. The resulting positive likelihood ratio (LR+) for each study was interpreted according to general guidelines for evaluating the probability increase of detecting the disease through a test (i.e., LR+ > 10 = large; 5 > LR+ > 10 = moderate; 2 > LR+ > 5 = small; 1 > LR+ > 2 = minimal; 0 > LR+ > 1 = no increase). Available scientific evidence regarding each of the topics was graded in terms of level of confidence (LoC: VL = very low, L = low, M = moderate, and H = high), as reported by the GRADE collaboration [74, 75]. In the GRADE system, valid diagnostic accuracy studies can provide high quality evidence of test accuracy. Quality of evidence (GRADE) for each study was evaluated based on LR+ values, LR+ probability increase, and the size of the sample included for each study (i.e., e.g., a study with a moderate LR+ probability increase but with a relatively small sample ($n = 20$) would be rated as low in terms of quality of evidence) (see Tables 1, 2, and 3).

In addition, we obtained a summary measure of effectiveness in each meta-analysis by weighting individual study effect measures according to their variance and by adopting a general inverse-variance weighted fixed-effects model to summarize individual effect measures (i.e., sensitivity analysis) and a Q test was performed to measure heterogeneity among studies. Sensitivity measures for each study were then arranged in a forest plot together with their 95% confidence intervals In order to represent the position of each study included over the central tendency, represented by the calculated summary fixed-effect sensitivity measure (see Figures 1(a), 1(b), and 1(c)).

2.3. Qualitative versus Quantitative Assessment. A description of differences in the levels of sensitivity and specificity for the standard visual FDG-PET scan or dichotomous

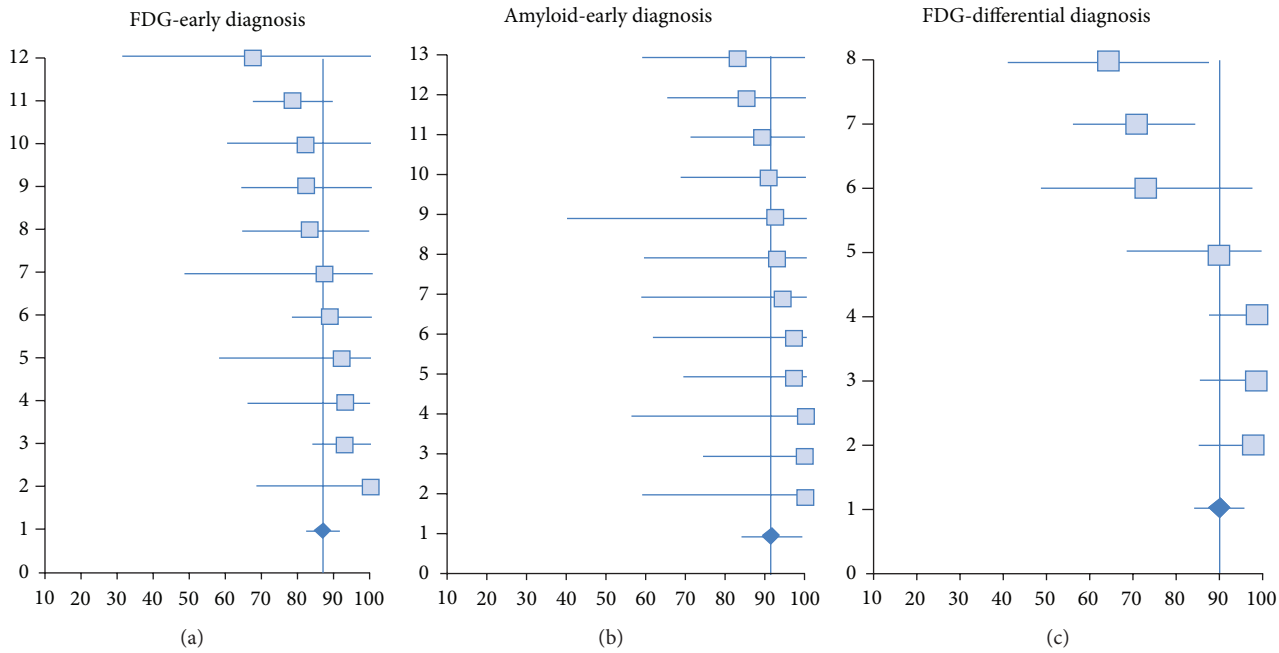

Figure 1: Forest plots of sensitivity measures and 95% confidence intervals for individual studies included in each meta-analysis.

readout based amyloid- PET with respect to parametric or semiquantitative analysis was performed on the basis of the data in literature reporting sensitivity and specificity of both the visual and the parametric methods in the same population.

3. Results

3.1. ^{18}F-FDG PET in the Early Diagnosis of AD. The systematic review identified a total of 10 studies that met our inclusion criteria (see Table 1); the most relevant findings were as follows.

Arnáiz et al. [79] showed that, in a cohort of $N = 20$ MCI followed for a mean observational period of 36 months, reduced glucose metabolism from left temporoparietal area could predict conversion with a 75% percentage of correct classification, resulting in 67% sensitivity and 82% specificity. Authors conclude that these measures of temporoparietal metabolism may aid (together also with neuropsychological data) in predicting evolution of MCI patients to AD.

In a landmark study, Herholz and colleagues [42] investigated metabolic abnormalities with ^{18}F-FDG-PET in a cohort of $N = 110$ HC and $N = 395$ probable AD. Despite the cross-sectional nature of the study, useful information was provided about an early diagnosis of AD because of the fragmentation of the pAD group in different subgroups related to probable disease severity (e.g., very mild probable AD group, MMSE ≥24). Authors calculated an AD t-sum score for each individual, and this score was applied to discriminate between various subgroups and controls. This method yielded 93% sensitivity and 93% specificity in classification of pAD versus HC, acting as a very useful tool to early diagnosis of AD.

Similarly, Mosconi and colleagues [80] followed a group of $N = 37$ MCI patients for a 12-month period. At the followup, $N = 8$ MCI converted while $N = 29$ remained stable. Authors analyzed, with a voxel-based method and analysis of variance, regional differences in cerebral glucose metabolism, using conversion (y/n) as outcome and APOE genotype (E4+/E4−) as grouping factor. Results show that for the whole MCI sample, inferior parietal cortex hypometabolism could predict conversion to AD with 84% diagnostic accuracy, 100% sensitivity, and 95% specificity. Furthermore, E4 carriers (E4+) converters ($N = 5$) presented significantly decreased metabolism in frontal areas, such as anterior cingulate cortex (ACC) and inferior frontal cortex (IFC). The authors' conclusion is that ^{18}F-FDG-PET may improve prediction of the MCI-AD conversion especially when combined with APOE genotype information.

Anchisi and coworkers [17] investigated in a longitudinal study a cohort of $N = 67$ amnestic-MCI patients of which $N = 48$ underwent follow-up examination at a (at least) 12-month interval. The ROC curve calculated for the glucose metabolism measured in two voxel ROIs (posterior cingulate and temporoparietal) showed an area under the curve (AUC) of 0.0863. With a cut-off at 1.138, authors reported 92.9% and 82.4% as, respectively, sensitivity and specificity in discriminating converters versus nonconverters. In addition, negative predictive value of 96.55% and a positive predictive value of 68.4% were reported. Furthermore, authors combined functional metabolism impairment with memory test score (Long free delay recall part of the California verbal learning test, CVLT-LFDR) [81] showing an inverse pattern: lower sensitivity (85.7%), higher specificity (97.1%), lower negative predictive value (94.3%), and a higher positive predictive value (92.3%). Authors claim that using

^{18}F-FDG-PET may help in predicting short-term conversion to AD, particularly combined with memory scores and also to account for the functional heterogeneity among subjects with aMCI.

Drzezga and coworkers [82] in a longitudinal prospective study on 30 MCI patients (mean observation period, 16 months) assessed the value of FDG-PET in detecting brain metabolic abnormalities in early AD, by using Neurostat [83] to perform an observer-independent statistical comparison with an age-matched reference database. The authors reported that the sensitivity and specificity of FDG-PET with regard to early diagnosis of AD in MCI patients were 92% and 89%, respectively.

Haense et al. [84] also investigated performance of ^{18}F-FDG-PET for detection of AD within two different samples, from ADNI and Network for Standardisation of Dementia Diagnosis (NEST-DD). The cohort from ADNI consisted in $N = 102$ HC and $N = 89$ AD, while the sample from NEST-DD comprised $N = 36$ HC and $N = 237$ AD. The authors generated AD t-sum maps and used a preset cut point for discrimination. Results were twofold: (1) AD presented much higher AD t-sum maps than HC in both samples and (2) early onset-AD presented higher AD t-sum maps than late-onset AD. The cut-off threshold yielded sensitivity and specificity of 83% and 78%, respectively, in ADNI; in NEST-DD, results showed 78% sensitivity and 94% specificity. Authors conclude that this automated procedure to analyze ^{18}F-FDG-PET scans is useful for the discrimination and is also more accurate for early onset AD.

Yuan and colleagues [20] performed a meta-analysis to evaluate and compare the ability of FDG-PET, single-photon emission tomography (SPECT), and structural MR imaging to predict conversion to AD in patients with MCI. Relevant studies were identified with MEDLINE from January 1990 to April 2008 and a meta-regression was carried out from eligible studies on the diagnostic performance data for each technique. This study included data from 1112 MCI patients (of which $N = 280$ investigated by FDG-PET) and showed that FDG-PET had better concordance with follow-up results for the prediction of conversion to AD dementia. Approximately 88.9% of the patients with progressive MCI were detected as positive by FDG-PET, whereas 84.9% of stable patients had negative FDG-PET at first scanning time (sensitivity 88.9%, specificity 84.9%). Further, FDG-PET was found to perform better than SPECT and structural MR imaging in the prediction of conversion to AD in patients with MCI.

Recently, Landau and coworkers [85] compared different biomarkers of conversion and decline in MCI investigating a fairly large cohort throughout the different predictors (FDG-PET, MRI/hippocampal volume, CSF biomarkers, Memory Score/Rey Auditory Verbal Learning Test). As regards ^{18}F-FDG-PET, $N = 85$ MCI were followed for a period of (mean) 21 months. During the observation period, $N = 28$ converted (MCIc) while $N = 57$ remained stable (MCIs). To evaluate the power of the prediction with ^{18}F-FDG-PET measured metabolism (parametrically analyzed with SPM, metaROI global index), the authors obtained cut-off scores from an independent sample rather than using cut-off scores present in literature. To do so, $N = 102$ Healthy controls and $N = 97$ AD were screened, resulting in a cut-off set at 1.21 to discriminate between "AD(+)" and "AD(−)". ROC curve at this score showed 82% sensitivity, 70% specificity and an overall accuracy of 76% in discriminating between AD and controls. Thereafter, the derived cut-off was used to calculate predictive values of conversion for the MCI group, resulting in a positive predictive value of 41% and a negative predictive value of 78%. To say, the 78% of MCI classified as "AD(−)" at baseline remained stable, whereas MCI classified as "AD(+)" had a 2.72 greater risk of conversion. Then authors concluded that the FDG-PET was the most informative biomarker, especially when combined with RAVLT episodic memory score.

In a longitudinal study comparing ^{11}C-PIB-PET, ^{18}F-FDG-PET and MRI, Brück and coworkers [86] investigated MCI conversion in a sample of $N = 29$ MCI (of which, only $N = 22$ underwent also ^{18}F-FDG). Clinical follow-up was carried on at a 24-months interval. During the observation period $N = 13$ MCI converted to AD while $N = 9$ MCI remained stable. All the ^{18}F-FDG-PET were optimized and analyzed with region of interest approach and SPM methodology, deriving a cut-off of 1.16 in left lateral temporal cortex (internally derived). This cut point was used to classify patients in "High" and "Low" ^{18}F-FDG, resulting in a sensitivity of 87% and a specificity of 78% in predicting conversion to AD. Similarly, patients were divided in "High" and "Low" ^{11}C-PIB depending on PiB uptake in lateral frontal cortex (internally derived cut-off: 1.57), providing 65% sensitivity and 75% specificity. When combined, ^{18}F-FDG and ^{11}C-PIB (e.g., Low FDG-High PiB) resulted in 87.5% sensitivity and 71.4% specificity. The authors' claim is that ^{18}F-FDG and ^{11}C-PIB are better than hippocampal volume in predicting conversion.

Arbizu and colleagues very recently [87] proposed a new score for automated analysis of ^{18}F-FDG-PET, called AD-Conv score, as a tool for single-subject prediction of conversion to AD. Their cohort comprised $N = 80$ HC, $N = 121$ MCI of which $N = 36$ MCIc (at 18-months interval) and $N = 85$ MCIs (at 24-months interval) and $N = 67$ AD. Briefly, their method consisted in generating an "AD-PET-pattern" from an external reference population and based on z-score map obtained with SPM. This map was then compared with individual hypometabolism voxel-by-voxel resulting in an AD-PET-index, that combined with age and gender generated the AD-Score. Starting from this score, meant to discriminate between AD and HC, authors generated a score to discriminate between MCIc and MCIs applying several modifications. First, instead of using a whole brain z-map (the AD-PET-pattern), AD-PET index was segmented in five volumes-of-interest (VOIs), namely left parietal, right parietal, left temporal, right temporal and posterior cingulate, and then compared with individual hypometabolism resulting in the MCI-PET-Index. Furthermore, to compute the score, APOE genotype (E4+/E4−), years of education and MMSE were combined with age obtaining the AD-Conv-Score. Further statistical analysis

showed that only hypometabolism in posterior cingulate area was significant in differentiating MCIc from MCIs and, together with APOE4 genotype and MMSE, yielded the AD-Conv-Score parameter. With an AD-Conv cut-off score at 0.28, the method classified MCIc and MCIs with 91.7% sensitivity and 62.4% specificity. As regards predictive values, a positive predictive value of 51% and a negative predictive value of 95% were shown.

3.2. ^{18}F-FDG PET in Differential Diagnosis between Forms of Dementia. A total of 4 papers addressing the discrimination power of FDG-PET between different neurodegenerative forms met the criteria outlined above (see Table 2). Among the studies pinpointed in Table 2, three studies included patients with a clinical diagnosis of probable AD, three studies included patients diagnosed with Lewy-Body Dementia (LBD), and two studies included patients with a diagnosis of Frontotemporal lobar degeneration (FTLD).

Minoshima et al. [42] examined brain glucose metabolism of DLB and AD and showed that FDG-PET discriminates DLB from AD with 90% sensitivity and 80% specificity using autopsy confirmation. They also concluded that the presence of occipital hypometabolism preceded some clinical features of DLB and that FDG-PET sensitivity was superior in differentiating DLB from AD with respect to medical charts exclusively based on clinical diagnostic criteria.

Similarly, Gilman and coworkers [88] investigated metabolism differences between AD and DLB measured with ^{18}F-FDG-PET in a sample of $N = 25$ AD, $N = 20$ DLB and $N = 19$ elderly HC. ^{18}F-FDG scans were analyzed with Minoshima method on selected VOIs (global cortex and occipital cortex, known to discriminate between DLB and AD in terms of CMRglc). Furthermore discrimination power was estimated also for neuropsychological scores such as MMSE, confrontation naming test and verbal fluencies. Logistic regression showed that glucose metabolism in BA17 (visual cortex) presented 64.3% sensitivity and 65.2% specificity for diagnosis of DLB. To say, the hypometabolism patterns of these two diseases were similar except for the metabolic rate in visual cortex.

In the widely cited study by Foster et al. [33] the utility of ^{18}F-FDG statistical parametric maps rather than simple transaxial FDG-PET scans for dementia diagnosis was evaluated. Six experienced raters were forced to make a diagnosis about a cohort of $N = 45$ patients, all pathologically confirmed, of which $N = 31$ AD and $N = 14$ FTD. Results showed that the utilization of ^{18}F-FDG statistical maps (stereotactic surface projection maps SSP) yielded high diagnostic accuracy (89.6%), showing 73% sensitivity and 97.6% specificity. Authors conclude that also after a brief training in visual interpretation of ^{18}F-FDG statistical maps this method is more reliable and accurate than clinical methods alone.

Mosconi and colleagues [89], in a large multicenter study, examined FDG-PET measures in the differentiation of AD, FTD, and DLB from normal aging and from each other ($N = 548$ subjects, including 111 healthy individuals). Each PET scan was Z-transformed by using automated voxel-based comparison resulting in statistical maps of disease-specific patterns of brain ^{18}F-FDG uptake. The differentiation and classification of patients in independent groups between patients and controls and among dementia forms yielded 99% sensitivity, 65% specificity (97% accuracy) for AD compared with FTD; 99% sensitivity, 71% specificity (97% accuracy) for AD compared to DLB; 99% sensitivity, 98% specificity (98% accuracy) for differentiating between AD and healthy controls; 71% sensitivity, 65% specificity (68% accuracy) for DLB with respect to FTD. Thus, this study strongly supported the validity and diagnostic accuracy of FDG-PET in the differential diagnosis of the three major neurodegenerative disorders.

3.3. FDG-PET Summary. These data provide strong evidence for FDG-PET parametric imaging to detect pathological changes occurring in the brain. FDG-PET holds great promise for diagnostic assessment of patients with Alzheimer disease (AD) and the other two major neurodegenerative diseases (i.e., DLB and FTLD) to the point that the recently revised diagnostic criteria of AD [5, 9] as well as the new National Institute of Aging-Alzheimer Association criteria of MCI due to AD [6] for the first time recognize the specific role of FDG-PET as a topographical functional biomarker in Alzheimer disease definition. What is especially relevant in this context is that FDG-PET as a neurodegeneration biomarker has been placed before brain atrophy in specific regions, as shown by means of MRI, in the hypothetical cascade model of AD biomarkers [46]. In fact, FDG-PET maps distribution of glucose metabolism occurring mainly at synaptic level [90]. Thus, pathologic phenomena leading to neuritic dysfunction affects synaptic glucose consumption prior of causing cell death and detectable atrophy [91, 92]. As such, FDG-PET is a proxy of reduced glucose utilization at synaptic level of still alive neurons.

It must be acknowledged that voxel-based procedures for objective image analysis can now be easily applied clearly providing evidence for a role of FDG-PET in assessment of dementia through the identification of disease-specific hypometabolic patterns. The main advantages of automatic methods consist in the fact that images can be interpreted even by intermediate-skilled readers and that false positive results are virtually eliminated, thus increasing specificity.

The primary objective of both tabulated surveys was to select studies on the basis of the mandatory need for the evaluation of the FDG-PET scans based on an automatic, unbiased voxel-based analysis in order to achieve higher confidence in diagnostic accuracy to significantly reduce the gap with post-mortem gold standard confirmatory diagnosis. The evidence provided in the tabulated surveys supports the role of FDG-PET as an effective tool aiding in the early diagnosis and differential diagnosis of dementia. The diagnostic accuracy of FDG-PET resulted to be high also in subjects with prodromal disease, for whom the clinical diagnosis and differential diagnosis are especially challenging. In fact, [1] claimed that "the sensitivity and specificity available with

FDG-PET near the time of initial diagnosis of AD is similar to longitudinal clinical diagnosis over 3-4 years".

3.4. Amyloid-PET in the Diagnosis of AD. The systematic review identified a total of 12 studies that met our inclusion criteria (see Table 3); the most relevant findings were as follows.

In their study, Rowe and coworkers [93], investigated the reliability of the ^{18}F-BAY94-9172 (Florbetaben) in a relatively small cohort (N = 15 AD, N = 15 HC and N = 5 FTD) in discriminating between the three conditions. Authors analyzed quantitatively the neocortex uptake with SUVR measure, using the cerebellum as reference region. Experienced raters then visually inspected the maps of SUVR distributions. Visual inspection of SUVR maps yielded 100% sensitivity and 90% specificity in discriminating AD versus HC or FTLD. Authors conclude that florbetaben imaging can be included successfully in clinical use.

Using ^{18}F-Flutemetamol PET scan in 25 HC, 20 MCI and 37 AD patients, Vandenberghe et al. [94] using SUVR distributions showed 93.1% sensitivity and 93.3% specificity and a very high correlation with ^{11}C-PIB uptake (r = .89) for visual inspection. It is noteworthy that sensitivities and specificities did not differ significantly between qualitative (visual) and quantitative methods (SUVR cutoff automated classification in raised uptake category). Further, it has been shown that the tracer uptake highly correlated with percentage of brain area of amyloid measured by cortical biopsy [95].

Barthel and colleagues [96, 97] investigated the use of ^{18}F-Florbetaben (^{18}F-BAY94-9172) PET analysis in two contiguous studies (phase 0 and 2) involving 69 HC and 81 AD patients and found that visual assessment of PET images allowed 80% sensitivity and 91% specificity. On the other side, linear discriminant analysis of regional SUVR yielded an 85% sensitivity and 91% specificity. The same tracer has been demonstrated to be useful in discriminating different forms of dementia as well as patients from controls [12, 93]. The first results on florbetaben indicate that this radiopharmaceutical, while having a narrower dynamic range than ^{11}C-PiB PET, is able to clearly differentiate HC from AD patients with a comparable effect size [98]. Moreover, quantification of β-amyloid binding from florbetaben PET data is feasible and all β-amyloid binding parameters including SUVR are excellent in discriminating between β-amyloid positive and negative scans [99].

In the study by Rostomian et al. [58], ^{18}F-FDG and ^{11}C-PIB were compared to evaluate the power of diagnosis of the *in vivo* imaging of fibrillar beta-amyloid versus metabolism or CSF. The authors tried first in a test cohort composed by N = 10 patients with various clinical diagnosis and, when identified the correct iterative algorithm, analyzed a sample of N = 42 AD and N = 31 FTLD with both FDG-PET and C-PIB PET (these map were obtained from t-test with reference regions, such as cerebellar for PiB). Results showed that with PIB PET had 90.5% sensitivity and 83.9% specificity (for AD), versus the, respectively, 88.1% and 83.9% with FDG-PET. Temporal pole and neocortex was significant for both the compounds, whereas the frontal lobe was particularly significant for PIB-PET. Authors conclude that the combined use of these two compounds can be very useful for early diagnosis of AD.

Other amyloid-PET studies addressing AD and MCI cases in large series came out in the literature reporting high sensitivity and intermediate/low values of specificity [21, 46, 62, 100, 101].

In the study by Villemagne et al. [12] authors still evaluated ^{18}F-Florbetaben in imaging AD versus other dementia types. Their cohort consisted in N = 32 HC, N = 20 MCI, N = 30 AD, N = 11 FTD, N = 5 LBD, N = 5 Parkinson's Disease (PD) and N = 4 Vascular Dementia (VaD). SUVR values for whole brain neocortical retention were calculated using cerebellar cortex as reference region. Results showed that almost all of the AD group (96%) and more than half of the MCI group (60%) presented diffuse cortical retention whereas the other groups presented far minor cortical retention (FTLD = 9%, VaD = 25%, DLB = 29%, PD = 0%, HC = 16%). Semiquantitative SUVR analysis yielded a 97% sensitivity and 84% specificity in discriminating AD versus Healthy Controls. Authors conclude that ^{18}F-Florbetaben can be useful in distinguishing AD from other dementias (e.g., FTLD) and that its effectiveness is comparable with the results obtained by ^{11}C-PiB compound.

In a prospective cohort study by Clark et al. aimed to compare florbetapir PET with neuropathology at autopsy for detecting neuritic amiloid-β plaques, also the relation between SUVR and neuritic plaque density was assessed [102]. Based on values from a series of young participants who were cognitively normal, Joshi et al. [73] had previously proposed a cutoff value of 1,10 to distinguish normal from abnormal scans. In the paper of Clark et al., all the cases with no or sparse plaques at autopsy had SUVR values of less than 1,10, and all but one with moderate or frequent plaques at autopsy had SUVR values greater than 1,10. SUVR analysis showed a 97% sensitivity and 99% specificity in detecting high or low burden of amyloid plaques with a 24-months autopsy reference.

Using PET with florbetapir to quantify brain amyloid load in a routine clinical environment to differentiate between patients with mild to moderate AD and MCI from HC, the quantitative assessment of the global cortex SUVR reached a sensitivity of 92.3% and specificity of 90.5% with a cut-off value of 1.12 [29].

3.5. Amyloid-PET Summary. Up to date, the literature demonstrates that ^{11}C-PiB PET allows reliable detection and in particular quantification of β-amyloid deposition in patients with AD.

However, because of the short half-life of ^{11}Carbon, which requires an on-site cyclotron and radiochemistry laboratory, ^{11}C-PiB has been compared with ^{18}F-labeled tracers like ^{18}F-Florbetapir, ^{18}F-Flutemetamol or ^{18}F-Florbetaben, which can be produced at central cyclotron and then delivered to clinical PET centers.

^{18}F-Florbetapir and ^{18}F-Flutemetamol are FDA approved in the US for clinical use, now also ^{18}F-Florbetapir by the EMA, whereas ^{18}F-florbetaben has not yet been approved in USA and Europe. These tracers could be largely used in detecting β-amyloid deposition and in distinguishing patients with AD from Frontotemporal dementia. As a limit, lipophilic plasma metabolites, which have been partially reported for ^{18}F-labeled tracers, could increase non-specific background activity.

The results of these included studies show a promising role of those ^{18}F-labeled tracers, but further data on larger number of patients also evaluated longitudinally are needed to clarify their diagnostic and prognostic potential roles in AD.

A central issue in PET estimation of amyloid load regards the use of semiquantitative analyses of images. In this view, a consensus regarding categorization of positive and negative subjects has not been established so far. For example, some groups have treated SUVR as a continuous variable whereas other groups have dichotomized subjects into positive and negative groups using a cut-off score, since the distribution of this variable is usually skewed. Further, there is variability in categorization approaches amongst studies that dichotomize into positive and negative groups. Some authors considered positive those subjects showing SUVR values that are 1, 1.5 or 2 standard deviations higher than normal controls [34, 56, 103–105], while others used more complex approaches such as cluster analyses [12, 48, 106, 107], iterative outlier removal [108] or complex functions [94]. SUVR cut-off values separating negative from positive subjects vary in the literature from 1.1 to 1.6, with a mean value around 1.3. The limit of classifying into positive and negative subjects relies on the fact that the threshold is often dependent on the distribution of SUVR values present in the control group under investigation rather than on a group of subjects lacking Aβ deposition.

In a recent study, ^{11}C-PiB and florbetapir PET were compared in a retrospective sample of cognitively normal older controls, patients with MCI, and patients with AD. ^{11}C-PiB and florbetapir retention ratios were strongly associated in the same individuals, and the relationship was consistent across several data analysis methods, despite scan-rescan intervals of more than a year. The findings of this study indicate that cutoff thresholds for determining positive or negative amyloid-β status can be reliably transformed from PIB to florbetapir units or vice versa using a population scanned with both radiopharmaceuticals [71].

Nordberg et al. [22] in a European multicentre PET study of fibrillar amyloid in AD based on very large datasets demonstrated the robustness of [^{11}C]-PIB PET as a marker of neocortical fibrillar amyloid deposition in brain when assessed in a multicentre setting. The variance of [^{11}C]PIB retention between different participating centers was low compared to the large differences between diagnostic groups, suggesting that results obtained from [^{11}C]PIB PET are highly consistent and reproducible. MCI PIB-positive patients showed more severe memory impairment than MCI PIB-negative patients and progressed to AD at an estimated rate of 25% per year. None of the MCI PIB-negative patients converted to AD, and thus PIB negativity had a 100% negative predictive value for progression to AD. This supports the notion that PIB-positive scans in MCI patients are an indicator of prodromal AD and that amyloid imaging is both a highly useful tool for diagnosis of AD in its earliest symptomatic stages and is suitable for identifying patients for antiamyloid therapy in multicentre clinical trials. The paper reports also the vast majority of healthy controls (46 out of 51) and showed neocortical [^{11}C]PIB retention ratios in the very narrow range of 1.13 to 1.39 (mean 1.26 ± 0.07). The upper 95% confidence limit in the normally distributed control population was 1.41, thus defining the normal limit.

One of the main issues since the advent of amyloid tracers remains and is represented by a percentage of HC showing an amyloid load in the range of patients with AD [22, 107, 109]. One of the future challenges in PET studies with ^{18}F amyloid tracers is to reach standardize quantitative measures (especially by means of longitudinal approaches) in order to establish reliable quantitative cut-offs that can be helpful in separating HC and AD subjects, in differential diagnosis of dementia and in providing prognostic indices for those subjects showing early signs of cognitive loss.

3.6. Qualitative versus Quantitative Assessment. Few papers in literature systematically investigated improvements in diagnostic accuracy and/or in differential diagnosis obtained by using quantified (or semiquantified) and qualitative analysis of FDG-PET scans. The results showed that the qualitative interpretation by visual reading of brain ^{18}F-FDG-PET scans and amyloid-PET scans clearly lacks clear-cut milestones to distinguish between a normal and a pathological scan. Indeed, in the already cited study by Foster and coworkers [33], authors compared five separate methods (clinical summaries, diagnostic checklist alone, summary and checklist, transaxial ^{18}F-FDG-PET scans and ^{18}F-FDG-PET stereotactic surface projection metabolic and statistical maps-SSP) for distinguishing AD from FTD in an autopsy-referenced cohort of $N = 31$ AD and M=14 FTD, adopted by six dementia experts. Data showed that the transaxial FDG-PET scans method yielded 96% sensitivity, 59% specificity and a mean accuracy of 84.8% in distinguishing AD versus FTD. On the other hand, the ^{18}F-FDG-PET SSP method improved sensitivity (97.6%), specificity (73.2%) and overall accuracy (89.2%). Authors conclude that ^{18}F-FDG-PET improves dementia diagnosis accuracy, especially when metabolism was quantitatively analyzed prior to visual expert rating and interpretation.

Recently, Rabinovici et al. [34] compared ^{11}C-PiB and ^{18}F-FDG in differential diagnosis of AD and FTLD in a cohort of $N = 62$ AD and $N = 45$ FTLD. It is noteworthy that the authors compared also qualitative (visual) and quantitative (DVR for ^{11}C-PiB, cut-off at 1.2 and regional ROI Z-score for ^{18}F-FDG) methods in their diagnostic efficacy. As regards qualitative evaluation of PET scans, ^{11}C-PiB PET yielded higher sensitivity for AD (89.5% versus 77.5%) and slightly lower specificity (83% versus 84%). Quantitative thresholds

for automated classification of scans provided interesting results. As a matter of fact, while ^{11}C-PiB PET DVRs yielded very similar results (89% sensitivity 83% specificity versus 89.5% sensitivity and 83% specificity), quantitative analysis of ^{18}F-FDG-PET increased specificity (98% versus. 84%). Authors conclude that with both methods ^{11}C-PiB PET was more sensitive, while ^{18}F-FDG-PET was more specific only when scans were interpreted quantitatively. Furthermore, a recent longitudinal study by Patterson et al. [35] showed that detection by Statistical Parametric Mapping (SPM) was more accurate ($N = 18$ subjects detected) than clinical evaluation of FDG-PET scans ($N = 10$ detected) in a cohort of $N = 31$ MCI followed for a 3-years period. Specifically, SPM detected correctly $N = 9$ MCI converters (versus $N = 5$ detected by subjective visual interpretation) and $N = 4$ subjects not meeting criteria for MCI (one of them was detected also visually), therefore highlighting a possible role for SPM in revealing metabolic defects anticipating clinical manifestations. Preliminary results in a study comparing inspection of visual FDG-uptake distribution maps and visual SPM hypometabolism maps in discrimination in a total cohort of $N = 95$ patients ($N = 45$ AD, $N = 30$ MCI, $N = 25$ FTLD) show higher sensitivity (96% versus 78%) and specificity (84% versus 50%) [110].

Other studies, even though not aiming as a primary endpoint to compare qualitative and quantitative analysis, provided results coherent with our claim. One of the most relevant findings is provided in the already cited study by Camus et al. [29] that investigated potential of ^{18}F-Florbetapir in discriminating AD versus HC. Their results showed that while visual assessment yielded 84.6% sensitivity and a 38.1% specificity, a quantitative global cortex SUVR analysis yielded 92.3% sensitivity and 90.5% specificity, with a cutoff point set at 1.122.

3.7. Meta-Analysis and GRADE Analysis. Tables 1, 2, and 3 show the characteristics of each study included in each meta-analysis, namely population sample, method employed, follow-up in months (i.e., only for early diagnosis), sensitivity and specificity measures, LR+, LR+ probability of increase, and GRADE evaluation [76, 77]. The total number of patients summed across all studies for each meta-analysis was computed and included 1322 patients for FDG-early diagnosis, 647 for amyloid-early diagnosis, and 1011 for FDG-differential diagnosis. Summary sensitivity effect measures were .86 for FDG-early diagnosis, .91 for amyloid-early diagnosis, and .90 for FDG-differential diagnosis. Q-test values for FDG-early diagnosis ($Q = 6{,}83$) and for amyloid-early diagnosis ($Q = 1, 94$) were below critical values assessed at $P < 0.05$, revealing low heterogeneity between studies included in each. The Q-value for studies included in the FDG-differential Diagnosis meta-analysis ($Q = 18.61$) was above critical values assessed at $P < 0.05$, indicating moderate heterogeneity. Forest plots for each meta-analysis show that the central tendency for the effectiveness of FDG-PET or amyloid-PET for the early or differential diagnosis of dementia is above 85%, however the 95% confidence intervals for studies FDG-early diagnosis reveal a lower degree of uncertainty with respect to amyloid-early diagnosis (see Figures 1(a) and 1(b)).

4. Discussion

Clinical, pathologic, and genetic evidence indicate that the primary dementias have different underlying aetiologies and pathogenetic mechanisms. Treatment approaches of these conditions are different and hopefully will be even more so in the future. Thus, accurate diagnosis is critical in order to maximize the efficacy and appropriateness of specific regimes. At present, best differential diagnosis of dementia relies on histopathological observations, usually available only at autopsy. When faced with a patient carrying a neurodegenerative disease possibly causing dementia, current guidelines suggest that the clinician must establish a probable etiopathogenic diagnosis based on evidence available from neurological and cognitive evaluation, blood tests, structural MRI neuroimaging, and PET imaging [5–8]. Attempts to differentiate between neurodegenerative diseases causing dementia based in the early prodromal phase can be hard, particularly when patients present with subtle prodromal symptoms or with clinical-neuropsychological characteristics that overlap between primary dementias or with an atypical profile of symptoms. Therefore, establishing valid and reliable markers of the main neurodegenerative diseases causing dementia which are capable to identify specific changes during the early clinical stages, or even in preclinical stages as it happens in genetic forms of AD, is a pivotal and strategical issue.

A decade ago, the American Academy of Neurology regarded CT and MR imaging as "optional" examinations for the diagnosis and evaluation of dementia [111]. This view was counterbalanced by a Consensus of the European Alzheimer Disease Consortium (EADC) in 2003, highlighting the changing philosophy on the role of neuroimaging in the dementia workup [112]. However, structural neuroimaging techniques, even if widely accepted and of high-value in the diagnosis and management, have no clear cut role in the very early stage of the diseases and at individual level. Attempts in measuring volumes of specific structures, such as the hippocampal formation, have been undertaken mainly in AD, with interesting results in group analysis, but still with lack of consistent and validated cut-off scores for individual analysis. In some neurodegenerative diseases other than AD, such as diffuse Lewy-body disease, MRI might present with multiple pattern of atrophy or even with null results in early stages. Thus, in the temporal dynamics of biomarkers in the Alzheimer's pathological cascade, atrophy represents the last phenomenon in comparison to biomarkers of brain dysfunction, early neurodegeneration, and amyloid deposition [46].

Functional neuroimaging techniques may aid in the early diagnosis of neurodegenerative disorders and to clearly support the final diagnosis. Positron emission topography (PET) allows the investigation of both the measurement

of cerebral glucose metabolism by ^{18}F-2-fluoro-2-deoxy-D-glucose (FDG) and the quantification of Aβ amyloid deposition through specific molecular imaging techniques involving radiopharmaceuticals binding to amyloid.

FDG-PET started to be used in AD about 30 years ago [37] but its role in the diagnostic road map of Alzheimer disease and related dementias has not gained general consensus up to few years ago. In fact, both the "Dubois" [5, 9] and the NIA-AA [6, 8] new diagnostic criteria have included FDG-PET as a valid tool for biomarker measure of neurodegeneration, by showing specific metabolic changes that precede atrophy as detected with MRI. The basic concept is that FDG-PET estimates glucose consumption at the synaptic-astrocyte level [90] thus picking-up very early changes already detectable even in asymptomatic subjects at high risk for AD [113, 114]. In AD, the core of such changes is the precuneus and the posterior cingulate cortex [17, 19], the MTL structures that are mainly highlighted with ROI-based than with voxel-based automatic approach, and the association posterior lateral parietal and temporal cortex. The same glucose utilization defect can be detected in other regions in FTLD [115, 116]; primary progressive aphasia (PPA) [117]; dementia with Lewy bodies (DLB) [88]. FDG-PET studies are therefore increasingly being used as an adjunct in the initial clinical evaluation of patients with suspected dementia, particularly to aid in early detection [17] or when clinical diagnosis is doubtful. As shown by the here included studies, voxel-based FDG-PET as *in vivo* biomarker measure plays a key role in the identification of early functional brain derangements. In this view, a recently introduced term designed to define the spectrum of cognitive function between healthy aging and dementia is mild cognitive impairment (MCI). It was [118] who first set out formal criteria for a diagnosis of MCI (subjective complaint of memory loss; objective impairment of ability; preserved general cognitive function; intact activities of daily living; individual does not meet criteria for dementia). People meeting these criteria are considered at higher risk of developing AD compared to general population [119]; consequently, MCI is considered the optimal clinical stage for both early detection and intervention of AD. More recently, the position paper by the International Working Group for New Research Criteria for the Diagnosis of AD [5] further introduced new concepts and distinguished between (i) preclinical states of AD, in which individuals are free of symptoms, yet have either biomarker evidence of Alzheimer's pathology or a monogenic form of AD and (ii) prodromal or predementia AD, referring to those clinically affected individuals who do not have dementia yet but are diagnosed to have AD on the basis of evidence of Alzheimer's pathology from biomarkers.

With regard to degenerative diseases such as AD, physicians' confidence in diagnosing dementia can be undermined by several factors such as young age of onset, high education level (where neuropsychological tests can fail to reveal a subtle, despite substantial, cognitive decline), atypical presentation, and presence of psychiatric or cognitive comorbidities. The information provided by FDG-PET can therefore satisfy a fundamental need not only as a disease confirmatory test (high sensitivity) but also as an exclusion test (high specificity), especially in the early stage of the disease.

On this regard, an international consortium of investigators argued that, due to its high sensitivity, a negative (i.e., normal) FDG-PET scan strongly favors a normal outcome at followup [1, 10].

Two decades of ^{18}F-FDG-PET studies in neurodegenerative diseases provided evidence for specific metabolic patterns [3].

Teune and colleagues [2] in a large study focusing on patients who had an FDG-PET scan at an early disease stage (96 patients: 20 patients with Parkinson's disease (PD), 21 with multiple system atrophy (MSA), 17 with progressive supranuclear palsy (PSP), 10 with corticobasal degeneration (CBD), 6 with dementia with Lewy bodies (DLB), 15 with Alzheimer's disease (AD), and 7 with frontotemporal dementia (FTD)) summarized the typical metabolic dysfunction in the different diseases. Each patient received a retrospectively confirmed diagnosis according to strictly defined clinical research criteria. FDG-PET images of each patient group were analyzed and compared with healthy controls using statistical parametric mapping (SPM5). The authors concluded that a combined method, including clinical information and voxel-based analysis technique, can discriminate patient groups across a spectrum of various neurodegenerative brain diseases, also at early disease stages. This implies that an early and more accurate diagnosis in individual patients can be made by comparing each subject's statistical objective map of brain glucose metabolism with a validated disease-specific hypometabolic pattern arising in specific brain areas, naturally grounded in a detailed clinical frame.

In the context of initial diagnosis, the exclusionary role of FDG-PET is especially clear in younger subjects with a suspicion of neurodegenerative disease. The high specificity of FDG-PET in AD, FTLD, and DLB implies that a negative, or normal, scan in the presence of the suspicion of dementia makes a diagnosis of a neurodegenerative disease very unlikely.

Based on the specificity of functional imaging with ^{18}F-FDG-PET that measures synaptic dysfunction in different networks, depending on the underlying pathology, and on the sufficiently large body of evidence in the literature, we strongly claim that ^{18}F-FDG-PET should be considered an essential component of the diagnostic workup of early onset dementia.

With regard to amyloid-PET, its potential clinical usefulness is strictly based on the assumption that early cerebral amyloidosis is virtually always detected in subjects on the path of AD. Even if there are still controversies about the so-called "amyloid hypothesis" in the pathogenesis of AD [120], the fact remains that amyloidosis is practically a held prerequisite for the diagnosis of AD. Nowadays, probably no physician would be highly confident with the diagnosis of AD in a patient in whom cerebral amyloidosis has not been confirmed. According to the temporal biomarker cascade hypothesis [52], brain amyloidosis would be a very early phenomenon, already detectable many years before the onset of symptoms.

As for differential diagnosis, amyloid-PET is less useful for the identification of DLB because most patients with this disease show brain amyloidosis that cannot be distinguished from that of AD patients [120]. In clinical practice, when a subject is evaluated because of cognitive symptoms, even if subtle, the demonstration of high brain amyloid load should strongly suggest one of the two main forms of neurodegenerative disease with amyloidosis, that is, AD or DLB. The topographic pattern of amyloid deposition is similar in these two conditions, but the pattern of neurodegeneration harbors significant differences because glucose hypometabolism specifically and extensively affects the occipital lobes in DLB and just marginally in AD whereas MTL hypometabolism, which is the classical fingerprint of AD, is seldom found in DLB [121]. Still in doubtful cases, the demonstration of nigrostriatal dopamine transporter deficit leads to identifying DLB with high accuracy [122].

Further, at least in AD, brain amyloid deposition seems to be a very early phenomenon and rather rapidly reaches a "plateau" at the time cognitive deficits become detectable [123], thus mirroring Aβ 1–42 levels in cerebrospinal fluid [124]. As such, the amount of amyloid deposition, along with Aβ 1–42 levels in cerebrospinal fluid, should not be viewed as an accurate index of disease progression. As a matter of fact, there is evidence that cognitive decline is much more related to the markers of neurodegeneration rather than to severity of amyloidosis, thus arguing for a higher sensitivity of PET-FDG and CSF levels of Tau and Phospho-Tau.

In the literature, visual inspection of amyloid burden has been reported to parallel the accuracy by quantification of the uptake (e.g., SUVR; see [34]). Other results, however, reported different findings (see [29]). It is of note that this may be true when discriminating mild to moderate AD with conditions in which amyloid retentions are null or nonsignificant (e.g., FTLD spectrum). When comparing early stages of AD pathology (MCI versus AD or even preclinical AD conditions), the methods based on quantification or semiquantification acquire relevance and might become mandatory. Typically, when considering patterns of accumulations in MCI during a follow-up period, quantitative analysis shows their power to detect changes [125].

In addition, while the *in vivo* detection of Aβ amyloid is gaining ground in the diagnosis of AD especially in MCI patients, the meaning of a positive PET scan in nondemented patients remains yet unclear. In our opinion, quantitative amyloid-PET scans, better defining the amount of amyloid load in these individuals, can prevent a positive amyloid scan to become a *de facto* diagnosis of AD. A paper from Mintun and colleagues [126] focused on this aspect by using ^{11}C-PiB PET scan in 41 nondemented subjects and 10 AD patients. Results showed that, globally, patients had greater uptake ratios, although 4 of the controls had cortical binding values that were comparable to those of AD patients, thus supporting the hypothesis that amyloid imaging could be used to detect preclinical stages of AD. A similar result has been described more recently by Mormino and coworkers [108] who found that the 15% of a large cohort of elderly HC showed positive ^{11}C-PiB uptake ratios. The clinical significance of these observations is still unclear and only long-term follow-up studies can clarify it. On the basis of the data available to date, it appears that these apparently healthy subjects with high amyloid load are likely to be on the path of AD, although we still ignore the time span from amyloid deposition and onset of first cognitive symptoms [46]. There is strong debate about the fate of "healthy" controls who displayed a positive amyloid-PET scan as we still ignore the time needed for an asymptomatic subject with amyloidosis to develop cognitive signs/symptoms. The time span has been indicated in a modeling of AD in the order of 10 years [46], but how to predict this time on an a real individual basis is still unknown. Noteworthy, recent evidence in individuals at risk for developing AD showed significant amyloid burden in autosomal dominant familial AD, even 15-16 years prior expected/predicted symptoms onset [113, 127] or 17 years before in sporadic AD cases [128]. The "nun" study has demonstrated that at least some individuals die with high brain amyloid load, but without any cognitive symptom or sign [129]. The biological evidence of amyloid load in human brains extended to elderly health individuals. This also implies ethical issues regarding what to communicate to an healthy volunteer found to be amyloid positive during clinical trials [130].

But just in this context of brain amyloidosis without symptoms, the demonstration of early signs of neurodegeneration in specific sites using voxel-based FDG-PET would be of great value. Starting from the observation that FDG-PET can be positive several years before the onset of dementia [64, 65], it would be possible to narrow the time of uncertainty in asymptomatic subject with amyloidosis. In other words, cognitively normal subjects showing cerebral amyloidosis through PET amyloid tracers along with glucose hypometabolism at specific sites would be at very high risk of developing a dementia process within few years. On the other hand, in a symptomatic patient with a suspicion of early AD, it has been proposed that amyloid-PET should precede any other evaluation just after morphological MRI [131] as a positive scan would strongly support the diagnosis of AD, thus avoiding most of the other diagnostic procedures, while a negative amyloid-PET scan would lead to search for other causes. Of utmost importance is the possibility to scan with amyloid-PET subjects in the MCI stage which represents a significant step toward the selection of groups with earlier AD for clinical trials. This would avoid including patients with a misdiagnosis and give experimental drugs the chance to be tested at the very onset of symptoms instead of when the disease has been already too progressed. While the potential of amyloid-PET is not a matter of debate in research, its misuse in clinical sets needs a careful regulation in order to give a proper role and a specific clinical context to this technique. That is why, recently, the Society of Nuclear Medicine and Molecular Imaging and the Alzheimer's Association have jointly convened the Amyloid Imaging Task Force (AIT) and published the Appropriate Use Criteria for amyloid-PET [132, 133]. They provided the appropriate use criteria for Amy-PET in which the circumstances for executing Amy-PET are listed.

According to those, Amy-PET will be appropriate for patients with persistent or progressive unexplained MCI, or satisfying core clinical criteria for possible AD (i.e., atypical clinical course or etiologically mixed presentation; for patients with atypically young-onset dementia). Crucially, the AIT also define the inappropriate use of amyloid-PET in the following conditions: (1) in patients with core clinical criteria for probable AD and with typical age of onset; (2) determination of dementia severity; (3) positive family history of dementia or presence of apolipoprotein E (APOE) $\varepsilon 4$; (4) in patients with a subjective cognitive complaint that is unconfirmed on clinical evaluation; (5) as an alternative to genotyping for suspected autosomal mutation carriers; (6) in asymptomatic individuals; (7) nonmedical uses such as (legal, insurance coverage, or employment screening).

In conclusion, on the basis of the present survey and also on the meta-analyses and GRADE analysis, we showed that there is moderate quality evidence for the effects of both modalities of PET imaging (FDG and Amyloid) in the early diagnosis of AD and conversion prediction, and, equally, moderate quality evidence for the differential diagnosis of patients with AD and the other major neurodegenerative dementia (i.e., DLB and FTLD). The three meta-analyses conducted through the three categories of studies (early diagnosis, disease progression and differential diagnosis), as remarked in the Results section, yielded significant results. Summary sensitivity effect measures were 0.86 for ^{18}F-FDG-PET (1322 cases), 0.91 for amyloid-PET (797 cases), and 0.90 for differential Diagnosis (1011 cases). Therefore, on the basis of the studies included in the present survey, amyloid-PET seems to be more sensitive than ^{18}F-FDG-PET in early diagnosis of AD. It is of note that our analysis included a sample of patients investigated by ^{18}F-FDG-PET larger than the cohort investigated by amyloid-PET. Hence, even if the effect measure is lower, we can interpret that result as more robust. In addition, the grade analysis classified more ^{18}F-FDG-PET studies as M (moderate, $N = 7$) than for amyloid-PET ($N = 5$) that is coherent with the previous claim. Lastly, as anticipated in Results section, the 95% confidence intervals for ^{18}F-FDG-PET early diagnosis and disease progression reveal a lower degree of uncertainty with respect to amyloid-PET early diagnosis (see Foster plots, Figure 1). For these reasons, we can definitely conclude that both the topographical and pathological PET markers are very accurate and sensitive to early diagnosis of AD, as well as to differential diagnosis with other dementia (e.g., FTD or DLB) when appropriate data analysis at single subject level is performed.

This survey and GRADE analysis show a good overall quality of evidence for PET functional (FDG) and molecular (amyloid) imaging in early and differential diagnosis of AD, on the basis of voxel-based or parametric data quantifications. This approach will allow net benefits in terms of diagnostic and prognostic value of the information provided by PET imaging considering its sensitivity and accuracy.

Conflict of Interests

The authors declare that there is no conflict of interests regarding the publication of this paper.

References

[1] W. Jagust, B. Reed, D. Mungas, W. Ellis, and C. DeCarli, "What does fluorodeoxyglucose PET imaging add to a clinical diagnosis of dementia?" *Neurology*, vol. 69, no. 9, pp. 871–877, 2007.

[2] L. K. Teune, A. L. Bartels, B. M. de Jong et al., "Typical cerebral metabolic patterns in neurodegenerative brain diseases," *Movement Disorders*, vol. 25, no. 14, pp. 2395–2404, 2010.

[3] V. Berti, A. Pupi, and L. Mosconi, "PET/CT in diagnosis of dementia," *Annals of the New York Academy of Sciences*, vol. 1228, no. 1, pp. 81–92, 2011.

[4] V. Berti, A. Pupi, and L. Mosconi, "PET/CT in diagnosis of movement disorders," *Annals of the New York Academy of Sciences*, vol. 1228, no. 1, pp. 93–108, 2011.

[5] B. Dubois, H. H. Feldman, C. Jacova et al., "Revising the definition of Alzheimer's disease: a new lexicon," *The Lancet Neurology*, vol. 9, no. 11, pp. 1118–1127, 2010.

[6] M. S. Albert, S. T. DeKosky, D. Dickson et al., "The diagnosis of mild cognitive impairment due to Alzheimer's disease: recommendations from the National Institute on Aging-Alzheimer's Association workgroups on diagnostic guidelines for Alzheimer's disease," *Alzheimer's & Dementia*, vol. 7, no. 3, pp. 270–279, 2011.

[7] G. M. McKhann, D. S. Knopman, H. Chertkow et al., "The diagnosis of dementia due to Alzheimer's disease: recommendations from the National Institute on Aging-Alzheimer's Association workgroups on diagnostic guidelines for Alzheimer's disease," *Alzheimer's & Dementia*, vol. 7, no. 3, pp. 263–269, 2011.

[8] R. A. Sperling, P. S. Aisen, L. A. Beckett et al., "Toward defining the preclinical stages of Alzheimer's disease: recommendations from the National Institute on Aging-Alzheimer's Association workgroups on diagnostic guidelines for Alzheimer's disease," *Alzheimer's & Dementia*, vol. 7, no. 3, pp. 280–292, 2011.

[9] B. Dubois, H. H. Feldman, C. Jacova et al., "Research criteria for the diagnosis of Alzheimer's disease: revising the NINCDS-ADRDA criteria," *The Lancet Neurology*, vol. 6, no. 8, pp. 734–746, 2007.

[10] D. H. S. Silverman, G. W. Small, C. Y. Chang et al., "Positron emission tomography in evaluation of dementia: regional brain metabolism and long-term outcome," *Journal of the American Medical Association*, vol. 286, no. 17, pp. 2120–2127, 2001.

[11] V. L. Villemagne, M. T. Fodero-Tavoletti, K. E. Pike, R. Cappai, C. L. Masters, and C. C. Rowe, "The ART of loss: Aβ imaging in the evaluation of Alzheimer's disease and other dementias," *Molecular Neurobiology*, vol. 38, no. 1, pp. 1–15, 2008.

[12] V. L. Villemagne, K. Ong, R. S. Mulligan et al., "Amyloid imaging with ^{18}F-florbetaben in Alzheimer disease and other dementias," *Journal of Nuclear Medicine*, vol. 52, no. 8, pp. 1210–1217, 2011.

[13] M. Signorini, E. Paulesu, K. Friston et al., "Rapid assessment of regional cerebral metabolic abnormalities in single subjects with quantitative and nonquantitative [^{18}F]FDG PET: a clinical validation of statistical parametric mapping," *NeuroImage*, vol. 9, no. 1, pp. 63–80, 1999.

[14] S. Minoshima, K. A. Frey, R. A. Koeppe, N. L. Foster, and D. E. Kuhl, "A diagnostic approach in Alzheimer's disease using three-dimensional stereotactic surface projections of fluorine-18-FDG PET," *Journal of Nuclear Medicine*, vol. 36, no. 7, pp. 1238–1248, 1995.

[15] A. Caroli, A. Prestia, K. Chen et al., "Summary metrics to assess Alzheimer disease-related hypometabolic pattern with

^{18}F-FDG PET: head-to-head comparison," *Journal of Nuclear Medicine*, vol. 53, no. 4, pp. 592–600, 2012.

[16] N. I. Bohnen, D. S. W. Djang, K. Herholz, Y. Anzai, and S. Minoshima, "Effectiveness and safety of ^{18}F-FDG PET in the evaluation of dementia: a review of the recent literature," *Journal of Nuclear Medicine*, vol. 53, no. 1, pp. 59–71, 2012.

[17] D. Anchisi, B. Borroni, M. Franceschi et al., "Heterogeneity of brain glucose metabolism in mild cognitive impairment and clinical progression to Alzheimer disease," *Archives of Neurology*, vol. 62, no. 11, pp. 1728–1733, 2005.

[18] O. Hansson, H. Zetterberg, P. Buchhave, E. Londos, K. Blennow, and L. Minthon, "Association between CSF biomarkers and incipient Alzheimer's disease in patients with mild cognitive impairment: a follow-up study," *The Lancet Neurology*, vol. 5, no. 3, pp. 228–234, 2006.

[19] L. Mosconi, R. Mistur, R. Switalski et al., "FDG-PET changes in brain glucose metabolism from normal cognition to pathologically verified Alzheimer's disease," *European Journal of Nuclear Medicine and Molecular Imaging*, vol. 36, no. 5, pp. 811–822, 2009.

[20] Y. Yuan, Z.-X. Gu, and W.-S. Wei, "Fluorodeoxyglucose-positron-emission tomography, single-photon emission tomography, and structural MR imaging for prediction of rapid conversion to Alzheimer disease in patients with mild cognitive impairment: a meta-analysis," *American Journal of Neuroradiology*, vol. 30, no. 2, pp. 404–410, 2009.

[21] A. Okello, J. Koivunen, P. Edison et al., "Conversion of amyloid positive and negative MCI to AD over 3 years: an ^{11}C-PIB PET study," *Neurology*, vol. 73, no. 10, pp. 754–760, 2009.

[22] A. Nordberg, S. F. Carter, J. Rinne et al., "A European multicentre PET study of fibrillar amyloid in Alzheimer's disease," *European Journal of Nuclear Medicine and Molecular Imaging*, vol. 40, no. 1, pp. 104–114, 2013.

[23] A. Prestia, A. Caroli, W. M. van der Flier et al., "Prediction of dementia in MCI patients based on core diagnostic markers for Alzheimer disease," *Neurology*, vol. 80, no. 11, pp. 1048–1056, 2013.

[24] J. L. Cummings, "Biomarkers in Alzheimer's disease drug development," *Alzheimer's & Dementia*, vol. 7, no. 3, pp. e13–e44, 2011.

[25] S. Ng, V. L. Villemagne, S. Berlangieri et al., "Visual assessment versus quantitative assessment of ^{11}C-PIB PET and ^{18}F-FDG PET for detection of Alzheimer's disease," *Journal of Nuclear Medicine*, vol. 48, no. 4, pp. 547–552, 2007.

[26] A. D. Cohen, W. Mowrey, L. A. Weissfeld et al., "Classification of amyloid-positivity in controls: comparison of visual read and quantitative approaches," *Neuroimage*, vol. 71, pp. 207–215, 2013.

[27] K. Herholz, E. Salmon, D. Perani et al., "Discrimination between Alzheimer dementia and controls by automated analysis of multicenter FDG PET," *NeuroImage*, vol. 17, no. 1, pp. 302–316, 2002.

[28] P. Edison, D. J. Brooks, F. E. Turkheimer, H. A. Archer, and R. Hinz, "Strategies for the generation of parametric images of [^{11}C]PIB with plasma input functions considering discriminations and reproducibility," *NeuroImage*, vol. 48, no. 2, pp. 329–338, 2009.

[29] V. Camus, P. Payoux, L. Barré et al., "Using PET with ^{18}F-AV-45 (florbetapir) to quantify brain amyloid load in a clinical environment," *European Journal of Nuclear Medicine and Molecular Imaging*, vol. 39, no. 4, pp. 621–631, 2012.

[30] C. A. Wiley, B. J. Lopresti, S. Venneti et al., "Carbon 11-labeled Pittsburgh Compound B and carbon 11-labeled (R)-PK11195 positron emission tomographic imaging in Alzheimer disease," *Archives of Neurology*, vol. 66, no. 1, pp. 60–67, 2009.

[31] G. Chételat, V. L. Villemagne, N. Villain et al., "Accelerated cortical atrophy in cognitively normal elderly with high β-amyloid deposition," *Neurology*, vol. 78, no. 7, pp. 477–484, 2012.

[32] R. J. Bateman, C. Xiong, T. Benzinger et al., "Erratum in "clinical and biomarker changes in dominantly inherited Alzheimer's disease"," *The New England Journal of Medicine*, vol. 367, no. 8, article 780, 2012.

[33] N. L. Foster, J. L. Heidebrink, C. M. Clark et al., "FDG-PET improves accuracy in distinguishing frontotemporal dementia and Alzheimer's disease," *Brain*, vol. 130, part 10, pp. 2616–2635, 2007.

[34] G. D. Rabinovici, H. J. Rosen, A. Alkalay et al., "Amyloid vs FDG-PET in the differential diagnosis of AD and FTLD," *Neurology*, vol. 77, no. 23, pp. 2034–2042, 2011.

[35] J. C. Patterson, D. L. Lilien, A. Takalkar, and J. B. Pinkston, "Early detection of brain pathology suggestive of early AD using objective evaluation of FDG-PET scans," *International Journal of Alzheimer's Disease*, vol. 2011, Article ID 946590, 9 pages, 2011.

[36] D. Attwell and C. Iadecola, "The neural basis of functional brain imaging signals," *Trends in Neurosciences*, vol. 25, no. 12, pp. 621–625, 2002.

[37] M. J. de Leon, S. H. Ferris, and A. E. George, "Computed tomography and positron emission transaxial tomography evaluations of normal aging and Alzheimer's disease," *Journal of Cerebral Blood Flow and Metabolism*, vol. 3, no. 3, pp. 391–394, 1983.

[38] D. E. Kuhl, "Imaging local brain function with emission computed tomography," *Radiology*, vol. 150, no. 3, pp. 625–631, 1984.

[39] M. J. de Leon, A. Convit, O. T. Wolf et al., "Prediction of cognitive decline in normal elderly subjects with 2-[^{18}F]fluoro-2-deoxy-D-glucose/positron-emission tomography (FDG/PET)," *Proceedings of the National Academy of Sciences of the United States of America*, vol. 98, no. 19, pp. 10966–10971, 2001.

[40] S. de Santi, M. J. de Leon, H. Rusinek et al., "Hippocampal formation glucose metabolism and volume losses in MCI and AD," *Neurobiology of Aging*, vol. 22, no. 4, pp. 529–539, 2001.

[41] L. Mosconi, "Brain glucose metabolism in the early and specific diagnosis of Alzheimer's disease: FDG-PET studies in MCI and AD," *European Journal of Nuclear Medicine and Molecular Imaging*, vol. 32, no. 4, pp. 486–510, 2005.

[42] S. Minoshima, N. L. Foster, A. A. Sima, K. A. Frey, R. L. Albin, and D. E. Kuhl, "Alzheimer's disease versus dementia with Lewy bodies: cerebral metabolic distinction with autopsy confirmation," *Annals of Neurology*, vol. 50, no. 3, pp. 358–365, 2001.

[43] S. Morbelli, A. Piccardo, G. Villavecchia et al., "Mapping brain morphological and functional conversion patterns in amnestic MCI: a voxel-based MRI and FDG-PET study," *European Journal of Nuclear Medicine and Molecular Imaging*, vol. 37, no. 1, pp. 36–45, 2010.

[44] J. L. Shaffer, J. R. Petrella, F. C. Sheldon et al., "Predicting cognitive decline in subject at risk for Alzheimer disease by using combined cerebrospinal fluid, MR imaging and PET biomarkers," *Radiology*, vol. 266, no. 2, pp. 583–591, 2013.

[45] C. Hinrichs, V. Singh, G. Xu, and S. C. Johnson, "Predictive markers for AD in a multi-modality framework: an analysis of MCI progression in the ADNI population," *NeuroImage*, vol. 55, no. 2, pp. 574–589, 2011.

[46] C. R. Jack Jr., D. S. Knopman, W. J. Jagust et al., "Hypothetical model of dynamic biomarkers of the Alzheimer's pathological cascade," *The Lancet Neurology*, vol. 9, no. 1, pp. 119–128, 2010.

[47] K. B. Walhovd, A. M. Fjell, J. Brewer et al., "Combining MR imaging, positron-emission tomography, and CSF biomarkers in the diagnosis and prognosis of Alzheimer disease," *American Journal of Neuroradiology*, vol. 31, no. 2, pp. 347–354, 2010.

[48] G. Chételat, V. L. Villemagne, P. Bourgeat et al., "Relationship between atrophy and β-amyloid deposition in Alzheimer disease," *Annals of Neurology*, vol. 67, no. 3, pp. 317–324, 2010.

[49] R. J. Castellani and M. A. Smith, "Compounding artefacts with uncertainty, and an amyloid cascade hypothesis that is "too big to fail"," *Journal of Pathology*, vol. 224, no. 2, pp. 147–152, 2011.

[50] C. C. Rowe and V. L. Villemagne, "Brain amyloid imaging," *Journal of Nuclear Medicine*, vol. 52, no. 11, pp. 1733–1740, 2011.

[51] C. A. Mathis, B. J. Bacskai, S. T. Kajdasz et al., "A lipophilic thioflavin-T derivative for Positron Emission Tomography (PET) imaging of amyloid in brain," *Bioorganic and Medicinal Chemistry Letters*, vol. 12, no. 3, pp. 295–298, 2002.

[52] W. E. Klunk, H. Engler, A. Nordberg et al., "Imaging brain amyloid in Alzheimer's disease with Pittsburgh Compound-B," *Annals of Neurology*, vol. 55, no. 3, pp. 306–319, 2004.

[53] A. Lockhart, J. R. Lamb, T. Osredkar et al., "PIB is a non-specific imaging marker of amyloid-beta (Aβ) peptide-related cerebral amyloidosis," *Brain*, vol. 130, no. 10, pp. 2607–2615, 2007.

[54] V. Leinonen, I. Alafuzoff, S. Aalto et al., "Assessment of β-amyloid in a frontal cortical brain biopsy specimen and by positron emission tomography with carbon 11-labeled pittsburgh Compound B," *Archives of Neurology*, vol. 65, no. 10, pp. 1304–1309, 2008.

[55] V. J. Lowe, B. J. Kemp, C. R. Jack Jr. et al., "Comparison of ^{18}F-FDG and PiB PET in cognitive impairment," *Journal of Nuclear Medicine*, vol. 50, no. 6, pp. 878–886, 2009.

[56] D. P. Devanand, A. Mikhno, G. H. Pelton et al., "Pittsburgh Compound B (^{11}C-PIB) and fluorodeoxyglucose (^{18}F-FDG) PET in patients with Alzheimer disease, mild cognitive impairment, and healthy controls," *Journal of Geriatric Psychiatry and Neurology*, vol. 23, no. 3, pp. 185–198, 2010.

[57] P. T. Meyer, S. Hellwig, F. Amtage et al., "Dual-biomarker imaging of regional cerebral amyloid load and neuronal activity in dementia with PET and ^{11}C-Labeled Pittsburgh Compound B," *Journal of Nuclear Medicine*, vol. 52, no. 3, pp. 393–400, 2011.

[58] A. H. Rostomian, C. Madison, G. D. Rabinovici, and W. J. Jagust, "Early ^{11}C-PIB frames and ^{18}F-FDG PET measures are comparable: a study validated in a cohort of AD and FTLD patients," *Journal of Nuclear Medicine*, vol. 52, no. 2, pp. 173–179, 2011.

[59] A. Kadir, O. Almkvist, A. Forsberg et al., "Dynamic changes in PET amyloid and FDG imaging at different stages of Alzheimer's disease," *Neurobiology of Aging*, vol. 33, no. 1, pp. 198.e1–198.e14, 2012.

[60] A. Kadir, N. Andreasen, O. Almkvist et al., "Effect of phenserine treatment on brain functional activity and amyloid in Alzheimer's disease," *Annals of Neurology*, vol. 63, no. 5, pp. 621–631, 2008.

[61] A. Forsberg, H. Engler, O. Almkvist et al., "PET imaging of amyloid deposition in patients with mild cognitive impairment," *Neurobiology of Aging*, vol. 29, no. 10, pp. 1456–1465, 2008.

[62] J. Koivunen, N. Scheinin, J. R. Virta et al., "Amyloid PET imaging in patients with mild cognitive impairment: a 2-year follow-up study," *Neurology*, vol. 76, no. 12, pp. 1085–1090, 2011.

[63] B. J. Lopresti, W. E. Klunk, C. A. Mathis et al., "Simplified quantification of Pittsburgh Compound B amyloid imaging PET studies: a comparative analysis," *Journal of Nuclear Medicine*, vol. 46, no. 12, pp. 1959–1972, 2005.

[64] B. L. Rosario, L. A. Weissfeld, C. M. Laymon et al., "Inter-rater reliability of manual and automated region-of-interest delineation for PiB PET," *NeuroImage*, vol. 55, no. 3, pp. 933–941, 2011.

[65] Y. Zhou, J. Sojkova, S. M. Resnick, and D. F. Wong, "Relative equilibrium plot improves graphical analysis and allows bias correction of standardized uptake value ratio in quantitative ^{11}C-PiB PET studies," *Journal of Nuclear Medicine*, vol. 53, no. 4, pp. 622–628, 2012.

[66] P. Edison, R. Hinz, A. Ramlackhansingh et al., "Can target-to-pons ratio be used as a reliable method for the analysis of [^{11}C]PIB brain scans?" *NeuroImage*, vol. 60, no. 3, pp. 1716–1723, 2012.

[67] S. Vallabhajosula, "Positron emission tomography radiopharmaceuticals for imaging brain beta-amyloid," *Seminars in Nuclear Medicine*, vol. 41, no. 4, pp. 283–299, 2011.

[68] K. Herholz and K. Ebmeier, "Clinical amyloid imaging in Alzheimer's disease," *The Lancet Neurology*, vol. 10, no. 7, pp. 667–670, 2011.

[69] C. M. Clark, J. A. Schneider, B. J. Bedell et al., "Use of florbetapir-PET for imaging β-amyloid pathology," *Journal of the American Medical Association*, vol. 305, no. 3, pp. 275–283, 2011, Erratum in *Journal of the American Medical Association*, vol. 305, no. 11, article 1096, 2011.

[70] A. S. Fleisher, K. Chen, X. Liu et al., "Using positron emission tomography and florbetapir F 18 to image cortical amyloid in patients with mild cognitive impairment or dementia due to Alzheimer disease," *Archives of Neurology*, vol. 68, no. 11, pp. 1404–1411, 2011.

[71] S. M. Landau, C. Breault, A. D. Joshi et al., "Amyloid-β imaging with Pittsburgh Compound B and florbetapir: comparing radiotracers and quantification methods," *Journal of Nuclear Medicine*, vol. 54, no. 1, pp. 70–77, 2013.

[72] W. J. Jagust, S. M. Landau, L. M. Shaw et al., "Relationships between biomarkers in aging and dementia," *Neurology*, vol. 73, no. 15, pp. 1193–1199, 2009.

[73] A. D. Joshi, M. J. Pontecorvo, C. M. Clark et al., "Performance characteristics of amyloid PET with florbetapir F 18 in patients with Alzheimer's disease and cognitively normal subjects," *Journal of Nuclear Medicine*, vol. 53, no. 3, pp. 378–384, 2012.

[74] J. L. Brozek, E. A. Akl, R. Jaeschke et al., "Grading quality of evidence and strength of recommendations in clinical practice guidelines: part 2 of 3. the GRADE approach to grading quality of evidence about diagnostic tests and strategies," *Allergy*, vol. 64, no. 8, pp. 1109–1116, 2009.

[75] J. Hsu, J. L. Brozek, L. Terracciano et al., "Application of GRADE: making evidence-based recommendations about diagnostic tests in clinical practice guidelines," *Implementation Science*, vol. 6, no. 1, article 62, 2011.

[76] G. H. Guyatt, A. D. Oxman, R. Kunz et al., "GRADE guidelines: 7. Rating the quality of evidence-inconsistency," *Chinese Journal of Evidence-Based Medicine*, vol. 11, no. 12, pp. 1444–1451, 2011.

[77] H. J. Schünemann, A. D. Oxman, J. Brozek et al., "GRADE: grading quality of evidence and strength of recommendations for diagnostic tests and strategies," *BMJ*, vol. 336, no. 7653, pp. 1106–1110, 2008.

[78] G. B. Frisoni and K. Blennow, "Biomarkers for Alzheimer's: the sequel of an original model," *The Lancet Neurology*, vol. 12, no. 2, pp. 126–128, 2013.

[79] E. Arnáiz, V. Jelic, O. Almkvist et al., "Impaired cerebral glucose metabolism and cognitive functioning predict deterioration in mild cognitive impairment," *NeuroReport*, vol. 12, no. 4, pp. 851–855, 2001.

[80] L. Mosconi, D. Perani, S. Sorbi et al., "MCI conversion to dementia and the APOE genotype: a prediction study with FDG-PET," *Neurology*, vol. 63, no. 12, pp. 2332–2340, 2004.

[81] D. C. Delis, J. Freeland, J. H. Kramer, and E. Kaplan, "Integrating clinical assessment with cognitive neuroscience: construct validation of the California Verbal Learning test," *Journal of Consulting and Clinical Psychology*, vol. 56, no. 1, pp. 123–130, 1988.

[82] A. Drzezga, T. Grimmer, M. Riemenschneider et al., "Prediction of individual clinical outcome in MCI by means of genetic assessment and ^{18}F-FDG PET," *Journal of Nuclear Medicine*, vol. 46, no. 10, pp. 1625–1632, 2005.

[83] K. Hosaka, K. Ishii, S. Sakamoto et al., "Validation of anatomical standardization of FDG PET images of normal brain: comparison of SPM and NEUROSTAT," *European Journal of Nuclear Medicine and Molecular Imaging*, vol. 32, no. 1, pp. 92–97, 2005.

[84] C. Haense, K. Herholz, W. J. Jagust, and W. D. Heiss, "Performance of FDG PET for detection of Alzheimer's disease in two independent multicentre samples (NEST-DD and ADNI)," *Dementia and Geriatric Cognitive Disorders*, vol. 28, no. 3, pp. 259–266, 2009.

[85] S. M. Landau, D. Harvey, C. M. Madison et al., "Comparing predictors of conversion and decline in mild cognitive impairment," *Neurology*, vol. 75, no. 3, pp. 230–238, 2010.

[86] A. Brück, J. R. Virta, J. Koivunen et al., "[^{11}C]PIB, [^{18}F]FDG and MR imaging in patients with mild cognitive impairment," *European Journal of Nuclear Medicine and Molecular Imaging*, vol. 40, no. 10, pp. 1567–1572, 2013.

[87] J. Arbizu, E. Prieto, P. Martínez-Lage et al., "Automated analysis of FDG PET as a tool for single-subject probabilistic prediction and detection of Alzheimer's disease dementia," *European Journal of Nuclear Medicine and Molecular Imaging*, vol. 40, no. 9, pp. 1394–1405, 2013.

[88] S. Gilman, R. A. Koeppe, R. Little et al., "Differentiation of Alzheimer's disease from dementia with Lewy bodies utilizing positron emission tomography with [^{18}F]fluorodeoxyglucose and neuropsychological testing," *Experimental Neurology*, vol. 191, supplement 1, pp. S95–S103, 2005.

[89] L. Mosconi, W. H. Tsui, K. Herholz et al., "Multicenter standardized ^{18}F-FDG PET diagnosis of mild cognitive impairment, Alzheimer's disease, and other dementias," *Journal of Nuclear Medicine*, vol. 49, no. 3, pp. 390–398, 2008.

[90] P. J. Magistretti, "Cellular bases of functional brain imaging: insights from neuron-glia metabolic coupling," *Brain Research*, vol. 886, no. 1-2, pp. 108–112, 2000.

[91] G. B. Frisoni, "Alzheimer disease: biomarker trajectories across stages of Alzheimer disease," *Nature Reviews Neurology*, vol. 8, pp. 299–300, 2012.

[92] C. R. Jack Jr., D. S. Knopman, W. J. Jagust et al., "Tracking pathophysiological processes in Alzheimer's disease: an updated hypothetical model of dynamic biomarkers," *The Lancet Neurology*, vol. 12, no. 2, pp. 207–216, 2013.

[93] C. C. Rowe, U. Ackerman, W. Browne et al., "Imaging of amyloid β in Alzheimer's disease with ^{18}F-BAY94-9172, a novel PET tracer: proof of mechanism," *The Lancet Neurology*, vol. 7, no. 2, pp. 129–135, 2008.

[94] R. Vandenberghe, K. van Laere, A. Ivanoiu et al., "^{18}F-flutemetamol amyloid imaging in Alzheimer disease and mild cognitive impairment a phase 2 trial," *Annals of Neurology*, vol. 68, no. 3, pp. 319–329, 2010.

[95] D. A. Wolk, I. D. Grachev, C. Buckley et al., "Association between in vivo fluorine 18-labeled flutemetamol amyloid positron emission tomography imaging and in vivo cerebral cortical histopathology," *Archives of Neurology*, vol. 68, no. 11, pp. 1398–1403, 2011.

[96] H. Barthel, H. Gertz, S. Dresel et al., "Cerebral amyloid-β PET with florbetaben (^{18}F) in patients with Alzheimer's disease and healthy controls: a multicentre phase 2 diagnostic study," *The Lancet Neurology*, vol. 10, no. 5, pp. 424–435, 2011.

[97] H. Barthel, J. Luthardt, G. Becker et al., "Individualized quantification of brain β-amyloid burden: results of a proof of mechanism phase 0 florbetaben PET trial in patients with Alzheimer's disease and healthy controls," *European Journal of Nuclear Medicine and Molecular Imaging*, vol. 38, no. 9, pp. 1702–1714, 2011.

[98] V. L. Villemagne, R. S. Mulligan, S. Pejoska et al., "Comparison of ^{11}C-PiB and ^{18}F-florbetaben for Aβ imaging in ageing and Alzheimer's disease," *European Journal of Nuclear Medicine and Molecular Imaging*, vol. 39, no. 6, pp. 983–989, 2012.

[99] G. A. Becker, M. Ichise, H. Barthel et al., "PET quantification of ^{18}F-florbetaben binding to β-amyloid deposits in human brains," *Journal of Nuclear Medicine*, vol. 54, no. 5, pp. 723–731, 2013.

[100] A. Forsberg, O. Almkvist, H. Engler, A. Wall, B. Långström, and A. Nordberg, "High PIB retention in Alzheimer's disease is an early event with complex relationship with CSF biomarkers and functional parameters," *Current Alzheimer Research*, vol. 7, no. 1, pp. 56–66, 2010.

[101] D. A. Wolk, J. C. Price, J. A. Saxton et al., "Amyloid imaging in mild cognitive impairment subtypes," *Annals of Neurology*, vol. 65, no. 5, pp. 557–568, 2009.

[102] C. M. Clark, M. J. Pontecorvo, T. G. Beach et al., "Cerebral PET with florbetapir compared with neuropathology at autopsy for detection of neuritic amyloid-β plaques: a prospective cohort study," *The Lancet Neurology*, vol. 11, no. 8, pp. 669–678, 2012.

[103] A. Forsberg, H. Engler, G. Blomquist, B. Långström, and A. Nordberg, "The use of PIB-PET as a dual pathological and functional biomarker in AD," *Biochimica et Biophysica Acta*, vol. 1822, no. 3, pp. 380–385, 2012.

[104] H. Shao, N. Okamura, K. Sugi et al., "Voxel-based analysis of amyloid positron emission tomography probe [C]BF-227 uptake in mild cognitive impairment and Alzheimer's disease," *Dementia and Geriatric Cognitive Disorders*, vol. 30, no. 2, pp. 101–111, 2010.

[105] M. Waragai, N. Okamura, K. Furukawa et al., "Comparison study of amyloid PET and voxel-based morphometry analysis in mild cognitive impairment and Alzheimer's disease," *Journal of the Neurological Sciences*, vol. 285, no. 1-2, pp. 100–108, 2009.

[106] C. R. Jack Jr., V. J. Lowe, M. L. Senjem et al., "^{11}C PiB and structural MRI provide complementary information in imaging of Alzheimer's disease and amnestic mild cognitive impairment," *Brain*, vol. 131, part 3, pp. 665–680, 2008.

[107] C. C. Rowe, K. A. Ellis, M. Rimajova et al., "Amyloid imaging results from the Australian Imaging, Biomarkers and Lifestyle (AIBL) study of aging," *Neurobiology of Aging*, vol. 31, no. 8, pp. 1275–1283, 2010.

[108] E. C. Mormino, M. G. Brandel, C. M. Madison et al., "Not quite PIB-positive, not quite PIB-negative: slight PIB elevations in elderly normal control subjects are biologically relevant," *NeuroImage*, vol. 59, no. 2, pp. 1152–1160, 2012.

[109] W. J. Jagust, D. Bandy, K. Chen et al., "The Alzheimer's Disease Neuroimaging Initiative positron emission tomography core," *Alzheimer's & Dementia*, vol. 6, no. 3, pp. 221–229, 2010.

[110] P. della Rosa, C. Cerami, A. Prestia et al., "Clinical validation of a grid-based SPM web tool for the automatic assessment of [^{18}F]FDG PET brain metabolic abnormalities in single subjects (P03.106)," *Neurology*, vol. 78, article P03.106, 2012.

[111] D. S. Knopman, S. T. DeKosky, J. L. Cummings et al., "Practice parameter: diagnosis of dementia (an evidence-based review): report of the quality standards subcommittee of the American Academy of Neurology," *Neurology*, vol. 56, no. 9, pp. 1143–1153, 2001.

[112] G. B. Frisoni, P. H. Scheltens, S. Galluzzi et al., "Neuroimaging tools to rate regional atrophy, subcortical cerebrovascular disease, and regional cerebral blood flow and metabolism: consensus paper of the EADC," *Journal of Neurology, Neurosurgery and Psychiatry*, vol. 74, no. 10, pp. 1371–1381, 2003.

[113] R. J. Bateman, C. Xiong, T. Benzinger et al., "Clinical and biomarker changes in dominantly inherited Alzheimer's disease," *The New England Journal of Medicine*, vol. 367, no. 8, pp. 795–804, 2012, Erratum in *The New England Journal of Medicine*, vol. 367, no. 8, article 780, 2012.

[114] E. M. Reiman, K. Chen, G. E. Alexander et al., "Correlations between apolipoprotein E ε4 gene dose and brain-imaging measurements of regional hypometabolism," *Proceedings of the National Academy of Sciences of the United States of America*, vol. 102, no. 23, pp. 8299–8302, 2005.

[115] Y. Jeong, S. S. Cho, J. M. Park et al., "^{18}F-FDG PET findings in frontotemporal dementia: an SPM analysis of 29 patients," *Journal of Nuclear Medicine*, vol. 46, no. 2, pp. 233–239, 2005.

[116] E. Salmon, G. Garraux, X. Delbeuck et al., "Predominant ventromedial frontopolar metabolic impairment in frontotemporal dementia," *NeuroImage*, vol. 20, no. 1, pp. 435–440, 2003.

[117] D. G. Clark, A. Charuvastra, B. L. Miller, J. S. Shapira, and M. F. Mendez, "Fluent versus nonfluent primary progressive aphasia: a comparison of clinical and functional neuroimaging features," *Brain and Language*, vol. 94, no. 1, pp. 54–60, 2005.

[118] R. C. Petersen, G. E. Smith, S. C. Waring, R. J. Ivnik, E. G. Tangalos, and E. Kokmen, "Mild cognitive impairment: clinical characterization and outcome," *Archives of Neurology*, vol. 56, no. 3, pp. 303–308, 1999, Erratum in *Archives of Neurology*, vol. 56, no. 6, article 760, 1999.

[119] R. C. Petersen, R. Doody, A. Kurz et al., "Current concepts in mild cognitive impairment," *Archives of Neurology*, vol. 58, no. 12, pp. 1985–1992, 2001.

[120] D. J. Brooks, "Imaging amyloid in Parkinson's disease dementia and dementia with Lewy bodies with positron emission tomography," *Movement Disorders*, vol. 24, supplement 2, pp. S742–S747, 2009.

[121] M. Weih, Ü. Degirmenci, S. Kreil et al., "Nuclear medicine diagnostic techniques in the era of pathophysiology-based csf biomarkers for Alzheimers disease," *Journal of Alzheimer's Disease*, vol. 26, supplement 3, pp. 97–103, 2011.

[122] I. McKeith, J. O'Brien, Z. Walker et al., "Sensitivity and specificity of dopamine transporter imaging with 123I-FP-CIT SPECT in dementia with Lewy bodies: a phase III, multicentre study," *The Lancet Neurology*, vol. 6, no. 4, pp. 305–313, 2007.

[123] H. Engler, A. Forsberg, O. Almkvist et al., "Two-year follow-up of amyloid deposition in patients with Alzheimer's disease," *Brain*, vol. 129, no. 11, pp. 2856–2866, 2006.

[124] T. Grimmer, M. Riemenschneider, H. Förstl et al., "Beta amyloid in Alzheimer's disease: increased deposition in brain is reflected in reduced concentration in cerebrospinal fluid," *Biological Psychiatry*, vol. 65, no. 11, pp. 927–934, 2009.

[125] N. Villain, G. Chételat, B. Grassiot et al., "Regional dynamics of amyloid-β deposition in healthy elderly, mild cognitive impairment and Alzheimer's disease: a Voxelwise PiB-PET Longitudinal study," *Brain*, vol. 135, part 7, pp. 2126–2139, 2012.

[126] M. A. Mintun, G. N. Larossa, Y. I. Sheline et al., "[^{11}C]PIB in a nondemented population: potential antecedent marker of Alzheimer disease," *Neurology*, vol. 67, no. 3, pp. 446–452, 2006.

[127] A. S. Fleisher, K. Chen, Y. T. Quiroz et al., "Florbetapir PET analysis of amyloid-β deposition in the presenilin 1 E280A autosomal dominant Alzheimer's disease kindred: a cross-sectional study," *The Lancet Neurology*, vol. 11, no. 12, pp. 1057–1065, 2012.

[128] V. L. Villemagne, S. Burnham, P. Bourgeat et al., "Amyloid β deposition, neurodegeneration, and cognitive decline in sporadic Alzheimer's disease: a prospective cohort study," *The Lancet Neurology*, vol. 12, no. 4, pp. 357–367, 2013.

[129] R. S. Briellmann, S. F. Berkovic, A. Syngeniotis, M. A. King, and G. D. Jackson, "Alzheimer's neurofibrillary pathology and the spectrum of cognitive function: findings from the Nun study," *Annals of Neurology*, vol. 51, no. 5, pp. 567–577, 2002.

[130] J. Karlawish, "Addressing the ethical, policy, and social challenges of preclinical Alzheimer disease," *Neurology*, vol. 77, no. 15, pp. 1487–1493, 2011.

[131] A. Drzezga, "Amyloid-plaque imaging in early and differential diagnosis of dementia," *Annals of Nuclear Medicine*, vol. 24, no. 2, pp. 55–66, 2010.

[132] K. A. Johnson, S. Minoshima, N. I. Bohnen et al., "Appropriate use criteria for amyloid PET: a report of the Amyloid Imaging Task Force, the Society of Nuclear Medicine and Molecular Imaging, and the Alzheimer's Association," *Journal of Nuclear Medicine*, vol. 54, no. 3, pp. 476–490, 2013.

[133] K. A. Johnson, S. Minoshima, N. I. Bohnen et al., "Update on appropriate use criteria for amyloid PET imaging: dementia experts, mild cognitive impairment, and education," *Alzheimer's & Dementia*, vol. 9, no. 4, pp. e106–e109, 2013.

Hindawi Publishing Corporation
BioMed Research International
Volume 2014, Article ID 327270, 6 pages
http://dx.doi.org/10.1155/2014/327270

Research Article

Functional MRI Study of Working Memory Impairment in Patients with Symptomatic Carotid Artery Disease

Shasha Zheng,[1,2] Miao Zhang,[1,2] Xiaoyi Wang,[1,2] Qingfeng Ma,[3] Hua Shu,[4] Jie Lu,[1,2] and Kuncheng Li[1,2]

[1] *Department of Radiology, Xuanwu Hospital of Capital Medical University, Beijing 100053, China*
[2] *Beijing Key Laboratory of Magnetic Resonance Imaging and Brain Informatics, Beijing 100053, China*
[3] *Department of Neurology, Xuanwu Hospital of Capital Medical University, Beijing 100053, China*
[4] *State Key Laboratory for Cognitive Neuroscience and Learning, Beijing Normal University, Beijing 100875, China*

Correspondence should be addressed to Jie Lu; imaginglu@hotmail.com

Received 29 November 2013; Accepted 14 January 2014; Published 20 February 2014

Academic Editor: Lijun Bai

The neuropsychological tests in patients with internal carotid artery (ICA) demonstrated cognitive deficits associated with frontal lobe dysfunction, but the pathophysiological mechanism of memory impairment is not fully understood. This study evaluated relationship between degree of ICA stenosis and frontal activations induced by working memory (WM) task using fMRI. The fMRI data of 21 patients with unilateral ICA stenosis (left/right, 11/10) and 21 controls were analyzed. In comparison with controls, ICA patients demonstrated significant activations in middle frontal gyrus (MFG) bilaterally, particularly in left MFG. In right ICA stenosis, there was slightly less MFG activation than that of controls. Importantly, lower MFG activity was associated with higher stenosis of ipsilateral ICA. For left ICA stenosis, weaker activation in left MFG was negatively correlated with degree of stenosis. Similarly, for right ICA stenosis, there was a significant negative correlation between right ICA stenosis and weaker activation of right MFG. Cognitive impairments in ICA stenosis were associated with frontal lobe dysfunctions. Left ICA stenosis had worse WM impairments than right ICA stenosis, which was affected by the degree of stenosis.

1. Introduction

Cerebrovascular diseases are associated with cognitive decline and dementia. Patients with occlusive diseases of the internal carotid artery (ICA) are at risk for cognitive impairment [1–3]. A systematic review of cognitive disorders in ICA patients finds subtle cognitive deficits in 70% of the studies reviewed [4]. Therefore, some patients may be in a preclinical stage of vascular dementia. Particularly, patients with carotid artery disease who have suffered a transient ischemic attack (TIA) can have lasting cognitive impairment, even without visible ischemic lesions on MRI [5, 6]. Similarly, neuropsychological tests show cognitive deficits in working memory (WM), attention, reasoning, psychomotor speed, and executive functions; frontal lobe dysfunction has been a consistent finding [4–7]. WM is the brain system that maintains a limited amount of information for short periods of time and manipulates that information [8]. The frontal cortex is involved in WM tasks with asymmetric activations in the left and right hemispheres during verbal and nonverbal WM tasks [9, 10]. Furthermore, several studies reported worse memory impairment in patients with left carotid artery disease than those with right carotid artery disease. The different patterns observed argue against that high-grade stenosis of ICA is simply a marker for vascular disease and its risk factors [6, 11, 12]. To date, the cognitive functions of carotid occlusive disease have been assessed using neuropsychological tests [4–7, 11, 13]. Various cognitive functions have been linked to specific brain regions. However, previous neuropsychological tests are not able to precisely reveal cognitive deficits in specific brain regions involving particular tasks. Therefore, the pathophysiological mechanism of memory impairment is not fully understood. Recently, functional magnetic resonance imaging (fMRI)

has increasingly been used to study cognitive function in humans. It has been explored for elucidating cognitive impairment mechanisms, especially WM impairment.

We hypothesized that brain dysfunction WM impairment in patients with symptomatic ICA disease; and specifically that the differences in brain dysfunction between left and right ICA disease were associated with the degree of stenosis in ipsilateral ICA, and the functional differences between left and right frontal lobes. Therefore, the purpose of the present study was as follows: (1) to investigate the abnormal frontal activations of digit WM in patients with ICA stenosis/occlusion and ipsilateral TIA and (2) to investigate the relationship between the activations in the frontal and the degree of ICA stenosis using fMRI.

2. Subjects and Methods

2.1. Subjects. This study was comprised of 49 consecutive patients who were assessed for neurocognitive effects of symptomatic carotid artery disease in the Department of Neurology. Symptomatic carotid stenosis is defined as stenosis having caused ischaemic events in the ipsilateral eye (transient monocular blindness) or cerebral hemisphere (transient ischaemic attack or stroke) in the past 6 months [14, 15]. The study protocol was approved by the local Institutional Review Board and written informed consent was obtained from all of subjects. 21 patients with symptoms of transient ischemia (lasting <24 hours) were enrolled. As determined by the use of a transcranial Doppler (TCD) or angiography, these patients demonstrated high-grade stenosis (70–99%) or unilateral internal carotid artery (ICA) occlusion. All patients had experienced at least one TIA and symptoms had occurred, at most, 6 months before inclusion in the study. All patients had normal intelligence; however, their total memory scale scores ($M = 72.54 \pm 21.96$) on the Clinical Memory Scale (CMS) were lower than the healthy subjects ($M = 88.54 \pm 14.57$) [16, 17]. The handedness of the subjects was assessed using the Edinburgh inventory [18]. The exclusion criteria included left-handedness; contralateral ICA occlusion or high-grade stenosis (≥70%); large infarct infarction or multiple lacunar infarctions (≥3) on MRI; severe white matter lesions (≥ Grade 3) on MRI, especially lacunar infarcts involved middle frontal gyrus and white matter lesions overstep the immediate subependymal region of the ventricles; history of other brain diseases; deafness and/or blindness. The severity of leukoaraiosis (LA) was graded using the visual rating scale proposed by Sakakibara et al. [19]. These patients were divided into two groups: left ICA stenosis or occlusion ($n = 11$, age range from 39 to 75 years, mean age 59.45 ± 11.72 years) and right ICA stenosis or occlusion ($n = 10$, age range from 38 to 70 years, mean age 56.10 ± 10.86 years) based on the TCD or digital subtraction angiography (DSA) study. The control group consisted of 21 healthy volunteers (age range was 33–69 years and mean age was 54.64 ± 11.85 years). These subjects were age- and education-matched to the patients (age: $t = 1.67$, $P > 0.05$; education: $t = 1.74$, $P > 0.05$). In the control group, carotid artery disease and intracerebral lesions were excluded by TCD and MRI examinations. All subjects were administered a battery of neuropsychological tests involving auditory digital memory and visual digital memory [20, 21]. All patients were found to have impaired WM compared with the control group. The demographic data of the study subjects were shown in Table 1.

2.2. MRI Data Acquisition. Scanning was performed on a 3.0-Tesla whole-body scanner (Trio Tim, Siemens). A T2-weighted (TR/TE: 3830 ms/98 ms; flip angle: 180°; slice thickness 5 mm; gap: 5 mm; FOV: 230 mm × 218 mm; matrix: 179 × 320) image was acquired for exclusion of intracranial lesions. High-resolution 3D magnetization prepared rapid gradient echo imaging (MPRAGE) and anatomical images (TR/TE: 1970 ms/3.93 ms; flip angle: 15°; thickness 1.70 mm; gap: 0.85 mm; FOV: 250 mm × 250 mm; matrix: 448 × 512) of the entire brain were obtained before the functional images were acquired. A $T2^*$-weighted gradient-echo echo-planar imaging (EPI) sequence was used to acquire functional images with 30 axial slices (TR/TE: 2000/30 ms; flip angle: 90°, thickness: 5 mm; gap: 0 mm; FOV: 240 × 240 mm; matrix: 64 × 64).

2.3. Working Memory Tasks. All subjects were required to perform a 3-item delayed-match-to-sample task with digit items [22, 23]. A fast event-related design was adopted. For the digital task the stimuli, ten different one-digit numbers (0–9), were projected randomly onto the center of a screen on the head coil. Subjects responded by pressing a keypad with their thumbs as quickly and accurately as possible. Prior to the MRI examination, all subjects were trained to perform 2 practice trials to ensure that they fully understood the tasks. A single trial of this digit working memory task is schematized in Figure 1. At the beginning, subjects were required to memorize a set of three items sequentially. Each item was shown for 500 milliseconds (ms) on the center of the screen with two 250 ms blank intervals in between each item. After the third item disappeared from the screen, an interruption mark was presented for 4 s, 6 s, or 8 s, respectively. Subjects were told to focus on the screen and hold the stimulus items in mind. The duration of the interruption mark presentation was randomly selected. Finally, a probe appeared for 1500 ms that contained half of the items presented in the previous set. Participants were instructed to press a button to decide whether or not the probe was the same as one of the three previously presented items (left hand indicated "Yes" and right indicated "No"). Reaction time and accuracy of the response were recorded during the scans for each subject. There were intertrial intervals (ITI) that consisted of a presentation of a blank screen. These intervals were used as a baseline epoch. The duration of ITIs ranged from 2 s to 14 s. The duration of each task was 8 min and 28 s and included 30 trials.

2.4. fMRI Data Analysis. The fMRI data were preprocessed and statistically analyzed using the Analysis of Functional Neuroimages (AFNI) software [24]. The first four scans for each participant were excluded from data to minimize the

Table 1: Demographic characteristics of patients and controls.

	Left ICA ($n = 11$)	Right ICA ($n = 10$)	Control ($n = 21$)
Age, years (mean ± SD)	59.45 ± 11.72	56.10 ± 10.86	54.64 ± 11.85
Gender M/F	8/3	3/7	11/10
Education, years (mean ± SD)	10.36 ± 4.03	11.60 ± 2.72	12.00 ± 2.95
Auditory digital memory (mean ± SD)	88.48 ± 8.16	89.63 ± 7.39	97.34 ± 3.28
Visual digital memory (mean ± SD)	90.37 ± 6.02	91.44 ± 6.71	98.02 ± 3.15
Severity of vessel stenosis			
70–99%, *n*	8	5	/
Occlusion, *n*	3	5	/
Hypertension, *n*	5	4	/
Hypercholesterolemia, *n*	1	2	/
Diabetes, *n*	1	1	/
Heart disease, *n*	1	1	/
Smokers, *n*	2	2	/
White matter lesions, *n*	6	5	/

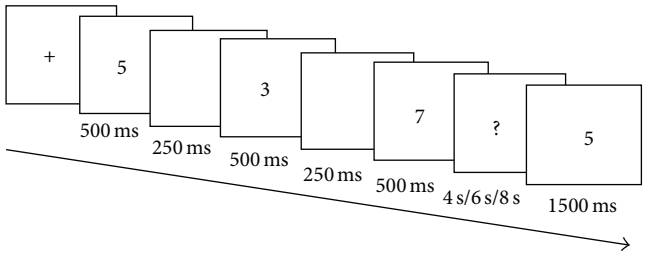

Figure 1: Digit working memory task.

transit effects of hemodynamic responses. Functional images were corrected for head motions by aligning all volumes to the fifth volume using a six-parameter rigid-body transformation. Statistical maps were spatially smoothed with a 6 mm full width at half maximum (FWHM) Gaussian kernel.

We analyzed the brain activities of working memory relative to the baseline of the resting period during the ITI. Individual anatomical images and functional t-maps were coregistered to the standard Talairach and Tournoux space [25]. All images were resized to 3 mm × 3 mm × 3 mm voxel. At the group level, the threshold of group maps was set at a voxel level of $t > 2.040$ ($P < 0.005$, number of voxels > 14) with a spatial extent correction. This threshold corresponded to an overall $\alpha < 0.05$ of family-wise error rate, as calculated with AlphaSim (http://afni.nimh.nih.gov) for all intracranial voxels in the image volumes. Previous WM studies have found that the bilateral frontal lobes play an important part in processing WM information [9, 10, 23, 26, 27]. For this reason we focused on the frontal lobes as our regions-of-interests (ROIs), to explore the relationship between the behavioral data of WM and the functional activation of ICA disease. The ROIs were defined functionally as spheres with a 6 mm radius on the basis of activation clusters in the bilateral frontal lobes from the group analysis (see Section 3). The peak activation coordinates from the cluster of the contrast analysis were selected as the center of each ROI. Then, these ROIs were employed as masks to extract the mean percent signal change (averaged over the ROI) in the blood oxygen level dependent (BOLD) response.

Table 2: Reaction time and accuracy of a digit working memory task in all subjects.

	Left ICA ($n = 11$)	Right ICA ($n = 10$)	Control ($n = 21$)
RT (ms)	1159.33 ± 310.28*	1099.83 ± 208.19*	983.28 ± 107.34
RA (%)	82.61 ± 19.42*	83.21 ± 20.67*	97.14 ± 4.32

Data are presented as mean ± SD. * $P < 0.05$ compared with controls.

2.5. Statistical Analysis. Neuropsychological data were analyzed using SPSS 11.0 computer software (SPSS Inc., Chicago, IL). The characteristics of patients and controls were compared using analysis of variance (ANOVA). The correlations between response time (RT), response accuracy (RA) of digit WM task, activation intensity within the defined frontal ROI, and the degree of ICA stenosis were analyzed using a Pearson's correlation.

3. Results

All subjects completed the fMRI digit task. The left and right ICA stenosis or occlusion patients showed significantly weaker (left: $P = 0.032$; right: $P = 0.041$) and less accurate responses (left: $P = 0.039$; right: $P = 0.043$) than those of the control subjects (Table 2). Higher degrees of left ICA stenosis were positively correlated with RT ($r = 0.412$, $P = 0.042$), but not with RA ($r = -0.243$, $P = 0.436$). Higher degrees of right ICA stenosis were not correlated with either RT ($r = 0.247$, $P = 0.424$) or RA ($r = -0.108$, $P = 0.671$).

The control group revealed a domain area of activation in the bilateral middle frontal gyrus (MFG), frontal gyrus, and supplementary motor area involving digit WM task. The peak of the activation was located in the bilateral MFG. The digit WM task induced significantly asymmetrical activations in the MFG (peak coordinate: (−31, 31, 23), $t = 5.915$)

Table 3: Medial frontal gyrus activations for a digit working memory task in subjects.

	Left MFG			Right MFG		
	Voxels	Peak (x, y, z)	t value	Voxels	Peak (x, y, z)	t value
Control	475	−31, 31, 23	5.915	294	34, 46, 32	5.085
LICA	241	−22, 46, 29	4.791	47	22, 19, 35	3.221
RICA	152	−34, −1, 47	3.506	15	−28, 1, 53	3.036
Control-LICA	129	−28, 34, 23	3.341	217	28, 28, −32	3.915
Control-RICA	26	−31, 31, 23	2.962	21	34, 46, −29	2.521

MFG: medial frontal gyrus; LICA: left internal carotid artery; RICA: right internal carotid artery.

and volume (475 voxels) in the left MFG. The left and right ICA groups showed similar activity clusters compared with those of the control group. MFG activations for digit WM task in subjects were listed in Table 3. A direct comparison between left ICA patients and control subjects revealed that the patients had significantly less activations in the left MFG and slightly less activations in the right MFG (Figure 2(a)). Right ICA patients demonstrated slightly less activation in the right MFG than control subjects (Figure 2(b)).

We selected the bilateral MFG for further ROI analysis. For the left ICA patients, there was a significant negative correlation between ICA stenosis and activation intensity in the left MFG ($r = -0.795$, $P = 0.009$), but not in the right MFG ($r = -0.254$, $P = 0.264$). By contrast, there was a significant negative correlation between the right ICA stenosis and activation intensity in the right MFG ($r = -0.483$, $P = 0.041$), but not in the left MFG ($r = -0.287$, $P = 0.218$). Correlation graphs of MFG activation and ICA stenosis are displayed in Figure 3.

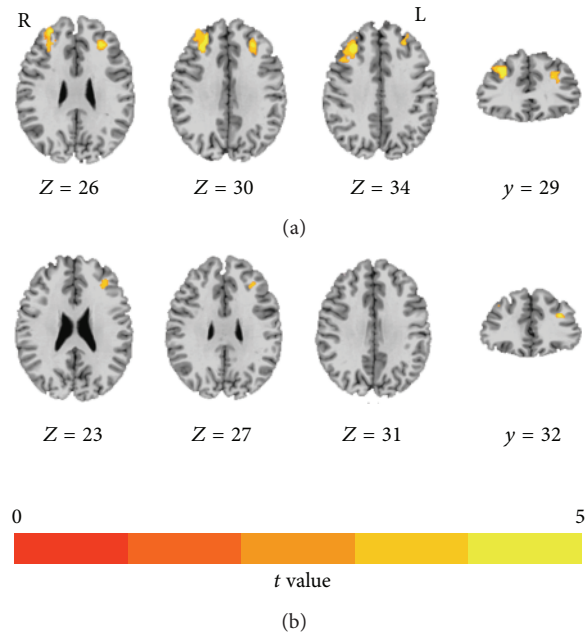

Figure 2: fMRI results for a digit WM task. (a) The left ICA patients showed significantly less activation in the left MFG as well as slightly less activation in the right MFG than control subjects. (b) The right ICA patients showed slightly less activation in the right MFG only than control subjects.

4. Discussion

The results from this study suggested that patients with left ICA disease have more severe frontal lobe dysfunctions than those of age- and sex-matched controls. Compared with controls, the right ICA patients found slightly less activation in the right MFG. Such weaker MFG activity was also associated with a higher stenosis of ipsilateral ICA. A significant negative correlation was found between left ICA stenosis and activation of left MFG in the left ICA patients. Similarly, there was a significant negative correlation between the right ICA stenosis and activation of right MFG in right ICA patients.

Behavioral studies have reported impaired frontal lobe function in patients with ICA disease. Patients demonstrated WM impairments by neuropsychological assessments [4–7, 11, 13]. In addition, results from fMRI and positron emission tomography (PET) imaging suggest that the frontal cortex plays a critical role in the WM [9, 10, 23, 26, 27]. MFG is the core region involving WM. Our results indicated that the activation of MFG (especially left MFG) is key region participant in digit WM. However, compared with controls, MFG activation was weaker in patients with left or right ICA disease. This finding demonstrates the ability of fMRI to detect abnormal frontal lobe activation in patients with mild cognitive impairment.

ICA disease may cause cognitive impairment but the mechanisms involved are poorly understood. Our results suggest that frontal lobe dysfunction may be one of the possible mechanisms. Since fMRI is based on hemodynamic coupling in activated brains, our results also imply that perfusion responses may be involved. Previous studies propose that compromised frontal lobe perfusion may be a cause of cognitive impairment in patients with ICA disease. Thus there is the suggestion that restoring, or at least improving, frontal perfusion with carotid endarterectomy or carotid artery stenting may enhance cognitive function [28, 29]. In this study, we did not examine changes in cerebral blood flow in our subjects. Future studies combining fMRI with perfusion imaging may be helpful for investigating this hypothesis.

Two forms of WM, namely, verbal and nonverbal WM, have been found to be asymmetrically represented in the left and right frontal cortex; however, this left-right specialization

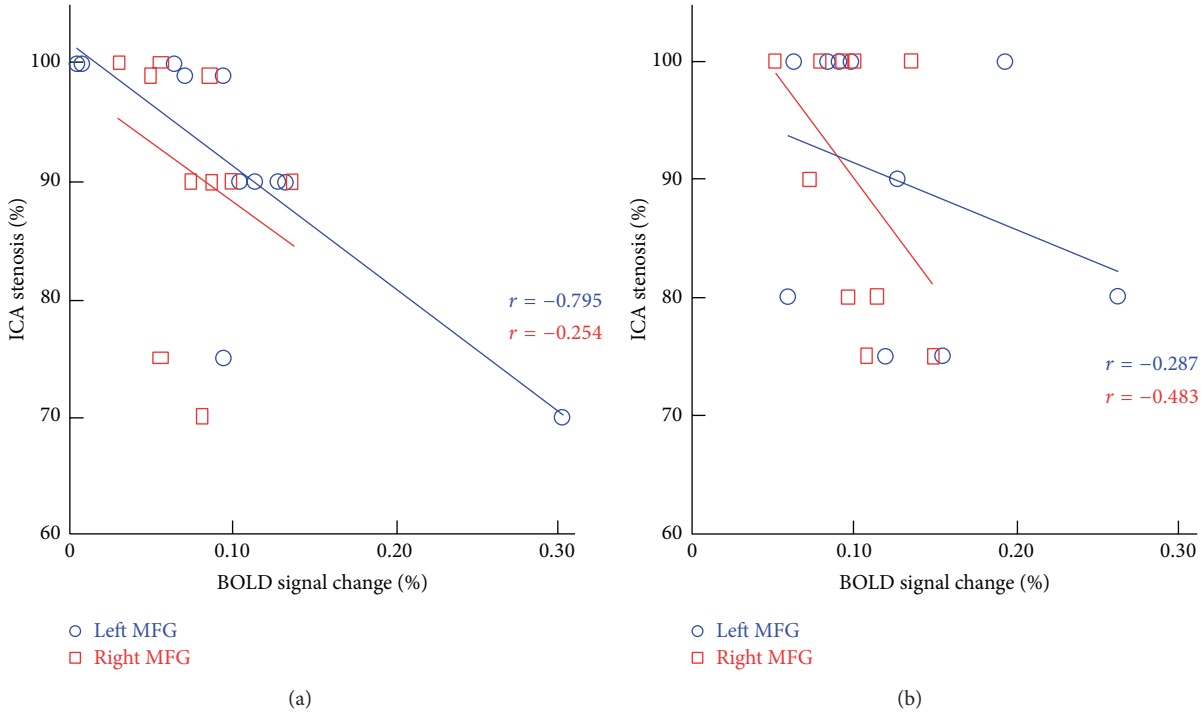

Figure 3: Relationship between MFG activation and the degree of ICA stenosis. (a) A significantly negative correlation was found between left ICA stenosis and lower activation intensity in the left MFG (blue), but not in the right MFG (red). (b) A significantly negative correlation was found between right ICA stenosis and lower activation intensity in the right MFG (red), but not in the left MFG (blue).

is relative [9, 10]. The digit WM is one of the most frequently used verbal WM tasks. Prior WM studies of digit task ability revealed activation within the MFG [23, 26]. In this study, digit WM in the control group demonstrated increased fMRI activation in the left MFG. This pattern of asymmetric activation in the MFG was disrupted in patients with left ICA disease. These patients presented with decreased activations in the bilateral MFG, especially in the left MFG, compared with the control group. In contrast, patients with right ICA disease retained the asymmetric pronounced left activation in the MFG. fMRI in the patient group showed no significant difference in the left MFG compared with the control group; however, there was less activation in the right MFG of patients. These fMRI results suggest that the left side of the ICA may reflect the left dominant frontal cortex in digit WM. For verbal WM, frontal dysfunction was worse in patients with left ICA disease than those with right ICA disease. Our results are consistent with previous neuropsychological findings which have reported that a higher degree of stenosis of the left ICA was associated with cognitive deficits and cognitive decline in the left cerebral hemisphere. However no such correlation was observed in right ICA stenosis [6, 11]. Additionally, even asymptomatic patients with left ICA stenosis appear mainly to have verbal deficits [11, 30].

A graded relationship has been shown between some neuropsychological tests and the degree of stenosis [31]. In the present study, the degree of left ICA stenosis was positively correlated with RT of digit WM. No correlation was found in right ICA disease. It is noted that the speed of decision making was reduced in patients with left ICA disease. The degree of left ICA stenosis was associated with lower activation in the left MFG, whereas the degree of right ICA stenosis was associated with lower activation in the right MFG. Previous fMRI studies of letter WM have suggested that increased intimal-medial thickening of the carotid wall is associated with lower signal intensity in MFG [27]. Viewed in combination, these findings not only suggest ICA stenosis as an independent risk factor for cognitive impairment, but may also be consistent with the idea that the degree of ICA stenosis may be a marker of cognitive decline in symptomatic patients.

In conclusion, our study suggests that cognitive impairments may be related with frontal dysfunctions in patients with symptomatic ICA disease. In the present study, patients with left ICA disease demonstrated worse verbal WM impairments due to more severe left frontal dysfunction. We also found that the degree of ICA stenosis may affect the severity of WM impairment. Further studies are warranted, perhaps utilizing multimodality MRI techniques such as perfusion and spectroscopy, in order to elucidate the mechanisms and markers of cognitive impairment in patients with symptomatic ICA disease.

Conflict of Interests

The authors declare that there is no conflict of interests regarding the publication of this paper.

References

[1] M. M. B. Breteler, "Vascular risk factors for Alzheimer's disease: an epidemiologic perspective," *Neurobiology of Aging*, vol. 21, no. 2, pp. 153–160, 2000.

[2] H. Hénon, I. Durieu, D. Guerouaou, F. Lebert, F. Pasquier, and D. Leys, "Poststroke dementia: incidence and relationship to prestroke cognitive decline," *Neurology*, vol. 57, no. 7, pp. 1216–1222, 2001.

[3] R. Rao, "The role of carotid stenosis in vascular cognitive impairment," *European Neurology*, vol. 46, no. 2, pp. 63–69, 2001.

[4] F. C. Bakker, C. J. M. Klijn, A. Jennekens-Schinkel, and L. J. Kappelle, "Cognitive disorders in patients with occlusive disease of the carotid artery: a systematic review of the literature," *Journal of Neurology*, vol. 247, no. 9, pp. 669–676, 2000.

[5] F. C. Bakker, C. J. M. Klijn, A. Jennekens-Schinkel, I. van der Tweel, C. A. F. Tulleken, and L. J. Kappelle, "Cognitive impairment in patients with carotid artery occlusion and ipsilateral transient ischemic attacks," *Journal of Neurology*, vol. 250, no. 11, pp. 1340–1347, 2003.

[6] J. E. Kim, B. R. Lee, J. E. Chun et al., "Cognitive dysfunction in 16 patients with carotid stenosis: detailed neuropsychological findings," *Journal of Clinical Neurology*, vol. 3, no. 1, pp. 9–17, 2007.

[7] R. Rao, S. Jackson, and R. Howard, "Neuropsychological impairment in stroke, carotid stenosis, and peripheral vascular disease: a comparison with healthy community residents," *Stroke*, vol. 30, no. 10, pp. 2167–2173, 1999.

[8] A. Baddeley, "Working memory," *Science*, vol. 255, no. 5044, pp. 556–559, 1992.

[9] E. E. Smith and J. Jonides, "Neuroimaging analyses of human working memory," *Proceedings of the National Academy of Sciences of the United States of America*, vol. 95, no. 20, pp. 12061–12068, 1998.

[10] L. E. Nystrom, T. S. Braver, F. W. Sabb, M. R. Delgado, D. C. Noll, and J. D. Cohen, "Working memory for letters, shapes, and locations: fMRI evidence against stimulus-based regional organization in human prefrontal cortex," *NeuroImage*, vol. 11, no. 5, part 1, pp. 424–446, 2000.

[11] S. C. Johnston, E. S. O'Meara, T. A. Manolio et al., "Cognitive impairment and decline are associated with carotid artery disease in patients without clinically evident cerebrovascular disease," *Annals of Internal Medicine*, vol. 140, no. 4, pp. 237–247, 2004.

[12] L. E. Philipose, H. Alphs, V. Prabhakaran, and A. E. Hillis, "Testing conclusions from functional imaging of working memory with data from acute stroke," *Behavioural Neurology*, vol. 18, no. 1, pp. 37–43, 2007.

[13] L. K. Sztriha, D. Nemeth, T. Sefcsik, and L. Vecsei, "Carotid stenosis and the cognitive function," *Journal of the Neurological Sciences*, vol. 283, no. 1-2, pp. 36–40, 2009.

[14] North American Symptomatic Carotid Endarterectomy Trial Collaborators, "Beneficial effect of carotid endarterectomy in symptomatic patients with high-grade carotid stenosis," *The New England Journal of Medicine*, vol. 325, no. 7, pp. 445–453, 1991.

[15] L. H. Bonati, S. T. Engelter, and P. A. Lyrer, "Carotid artery stenting," *Swiss Medical Weekly*, vol. 142, Article ID w13619, 2012.

[16] S. L. Xu and Z. Y. Wu, "Development of the clinical memory scale," *Acta Psychologica Sinica*, vol. 18, pp. 100–108, 1986.

[17] S. K. Sutherland, S. E. Purdon, C. H. Lai, L. J. Wang, G. Z. Liu, and J. J. Shan, "Memory enhancement from two weeks' exposure to North American ginseng extract HT1001 in young and middle aged healthy adults," *The Open Nutraceuticals Journal*, vol. 3, pp. 20–24, 2010.

[18] R. C. Oldfield, "The assessment and analysis of handedness: the edinburgh inventory," *Neuropsychologia*, vol. 9, no. 1, pp. 97–113, 1971.

[19] R. Sakakibara, T. Hattori, T. Uchiyama, and T. Yamanishi, "Urinary function in elderly people with and without leukoaraiosis: relation to cognitive and gait function," *Journal of Neurology Neurosurgery and Psychiatry*, vol. 67, no. 5, pp. 658–660, 1999.

[20] P. Gong, A. Zheng, D. Chen et al., "Effect of BDNF Val66Met polymorphism on digital working memory and spatial localization in a healthy chinese han population," *Journal of Molecular Neuroscience*, vol. 38, no. 3, pp. 250–256, 2009.

[21] S. Y. Shu, Y. M. Wu, X. M. Bao et al., "A new area in the human brain associated with learning and memory: immunohistochemical and functional MRI analysis," *Molecular Psychiatry*, vol. 7, no. 9, pp. 1018–1022, 2002.

[22] M. Raabe, V. Fischer, D. Bernhardt, and M. W. Greenlee, "Neural correlates of spatial working memory load in a delayed match-to-sample saccade task," *Neuroimage*, vol. 71, pp. 84–91, 2013.

[23] H. C. Bergmann, M. Rijpkema, G. Fernández, and R. P. C. Kessels, "Distinct neural correlates of associative working memory and long-term memory encoding in the medial temporal lobe," *NeuroImage*, vol. 63, no. 2, pp. 989–997, 2012.

[24] R. W. Cox, "AFNI: software for analysis and visualization of functional magnetic resonance neuroimages," *Computers and Biomedical Research*, vol. 29, no. 3, pp. 162–173, 1996.

[25] J. Talairach and P. Tournoux, *Co-Planar Stereotactic Atlas of the Human Brain-3-Dimensional Proportional System: An Approach to Cerebral Imaging*, Thieme Medical Publishers, Stuttgart, Germany, 1988.

[26] F. E. Cooper, M. Grube, K. Von Kriegstein et al., "Distinct critical cerebellar subregions for components of verbal working memory," *Neuropsychologia*, vol. 50, no. 1, pp. 189–197, 2012.

[27] A. P. Haley, L. H. Sweet, J. Gunstad et al., "Verbal working memory and atherosclerosis in patients with cardiovascular disease: an fMRI study," *Journal of Neuroimaging*, vol. 17, no. 3, pp. 227–233, 2007.

[28] K. Kishikawa, M. Kamouchi, Y. Okada, T. Inoue, S. Ibayashi, and M. Iida, "Effects of carotid endarterectomy on cerebral blood flow and neuropsychological test performance in patients with high-grade carotid stenosis," *Journal of the Neurological Sciences*, vol. 213, no. 1-2, pp. 19–24, 2003.

[29] W. Mlekusch, I. Mlekusch, M. Haumer et al., "Improvement of neurocognitive function after protected carotid artery stenting," *Catheterization and Cardiovascular Interventions*, vol. 71, no. 1, pp. 114–119, 2008.

[30] M. Silvestrini, I. Paolino, F. Vernieri et al., "Cerebral hemodynamics and cognitive performance in patients with asymptomatic carotid stenosis," *Neurology*, vol. 72, no. 12, pp. 1062–1068, 2009.

[31] E. B. Mathiesen, K. Waterloo, O. Joakimsen, S. J. Bakke, E. A. Jacobsen, and K. H. Bønaa, "Reduced neuropsychological test performance in asymptomatic carotid stenosis: the Tromsø Study," *Neurology*, vol. 62, no. 5, pp. 695–701, 2004.

Hindawi Publishing Corporation
BioMed Research International
Volume 2014, Article ID 548392, 7 pages
http://dx.doi.org/10.1155/2014/548392

Research Article

Loss of Microstructural Integrity in the Limbic-Subcortical Networks for Acute Symptomatic Traumatic Brain Injury

Yanan Zhu,[1,2] Zhengjun Li,[2] Lijun Bai,[3] Yin Tao,[3] Chuanzhu Sun,[3] Min Li,[1] Longmei Zheng,[2] Bao Zhu,[2] Jun Yao,[2] Heping Zhou,[2] and Ming Zhang[1]

[1] *Department of Medical Imaging, First Affiliated Hospital of Medical College of Xi'an Jiaotong University, Xi'an 710061, China*
[2] *Medical Imaging Centre, An Kang Central Hospital, 85-Jinzhou South Road, AnKang 725000, China*
[3] *The Key Laboratory of Biomedical Information Engineering, Ministry of Education, Department of Biomedical Engineering, School of Life Science and Technology, Xi'an Jiaotong University, Xi'an 710049, China*

Correspondence should be addressed to Lijun Bai; bailj4152615@gmail.com and Ming Zhang; profzmmri@gmail.com

Received 18 December 2013; Accepted 14 January 2014; Published 20 February 2014

Academic Editor: Lin Ai

Previous studies reported discrepant white matter diffusivity in mild traumatic brain injury (mTBI) on the base of Glasgow Coma Scale, which are unreliable for some TBI severity indicators and the frequency of missing documentation in the medical record. In the present study, we adopted the Mayo classification system for TBI severity. In this system, the mTBI is also divided into two groups as "probable and symptomatic" TBI. We aimed to investigate altered microstructural integrity in symptomatic acute TBI (<1 week) by using tract-based spatial statics (TBSS) approach. A total of 12 patients and 13 healthy volunteers were involved and underwent MRI scans including conventional scan, and SWI and DTI. All the patients had no visible lesions by using conventional and SWI neuroimaging techniques, while showing widespread declines in the fractional anisotropy (FA) of gray matter and white matter throughout the TBSS skeleton, particularly in the limbic-subcortical structures. By contrast, symptomatic TBI patients showed no significant enhanced changes in FA compared to the healthy controls. A better understanding of the acute changes occurring following symptomatic TBI may increase our understanding of neuroplasticity and continuing degenerative change, which, in turn, may facilitate advances in management and intervention.

1. Introduction

Mild traumatic brain injury (mTBI) is one of the most common injuries seen in emergency departments [1]. Approximately 15 to 30% of mTBI patients will experience kinds of cognitive and clinical symptoms known as the postconcussion syndrome (PCS) and do not resolve following the first 3 months after injury [2]. Furthermore, in some cases, the PCS-related complaints last several months to years, leading to even long-term disability [3]. TBI is one of the most consistent candidates for initiating the molecular cascades that result in Alzheimer's disease (AD), Parkinson's disease (PD), and amyotrophic lateral sclerosis [4]. The debate about the pathophysiology of mild TBI and its neurobehavioural symptomatology comes from psychogenic or physiogenic origin that has been strongly argued. Since these symptoms may be derived from more subtle neurological alterations and cannot be detected by only using conventional neuroimaging techniques such as conventional CT and MRI [5], recent upsurge of interest has been directed toward developing both diagnostic and prognostic biomarkers that can predict which individuals are relatively more likely to progress clinically.

Diffusion tensor imaging (DTI) is a technique that makes it possible to investigate white matter in vivo, since it provides information about white matter anatomy unavailable by any other method—either in vivo or in vitro [6]. Recent study suggests that subtle white matter abnormalities can be better detected by DTI than by conventional imaging [7]. These subtle abnormalities were potentially responsible for persistent postconcussive symptoms.

Taking the advantages of DTI, growing studies have focused on the correlation between structural integrity and

mTBI recently. However, it was still unclear how these structural pictures evolved in mTBI patients. Arfanakis and coworkers firstly used DTI to investigate diffuse axonal injuries in acute mTBI (within 24 h of injury) and pointed out no significant mean diffusivity (MD) differences between mTBI patients and controls but attenuated fractional anisotropy (FA) in corpus callosum and the internal capsule in patients with mTBI [8]. Other study aimed to evaluate the correlation of the changes in FA and individual behavior performance. Niogi et al. found that subacute and chronic mTBI patients showed significant losses of FA in the left anterior corona radiate and uncinate fasciculus, which were significantly correlated with individual performances in attention control as well as memory, respectively [9]. And they inferred that FA can be used as a biomarker for neurocognitive function and dysfunction [10]. In addition, a longitudinal investigation demonstrated that mTBI was noted as a significant increase in fractional anisotropy and decrease in radial diffusivity in several left hemisphere tracts, and these trends even occurred after 3 to 5 months after injury [11]. Another study further explored that acute and chronic mTBI patients showed heterogeneous changes in the FA [12], and the main changes in FA for acute mTBI were significantly correlated with their postconcussion symptoms [13].

These discrepant findings do not necessarily conflict with each other, as there are many sources of variability inherent in MRI investigations that may contribute to the reported differences. Of various factors, one major effect is derived from the subtle difference in physiological state of mTBI. Previous study often adopted single indicators such as the Glasgow Coma Scale to classify different stages of TBI. However, this measure is often unreliable for some TBI severity indicators and the frequency of missing documentation in the medical record. In the present study, we adopted the Mayo classification system for TBI severity [14]. In this system, the mTBI is also divided into two groups as "probable and symptomatic" TBI.

In the present study, we aimed to investigate altered microstructural integrity in symptomatic acute TBI by using tract-based spatial statics (TBSS) approach. We hypothesized that (1) significant altered microstructural integrity occurred in the symptomatic acute TBI. (2) Though previous DTI studies have generally demonstrated lower integrity of white matter tracts in frontal and temporal regions in mTBI, we predicted the loss of integrity of limbic-subcortical in acute symptomatic TBI patients which were associated with emotional as well as executive dysfunction.

2. Materials and Methods

2.1. Participants. A total of 12 patients with acute symptomatic TBI (10 male, mean age 35.7, range 19–50) were recruited from the Emergency Department of An kang Central Hospital. Inclusion criteria were (1) first-episode, (2) symptomatic TBI defined according to the Mayo classification system for TBI severity, and (3) acute stage of TBI (<1 week). Exclusion criteria of symptomatic TBI were defined as current or previous drug or alcohol abuse, previous TBI, contraindications to MRI, penetrating injury, administration of sedatives/psychotropic/antiepileptic medication, spinal cord injury, neurological signs or multiple disabilities, history of psychiatric or psychological or neurological disease, MRI artifacts, and/or poor image quality. The control group comprised 13 healthy volunteers matched by the age, sex, and educational level. None had a history of neurological or psychiatric diseases. Their demographic characteristics were provided in Table 1. The study was approved by the local medical research ethics committee and institutional review board of local research ethics committees. All participants gave written informed consents.

Table 1: Demographic and injury characteristics of TBI.

Patient ID	Gender	Age	Education (years)	Days after injury	Causes
1	F	38	4	6	Assaults
2	M	36	15	1	RTA
3	M	19	13	1	Assaults
4	M	50	5	7	Assaults
5	M	21	7	5	Falls
6	F	29	15	7	RTA
7	M	48	1	7	Falls
8	M	42	6	7	RTA
9	M	46	9	4	RTA
10	M	26	12	7	Assaults
11	M	23	9	7	RTA
12	M	50	9	7	Assaults

ATBI: traumatic brain injury; M: male; F: female; RTA: road traffic accidents.

2.2. Image Acquisition. The MRI protocol consisted of structural and functional images acquired on a 1.5 T Siemens Magnetom Avanto MRI scanner. Image acquisition was as follows: high-resolution T1-weighted anatomic images were obtained (TR = 1900 ms, TI = 1000 ms, TE = 2.8 ms, flip angle = 8°, 144 contiguous slices of 1.0 mm thickness, FOV = 256 × 256 mm^2, and matrix = 256 × 256). T2-weighted images were obtained (TR = 4000 ms, TE = 79 ms, thickness = 5.5 mm, flip angle = 150°, FOV = 230 × 230 mm^2, and matrix = 231 × 384). SWI images were obtained (TR = 49 ms, TE = 40 ms, flip angle = 15°, 72 contiguous slices of 2.0 mm thickness, FOV = 230 × 230 mm^2, and matrix = 221 × 320). DTI scans were obtained (TR = 7300 ms, TE = 99 ms, thickness = 3 mm, directions = 30, FOV = 256 × 256 mm^2, matrix = 128 × 128, Averages = 2, and b-value = 1,000/0 s/mm^2).

2.3. Clinical Imaging. Patients were assessed by using standard T2 MRI to assess evidence of focal brain injury and SWI imaging to identify microbleeds, a marker of diffuse axonal injury. A senior consultant neuroradiologist reviewed all study MRI scans.

2.4. DTI Statistical Analyses. Diffusion data were preprocessed and analyzed using tools from the Oxford University Centre for Functional MRI of the Brain (FMRIB) software library (FSL Version 4.1). First, the b0 image of each subject was skull-stripped using the brain extraction tool. The data was corrected for subject motion and eddy-current-induced geometrical distortions, and the diffusion sensitizing gradients were rotated to correct for motion. Using FDT, the diffusion tensor model was fit to the data, from which FA images were calculated.

For tract-based spatial statistics (TBSS), all subjects' FA data was registered to a common space (the FA158 MNI space template) using a combination of affine and nonlinear registration. A mean FA image was created and eroded to a skeleton and threshold at FA > 0.2. Each subject's aligned FA data were then projected onto this skeleton and the resulting alignment-invariant representation of the central trajectory of white matter pathways was used for voxelwise statistical analysis (Randomize, 5000 permutations). The contrast TBI < controls was examined using threshold-free cluster enhancement (TFCE), with correction for multiple comparisons at $P < 0.05$.

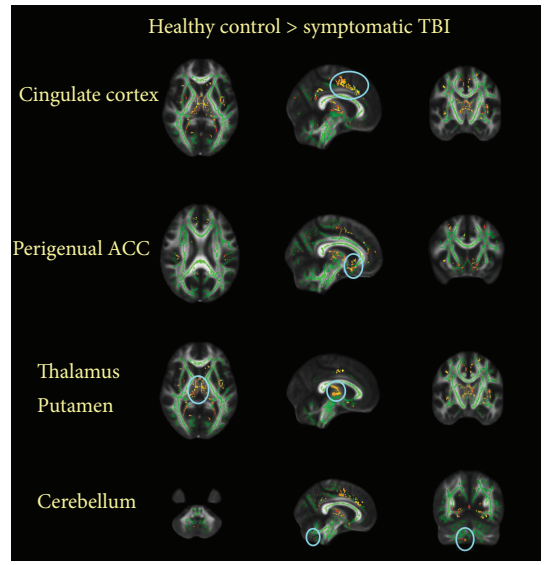

Figure 1: Group differences in mean FA. Symptomatic TBI patients showed a widespread decline in fractional anisotropy (FA) of gray and white matter throughout the TBSS skeleton (threshold at FA > 0.2, $P < 0.05$, corrected) overlaid on the TBSS skeleton (green).

3. Results

3.1. Demographic Results. Participants had to be between the ages of 18 and 60. Injuries were secondary to road traffic accidents (42%), assaults (42%), and falls (16%). Average scanning time after TBI was 5.5 days (range 1–7 days; SD 2.32). For a detailed list of means and demographic and injury characteristics, please see Table 1.

3.2. Clinical Imaging of Data. All of 12 patients with symptomatic TBI had a CT scan at the time of their emergency room visit, but none of the CT scans were deemed to contain trauma-related pathology by a nonblinded neuroradiologist. In addition, T2-weighted and SWI MRI images were reviewed by a neuroradiologist blinded to patient diagnosis. None of the patients had the well-defined evidence of lesion. Therefore, all the patients had no visible lesions by using conventional neuroimaging techniques.

3.3. Diffusion Tensor Imaging Scalar Analyses. Symptomatic TBI patients showed a widespread decline in fractional anisotropy (FA) of gray matter throughout the TBSS skeleton (shown in Figure 1). These regions included the bilateral frontal cortex (dorsal lateral prefrontal cortex, DLPFC; orbitofrontal cortex, OFC), the limbic system (bilateral subgenual and perigenual anterior cingulated cortex, sACC and pACC; bilateral posterior cingulate cortex, PCC; bilateral amygdala and parahippocampal gyrus), subcortical regions (bilateral caudate, claustrum, putamen, insula, and thalamus), occipital lobe (BA 7, 18, and 19), and temporal lobe (BA 20 and 37). In addition, the cerebellum also presented attenuated FA changes, primarily in the cerebellar lingual, declive, and uvula; please see Table 2. However, symptomatic TBI patients showed no significant enhanced changes in FA compared to the healthy controls.

The white matter of symptomatic TBI patients also exhibited FA decreases. Primarily, these regions located in the corpus callosum, limbic system (anterior cingulate, parahippocampal gyrus, and posterior cingulate) and sublobar areas (insula and extranuclear) as well as the frontal, temporal, occipital, and parietal lobe (precuneus) (see Table 3). However, symptomatic TBI patients showed no significant enhanced changes in FA compared to the healthy controls.

4. Discussion

In the current study, we observed a loss of structural integrity in multiple brain domains in acute symptomatic TBI patients (based on the Mayo classification system for TBI severity), who presented decreased fractional anisotropy values in widespread regions specially located in frontal lobe, limbic system, and sublobar areas compared with healthy controls.

In previous studies, DTI proved a sensitive technique that gave access in vivo to the structural integrity in mild TBI (mTBI) patients [7]. However, most of these studies generally induced discrepant findings only defining the mild TBI sample on the base of scores derived from Glasgow Coma Score (GCS). Single indicator such as the GCS was hardly to classify different stages of TBI. It is noted that about 6%–10% mTBI patients had visible lesions on CT [15]; these patients with positive CT scans tend to experience more neurobehavioral symptoms and poorer prognoses [16]. Therefore, this measures was often unreliable for some TBI severity indicators and the frequency of missing documentation in the medical record, leading to discrepant findings.

In the current study, we adopted the first-episode symptomatic TBI patients according to the Mayo classification system, based on available indicators including death due

Table 2: Gray matter regions of significant FA reductions in 12 sTBI.

	Talairach			t	Voxels
	x	y	z	Value	
Caudate head					
L	−13	20	−1	2.40	128
Claustrum					
L	−31	3	7	2.88	31
R	36	−8	6	3.00	34
Insula					
L	−36	0	10	2.24	39
R	34	20	5	3.31	50
Putamen					
L	−25	−3	−2	3.24	138
R	23	−1	3	3.30	176
Thalamus					
L	−10	−8	15	2.99	297
R	15	−30	2	4.03	282
AN_Thalamus					
L	−10	−9	14	2.55	45
R	10	−6	13	2.79	61
MDN_Thalamus					
L	−7	−20	7	2.66	204
R	12	−19	6	3.65	184
Pulvinar_Thalamus					
L	−5	−23	9	2.92	166
R	17	−24	6	3.38	301
VLN_Thalamus					
L	−9	−8	6	1.96	67
R	11	−11	−17	2.47	66
sACC BA 25					
L	−7	17	−10	2.14	30
R	8	17	−10	2.20	47
pACC BA 32					
L	−12	36	17	3.67	71
R	10	37	19	2.96	80
Cigulate cortex BA 32/24					
L	−7	−7	39	2.23	218
R	9	−2	47	4.93	326
Amygdala					
L	−28	−6	−12	1.64	28
PH BA 36/37					
L	−23	−30	−12	3.84	185
R	23	−30	−4	3.14	143
PCC BA 23					
L	−1	−56	15	1.60	26
R	5	−47	24	3.37	199
OFC BA 10/47					
L	−10	−13	49	4.38	112
DLPFC BA 6/9					
L	−10	−13	49	4.38	112
R	5	−22	50	3.14	82
Lingual gyrus BA 18/19					
L	−17	−64	0	2.51	86
R	13	−52	3	3.45	149
Fusiform gyrus BA 37/20					
L	−44	−39	−17	2.36	45
R	32	−36	−17	1.27	24
R	20	−42	−7	1.39	21

AsTBI: symptomatic traumatic brain injury; LN: lentiform nucleus; AN: anterior nucleus; MDN: medial dorsal nucleus; VLN: ventral lateral nucleus; sACC: subgenual anterior cingulate cortex; pACC: perigenual anterior cingulate cortex; PH: parahippocampal gyrus; PCC: posterior cingulate cortex; OFC: orbitofrontal cortex; DLPFC: dorsolateral prefrontal cortex; BA: Brodmann area; PH: parahippocampus; AL: anterior lobe.

to TBI, trauma-related neuroimaging abnormalities, GCS, Posttraumatic Amnesia (PTA), loss of consciousness, and specified postconcussive symptoms. We supposed that, even in the stage of symptomatic TBI, there might be significant damage related to TBI that needed acute and proper treatment which was probably beneficial to the long-term prognosis.

Many studies reported discrepant white matter diffusivity in mTBI, increased, reduced, or unchanged. One of major factors was the unequal scanning time after mTBI. Recently, traumatic axonal injury (TAI) has been suggested encompassing not only the primary axonal damage specifically caused by shear/strain injury but also secondary alterations of white matter such as metabolic, hypoxic, and microvascular damage or excitotoxicity [17]. Moreover, axonal pathology is more pronounced in the acute phase of injury [18]. In the current study, we aimed to investigate the symptomatic TBI during the acute period after postinjury period that helped us to draw original patterns of TBI damage, which we can use as the baseline of longitudinal study to observe the recovery and/or deterioration of traumatic axonal injury.

Standard DTI analysis consisted of the placement of regions of interest, the tract-based spatial statistics. The former is restricted to assessment of the a priori defined regions, and only a small amount of the total white matter is usually investigated [9]. The latter allows the voxelwise assessment of all parts of large white matter tracts in an automated way [19], providing whole-brain voxelwise measures. It was clear that traumatic brain injury produced a complex pattern of diffuse axonal injury at wide range of brain regions and so it was hard to define regions with a priori information.

Fractional anisotropy (FA) is the DTI metric, which was commonly applied and measures preferential water diffusion along white matter tracts, and served as a usable marker of tissue integrity. In recent studies, FA has also been proposed as the most feasible biomarker of TAI and one of the best indicators of TBI severity [20, 21]. In the current study, we evaluated the structural integrity by observing the changes of FA values, which showed reductions in the TBI cohort. This finding was coincident with animal models of TBI, which

Table 3: White matter regions of significant FA reduction in 12 sTBI.

	Talairach			t	Voxels
	x	y	z	Value	
MFG					
L	−10	53	8	3.81	140
R	10	43	21	4.37	153
PG					
L	−46	−7	36	1.66	33
R	41	−10	38	2.55	52
SG					
L	−13	12	−11	3.45	62
R	9	15	−13	3.47	58
Subgyral					
L	−20	−7	56	3.05	282
R	11	−23	46	3.75	329
PH					
L	−30	−38	−5	4.96	537
R	32	−30	−11	4.12	461
PCC					
L	32	−58	15	2.11	33
R	32	−59	8	3.48	22
ACC					
L	−6	40	−4	3.43	145
R	13	44	−6	2.48	95
Cingulate cortex					
L	−12	−3	32	3.60	102
R	8	−1	46	3.71	173
Extranuclear					
L	32	−29	13	3.23	667
R	32	−14	15	3.90	487
Corpus callosum					
L	32	−14	18	2.05	23
R	32	−42	6	3.02	46
Insula					
L	32	−11	10	2.77	327
R	32	19	5	3.73	186
Cuneus					
L	32	−59	6	1.95	65
Lingual gyrus					
L	32	−58	3	3.09	283
R	32	−60	0	3.33	260
Precuneus					
L	−10	−57	35	4.88	29
R	12	−51	40	2.52	49
MTG					
L	32	−34	2	2.09	28

AMFG: middle frontal gyrus; PeCG: precentral gyrus; SG: subcallosal gyrus; PH: parahippocampal gyrus; PCC: posterior cingulate cortex; ACC: anterior cingulate cortex; LG: Lingual Gyrus; MTG: middle temporal gyrus.

have consistently indicated reduced anisotropic white matter water diffusion in the acute and semiacute injury stages [22]. But this finding appeared to be inconsistent with Ling et al. 's study, which proved increased FA in semiacute mTBI [23]. The possible reason was that the symptomatic TBI in the current study were different from their mild TBI, that all experienced an alteration in mental status, and the majority of the sample also experienced a loss of consciousness. The other reason was the earlier neuroimaging in the current study. If both reasons were all reasonable, we may suggest that the decreased FA probably indicated the original damage to the axon and the increased one indicated the recovery; we also suggested that an increase in FA may indicate more severe TBI correlated with poor clinical outcomes.

In the current study, we conducted the group comparison through FA skeleton maps, revealing significant FA reductions in the acute symptomatic TBI patients as compared to controls in the following areas: frontal lobe (DLPFC; OFC), the limbic-system (bilateral sACC and pACC, bilateral PCC, bilateral amygdala, and parahippocampal gyrus), subcortical regions (bilateral caudate, claustrum, putamen, insula, and thalamus), occipital lobe (BA 7, 18, and 19), temporal lobe (BA 20 and 37), and the corpus callosum (CC). These regions were generally in coincidence with a volumetric studies by the voxel-based morphometry (VBM) method and revealed reduced density of gray and/or white matter in the corpus callosum, limbic system, frontal lobe, subcortical areas, temporal lobe, and the cerebellum [24–26]. However, these findings about lower integrity domains of current study were only somewhat similar with previous DTI studies, in which the frontal and temporal regions proved the general lower integrity domains with mTBI [27]. The studies utilizing voxel-based techniques showed the discrepant losses in the brain areas. In Lipton et al.'s work, the domains were CC, subcortical white matter, and internal capsules, bilaterally in chronic mTBI [28]. In another study, in the acute mTBI (≤2 weeks), the significant changes were mainly located in the frontal white matter, including the dorsolateral prefrontal cortex [29]. The FA attenuated regions were also found in the right temporal subcortical white matter including the inferior frontooccipital fasciculus in the subacute mTBI [30]. Obviously, the current findings included almost all regions of previous studies, potentially deriving from the more sensitive analysis method and assessment to the whole brain including white and gray matters. Notably, we observed the pronounced FA reduction in the thalamus, which was a key node in many of brain function networks [31] but was often overlooked in previous DTI studies. The damage to the thalamus-seeded structural connectivity is an important determinant of outcomes after TBI [32]. Our findings suggested a loss of integrity in the precuneus which served as an important node within the default mode network (DMN). The locations of thalamus and the precuneus provided us with a novel idea that perhaps the damage which resulted by TBI was not only the focal lesion but also the disconnection of brain network. Standing at this point, the following study will use the combination of multiple tractographical, analytical, and statistical methods to detect more tiny damage to the specific brain network in the whole brain range.

5. Conclusions

We demonstrated the sensitivity of DTI in identifying microstructural abnormalities in patients classified as

"symptomatic" TBI with the minimal severity, no loss of consciousness, posttraumatic anterograde amnesia, and no contusions and microhemorrhage on conventional neuroimaging. A better understanding of the acute changes occurring following symptomatic TBI may increase our understanding of neuroplasticity and continuing degenerative changes, which. in turn, may facilitate advances in management and intervention. Future analyses will include additional examination of the relation of imaging changes to cognitive and functional outcome as well as multimodal imaging analyses of symptomatic TBI.

Conflict of Interests

There is no competing interests.

Acknowledgments

This study was supported by the National Natural Science Foundation of China (Grant nos. 81071217, 81371630, and 81371530), the Fundamental Research Funds for the Central Universities, the Beijing Nova program (Grant no. Z111101054511116), and the Beijing Natural Science Foundation (Grant no. 4122082).

References

[1] J. D. Cassidy, L. J. Carroll, P. M. Peloso et al., "Incidence, risk factors and prevention of mild traumatic brain injury: results of the WHO Collaborating Centre Task Force on Mild Traumatic Brain Injury," *Journal of Rehabilitation Medicine, Supplement*, no. 43, pp. 28–60, 2004.

[2] E. D. Bigler, "Neuropsychology and clinical neuroscience of persistent post-concussive syndrome," *Journal of the International Neuropsychological Society*, vol. 14, no. 1, pp. 1–22, 2008.

[3] B. Willer and J. J. Leddy, "Management of concussion and post-concussion syndrome," *Current Treatment Options in Neurology*, vol. 8, no. 5, pp. 415–426, 2006.

[4] B. E. Gavett, R. A. Stern, R. C. Cantu, C. J. Nowinski, and A. C. McKee, "Mild traumatic brain injury: a risk factor for neurodegeneration," *Alzheimer's Research and Therapy*, vol. 2, no. 3, article 18, 2010.

[5] R. Green, Y. Koshimori, and G. Turner, "Research digest. Understanding the organic basis of persistent complaints in mTBI: findings from functional and structural neuroimaging," *Neuropsychological Rehabilitation*, vol. 20, no. 3, pp. 471–478, 2010.

[6] Y. Assaf and O. Pasternak, "Diffusion tensor imaging (DTI)-based white matter mapping in brain research: a review," *Journal of Molecular Neuroscience*, vol. 34, no. 1, pp. 51–61, 2008.

[7] M. E. Shenton, H. M. Hamoda, J. S. Schneiderman et al., "A review of magnetic resonance imaging and diffusion tensor imaging findings in mild traumatic brain injury," *Brain Imaging and Behavior*, vol. 6, no. 2, pp. 137–192, 2012.

[8] K. Arfanakis, V. M. Haughton, J. D. Carew, B. P. Rogers, R. J. Dempsey, and M. E. Meyerand, "Diffusion tensor MR imaging in diffuse axonal injury," *American Journal of Neuroradiology*, vol. 23, no. 5, pp. 794–802, 2002.

[9] S. N. Niogi, P. Mukherjee, J. Ghajar et al., "Structural dissociation of attentional control and memory in adults with and without mild traumatic brain injury," *Brain*, vol. 131, no. 12, pp. 3209–3221, 2008.

[10] S. N. Niogi, P. Mukherjee, J. Ghajar et al., "Extent of microstructural white matter injury in postconcussive syndrome correlates with impaired cognitive reaction time: a 3T diffusion tensor imaging study of mild traumatic brain injury," *American Journal of Neuroradiology*, vol. 29, no. 5, pp. 967–973, 2008.

[11] A. R. Mayer, J. Ling, M. V. Mannell et al., "A prospective diffusion tensor imaging study in mild traumatic brain injury," *Neurology*, vol. 74, no. 8, pp. 643–650, 2010.

[12] M. Inglese, S. Makani, G. Johnson et al., "Diffuse axonal injury in mild traumatic brain injury: a diffusion tensor imaging study," *Journal of Neurosurgery*, vol. 103, no. 2, pp. 298–303, 2005.

[13] E. A. Wilde, S. R. McCauley, J. V. Hunter et al., "Diffusion tensor imaging of acute mild traumatic brain injury in adolescents," *Neurology*, vol. 70, no. 12, pp. 948–955, 2008.

[14] J. F. Malec, A. W. Brown, C. L. Leibson et al., "The mayo classification system for traumatic brain injury severity," *Journal of Neurotrauma*, vol. 24, no. 9, pp. 1417–1424, 2007.

[15] M. Smits, D. W. J. Dippel, G. G. de Haan et al., "Minor head injury: guidelines for the use of CT—a multicenter validation study," *Radiology*, vol. 245, no. 3, pp. 831–838, 2007.

[16] R. T. Lange, G. Iverson, and M. D. Franzen, "Neuropsychological functioning following complicated vs. uncomplicated mild traumatic brain injury," *Brain Injury*, vol. 23, no. 2, pp. 83–91, 2009.

[17] A. Büki and J. T. Povlishock, "All roads lead to disconnection? Traumatic axonal injury revisited," *Acta Neurochirurgica*, vol. 148, no. 2, pp. 181–193, 2006.

[18] A. Spain, S. Daumas, J. Lifshitz et al., "Mild fluid percussion injury in mice produces evolving selective axonal pathology and cognitive deficits relevant to human brain injury," *Journal of Neurotrauma*, vol. 27, no. 8, pp. 1429–1438, 2010.

[19] K. M. Kinnunen, R. Greenwood, J. H. Powell et al., "White matter damage and cognitive impairment after traumatic brain injury," *Brain*, vol. 134, no. 2, pp. 449–463, 2011.

[20] T. A. G. M. Huisman, L. H. Schwamm, P. W. Schaefer et al., "Diffusion tensor imaging as potential biomarker of white matter injury in diffuse axonal injury," *American Journal of Neuroradiology*, vol. 25, no. 3, pp. 370–376, 2004.

[21] R. R. Benson, S. A. Meda, S. Vasudevan et al., "Global white matter analysis of diffusion tensor images is predictive of injury severity in traumatic brain injury," *Journal of Neurotrauma*, vol. 24, no. 3, pp. 446–459, 2007.

[22] Y. van de Looij, F. Mauconduit, M. Beaumont et al., "Diffusion tensor imaging of diffuse axonal injury in a rat brain trauma model," *NMR in Biomedicine*, vol. 25, no. 1, pp. 93–103, 2012.

[23] J. M. Ling, A. Peña, R. A. Yeo et al., "Biomarkers of increased diffusion anisotropy in semi-acute mild traumatic brain injury: a longitudinal perspective," *Brain*, vol. 135, no. 4, pp. 1281–1292, 2012.

[24] S. D. Gale, L. Baxter, N. Roundy, and S. C. Johnson, "Traumatic brain injury and grey matter concentration: a preliminary voxel based morphometry study," *Journal of Neurology, Neurosurgery and Psychiatry*, vol. 76, no. 7, pp. 984–988, 2005.

[25] C. H. Salmond, D. A. Chatfield, D. K. Menon, J. D. Pickard, and B. J. Sahakian, "Cognitive sequelae of head injury: involvement of basal forebrain and associated structures," *Brain*, vol. 128, no. 1, pp. 189–200, 2005.

[26] F. Tomaiuolo, K. J. Worsley, J. Lerch et al., "Changes in white matter in long-term survivors of severe non-missile traumatic brain injury: a computational analysis of magnetic resonance images," *Journal of Neurotrauma*, vol. 22, no. 1, pp. 76–82, 2005.

[27] S. N. Niogi and P. Mukherjee, "Diffusion tensor imaging of mild traumatic brain injury," *Journal of Head Trauma Rehabilitation*, vol. 25, no. 4, pp. 241–255, 2010.

[28] M. L. Lipton, E. Gellella, C. Lo et al., "Multifocal white matter ultrastructural abnormalities in mild traumatic brain injury with cognitive disability: a voxel-wise analysis of diffusion tensor imaging," *Journal of Neurotrauma*, vol. 25, no. 11, pp. 1335–1342, 2008.

[29] M. L. Lipton, E. Gulko, M. E. Zimmerman et al., "Diffusion-tensor imaging implicates prefrontal axonal injury in executive function impairment following very mild traumatic brain injury," *Radiology*, vol. 252, no. 3, pp. 816–824, 2009.

[30] M. Smits, G. C. Houston, D. W. J. Dippel et al., "Microstructural brain injury in post-concussion syndrome after minor head injury," *Neuroradiology*, vol. 53, no. 8, pp. 553–563, 2011.

[31] B. Alkonyi, C. Juhász, O. Muzik, M. E. Behen, J.-W. Jeong, and H. T. Chugani, "Thalamocortical connectivity in healthy children: asymmetries and robust developmental changes between ages 8 and 17 years," *American Journal of Neuroradiology*, vol. 32, no. 5, pp. 962–969, 2011.

[32] J. H. Adams, D. I. Graham, and B. Jennett, "The neuropathology of the vegetative state after an acute brain insult," *Brain*, vol. 123, no. 7, pp. 1327–1338, 2000.